Optimisation de méthodes bidimensionnelles en ligne LCxLC-UV/MS et LCxSFC-UV pour l'analyse d'échantillons complexes

Morgan Sarrut

N°d'ordre NNT : 2016LYSE1189

THESE de DOCTORAT DE L'UNIVERSITE DE LYON

opérée au sein de

l'Université Claude Bernard Lyon 1

École Doctorale N° 206

École doctorale de Chimie de Lyon

Spécialité de doctorat : **Chimie Analytique**

Soutenue publiquement le 17/10/2016, par :

Morgan SARRUT

Optimisation de méthodes bidimensionnelles en ligne LCxLC-UV/MS et LCxSFC-UV pour l'analyse d'échantillons complexes

Devant le jury composé de :

BECK, Alain	Chercheur	Laboratoires Pierre Fabre	Examinateur
FOCANT, Jean-François	Professeur	Université de Liège	Rapporteur
HEINISCH, Sabine	Ingénieur de Recherche	Université Lyon 1	Directrice de thèse
MORELL, Christophe	Professeur	Université Lyon 1	Président du jury
VEUTHEY, Jean-Luc	Professeur	Université de Genève	Rapporteur
WEST Caroline	Maître de Conférences	Université d'Orléans	Examinateur

UNIVERSITE CLAUDE BERNARD - LYON 1

Président de l'Université	**M. le Professeur Frédéric FLEURY**
Président du Conseil Académique	M. le Professeur Hamda BEN HADID
Vice-président du Conseil d'Administration	M. le Professeur Didier REVEL
Vice-président du Conseil Formation et Vie Universitaire	M. le Professeur Philippe CHEVALIER
Vice-président de la Commission Recherche	M. Fabrice VALLÉE
Directeur Général des Services	M. Alain HELLEU

COMPOSANTES SANTE

Faculté de Médecine Lyon Est – Claude Bernard	Directeur : M. le Professeur J. ETIENNE
Faculté de Médecine et de Maïeutique Lyon Sud – Charles Mérieux	Directeur : Mme la Professeure C. BURILLON
Faculté d'Odontologie	Directeur : M. le Professeur D. BOURGEOIS
Institut des Sciences Pharmaceutiques et Biologiques	Directeur : Mme la Professeure C. VINCIGUERRA
Institut des Sciences et Techniques de la Réadaptation	Directeur : M. le Professeur Y. MATILLON
Département de formation et Centre de Recherche en Biologie Humaine	Directeur : Mme la Professeure A-M. SCHOTT

COMPOSANTES ET DEPARTEMENTS DE SCIENCES ET TECHNOLOGIE

Faculté des Sciences et Technologies	Directeur : M. F. DE MARCHI
Département Biologie	Directeur : M. le Professeur F. THEVENARD
Département Chimie Biochimie	Directeur : Mme C. FELIX
Département GEP	Directeur : M. Hassan HAMMOURI
Département Informatique	Directeur : M. le Professeur S. AKKOUCHE
Département Mathématiques	Directeur : M. le Professeur G. TOMANOV
Département Mécanique	Directeur : M. le Professeur H. BEN HADID
Département Physique	Directeur : M. le Professeur J-C PLENET
UFR Sciences et Techniques des Activités Physiques et Sportives	Directeur : M. Y.VANPOULLE
Observatoire des Sciences de l'Univers de Lyon	Directeur : M. B. GUIDERDONI
Polytech Lyon	Directeur : M. le Professeur E.PERRIN
Ecole Supérieure de Chimie Physique Electronique	Directeur : M. G. PIGNAULT
Institut Universitaire de Technologie de Lyon 1	Directeur : M. le Professeur C. VITON
Ecole Supérieure du Professorat et de l'Education	Directeur : M. le Professeur A. MOUGNIOTTE
Institut de Science Financière et d'Assurances	Directeur : M. N. LEBOISNE

REMERCIEMENTS

J’ai vécu trois années passionnantes et inoubliables. Bien sûr la science, les différents projets et collaborations y sont pour quelque chose. Mais plus encore ce sont les rencontres humaines qui donnent l’envie et la motivation d’explorer, de progresser, de transmettre aussi.

Je remercie Madame Sabine Heinisch pour sa confiance, son investissement total, son exigence et son désir de transmettre. Sabine, ma reconnaissance est infinie.

Un grand merci à Monsieur Gérard Crétier pour sa présence et pour tous ces échanges scientifiques et autres discussions qui m’ont fait progresser plus vite que je n’aurais pu l’espérer.

Je souhaite exprimer ma gratitude aux membres du jury pour avoir accepté d’évaluer ce travail de thèse. Merci à Messieurs Jean-François Focant et Jean-Luc Veuthey d’avoir accepté de rapporter ce manuscrit, merci à Madame Caroline West et Messieurs Alain Beck et Christophe Morell pour l’examen de ces travaux.

Je voudrais bien sûr remercier toutes les personnes que j’ai particulièrement côtoyées durant ma thèse. Amélie pour ces 9 mois fantastiques (qui continuent !), Audrey avec qui les congrès deviennent des aventures (l’avion, le coiffeur, le taxi, sans parler des irlandais(e)s...), Élodie et nos discussions, thank you Marie, Josiane, Féfé, Marion (allez l’OM), Léa, Magali. Florent, t’inquiètes je ne t’oublie pas ! Tu es le plus grand flemmard passionné que je connaisse ! Mais toujours là. Karine, tu sais que je suis maintenant convaincu que la CPC est de la chromatographie !

Merci aux membres du CA du Club Lyonnais de Chromatographie pour leur accueil, il y a trois ans, et leur sympathie.

Je voudrais également remercier Philippe Mériglier de la société Waters pour son aide précieuse et spontanée. Merci à Davy Guillarme de l’université de Genève et Alain Beck des Laboratoires Pierre Fabre ainsi que leurs équipes pour leur aide durant nos projets communs. Merci aussi à Christelle Margoum, Philippe Bados et Céline Guillemain d’Irstea pour leur disponibilité et leur confiance pour l’utilisation de leur matériel.

Je profite de l’occasion pour lancer un message à mes amis sudistes qui pour la plupart ont réussi à rester proches du soleil et que je revois toujours avec grand plaisir : le Vince, Bastien, Manon, Kévin... Un jour je reviendrai ! Mathieu, Sylvain, déjà 5 ans…

Enfin j’ai une pensée pour mes parents, mes grand-parents et mon frère qui ont suivi ma thèse, souvent sans tout comprendre, mais qui ont toujours essayé. Merci Laurianne pour ta présence au quotidien.

TITRE en français : Optimisation de méthodes bidimensionnelles en ligne LCxLC-UV/MS et LCxSFC-UV pour l'analyse d'échantillons complexes

RÉSUMÉ en français : La chromatographie en phase liquide bidimensionnelle « comprehensive » en ligne (LCxLC) est une technique à très haut pouvoir de séparation. Après avoir établi son intérêt mais aussi les enjeux liés au développement de méthodes et les conditions expérimentales utilisées, une attention particulière est portée à l'optimisation des méthodes en LCxLC. Une procédure d'optimisation basée la méthode « Pareto-optimal » est décrite. Les conditions optimales prédites sont ensuite appliquées à la séparation RPLCxRPLC d'un mélange complexe de peptides et comparée avec la 1D-RPLC en termes de capacité de pics, temps d'analyse et facteur de dilution démontrant l'avantage fournit par la RPLCxRPLC. L'optimisation d'une méthode HICxRPLC-UV/MS en ligne permettant la caractérisation exhaustive d'un anticorps conjugué est réalisée soulignant, entre autres, la grande complémentarité entre les différents modes de détection employés en ^{1}D et ^{2}D.
Enfin, la possibilité de développer un couplage RPLCxSFC est explorée dans le but d'augmenter l'espace de séparation pour des composés neutres. La méthode RPLCxSFC optimisée est comparée avec une séparation RPLCxRPLC optimisée pour l'analyse d'une bio-huile montrant qu'elle peut être considérée comme une alternative crédible pour la séparation de tels échantillons.

TITRE en anglais : Optimization of on-line two-dimensional LCxLC-UV/MS and LCxSFC-UV methods for the analysis of complex matrices

RÉSUMÉ en anglais : Comprehensive two-dimensional liquid chromatography is a powerful but complex separative technique. After detailing the interest of such a technique, the method development issues and the experimental conditions employed throughout this work, a particular attention is paid to the optimization of LCxLC methods. Accordingly an optimization procedure based on Pareto-optimal method is described. The predicted optimal conditions are then applied to experimental RPLCxRPLC separations of complex samples of peptides and compared with 1D-RPLC in terms of peak capacity, analysis time and sensitivity clearly showing the advantage of RPLCxRPLC approach.The optimization of a HICxRPLC-UV/MS method for the exhaustive characterization of an antibody-drug conjugate is achieved highlighting the high complementarity of the different detection modes used both in ^{1}D and ^{2}D. Finally, a proof of concept concerning the implementation of RPLCxSFC coupling is achieved with the aim of increasing the separation space coverage for neutral compounds. The optimized RPLCxSFC separation is then compared with an optimized RPLCxRPLC approach for the analysis of a bio-oil sample showing that RPLCxSFC is a credible alternative for the separation of such a sample.

Discipline : Chimie analytique

MOTS-CLÉS : Chromatographie bidimensionnelle en ligne, peptides, anticorps conjugués (ADC), biomolécules, bio-huile, SFC, RPLC, HIC, spectrométrie de masse

ADRESSE DU LABORATOIRE : Institut des Sciences Analytiques (ISA). 5 rue de la Doua. 69100 Villeurbanne (France)

PRINCIPALES ABRÉVIATIONS

AA	Acétate d'ammonium
ADC	Anticorps conjugué
As	Asymétrie du pic
b	Pente de gradient dans la relation de Snyder « gradient steepness »
C_e	Composition en solvant organique du gradient à l'élution
C_i	Composition initiale en solvant organique du gradient
C_f	Composition finale en solvant organique du gradient
C_F	Facteur de compression
^1D	Première dimension
^2D	Seconde dimension
DAD	Détecteur à barrettes de diodes
ΔC	Plage de composition en solvant organique du gradient
d_i	Diamètre interne de la colonne
D_m	Coefficient de diffusion
d_p	Diamètre des particules
η	Viscosité de la phase mobile
D_f	Facteur de dilution
ε_t	Porosité totale de la colonne
ESI	Electrospray
EIC	Courant ionique extrait
F	Débit
FA	Acide formique
γ	Taux d'occupation de l'espace 2D
HIC	Chromatographie d'interaction hydrophobe
HRMS	Spectrométrie de masse haute résolution
HT	Haute température
k	Facteur de rétention
k_0	Facteur de rétention dans le solvant le plus faible
k_e	Facteur de rétention à l'élution
L	Longueur de la colonne
LC	Chromatographie en phase liquide
LCxLC	Chromatographie en phase liquide bidimensionnelle « comprehensive »
log P	Coefficient de partage octanol/eau
LSS	Linear Solvent Strength
mAb	Anticorps monoclonaux
MS	Spectrométrie de masse
M_W	Masse moléculaire
N	Nombre de plateaux
$n_{2D,effective}$	Capacité de pics effective en 2D
n	Capacité de pics
Na_2HPO_4	Hydrogénophophaste disodique
NaH_2PO_4	Dihydrogénophosphate de sodium

RPLC	Chromatographie en phase liquide à polarité des phases inversées
σ^2_{col}	Dispersion colonne
σ^2_{ext}	Dispersion extra-colonne
σ_i^2	Dispersion liée à l'injection
σ^2_{split}	Dispersion liée au split
σ_t	Écart type du pic en temps
σ_v	Écart type du pic en volume
s	Pente normalisée de gradient
S	Pente pour la relation LSS
SFC	Chromatographie en fluide supercritique
SIM	Acquisition du suivi d'un ion « single ion monitoring »
T	Température
τ	Taux d'échantillonnage en D1
t_0	Temps mort de la colonne
t_D	Temps de délai
TFA	Acide trifluoroacétique
t_G	Temps de gradient
TIC	Courant ionique total
TOF	Spectromètre de masse à temps de vol « time of flight »
t_R	Temps de rétention
UHPLC	Système chromatographique à très hautes pressions
UV	Détecteur ultraviolet
V_0	Volume mort de la colonne
V_i	Volume injecté
v	Vitesse linéaire réduite
$w_{10\%}$	Largeur à 10% de la hauteur du pic
$w_{4\sigma}$	Largeur du pic à 4σ
z	Rapport de split

Les exposants 1 et 2 sont utilisés pour préciser s'il s'agit d'une grandeur de première ou seconde dimension.

SOMMAIRE

INTRODUCTION GÉNÉRALE

La chromatographie en phase liquide (LC) est une technique de choix dans de très nombreux domaines (pharmaceutiques, environnementaux, cosmétiques, fraudes…).

Pour faire face à des échantillons de plus en plus complexes et obtenir un maximum d'informations, la chromatographie en phase liquide bidimensionnelle « comprehensive » (LCxLC) est une technique à fort potentiel grâce à son très haut pouvoir séparatif théorique.

Les approches bidimensionnelles (2D) peuvent être réalisées en mode hors ligne ou en ligne. Le mode hors-ligne requiert une optimisation classique des conditions chromatographiques mais présente plusieurs inconvénients à savoir (i) une durée totale d'analyse très élevée qui comprend différentes étapes non automatisables tels que l'analyse de 1ère dimension, la collecte des fractions, bien souvent un traitement de celles-ci (évaporation du solvant, regroupement de fractions) puis les injections successives en 2ème dimension (une fraction = une analyse), (ii) des risques de contamination, d'effets mémoires, et (iii) des pertes et/ou dégradations d'échantillons.

Pour pallier ces limitations, le mode en ligne a été privilégié tout au long de ce travail. Toutefois, l'optimisation de méthodes LCxLC en ligne est beaucoup plus complexe. En effet, il faut considérer les deux dimensions chromatographiques non plus de façon distinctes mais comme un système unique dans lequel tous les facteurs (conditions opératoires et contraintes instrumentales) sont interconnectés. Ceux-ci influencent de façon conflictuelle les trois objectifs désirés dans le développement d'une méthode chromatographique à savoir (i) une capacité de pics élevée, (ii) une sensibilité élevée et (iii) un temps d'analyse le plus court possible. Il est donc nécessaire d'établir des relations mathématiques qui permettent de suivre le comportement chromatographique des molécules à séparer dans le système 2D envisagé reliant ainsi les conditions opératoires à ces trois descripteurs de performance afin de pouvoir les optimiser simultanément. Malgré l'enjeu, peu de travaux ont été décrits concernant l'optimisation de méthodes en LCxLC en ligne. Aucun ou presque ne présente d'application expérimentale basée sur une stratégie prédictive.

Un état des lieux concernant les grands principes à appliquer lors d'un développement de méthodes en LCxLC en ligne, ainsi que les différentes stratégies d'optimisation proposées dans la littérature est donc proposé dans le chapitre 1. Une analyse critique de ces différentes approches est effectuée et des pistes d'améliorations sont suggérées.

Après avoir décrit, dans le chapitre 2, les conditions expérimentales utilisées dans les différentes études, le chapitre 3 développe une nouvelle méthodologie pour l'optimisation des conditions en RPLCxRPLC en ligne. Basée sur une approche

"Pareto optimal", cette méthodologie tient simultanément compte des trois critères d'optimisation en intégrant les aspects cinétiques et thermodynamiques pour décrire le comportement des molécules, mais aussi les contraintes instrumentales dans chacune des dimensions. L'objectif est double : (i) prédire quels sont les meilleurs paramètres (longueur de colonne, diamètre de particules, température, ratio de split, etc…) à choisir pour dimensionner une séparation RPLCxRPLC optimale et (ii) pouvoir directement appliquer ces conditions expérimentalement. Dans ce travail, l'approche théorique est ensuite appliquée à la séparation de peptides. Les résultats sont comparés avec ceux obtenus en 1D-RPLC dans des conditions également optimisées.

Le couplage en ligne de méthodes orthogonales couplées à la spectrométrie de masse haute résolution a également été développé pour la caractérisation de biomolécules à très hauts poids moléculaires (≈ 25 à 150 kDa), des anticorps conjugués (ADCs). Ces nouvelles molécules thérapeutiques à très haute valeur ajoutée allient la spécificité d'un anticorps monoclonal (mAb) et la puissance de molécules cytotoxiques conjuguées sur le mAb. Utilisées pour le traitement du cancer, elles sont particulièrement propices au développement d'outils bidimensionnels du fait de leurs propriétés et de leur complexité. En effet, de nombreuses techniques analytiques sont nécessaires pour caractériser ces molécules et l'intérêt de pouvoir combiner les informations obtenues à partir de deux techniques différentes lors d'une même analyse est évident. Dans cette optique, le chapitre 4 détaille l'optimisation d'une méthode bidimensionnelle « comprehensive » en ligne entre la chromatographie d'interaction hydrophobe (HIC) et la chromatographie en phase inverse (RPLC) couplée à la spectrométrie de masse haute résolution (HRMS). Cette méthode HICxRPLC-UV/MS a pour but de déterminer, en une seule analyse, le nombre moyen de molécules cytotoxiques conjuguées au mAb, en HIC (conditions non dénaturantes), puis d'obtenir des informations structurales en RPLC-UV/MS (conditions dénaturantes). En plus de l'aspect séparatif, la deuxième dimension doit permettre l'élimination de la grande quantité de sels présents dans la phase mobile de 1ère dimension avant son entrée dans le spectromètre de masse afin d'éviter toute contamination. Cette étape de dessalage en ligne constitue également un aspect particulièrement intéressant d'un couplage LCxLC-MS.

Alors qu'il est assez aisé de trouver des conditions relativement orthogonales en LCxLC pour des composés ionisables par simple modification du pH entre les deux dimensions (chapitre 3) ou en utilisant des conditions non dénaturantes/dénaturantes dans le cas de biomolécules telles que les ADCs (chapitre 4), il est beaucoup plus difficile de trouver des sélectivités différentes en RPLCxRPLC pour des molécules neutres. Des alternatives comme le couplage entre la phase normale (NP) et la phase inverse (RP) peuvent être envisagées mais se heurtent au manque de compatibilité des phases mobiles entre les deux dimensions. De plus la NP présente les inconvénients d'être peu répétable, d'utiliser des éluants souvent toxiques et d'offrir peu de choix dans les chimies des phases stationnaires. De ce fait, les séparations RPLCxRPLC sont souvent privilégiées malgré le manque d'orthogonalité. Le chapitre 5 propose une nouvelle alternative pour la séparation de mélanges complexes de

composés neutres. Il s'agit de coupler la RPLC, en 1ère dimension, avec la chromatographie en fluide supercritique (SFC), en 2ème dimension. L'utilisation de la SFC en 2ème dimension se justifie notamment par la possibilité de conduire des analyses ultra-rapides (< 1min). D'autre part, la phase mobile constituée de CO_2, mélangé à de faibles proportions de solvant organique (5-10% en général) en SFC est considérée comme " verte" et peu onéreuse. Afin d'assurer la compatibilité entre les phases mobiles, une étude concernant le choix de plusieurs paramètres critiques a été effectuée (nature de la phase stationnaire, volume injecté, volumes des boucles, composition du solvant d'injection). À partir de ces résultats, l'optimisation d'une méthode RPLCxSFC en ligne a été menée sur un échantillon de standards puis étendue à l'analyse d'un mélange complexe de composé neutres issus d'un extrait aqueux d'une bio-huile. Les résultats ont ensuite été comparés à ceux obtenus à l'aide d'une méthode RPLCxRPLC optimisée.

Six études sont présentées sous forme d'articles :

Article 1 (chapitre 1)

"Theoretical and practical interest in UHPLC technology for 2D-LC ";

M. Sarrut, G. Crétier, S. Heinisch, TrAC Trends Anal. Chem. 63 (2014) 104–112. doi:10.1016/j.trac.2014.08.005.

Article 2 (chapitre 3)

"Optimization of conditions in on-line comprehensive two-dimensional reversed phase liquid chromatography. Experimental comparison with one-dimensional reversed phase liquid chromatography for the separation of peptides";

M. Sarrut, A. D'Attoma, S. Heinisch, J. Chromatogr. A. 1421 (2015) 48–59. doi:10.1016/j.chroma.2015.08.052.

Article 3 (chapitre 3)

"Theoretical and experimental comparison of one dimensional versus on-line comprehensive two dimensional liquid chromatography for optimized sub-hour separations of complex peptide samples";

M. Sarrut, F. Rouvière, S. Heinisch, J. Chromatogr. A, (2017), In press

Article 4 (chapitre 4)

"Analysis of antibody-drug conjugates by comprehensive on-line two-dimensional hydrophobic interaction chromatography x reversed phase liquid chromatography hyphenated to high resolution mass spectrometry. I- Optimization of chromatographic conditions";

M. Sarrut, A. Corgier, S. Fekete, D. Guillarme, D. Lascoux, M-C. Janin-Bussat, A. Beck, S. Heinisch, J. Chromatogr. B, 1032 (2016), 103-111

Article 5 (chapitre 4)

“Analysis of antibody-drug conjugates by comprehensive on-line twodimensional hydrophobic interaction chromatography x reversed phase liquid chromatography hyphenated to high resolution mass spectrometry. II- Identification of sub-units for the characterization of even and odd load drug species”;

M. Sarrut, S. Fekete, M-C. Janin-Bussat, D. Guillarme, O. Colas, D. Guillarme, A. Beck, S. Heinisch, J. Chromatogr. B, 1032 (2016), 91-102

Article 6 (chapitre 5)

“Potential and limitations of on-line comprehensive reversed phase liquid chromatography × supercritical fluid chromatography for the separation of neutral compounds: An approach to separate an aqueous extract of bio-oil“;

M. Sarrut, A. Corgier, G. Crétier, A. Le Masle, S. Dubant, S. Heinisch J. Chromatogr. A. 1402 (2015) 124–133. doi:10.1016/j.chroma.2015.05.005.

CHAPITRE 1 – CONTEXTE

Ce chapitre a fait l'objet d'une publication :

Article 1

"Theoretical and practical interest in UHPLC technology for 2D-LC ";

M. Sarrut, G. Crétier, S. Heinisch, TrAC Trends Anal. Chem. 63 (2014) 104–112. doi:10.1016/j.trac.2014.08.005.

INTRODUCTION

La chromatographie liquide bidimensionnelle « comprehensive » en ligne est une technique séparative à très fort potentiel qui permet théoriquement d'obtenir une capacité de pics très élevée. En effet, la capacité de pics théorique est égale au produit des capacités de pics dans chaque dimension. Le couplage d'un tel pouvoir de séparation associé à la dimension supplémentaire fournie par la spectrométrie de masse conduit à un pouvoir de résolution très important donnant ainsi la possibilité de caractériser des échantillons complexes.

Néanmoins, atteindre le plein potentiel d'une analyse bidimensionnelle « comprehensive » en ligne est un challenge analytique. Cela requiert l'utilisation des grandeurs théoriques impliquées dans les processus chromatographiques et des équations qui les relient mais aussi la prise en compte des contraintes instrumentales afin de trouver le meilleur compromis entre des objectifs contradictoires, les objectifs prioritaires étant de maximiser la capacité de pics tout en minimisant à la fois le facteur de dilution et le temps d'analyse.

Ce chapitre 1 aborde dans une première partie les notions théoriques indispensables à la mise en place d'une démarche d'optimisation des conditions bidimensionnelles. Un regard particulier est mis sur l'avantage d'utiliser la chromatographie liquide à très haute performance (jusqu'à 1200 bar) associée à des températures élevées (HT-UHPLC) en ^{2}D. Une revue des applications employant des conditions UHPLC en ^{2}D est présentée.

Une deuxième partie récapitule les stratégies d'optimisation multi-critères employées pour l'optimisation de méthodes LCxLC.

Finalement, une troisième partie s'intéresse aux différents moyens employés pour limiter la variance à l'injection lors du transfert de l'échantillon de la ^{1}D à la ^{2}D.

A. INTÉRÊTS ET CHALLENGES EN CHROMATOGRAPHIE EN PHASE LIQUIDE « COMPREHENSIVE » BIDIMENSIONNELLE EN LIGNE

1. Apport de l'HT-UHPLC en LCxLC en ligne

Article 1

"Theoretical and practical interest in UHPLC technology for 2D-LC ";

M. Sarrut, G. Crétier, S. Heinisch, TrAC Trends Anal. Chem. 63 (2014) 104–112. doi:10.1016/j.trac.2014.08.005.

Trends in Analytical Chemistry 63 (2014) 104–112

Contents lists available at ScienceDirect

Trends in Analytical Chemistry

journal homepage: www.elsevier.com/locate/trac

Theoretical and practical interest in UHPLC technology for 2D-LC

Morgan Sarrut, Gérard Crétier, Sabine Heinisch *

Institut des Sciences Analytiques, UMR CNRS 5280, Université de Lyon, 5 rue de la Doua, Villeurbanne 69100, France

ARTICLE INFO

Keywords:
2D-LC
LC x LC
Comprehensive two-dimensional liquid chromatography (LC x LC)
Food analysis
High-temperature-UHPLC (HT-UHPLC)
HT-UHPLC
Polymer analysis
Two-dimensional liquid chromatography (2D-LC)
UHPLC
Ultra-high-pressure liquid chromatography (UHPLC)

ABSTRACT

Comprehensive two-dimensional liquid chromatography (LC x LC) has significantly improved the separation power of LC for complex samples. Our review opens with theoretical considerations about on-line LC x LC in order to explain why ultra-high-pressure LC (UHPLC) and more specifically, high-temperature (HT)-UHPLC are very convenient in the second dimension. We present some recent applications involving UHPLC in LC x LC. They cover a wide range of analytical fields, such as food analysis, life sciences, bioenergy and polymers.

Contents

1. Introduction

Two-dimensional chromatographic separations can be heart-cutting or comprehensive in approach, as stated by Giddings [1]. Definitions, nomenclature and symbols were further standardized by Marriott et al. [2].

Unlike heart-cutting, wherein only a fraction of the chromatogram is sent to a second dimension, "comprehensive" means that the whole sample is subjected to two different separations. The interest in two-dimensional separation techniques has grown considerably in the past decade. Comprehensive two-dimensional gas chromatography (GC x GC) is now accepted as a powerful technique for the separation of complex samples (e.g., those encountered in the fields of oil products or perfumes). By contrast, comprehensive two-dimensional liquid chromatography (LC x LC), although very promising, is still emerging and is not yet used as a routine technique in industry.

In LC x LC, the total peak capacity is theoretically the product of peak capacities in each dimension. As a result, whereas hours or even days are necessary in one-dimensional LC to reach peak capacities exceeding 1000 [3], impressive theoretical peak capacities may be achieved rapidly in LC x LC (e.g., peak capacities as low as 50 in each dimension should provide 2500 as the theoretical peak capacity in LC x LC).

The advantage of UHPLC for heart-cutting methods (LC-LC) can be considered similar to those for conventional LC methods, so we

* Corresponding author. Tel.: +33 437 423 551.
E-mail address: sabine.heinisch@univ-lyon1.fr (S. Heinisch).

http://dx.doi.org/10.1016/j.trac.2014.08.005
0165-9936/

do not deal with this subject in this review, which focuses on the advantages of UHPLC for LC x LC techniques. The growing interest in LC x LC is driven by the following observations:

1 the sample complexity increases in many fields (-omics science, biofuels, pharmaceuticals, environmental research, food and natural products);
2 there is a trend towards the reduction of sample preparation, which is made easier using two chromatographic dimensions, as already shown by the success of heart-cutting methods;
3 two-dimensional techniques may quantify compounds at levels significantly lower than those possible by one-dimensional techniques, thanks to focusing methods; and,
4 coupling to mass spectrometry (MS) requires compatible mobile phases capable of providing suitable ionization.

With a two-dimensional separation system, while the second dimension mobile phase has to be MS compatible, the choice of the first dimension (^{1}D) mobile phase is driven by separation considerations only, making separation methods in 2D much more flexible than any 1D ones [4].

Whereas heart-cutting methods are extensively used in routine analysis, comprehensive methods are scarcely used and when they are, they are most often in off-line mode. Yet, on-line methods are very advantageous in many respects, as reported by recent very interesting reviews [5–10]. They avoid the risk of sample contamination, sample loss or sample degradation during sample handling and, solvent evaporation and furthermore, they are less time-consuming. In spite of their great potential, on-line LC X LC methods have essentially been evaluated by academic research and have very rarely been used in industrial projects. This can be due to both the complexity of current data analysis while suitable software is still missing and the difficulty in optimizing 2D conditions, considering the huge amount of parameters and the conflicting objectives (increasing peak capacity, decreasing analysis time and increasing sensitivity). The possibility of using very high pressure associated with short efficient columns in the second dimension is currently enhancing interest in on-line LC x LC. A theoretical section draws the fundamentals of LC x LC with a focus on the need for very fast separations in the second dimension. A second section deals with applications in on-line LC x LC that involve UHPLC.

2. Theoretical advantage of UHPLC in 2D-LC

2.1. Peak capacity in 1D-LC

The concept of peak capacity was first introduced by Giddings to provide a valuable tool capable of assessing the separation power. It was defined as the number of peaks that can be ideally placed between the first peak (often represented by the column dead time) and the last peak of interest with unity resolution between all peaks [11]. According to Neue [12], if the peak width is changing with retention time, the sample peak capacity, n, as defined by Dolan et al. [13], can be expressed as:

$$n = 1 + \int_{t1}^{tn} \frac{1}{4 \cdot \sigma_{t,total}} dt \quad (1)$$

where t_n and t_1 are the gradient retention times of the most and the least retained compounds, respectively, and $\sigma_{t,total}$ is the total peak standard deviation in time unit.

A solution to this general equation exists for linear solvent strength (LSS) gradients according to the LSS model developed by Snyder et al. [14]. LSS behavior is usually assumed for linear gradients in reversed-phase LC (RPLC) and, to a certain extent, hydrophilic interaction LC (HILIC) [15]. In this case, the practical peak capacity becomes [12]:

$$n = 1 + \frac{\sqrt{N}}{4} \cdot \frac{1}{2.3b+1} \cdot \ln\left(\frac{2.3b+1}{2.3b} \cdot e^{2.3S \cdot \Delta C} - \frac{1}{2.3b} \right) \quad (2)$$

where S is the average value of the slope of the relationship between the logarithm of the retention factor and the solvent composition, ΔC is the composition range, and b is the LSS gradient steepness:

$$b = \frac{S \cdot \Delta C \cdot t_0}{T_G} \quad (3)$$

with T_G, the gradient time and t_0, the column dead time.

It should be noted that, for rapid gradients (T_G is low) or for large molecules (S$\times\Delta$C is high), the peak width is nearly constant all over the gradient run and Equation (2) simplifies to:

$$n = 1 + \frac{t_n - t_1}{4\sigma_{t,total}} = 1 + 2.3 \cdot S \cdot \Delta C_e \times \frac{1}{1+2.3b} \times \frac{\sqrt{N}}{4} \quad (4)$$

ΔC_e, being the range of compositions at elution covered by the sample.

When considering Equation (4), it appears that the highest peak capacity is obtained for b close to 0. In this case, n depends on the product S$\times\Delta C_e$ (typically of the order 3–10, depending on the S value, which increases with molecule size) and on the column plate number. That leads to a maximum peak capacity equal to 2–5 times the square root of the plate number (n_{max} = 2–5$\sqrt{N}$). For example, 100,000 plates are potentially sufficient to reach 600–1500 as peak capacity.

2.2. Peak capacity in LC x LC

In off-line LC x LC, the two separations are decoupled so that peak capacities in both first dimension (^{1}D) and second dimension (^{2}D) might be as high as that in 1D-LC. The advantage of UHPLC in off-line LC x LC is similar to that of 1D-LC. If the two LC systems are fully orthogonal, the total peak capacity can theoretically attain the product of the maximum peak capacities obtained in one single dimension, (e.g., 600 × 600 = 360,000 for a small analyte). However, it is obviously unrealistic, considering the huge number of runs in ^{2}D (>1000) and, more importantly, the lengthy total analysis time (many days). As a result, the chromatographer has to choose the best trade-off between peak capacity and analysis time for his own requirements.

Conversely, in on-line LC x LC, the two separations are linked by the analysis time in ^{2}D being a fraction of the ^{1}D peak width. It is therefore impossible to deal with the peak capacity in ^{2}D separately from that in ^{1}D. In on-line LC x LC, the effective peak capacity must be calculated by taking into account three correction factors [16]:

- γ, to take into account the retention surface coverage, which depends on the degree of orthogonality between the two systems [15];
- α, to correct the peak capacity in ^{1}D due to under-sampling; and,
- β, to correct the peak capacity in ^{2}D due to non-ideal transfer of the sample fraction from ^{1}D to ^{2}D [17].

As a result, the effective peak capacity is given by:

$$n_{2D,effective} = \alpha \cdot (1-\gamma) \cdot {}^1n + \alpha \cdot \beta \cdot \gamma \cdot {}^1n \cdot {}^2n \quad (5)$$

where ^{1}n and ^{2}n are the peak capacities in the ^{1}D and ^{2}D, respectively, and can be predicted, in case of LSS gradients, according to Equation (2).

If γ is high enough (close to 1), Equation (5) simplifies to [17]:

$$n_{2D,effective} = \alpha \cdot \beta \cdot \gamma \cdot {}^1n \cdot {}^2n \quad (6)$$

As the three correction factors are less than 1, it is clear that the effective peak capacity in LC x LC can be significantly lower than that expected from the calculation of theoretical peak capacity (^1n x ^2n). Vivo-Truyols et al. [18] showed that, under certain circumstances, the loss in peak capacity may reach 75%. It is therefore of crucial importance to find a way to evaluate these correction factors correctly in calculating the effective peak capacity and optimizing LC x LC parameters.

The estimation of γ can be made graphically. It can also be predicted from data obtained with a representative sample in a given LC x LC configuration [15,19,20].

As regards the correction factor, α, Davis et al. [16] derived an empirical equation to estimate it. This equation is now widely used to evaluate the effective peak capacity:

$$\alpha = \frac{1}{\sqrt{1+0.21\cdot\lambda^2}} \quad (7)$$

with:

$$\lambda = t_s / {}^1\sigma_{t,total} \quad (8)$$

t_s is the sampling time and the total analysis time in ^{2}D. It corresponds to a multiple, λ, of the peak standard deviation in ^{1}D. λ cannot be too high because the analysis time in ^{2}D would be too short and cannot be too low because under-sampling would be too severe. This issue was first addressed by Murphy et al. [21], who showed that λ should be 2–2.7 roughly to maintain the resolution obtained in ^{1}D. However, it is difficult to find a balance between the decrease in ^{1}n due to large t_s, on the one hand, and the decrease in ^{2}n due to short t_s, on the other hand. To maximize $n_{2D,effective}$ for LC x LC with gradients in both dimensions, Horie et al. showed that λ should be 2–3.6 [22], which corresponds to 1.7–3 runs in ^{2}D per peak in ^{1}D. According to Equation (7), ^{1}n is decreased by 25% with λ = 2 and 50% with λ = 3.6.

The total analysis time in ^{2}D, t_s, is related to gradient time ^2T_G according to:

$$t_s = {}^2t_0 \cdot \left(\frac{{}^2T_G}{{}^2t_0} + \frac{{}^2V_D}{{}^2V_0} + (1+x) \right) \quad (9)$$

with ^2V_D, the gradient dwell volume in ^{2}D; $^2V_0$, the column dead volume; $^2t_0$, the column dead time; and, x, the number of column volumes used for column equilibration. As highlighted in Equations (2) and (3), the peak capacity in ^{2}D strongly depends on the ratio $^2T_G/^2t_0$. Equation (9) emphasizes the necessity to consider both equilibration time and dwell time when optimizing LC x LC conditions.

It is clear that $t_s/^2t_0$ should be as high as possible and at least higher than $\left(\frac{^2V_D}{^2V_0} + 1 + x \right)$.

It is usually recommended that the dwell volume is of the same order of magnitude as the column dead volume. However, it was shown that only two column volumes (x = 2) can provide good run-to-run repeatability in UHPLC conditions, even with charged compounds [23–25]. Starting from these values, the requirement in on-line LC x LC becomes:

$$\frac{t_s}{{}^2t_0} >> 4 \quad (10)$$

Two very important conclusions for the interest in UHPLC for LC x LC can then be drawn from Equation (10), as follows.

1 In ^{2}D, $^2t_0$ must be minimized while keeping good column efficiency. Small particle sizes working at maximum allowable pressure and/or maximum deliverable flow-rate are therefore strongly recommended in the ^{2}D, as illustrated in Fig. 1, showing calculated ^{2}n as a function of flow-rate for conventional HPLC, high-temperature LC (HTLC), UHPLC and high-temperature UHPLC (HT-UHPLC) [26]. The calculations were carried out with 60 s as sampling time and a 50 × 2.1 mm column in ^{2}D. As expected from Equation (9), $^2T_G/^2t_0$ and, hence, ^{2}n increase with the flow-rate, the minimum value of which (here 0.4 mL/min) is:

$${}^2F_{min} = \frac{{}^2V_0}{t_s} \cdot \left(\frac{{}^2V_D}{{}^2V_0} + 1 + x \right) \quad (11)$$

As shown in Fig. 1, the highest peak capacity is achieved in HT-UHPLC (170). In UHPLC, the maximum peak capacity is lower (100) because of lower attainable flow-rate. However both techniques are better than conventional techniques with maximum peak capacities of only 70 and 40 in HTLC and HPLC respectively. It should be noted that although high temperatures associated with UHPLC conditions are very attractive to enhance peak capacities for a given sampling time, there are some potential issues when operating at high column temperature [27]. They include: (1) possible sample degradation; (2) reduction of column lifetime; and, (3) decrease in the eluent strength of the solvent entering the ^{2}D and hence reduction of the compression factor.

2 In ^{1}D, t_s and hence $\lambda {}^1\sigma_{t,total}$ should be high enough (at least higher than 4^2t_0). For small column length and/or low ^1T_G, it may be necessary to decrease significantly the linear velocity, ^{1}u, sometimes well below the optimum value, in order to fulfill the condition of Equation (10). Thus, resulting conditions in ^{1}D often have to be far from UHPLC conditions. However, as discussed elsewhere [28], the effective peak capacity in fast on-line LC x LC (<2 h) weakly depends on the ^{1}D peak capacity and, as a result, UHPLC conditions are unnecessary in this case

In preceding calculations of ^{2}n, peak-band broadening due to injection effects were not considered. However, there may be significant peak distortion if large fractions of ^{1}D are injected in ^{2}D. The effect of a large injection volume on peak variance has been studied [29]. The correction factor, β, for ^{2}n can be related to the injection volume in ^{2}D, ^2V_i, and derived as:

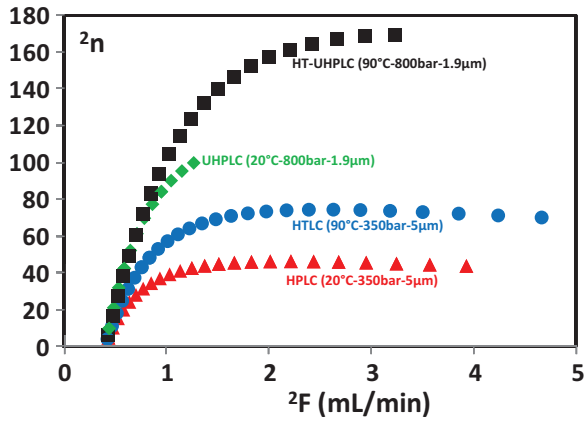

Fig. 1. Variation of peak capacity in the second dimension with flow-rate in different conditions. Data were calculated for a sampling time of 1 min with 50 × 2.1 mm column in ^{2}D, a dwell volume of 120 µL and two column volumes for equilibration (x = 2). {Adapted from [26]}.

$$\beta = \frac{{}^2\sigma_{v,col}}{{}^2\sigma_{v,total}} = \frac{1}{\sqrt{1 + \frac{1}{\delta_i^2} \times \frac{{}^2V_i^2}{{}^2\sigma_{v,col}^2} \times \frac{1}{C_F^2}}} \quad (12)$$

δ^2_i depends on the injection process (=12 for plug injection and close to 3–4 in practice). ${}^2\sigma_{v,\,col}$ is the peak standard deviation in volume units resulting from peak band broadening in the second column, ${}^2\sigma_{v,\,total}$ is the total peak standard deviation in ^{2}D and C_F is the compression factor [30]. C_F is related to the two solute retention factors in ^{2}D, the first one with the ^{1}D mobile phase and the second one at elution with the ^{2}D mobile phase [18,30,31]. The compression factor is high if the injection solvent in the transferred fraction is weak.

${}^2V_i$ is related to both the total peak standard deviation (in volume units) in ^{1}D and the split ratio potentially designed for reducing the flow-rate entering ^{2}D ($0 < z \leq 1$) [32]:

$${}^2V_i = \lambda \times {}^1\sigma_{v,total} \cdot z \quad (13)$$

The combination of Equations (12) and (13) yields:

$$\beta = \frac{1}{\sqrt{1 + \frac{\lambda^2 \cdot z^2}{\delta_i^2} \times \frac{{}^1\sigma_{v,total}^2}{{}^2\sigma_{v,col}^2} \times \frac{1}{C_F^2}}} \quad (14)$$

From Equation (14), it appears that β can be tuned or maintained at an acceptable value (for example, >0.9, which means that less than 10% of the peak capacity is lost in ^{2}D as a result of injection effect) by various means:

- increasing the compression factor; in RPLC x RPLC, this can be obtained with relative smooth gradient steepness in ^{1}D while steeper gradient in ^{2}D and/or with more retentive stationary phase in ^{2}D than that in ^{1}D;
- decreasing ${}^1\sigma_{v,total}/{}^2\sigma_{v,col}$ and hence the ratio of internal column diameters (${}^1d_i/{}^2d_i$), and/or, decreasing ${}^1\sigma_{v,total}$, which means, for a given t_s, decreasing ^{1}F and hence the column pressure; or,
- decreasing the split ratio ($z < 1$); however, one should be careful not to significantly increase extra-column band broadening with low split ratio ($z << 1$), thereby decreasing ^{1}n [33].

Depending on the column geometry in both dimensions, a suitable compromise has to be found between the decrease in z and the decrease in ^{1}F.

2.3. Optimization of on-line LC x LC parameters

Once the two chromatographic systems are chosen with respect to their degree of orthogonality, the operating conditions have to be carefully optimized. Those include gradient conditions, column dimensions and particle diameters in both dimensions, as well as the split ratio. The optimization procedure must deal with:

- on the one hand, conflicting objectives, including maximizing the effective peak capacity, minimizing the analysis time (represented by the gradient time in ^{1}D) and minimizing the dilution; and,
- on the other hand, instrumental limits in terms of pressure, flow-rate, column length, temperature and dwell time.

It is therefore of prime importance to find a way to make the situation less complex.

The dilution factor, D_F, is often considered as the product of the dilution factors in each dimension ($D_F = {}^1D_F \times {}^2D_F$) [34]. That would be fully correct if the maximum injection concentration in ^{2}D was the concentration at the peak apex in ^{1}D (${}^1C_{max}$), namely if the fraction number was infinite. A more accurate approach involves the "ERF function", which allows calculation of the fraction of peak area corresponding to the sampling [35]. However, for sake of clarity, the product of dilution factors is usually maintained to evaluate D_F:

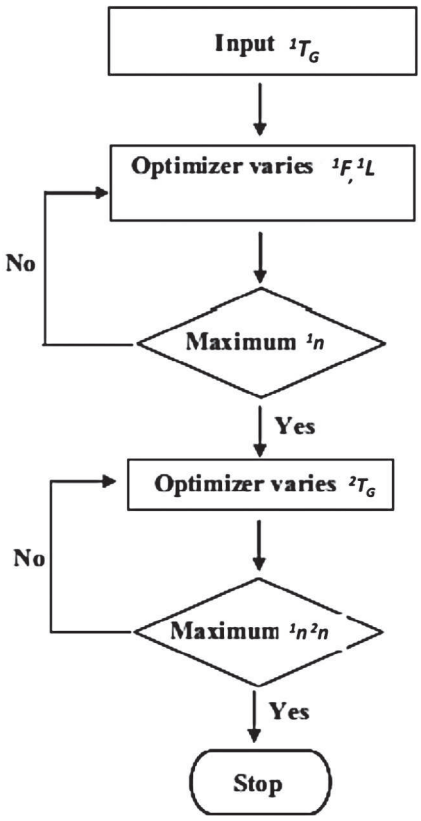

Fig. 2. Two-step optimization diagram in LC x LC. {Adapted from [36]}.

$$D_F = \frac{\sqrt{2\pi}}{\beta} \times \frac{{}^2\sigma_{v,col}}{{}^2V_i} \times {}^1D_F \quad (15)$$

which yields, by combining Equations (12) and (15):

$$D_F = \frac{\sqrt{2\pi}}{\delta_i \cdot \sqrt{1-\beta^2}} \times \frac{1}{C_F} \times {}^1D_F \quad (16)$$

Two different optimization protocols were recently proposed [36] for maximizing peak capacity with gradient conditions in both dimensions. The more robust method involved a two-step optimization, first maximizing ^{1}n and then maximizing $n_1 \times n_2$. The flow diagram is shown in Fig. 2.

Other attempts were made to optimize the peak capacity while keeping an acceptable analysis time [30,37,38]. The compromise between peak capacity and analysis time was established by means of an attractive pareto-optimality approach [18]. In this study, the calculations were made easier by:

1 setting, in both dimensions, a value of 10 for the ratio of the gradient time to the column dead time ($T_G/t_0 = 10$);
2 working, in both dimensions, at the maximum pressure allowed by the instrument; and,
3 neglecting dwell times and equilibration times.

In addition, the sampling rate was not kept constant but was allowed to vary. Consequently, the authors used Equation (7) to

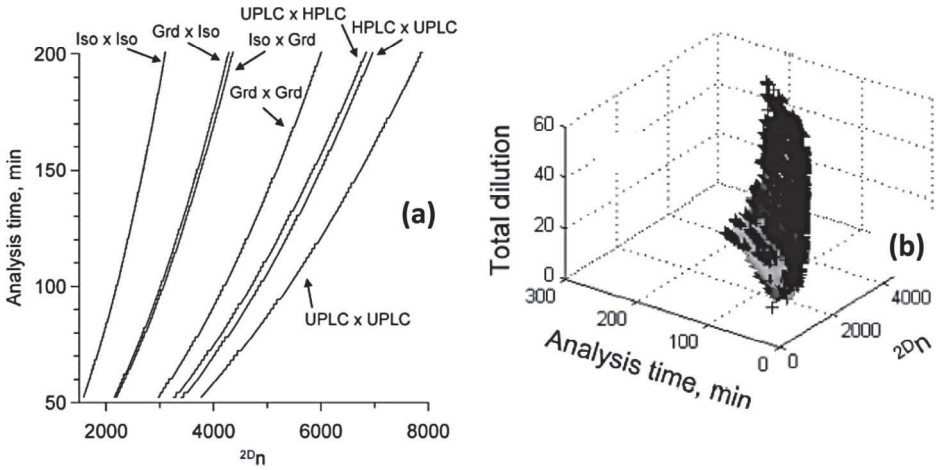

Fig. 3. (a)Pareto curves and (b) Pareto surfaces for optimizing conditions in LC x LC. {Adapted from [18]}.

correct the effective peak capacity. The results are shown in Fig. 3a. As expected, the gain in peak capacity is achieved at the expense of longer analysis time. It seems from these curves that the use of UHPLC in both dimensions represents the best configuration with peak-capacity improvement by 30% compared to HPLC x HPLC systems. The dilution factors were not taken into account in the different situations presented in Fig. 3a. Yet, as underlined by the authors, the best conditions in Fig. 3a lead to very high dilution. The authors therefore also considered low dilution as a separate objective in the optimization procedure. The results are shown in Fig. 3b, which displays the Pareto surfaces for the simultaneous optimization of peak capacity, analysis time and dilution factor.

From Equation (16), it is clear that maximizing the effective peak capacity (i.e., β close to 1) is a conflicting objective with decreasing the dilution factor ((i.e., β close to 0). However, for given β and ^1D_F, D_F becomes dependent on only the compression factor, and it is very interesting to note that increasing C_F is beneficial for both peak capacity (β increases) and sensitivity (D_F decreases), as illustrated in Fig. 4.

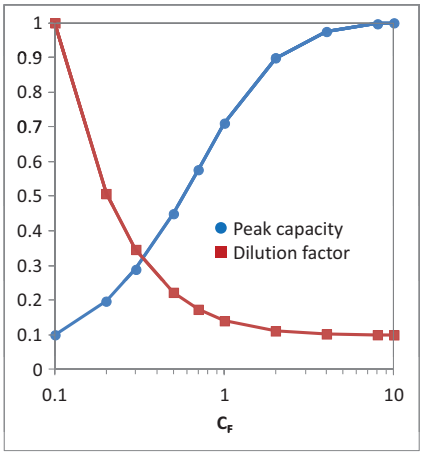

Fig. 4. Variation of dilution factor and peak capacity (normalized scale) with the compression factor. Data calculated from Equations (12) and (15), with $\delta_i^2 = 4$ and $^2V_i = {}^2\sigma_{v,col}$.

3. The quest for large separation power in on-line LC x LC applications

In the past few years, researchers performed comprehensive on-line two-dimensional separations by adapting the chromatographic conditions in order to find a good trade-off between speed and peak capacity in the ^{2}D. As discussed in Section 2, the peak capacity in the ^{2}D is increased with $^2T_G/{}^2t_0$. Although the stop-flow mode seems to be convenient to increase ^2T_G [39–41], it is time consuming [40] even with UHPLC conditions in the ^{2}D [41,42], and, in addition, it requires additional hardware. Moreover, axial dispersion may be a critical issue, particularly for the most retained compounds, thereby leading to significant peak band broadening [8]. Yet, large molecules with low diffusion coefficients are relatively little subjected to axial dispersion [43].

An alternative approach to increase peak capacity in the ^{2}D involves using two columns in parallel [30,44–47]. François et al. designed an interface [48] consisting of two identical two-position 10-port switching valves, each equipped with two identical loops. The second switching valve offered the possibility to double the analysis time in the ^{2}D, thereby increasing the gradient time and hence the peak capacity. However, the use of two columns in parallel requires complex interfaces and introduces additional difficulties for data processing, particularly because consecutive separations are performed on two different columns that can be slightly different [49].

The use of HT-HPLC was also investigated to reduce the mobile-phase viscosity and hence to increase the flow rate while keeping an acceptable pressure [50–52]. According to Equation (9), dead time, delay time and equilibration time are also decreased resulting in higher peak capacity. However, as discussed in Section 2, UHPLC and especially HT-UHPLC are the techniques of choice in the ^{2}D. Some LC x LC applications involving UHPLC in the ^{2}D were recently reported. They covered a wide range of analytical fields, such as food analysis, life sciences, bioenergy and polymers. These applications are summarized in Table 1 and discussed below.

3.1. LC x UHPLC in food analysis

The complexity of food matrices makes LC x LC coupled to MS a powerful technique for solute identification. The first application involving UHPLC in the ^{2}D dealt with the separation of phenolic

Table 1
On-line comprehensive two-dimensional liquid chromatography (LC x LC) separations using ultra-high-pressure liquid chromatography (UHPLC)

Ref.	Configuration	Column dimensions; Flow-rate; Temperature		Sampling time	Application
		First dimension, ^{1}D	Second dimension, ^{2}D		
[53]	RPLC x RPLC	150 × 2.1 mm, 3 μm; 100 μL/min; ND[a]	50 × 2.1 mm, 1.7 μm; 0.8 mL/min; ND	120 s	Food analysis
[42]	HILIC x RPLC	250 × 1.0 mm, 5 μm; 25 μL/min; Ambient	50 × 4.6 mm, 1.8 μm; 1.5 mL/min, 50°C	120 and 180 s	Food analysis
[54]	HILIC x RPLC	250 × 1.0 mm, 5 μm; 20 μL/min; Ambient	30 × 2.1 mm, 1.8 μm; 3.4 mL/min, 70°C	20 s	Food analysis
[55]	HILIC x RPLC	250 × 1.0 mm, 5 μm; 50 μL/min; Ambient	50 × 4.6 mm, 1.8 μm; 1.2 mL/min, 48°C	120 s	Food analysis
[56]	NPLC x RPLC	250 × 1.0 mm, 5 μm; 10 μL/min; 30°C	60 × 4.6 mm, 2.7 μm; 4 mL/min; 65°C	90 s and 60 s	Food analysis
[57]	RPLC x RPLC	50 × 1.0 mm, 3 μm; 10 μL/min; 30°C	50 × 2.1 mm, 2.6 μm; 1.8 mL/min; 60°C	55.5 s	Life sciences
[57]	RPLC x HILIC	50 × 1 mm, 3 μm; 10 μL/min; 30°C	50 × 2.1 mm, 1.7 μm; 1.8 mL/min; 60°C	46.2 s	Life sciences
[58]	RPLC x RPLC	100 × 1.0 mm, 5 μm; 10 μL/min; 60°C	50 × 2.1 mm, 1.7 μm; 1.4 mL/min; 80°C	69 s	Bioenergy
[59]	RPLC x SEC	250 × 2.1 mm, 1.7 μm; 200 μL/min; 25°C	150 × 4.6 mm, 1.7 μm; 2 mL/min; 30°C	54 s	Polymer
[59]	RPLC x SEC	250 × 2.1 mm, 1.7 μm; 100 μL/min; 55°C	150 × 4.6 mm, 1.7 μm; 2 mL/min; 50°C	30 s	Polymer

[a] ND: No Data.

compounds in wines [53]. In this work, the authors compared several combinations:

- HPLC x HPLC (packed);
- HPLC x HPLC (monolith);
- HPLC x UHPLC with the ^{2}Ds performed in isocratic mode; and,
- HPLC x UHPLC with gradient conditions in the ^{2}D.

^{1}D conditions were the same for all experiments. Surprisingly, the best performance in terms of peak capacity was obtained with the two HPLC x HPLC configurations. However, the lower peak capacity in HPLC x UHPLC compared to HPLC x HPLC (monolith) was explained by significant additional peak band broadening resulting from injection on the UHPLC column (200 μL injected on a 50 × 2.1 mm column *versus* 150 μL on the 50 × 4.6 mm monolithic column). Moreover, the potential of UHPLC was not fully exploited (only 520 bar as column pressure).

The separation of matrices of phenolic compounds in HILIC x RP-UHPLC has been studied at different temperatures for the ^{2}D {i.e., 70°C [54]; 48°C [55]; and, 50°C [42]}. In these different studies, a 250 × 1 mm column with 5-μm particle size was used in ^{1}D. Kalili et al. [42] compared off-line, stop-flow and on-line comprehensive analysis of procyanidins in cocoa extracts, while Beelders et al. [55] compared off-line and on-line comprehensive analysis of phenolics (flavonoids, phenolic acids, coumarins amongst others) contained in rooibos. They both used the same C18 50 × 4.6 mm column with 1.8-μm particle size in the ^{2}D. The second separation was performed at the maximum pressure withstood by the column (600 bar). Both studies showed that, although stop-flow and off-line modes provide much higher peak capacity than the on-line mode, the peak-production rate (peaks/min) was 2–4 times greater in the on-line mode. In both cases, the flow was split to avoid extra-column peak band broadening due to large injection volumes. However, that increased dilution, which, in turn, decreased peak sensitivity. Conversely, the repeatability of ^{2}D retention times was found to be very good (<2%).

Similarly, the separation of 10 stevia glycoside and polyphenol compounds contained in *Stevia rebaudiana* extract was achieved in 100 min in HILIC x RPLC [54]. A very short narrow-bore, sub-2-μm column (30 × 2.1 mm, 1.8 μm) was used at 70°C in order to obtain very fast analysis in the ^{2}D (20 s as cycle time with a flow rate of 3.4 mL/min). In these conditions, the system pressure attained 922 bar and the ^2T_G value was only 15.6 s. The effective peak capacity was calculated according to the geometric approach developed by Liu et al. [19] and estimated at 1850. Despite the very short analysis time, the retention-time repeatability obtained was acceptable (<5%).

Finally, in a recent study [56], two different NPLC x RPLC configurations (HPLC x HPLC and HPLC x UHPLC) were compared for the separation of 33 compounds belonging to 10 different classes of carotenoids contained in red chili-pepper extracts. IT-TOF-MS detection was used in both configurations for compound identification. A microbore cyano column (250 × 1 mm; 5 μm) was used in ^{1}D while macrobore superficially porous C18 columns (30 × 4.6 mm, 2.7 μm in HPLC and 2 × 30 × 4.6 mm, 2.7 μm in UHPLC) were used in ^{2}D at 65°C. Such a large difference in column diameters between ^{1}D and ^{2}D was designed to circumvent the incompatibility of the solvents used in the two dimensions. In the LC x UHPLC system, two columns were serially coupled with a view to increasing peak capacity. ^{2}D separations were carried out at a flow rate of 4 mL/min, allowing very fast analyses and generating a backpressure of 450 bar (HPLC) and 900 bar (UHPLC). As expected from Equations (2) and (4), the peak capacity in ^{2}D was multiplied by a factor $\sqrt{2}$ from RP-HPLC with a sampling time of 0.75 min to RP-UHPLC with a sampling time of 1.5 min (22 *versus* 31). The theoretical peak capacity was therefore significantly increased (from 990 to 1375). However, the effective peak capacity, corrected for under-sampling [Equation (7)] and for orthogonality, became higher with HPLC compared to UHPLC (526 *versus* 373). As the sampling time was larger in the second case, the under-sampling was more severe and that, in turn, could explain this result. After decreasing the sampling time from 1.5 min to 1 min, an effective peak capacity of 639 was obtained in UHPLC conditions, thereby highlighting the interest in increasing pressure.

3.2. LC x UHPLC in life sciences

Biological samples require techniques with very high resolving power and high sensitivity in order to identify the maximum number of sample components. On-line HPLC x HT-UHPLC separations of tryptic digest of three proteins were recently achieved in both RPLC x RPLC and RPLC x HILIC with UHPLC as ^{2}D [57]. The peak capacities obtained, corrected for surface coverage, were 3300 ($\gamma = 0.39$) and 2600 ($\gamma = 1$), respectively, both in 200 min. The two ^{2}Ds were performed at the maximum flow rate authorized by the instrument (i.e., 2 mL/min). The aim of this work was to evaluate the benefit of 2D-LC separations of peptides compared to 1D-LC separations using a Pareto optimal approach. The ^{1}D column was a microbore C18 column (50 × 1 mm, 3 μm). Short narrow-bore columns (50 × 2.1 mm) were used in the ^{2}D in order to have a short cycle time and to limit the dilution factor. The rapid calculation of the ultimate peak capacity in 1D-LC, as presented in Section 2, does not give any information on the time it would take, or on the real possibilities of achieving such high peak capacities taking instrument limitations into account. This information is given in Fig. 5, which shows analysis time as a function of peak capacity for 1D data that were found in the literature (represented by squares). Most data were obtained in UHPLC or HT-UHPLC; the data corresponding to the upper square were obtained with a long silica monolith column [60]. The dotted curve represents the Pareto front for two objectives, namely minimizing the analysis time and maximizing the peak

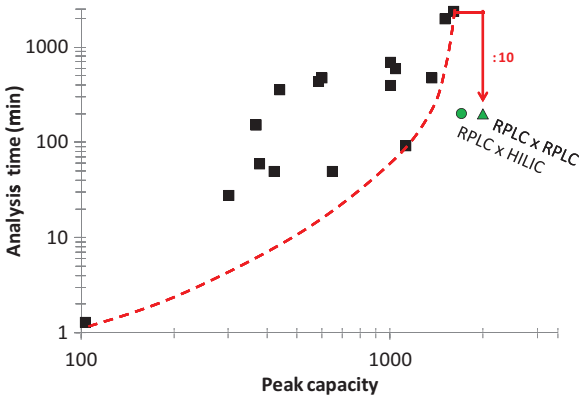

Fig. 5. Plots of analysis time *versus* peak capacity for the separation of peptides. Black squares correspond to data recently published in the literature (see [57] for more information). The dotted line represents the Pareto curve for analysis time and peak capacity. The data obtained in RPLC x HILIC and RPLC x RPLC are indicated by a circle and a triangle, respectively. {Adapted from [57]}.

capacity. It can illustrate the current limit attained in 1D-LC according to published results. After correction for under-sampling, the effective peak capacities obtained in RPLC x HILIC (1700) and RPLC x RPLC (2000) were placed in Fig. 5. As can be seen, they are located outside the Pareto curve. The gain in speed and the gain in peak capacity was 10 and 1.3, respectively, compared to the best result obtained in 1D-LC. A similar effective peak capacity (1800) was also obtained in RPLC x RPLC in 200 min [61]. However, this separation performed under conventional HPLC conditions made use of a very long column ($4 \times 150 \times 2.1$ mm serially coupled columns) in the ^{1}D.

3.3. LC x UHPLC in bioenergy

Le Masle et al. [58] used on-line RPLC x RPLC for the characterization of bio-oils obtained by fast pyrolysis of lignocellulosic biomass (mainly neutral and acidic compounds). Accurate knowledge of bio-oil composition is essential for optimizing the process of upgrading bio-oil to biofuel.

Based on preliminary data obtained with a sample of 38 representative compounds, an LC x LC configuration was selected. It comprised a stationary phase based on porous graphitic carbon (Hypercarb column 100×1 mm, 5 µm) in ^{1}D and a Phenyl Hexyl column in ^{2}D (50×2.1 mm, 1.7 µm). The authors relied on the difference in selectivity between these two different columns to generate high peak capacity, and on HT-UHPLC conditions to get fast analyses in ^{2}D. Accordingly, the temperature of the ^{2}D was set at 80°C with 1.15 min as sampling time, ensuring 3.6 cuts by peak of ^{1}D. The gradient time was 0.73 min at 1.4 mL/min. The LC x LC analysis of a partly dehydroxygenated bio-oil provided an effective peak capacity of 1940, corresponding to the separation of more than 120 compounds with an average peak width of 0.85 s ($4x^2\sigma_{t,total}$) and a total analysis time of 285 min. This 2D separation is shown in Fig. 6.

3.4. UHPLC x UHPSEC in polymer analysis

For polymer samples, RPLC x SEC is a powerful technique that can provide simultaneous information on both chemical composition and molecular-weight distribution. According to Uliyanchenko et al. [62], the commonly used LC x SEC configuration provides satisfactory information, but its implementation in industry is very time consuming (several hours). To overcome this constraint, the authors developed an on-line UHPLC x UHPSEC for the separation of samples of polyurethane (PU) and polymethacrylate (PMMA). In ^{1}D, three

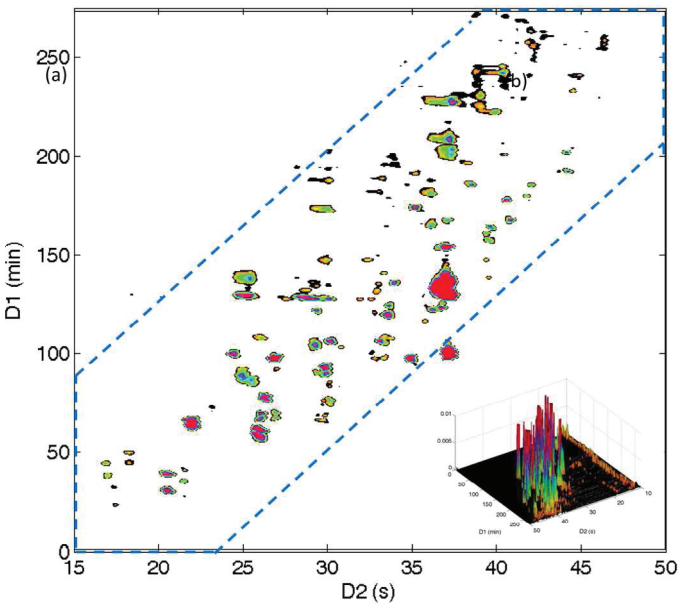

Fig. 6. RPLC × RPLC separation of a partially dehydroxygenated bio-oil using the coupling of Hypercarb (100×1 mm, 5 µm) in ^{1}D and Acquity CSH phenyl-Hexyl (50×2.1 mm, 1.7 µm) in ^{2}D. {Adapted from [58]}.

Acquity BEH C18 columns (2.1 mm i.d.) with a total length of 250 mm were serially coupled and used at a flow-rate of 0.2 mL/min and 0.1 mL/min for PMMA and PU, respectively. In ^{2}D, an Acquity BEH C18 column (150×4.6 mm, 1.7 µm) with a sampling time of 0.9 min and an Acquity BEH HILIC column with a sampling time of 0.5 min (150×4.6 mm, 1.7 µm) were used at 2 mL/min for PMMA samples and PU samples, respectively. With these two LC x LC systems, the analyses were performed in only 22 min for PMMA and 60 min for PU. Both analysis times were much shorter than those obtained in conventional LC x SEC, which can reach 4 h for PMMA analyses [59]. According to the authors, in addition to the shorter analysis time due to using UHPLC conditions, the resulting information was relevant to assess the composition of the polymer samples.

4. Conclusion

It was shown that, whereas UHPLC conditions (very small particles with very high pressure) are highly recommended in the ^{2}D of on-line LC x LC separations in order to reduce the gradient time, they may be quite counterproductive in the ^{1}D.

In the ^{2}D, UHPLC conditions with short columns are very attractive because they can generate enough separation power to increase significantly the total effective peak capacity compared to unidimensional techniques, as was recently proved for the separation of peptides. Elevated temperatures associated with UHPLC conditions can further improve the separation power in the ^{2}D but they may be detrimental to samples and instrumentation.

Numerous parameters are available to optimize the quality of analysis, which can be well described by three conflicting criteria: effective peak capacity; analysis time in ^{1}D; and, method sensitivity. Although efficient strategies have already been developed, much work is still required to have convenient, reliable tools able to predict and to optimize LC x LC separations.

References

[1] J.C. Giddings, Concepts and comparisons in multidimensional separation, J. High Resolut. Chromatogr. 10 (1987) 319–323, doi:10.1002/jhrc.1240100517.

[2] P.J. Marriott, P. Schoenmakers, Z.-Y. Wu, Nomenclature and conventions in comprehensive multidimensional chromatography – an update, LC GC Eur. 25 (2012).
[3] G. Guiochon, The limits of the separation power of unidimensional column liquid chromatography, J. Chromatogr. A 1126 (2006) 6–49, doi:10.1016/j.chroma.2006.07.032.
[4] X. Zhang, A. Fang, C.P. Riley, M. Wang, F.E. Regnier, C. Buck, Multi-dimensional liquid chromatography in proteomics – a review, Anal. Chim. Acta 664 (2010) 101–113, doi:10.1016/j.aca.2010.02.001.
[5] P. Donato, F. Cacciola, L. Mondello, P. Dugo, Comprehensive chromatographic separations in proteomics, J. Chromatogr. A 1218 (2011) 8777–8790, doi:10.1016/j.chroma.2011.05.070.
[6] I. François, K. Sandra, P. Sandra, Comprehensive liquid chromatography: fundamental aspects and practical considerations – a review, Anal. Chim. Acta 641 (2009) 14–31, doi:10.1016/j.aca.2009.03.041.
[7] P. Dugo, F. Cacciola, T. Kumm, G. Dugo, L. Mondello, Comprehensive multidimensional liquid chromatography: theory and applications, J. Chromatogr. A 1184 (2008) 353–368, doi:10.1016/j.chroma.2007.06.074.
[8] G. Guiochon, N. Marchetti, K. Mriziq, R.A. Shalliker, Implementations of two-dimensional liquid chromatography, J. Chromatogr. A 1189 (2008) 109–168, doi:10.1016/j.chroma.2008.01.086.
[9] D.R. Stoll, X. Li, X. Wang, P.W. Carr, S.E.G. Porter, S.C. Rutan, Fast, comprehensive two-dimensional liquid chromatography, J. Chromatogr. A 1168 (2007) 3–43, doi:10.1016/j.chroma.2007.08.054.
[10] P. Jandera, Programmed elution in comprehensive two-dimensional liquid chromatography, J. Chromatogr. A 1255 (2012) 112–129, doi:10.1016/j.chroma.2012.02.071.
[11] J.C. Giddings, Maximum number of components resolvable by gel filtration and other elution chromatographic methods, Anal. Chem. 39 (1967) 1027–1028, doi:10.1021/ac60252a025.
[12] U.D. Neue, Theory of peak capacity in gradient elution, J. Chromatogr. A 1079 (2005) 153–161, doi:10.1016/j.chroma.2005.03.008.
[13] J.W. Dolan, L.R. Snyder, N.M. Djordjevic, D.W. Hill, T.J. Waeghe, Reversed-phase liquid chromatographic separation of complex samples by optimizing temperature and gradient time: I. Peak capacity limitations, J. Chromatogr. A 857 (1999) 1–20, doi:10.1016/S0021-9673(99)00765-7.
[14] L.R. Snyder, J.W. Dolan, J.R. Gant, Gradient elution in high-performance liquid chromatography: I. Theoretical basis for reversed-phase systems, J. Chromatogr. A 165 (1979) 3–30, doi:10.1016/S0021-9673(00)85726-X.
[15] A.D. Attoma, C. Grivel, S. Heinisch, On-line comprehensive two-dimensional separations of charged compounds using reversed-phase high performance liquid chromatography and hydrophilic interaction chromatography. Part I: orthogonality and practical peak capacity considerations, J. Chromatogr. A 1262 (2012) 148–159, doi:10.1016/j.chroma.2012.09.028.
[16] J.M. Davis, D.R. Stoll, P.W. Carr, Effect of first-dimension undersampling on effective peak capacity in comprehensive two-dimensional separations, Anal. Chem. 80 (2008) 461–473, doi:10.1021/ac071504j.
[17] F. Bedani, P.J. Schoenmakers, H.-G. Janssen, Theories to support method development in comprehensive two-dimensional liquid chromatography – a review, J. Sep. Sci. 35 (2012) 1697–1711, doi:10.1002/jssc.201200070.
[18] G. Vivó-Truyols, S. van der Wal, P.J. Schoenmakers, Comprehensive study on the optimization of online two-dimensional liquid chromatographic systems considering losses in theoretical peak capacity in first- and second-dimensions: a Pareto-optimality approach, Anal. Chem. 82 (2010) 8525–8536, doi:10.1021/ac101420f.
[19] Z. Liu, D.G. Patterson, M.L. Lee, Geometric approach to factor analysis for the estimation of orthogonality and practical peak capacity in comprehensive two-dimensional separations, Anal. Chem. 67 (1995) 3840–3845, doi:10.1021/ac00117a004.
[20] M. Gilar, P. Olivova, A.E. Daly, J.C. Gebler, Orthogonality of separation in two-dimensional liquid chromatography, Anal. Chem. 77 (2005) 6426–6434, doi:10.1021/ac050923i.
[21] R.E. Murphy, M.R. Schure, J.P. Foley, Effect of sampling rate on resolution in comprehensive two-dimensional liquid chromatography, Anal. Chem. 70 (1998) 1585–1594, doi:10.1021/ac971184b.
[22] K. Horie, H. Kimura, T. Ikegami, A. Iwatsuka, N. Saad, O. Fiehn, et al., Calculating optimal modulation periods to maximize the peak capacity in two-dimensional HPLC, Anal. Chem. 79 (2007) 3764–3770, doi:10.1021/ac062002t.
[23] C. Grivel, J.-L. Rocca, D. Guillarme, J.-L. Veuthey, S. Heinisch, Selection of suitable operating conditions to minimize the gradient equilibration time in the separation of drugs by Ultra-High-Pressure Liquid Chromatography with volatile (mass spectrometry-compatible) buffers, J. Chromatogr. A 1217 (2010) 459–472, doi:10.1016/j.chroma.2009.11.059.
[24] A.P. Schellinger, D.R. Stoll, P.W. Carr, High-speed gradient elution reversed-phase liquid chromatography of bases in buffered eluents: part I. Retention repeatability and column re-equilibration, J. Chromatogr. A 1192 (2008) 41–53, doi:10.1016/j.chroma.2008.01.062.
[25] A.P. Schellinger, D.R. Stoll, P.W. Carr, High speed gradient elution reversed phase liquid chromatography of bases in buffered eluents: part II. Full equilibrium, J. Chromatogr. A 1192 (2008) 54–61, doi:10.1016/j.chroma.2008.02.049.
[26] S. Heinisch, Using elevated temperature in UHPLC: interest and limitations, in: D. Guillarme, J.-L. Veuthey (Editors), UHPLC in Life Sciences, Royal Society of Chemistry, London, 2012, pp. 102–130.
[27] S. Heinisch, J.-L. Rocca, Sense and nonsense of high-temperature liquid chromatography, J. Chromatogr. A 1216 (2009) 642–658, doi:10.1016/j.chroma.2008.11.079.
[28] X. Li, D.R. Stoll, P.W. Carr, Equation for peak capacity estimation in two-dimensional liquid chromatography, Anal. Chem. 81 (2009) 845–850, doi:10.1021/ac801772u.
[29] J.C. Sternberg, Extracolumn contributions to chromatography band broadening, in: J.C. Giddings, R.A. Keller (Editors), Advances in Chromatography, vol. 2, M. Dekker Inc., New York, 1966, p. 205.
[30] P. Jandera, P. Česla, T. Hájek, G. Vohralík, K. Vyňuchalová, J. Fischer, Optimization of separation in two-dimensional high-performance liquid chromatography by adjusting phase system selectivity and using programmed elution techniques, J. Chromatogr. A 1189 (2008) 207–220, doi:10.1016/j.chroma.2007.11.053.
[31] J. Lankelma, H. Poppe, Determination of methotrexate in plasma by on-column concentration and ion-exchange chromatography, J. Chromatogr. A 149 (1978) 587–598, doi:10.1016/S0021-9673(00)81013-4.
[32] M.R. Filgueira, Y. Huang, K. Witt, C. Castells, P.W. Carr, Improving peak capacity in fast online comprehensive two-dimensional liquid chromatography with post-first-dimension flow splitting, Anal. Chem. 83 (2011) 9531–9539, doi:10.1021/ac202317m.
[33] A. D'Attoma, Thesis, University of Lyon, 2013.
[34] M.R. Schure, Limit of detection, dilution factors, and technique compatibility in multidimensional separations utilizing chromatography, capillary electrophoresis, and field-flow fractionation, Anal. Chem. 71 (1999) 1645–1657, doi:10.1021/ac981128q.
[35] K. Horváth, J.N. Fairchild, G. Guiochon, Detection issues in two-dimensional on-line chromatography, J. Chromatogr. A 1216 (2009) 7785–7792, doi:10.1016/j.chroma.2009.09.016.
[36] H. Gu, Y. Huang, P.W. Carr, Peak capacity optimization in comprehensive two dimensional liquid chromatography: a practical approach, J. Chromatogr. A 1218 (2011) 64–73, doi:10.1016/j.chroma.2010.10.096.
[37] P.J. Schoenmakers, G. Vivó-Truyols, W.M.C. Decrop, A protocol for designing comprehensive two-dimensional liquid chromatography separation systems, J. Chromatogr. A 1120 (2006) 282–290, doi:10.1016/j.chroma.2005.11.039.
[38] P. Jandera, T. Hájek, M. Staňková, K. Vyňuchalová, P. Česla, Optimization of comprehensive two-dimensional gradient chromatography coupling in-line hydrophilic interaction and reversed phase liquid chromatography, J. Chromatogr. A 1268 (2012) 91–101, doi:10.1016/j.chroma.2012.10.041.
[39] K.M. Kalili, A. de Villiers, Systematic optimisation and evaluation of on-line, off-line and stop-flow comprehensive hydrophilic interaction chromatography × reversed phase liquid chromatographic analysis of procyanidins, Part I: theoretical considerations, J. Chromatogr. A 1289 (2013) 58–68, doi:10.1016/j.chroma.2013.03.008.
[40] P. Dugo, N. Fawzy, F. Cichello, F. Cacciola, P. Donato, L. Mondello, Stop-flow comprehensive two-dimensional liquid chromatography combined with mass spectrometric detection for phospholipid analysis, J. Chromatogr. A 1278 (2013) 46–53, doi:10.1016/j.chroma.2012.12.042.
[41] S. Wang, J. Li, X. Shi, L. Qiao, X. Lu, G. Xu, A novel stop-flow two-dimensional liquid chromatography–mass spectrometry method for lipid analysis, J. Chromatogr. A 1321 (2013) 65–72, doi:10.1016/j.chroma.2013.10.069.
[42] K.M. Kalili, A. de Villiers, Systematic optimisation and evaluation of on-line, off-line and stop-flow comprehensive hydrophilic interaction chromatography × reversed phase liquid chromatographic analysis of procyanidins. Part II: application to cocoa procyanidins, J. Chromatogr. A 1289 (2013) 69–79, doi:10.1016/j.chroma.2013.03.009.
[43] F. Bedani, W.T. Kok, H.-G. Janssen, A theoretical basis for parameter selection and instrument design in comprehensive size-exclusion chromatography × liquid chromatography, J. Chromatogr. A 1133 (2006) 126–134, doi:10.1016/j.chroma.2006.08.048.
[44] N. Tanaka, H. Kimura, D. Tokuda, K. Hosoya, T. Ikegami, N. Ishizuka, et al., Simple and comprehensive two-dimensional reversed-phase HPLC using Monolithic Silica columns, Anal. Chem. 76 (2004) 1273–1281, doi:10.1021/ac034925j.
[45] E. Machtejevas, H. John, K. Wagner, L. Ständker, G. Marko-Varga, W.-G. Forssmann, et al., Automated multi-dimensional liquid chromatography: sample preparation and identification of peptides from human blood filtrate, J. Chromatogr. B 803 (2004) 121–130, doi:10.1016/j.jchromb.2003.07.015.
[46] I. François, D. Cabooter, K. Sandra, F. Lynen, G. Desmet, P. Sandra, Tryptic digest analysis by comprehensive reversed phase × two reversed phase liquid chromatography (RP-LC × 2RP-LC) at different pH's, J. Sep. Sci. 32 (2009) 1137–1144, doi:10.1002/jssc.200800578.
[47] C.J. Venkatramani, Y. Zelechonok, An automated orthogonal two-dimensional liquid chromatograph, Anal. Chem. 75 (2003) 3484–3494, doi:10.1021/ac030075w.
[48] I. François, A. de Villiers, B. Tienpont, F. David, P. Sandra, Comprehensive two-dimensional liquid chromatography applying two parallel columns in the second dimension, J. Chromatogr. A 1178 (2008) 33–42, doi:10.1016/j.chroma.2007.11.032.
[49] A. Felinger, M. Kele, G. Guiochon, Identification of the factors that influence the reproducibility of chromatographic retention data, J. Chromatogr. A 913 (2001) 23–48, doi:10.1016/S0021-9673(00)01044-X.
[50] D.R. Stoll, P.W. Carr, Fast, comprehensive two-dimensional HPLC separation of tryptic peptides based on high-temperature HPLC, J. Am. Chem. Soc. 127 (2005) 5034–5035, doi:10.1021/ja050145b.
[51] D.R. Stoll, J.D. Cohen, P.W. Carr, Fast, comprehensive online two-dimensional high performance liquid chromatography through the use of high temperature ultra-fast gradient elution reversed-phase liquid chromatography, J. Chromatogr. A 1122 (2006) 123–137, doi:10.1016/j.chroma.2006.04.058.
[52] A. Ginzburg, T. Macko, F. Malz, M. Schroers, I. Troetsch-Schaller, J. Strittmatter, et al., Characterization of functionalized polyolefins by high-temperature

two-dimensional liquid chromatography, J. Chromatogr. A 1285 (2013) 40–47, doi:10.1016/j.chroma.2013.01.067.
[53] M. Kivilompolo, T. Hyötyläinen, Comparison of separation power of ultra performance liquid chromatography and comprehensive two-dimensional liquid chromatography in the separation of phenolic compounds in beverages, J. Sep. Sci. 31 (2008) 3466–3472, doi:10.1002/jssc.200800287.
[54] F. Cacciola, P. Delmonte, K. Jaworska, P. Dugo, L. Mondello, J.I. Rader, Employing ultra high pressure liquid chromatography as the second dimension in a comprehensive two-dimensional system for analysis of Stevia rebaudiana extracts, J. Chromatogr. A 1218 (2011) 2012–2018, doi:10.1016/j.chroma .2010.08.081.
[55] T. Beelders, K.M. Kalili, E. Joubert, D. de Beer, A. de Villiers, Comprehensive two-dimensional liquid chromatographic analysis of rooibos (Aspalathus linearis) phenolics, J. Sep. Sci. 35 (2012) 1808–1820, doi:10.1002/jssc.201200060.
[56] F. Cacciola, P. Donato, D. Giuffrida, G. Torre, P. Dugo, L. Mondello, Ultra high pressure in the second dimension of a comprehensive two-dimensional liquid chromatographic system for carotenoid separation in red chili peppers, J. Chromatogr. A 1255 (2012) 244–251, doi:10.1016/j.chroma.2012.06.076.
[57] A.D. Attoma, S. Heinisch, On-line comprehensive two dimensional separations of charged compounds using reversed-phase high performance liquid chromatography and hydrophilic interaction chromatography. Part II: application to the separation of peptides, J. Chromatogr. A 1306 (2013) 27–36, doi:10.1016/j.chroma.2013.07.048.
[58] A. Le Masle, D. Angot, C. Gouin, A.D. Attoma, J. Ponthus, A. Quignard, et al., Development of on-line comprehensive two-dimensional liquid chromatography method for the separation of biomass compounds, J. Chromatogr. A (2014) doi:10.1016/j.chroma.2014.03.020.
[59] A. van der Horst, P.J. Schoenmakers, Comprehensive two-dimensional liquid chromatography of polymers, J. Chromatogr. A 1000 (2003) 693–709, doi:10.1016/S0021-9673(03)00495-3.
[60] K. Horie, Y. Sato, T. Kimura, T. Nakamura, Y. Ishihama, Y. Oda, et al., Estimation and optimization of the peak capacity of one-dimensional gradient high performance liquid chromatography using a long monolithic silica capillary column, J. Chromatogr. A 1228 (2012) 283–291, doi:10.1016/j.chroma .2011.12.088.
[61] P. Donato, F. Cacciola, E. Sommella, C. Fanali, L. Dugo, M. Dachà, et al., Online comprehensive RPLC × RPLC with mass spectrometry detection for the analysis of proteome samples, Anal. Chem. 83 (2011) 2485–2491, doi:10.1021/ac102656b.
[62] E. Uliyanchenko, P.J.C.H. Cools, S. van der Wal, P.J. Schoenmakers, Comprehensive two-dimensional ultrahigh-pressure liquid chromatography for separations of polymers, Anal. Chem. 84 (2012) 7802–7809, doi:10.1021/ac3011582.

2. Stratégies d'optimisation de méthodes LCxLC en ligne

L'optimisation de méthodes LCxLC en ligne est beaucoup plus complexe qu'en 1D-LC. Ceci est dû au très grand nombre de paramètres qui peuvent influencer la qualité de la séparation (en général évaluée en terme de capacité de pics), le facteur de dilution et le temps d'analyse (correspondant au temps d'analyse de première dimension). De ce fait, l'optimisation doit considérer l'ensemble des paramètres du système LCxLC, la modification d'un paramètre pouvant s'avérer avantageux pour la capacité de pics de première dimension, par exemple, mais finalement défavorable pour la capacité de pics effective en LCxLC. Cependant, très peu d'études proposent l'optimisation simultanée de ces trois critères.

2.1. Optimisation de la capacité de pics

À partir du travail de Davis et coll. [1] concernant le taux d'échantillonnage optimal de la séparation ^{1}D (lié au facteur de correction α, (cf. Chap.1-A.1.)) et du travail de Li et coll. [2], Gu et coll. ont développé deux protocoles pour maximiser la capacité de pics effective en LCxLC [3].

L'équation qu'ils ont utilisée pour la capacité de pics effective est la suivante :

$$n_{2D,effecive} = \frac{{}^1t_{r,last} - {}^1t_{r,first}}{(({}^1w_{4\sigma})^2 + 3.35({}^2t_g + 3)^2)} \times a_1 \times (1 - \exp(-a_2 \times {}^2t_g)) \qquad \text{Eq. 1}$$

avec ${}^1t_{r,last}$ et ${}^1t_{r,first}$ le temps de rétention du dernier et du premier pic en ^{1}D, ${}^1w_{4\sigma}$ la largeur d'un pic ^{1}D à 4 sigma et ^2t_g le temps de gradient de ^{2}D. A noter que ${}^2t_g + 3$ représente le temps d'échantillonnage, la valeur de 3 correspondant au temps d'équilibrage, en secondes, utilisé dans cette étude ($2\times{}^2t_0$). Les coefficients a_1 et a_2 sont propres à chaque système chromatographique utilisé.

Après avoir choisi la valeur de ^1t_g, le protocole 1 se déroule en deux étapes indépendantes. Il consiste tout d'abord à faire varier ^{1}L avec ^{1}F fixe pour maximiser la capacité de pics de la ^{1}D puis à optimiser ^2t_g (et donc le temps d'échantillonnage de ^{1}D). Le protocole 2 permet d'optimiser simultanément ^{1}F, ^{1}L, et ^2t_g. Tous les autres paramètres (^{2}L, ^1d_c, ^2d_c, ^1d_p, ^2d_p) sont fixes dans les deux protocoles.

Les calculs obtenus montrent qu'un faible taux d'échantillonnage ($\alpha \ll 1$) peut être compensé par un ^2t_g plus long (soit ^{2}n plus grand) et que ^2t_g optimal augmente lorsque ^1t_g augmente. Il apparaît également avec le protocole 2 qu'une capacité de pics maximale ^{1}n, ne génère pas nécessairement une $n_{2D,effective}$ maximale. Ce dernier résultat démontre l'importance du compromis entre t_s (liée au nombre de fractions par pics de ^{1}D) et ^{2}n pour obtenir une $n_{2D,effective}$ maximale.

La capacité de pics calculée par ces protocoles d'optimisation tient donc compte du sous échantillonnage en ^{1}D (facteur de correction α) pour un taux d'occupation de l'espace donné. Cependant la dispersion engendrée par des volumes injectés en ^{2}D

souvent très importants (60 et 230% $^2V_0$ dans [3]) n'est pas prise en compte. Les capacités de pics effectives LCxLC calculées à partir de ces deux approches peuvent donc être largement surestimées selon les volumes injectés en ^{2}D et la force éluante du solvant d'injection. Les conditions optimales pourraient donc s'avérer différentes si la démarche tenait compte de cette dispersion. Par ailleurs, la prise en compte du facteur de dilution comme critère additionnel devrait également conduire à des conditions optimales différentes.

2.2. Optimisation multi-critères

2.2.1. Approche générale

Le groupe de Schoenmakers a développé des stratégies plus exhaustives qui tiennent compte simultanément de la capacité de pics, du temps d'analyse et du facteur de dilution.

Dans un premier article [4], les auteurs ont proposé un protocole d'optimisation, présenté Fig.1, basé sur la méthode dite « Poppe plots » qui est une méthode définissant le meilleur compromis entre la capacité de pics et le temps de gradient en 1D-LC pour des paramètres donnés (diamètre de particules, viscosité de la phase mobile, coefficient de diffusion de l'analyte, coefficients expérimentaux de l'équation de Van Deemter) et pour une contrainte en pression donnée. Les temps de gradients utilisés dans cette étude théorique sont fixés à $t_G = 10 \times t_0$ pour toute l'étude et dans chaque dimension.

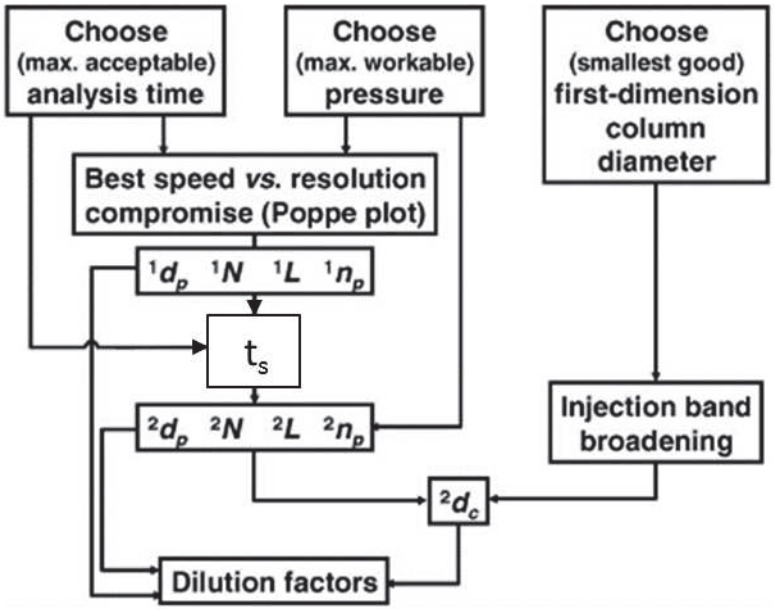

Figure 1 : Protocole d'optimisation en LCxLC en ligne proposé par [4]. Adaptée de [4].

Dans ce protocole, l'utilisateur définit une pression maximale pour les deux dimensions et une valeur minimum du diamètre de la colonne de ^{1}D, ^1d_c. Ensuite, les « Poppe plots » déterminent les valeurs optimales de ^{1}N associées à ^{1}L pour plusieurs

valeurs de ^1d_p. Il est donc possible de calculer ^1n, $^1\sigma_t$ et le temps d'échantillonnage, t_s, selon $t_s = {}^1\sigma_t$. Enfin les valeurs de ^2d_p, ^2N et ^2L sont obtenues de la même façon qu'en ^1D. L'utilisateur définit alors une valeur de ^1d_c impliquant une valeur de ^1F et donc un volume injecté en ^2D. Un ^2d_c approprié est finalement calculé afin d'éviter les effets à l'injection (selon $\sigma_i^2 = \frac{V_i^2}{\delta^2}$) tout en minimisant le facteur de dilution. Grâce à cette stratégie, en supposant une couverture maximale de l'espace de rétention, une capacité de pics de 4000 associée à un facteur de dilution de 12 a été calculée pour un temps d'analyse de 220 min dans des conditions HPLC (400 bar). Il a été suggéré, par la suite, que cette valeur de capacité de pics pourrait être augmentée en considérant t_s compris entre $2{}^1\sigma_t$ et $3.6{}^1\sigma_t$ au lieu de ${}^1\sigma_t$ selon [5–7]. Par ailleurs, la prise en compte du facteur de compression qui n'est pas considéré dans cette étude pourrait réduire le facteur de dilution sans affecter la capacité de pics. Ceci explique notamment le choix défavorable du rapport des diamètres de colonne ($\frac{^1d_c}{^2d_c} \ll 1$ avec des diamètres de 1 mm et 4.6 mm en ^1D et ^2D respectivement) pour éviter les effets à l'injection.

Vivó-Truyols et coll. ont proposé en 2010 l'utilisation d'une méthode « Pareto-optimal » [8]. Cette méthode permet de calculer la (ou les) condition(s) optimale(s) lorsque plusieurs objectifs conflictuels doivent être pris compte [9]. En pratique, les paramètres tels que la perte de charge maximum, le diamètre des colonnes, le volume d'injection de ^1D, le diamètre de particules et le temps d'échantillonnage sont définis par l'utilisateur. À partir de ces données et de paramètres pré-établis liés au système (coefficients de l'équation de Van Deemter, coefficients de diffusion, viscosité, porosité des colonnes, facteur de résistance à l'écoulement) cette méthode permet de générer des valeurs optimales pour les longueurs de colonnes et les débits. L'algorithme « Pareto optimal » permet la sélection des meilleures conditions considérant les trois critères, capacité de pics, temps d'analyse et facteur de dilution. Les résultats montrent clairement l'avantage d'utiliser le mode gradient dans les deux dimensions ainsi que des conditions UHPLC (cf. Chap.1-A.1). Contrairement à la méthode décrite précédemment, le facteur de compression (C_F) a été considéré et permet, pour un même temps d'analyse (2h) et une même capacité de pics (4000), de diviser par 4 le facteur de dilution passant de 40 (C_F=1) à 10 (C_F=5) montrant ainsi l'importance de considérer ce facteur lors de l'optimisation.

En conclusion, la méthode basée sur les « Poppe plots » et celle basée sur la méthode optimale de Pareto sont des outils intéressants pour l'optimisation de méthodes en LCxLC en ligne. L'avantage d'une approche « Pareto optimal » réside dans sa capacité à optimiser simultanément plusieurs objectifs conflictuels [6]. Il est également important de noter que ces deux études sont purement théoriques et qu'aucune séparation n'a été réalisée expérimentalement à partir des valeurs optimales prédites. De plus, le volume de délai de l'appareillage qui dépend en partie de la boucle d'injection et donc du volume injecté, le temps d'équilibrage ou encore

l'utilisation de débits splittés n'ont pas été pris en compte et devront aussi être considérés.

2.2.2. Approche ciblée

Dans un très récent article, Pirok et coll. [10] ont développé une stratégie pour optimiser la séparation de 54 colorants synthétiques par chromatographie d'échange d'anions en ^{1}D et en chromatographie d'appariement d'ions C18 en ^{2}D (SCX x Ion Pair-RP). Leur méthodologie consiste à réaliser deux séparations LCxLC avec des pentes de gradient normalisées très différentes dans les deux dimensions et de réaliser du « peak tracking » afin de déterminer un modèle de rétention linéaire pour chaque composé et ainsi prédire les temps de rétention dans des conditions de gradients données. A partir de ces modèles, une approche « Pareto-optimal » est utilisée pour définir le meilleur compromis entre le temps d'analyse et la résolution entre chaque pic en tenant compte du temps d'échantillonnage de la ^{1}D et des effets à l'injection en ^{2}D. La résolution entre chaque pic est calculée selon un algorithme développé par Schure et coll. [11] et une fonction de désirabilité de Derringer est employée délivrant un score compris entre 0 (co-élution totale) et une valeur de 1 (résolution ≥ 1.5). Finalement, le produit de chaque fonction est calculé pour évaluer la qualité globale de la séparation, une valeur de 1 signifiant que tous les pics sont séparés en LCxLC. Cette approche est intéressante pour des échantillons pour lesquels il est possible d'identifier et de suivre des composés mais est impossible à appliquer pour des échantillons très complexes.

2.3. 1D-LC vs LCxLC : Quelle capacité de pics, en combien de temps ?

Différents groupes ont cherché à définir le temps au bout duquel la capacité de pics devient égale entre une analyse 1D-LC et LCxLC appelé « crossover time » [12–14] pour la séparation de molécules de bas poids moléculaires (150-400 Da). Dans une étude théorique Potts et Carr ont montré que ce « crossover time » était situé entre 3 et 8 min (Fig.2) [14].

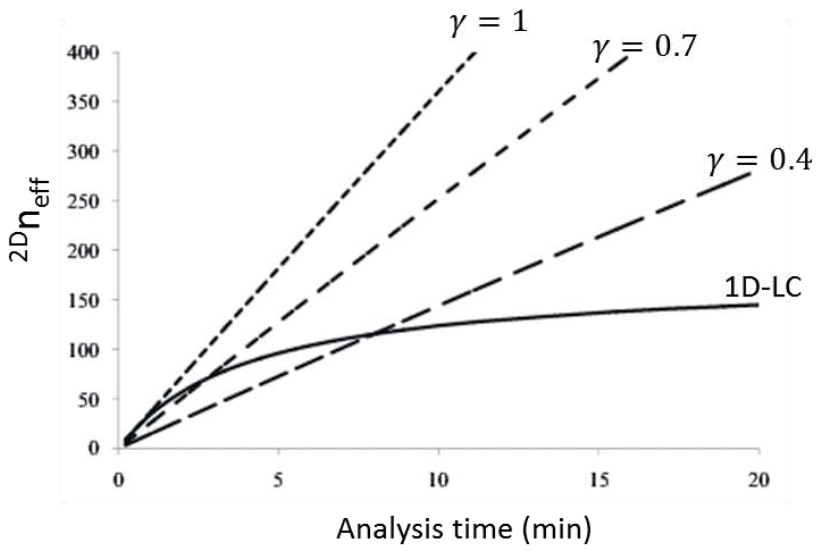

Figure 2 : Comparaison théorique des capacités de pics effectives en LCxLC et 1D-LC en fonction du temps d'analyse pour différents taux d'occupation de l'espace (1, 0.7 et 0.4). La ligne pleine correspond à l'analyse 1D-LC. Conditions détaillées en [14]. Figure adaptée de [14].

Les auteurs ont comparé des analyses 1D-LC optimisées selon une méthode analogue à celle des Poppe-plots [15] (ΔP_{max}=400 bar) avec différentes analyses LCxLC pour des temps d'analyses de 15, 30 et 60 min. L'optimisation des analyses LCxLC utilisait la méthode décrite dans la 2.2.1 de ce même chapitre. Le crossover time théorique est environ 4-5 min pour γ≈0.7. Il est encore diminué par l'utilisation d'un split en amont de la colonne de ^{1}D qui a pour but de permettre une augmentation de ^{1}F et donc une diminution du temps nécessaire pour l'équilibrage de la colonne en fin d'analyse. En conséquence, la pente normalisée de ^{1}D diminue et ^{1}n augmente d'autant plus que ^{1}F se rapproche du débit optimal. Les auteurs soulignent l'importance de γ, du taux d'échantillonnage et de la nature des composés sur ces résultats. Ces observations théoriques sont en accord avec les résultats expérimentaux obtenus par Stoll et coll. [12] et Huang et coll. [13] sur un échantillon de graines de maïs mutées.

À nouveau, les études théoriques ne tiennent pas compte des potentiels effets à l'injection en ^{2}D qui peuvent pourtant diviser par deux la capacité de pics en LCxLC selon Vivó-Truyols et coll. [8]. Le facteur de dilution n'est pas non plus abordé. En conséquence, les résultats expérimentaux pourraient être améliorés par un meilleur dimensionnement de l'analyse bidimensionnelle.

3. Minimisation de la variance liée à l'injection en deuxième dimension

Comme évoqué précédemment le transfert de l'échantillon de l'une à l'autre des deux dimensions est un point critique affectant l'optimisation d'une analyse LCxLC.

Il est donc crucial de réduire la contribution de la variance à l'injection en ^{2}D, autrement dit de maximiser le facteur β (cf. article 1). La dispersion à l'injection peut être due (i) à un volume injecté trop important [16] associé à une force éluante plus importante que celle de la phase mobile pouvant même dans certains cas conduire à un phénomène de breakthrough [17,18], (ii), à des problèmes de miscibilité entre les phases mobiles ^{1}D et ^{2}D [19,20], et/ou (iii) à une différence de viscosité entre le solvant d'injection et la phase mobile (« viscous fingering ») [21,22].

Le facteur de correction β décrit la perte en capacité de pics liée au premier cas évoqué ci-dessus. Son expression (cf. article 1) est à nouveau décrite ici pour faciliter le raisonnement :

$$\beta = \frac{^2\sigma_{v,col}}{^2\sigma_{v,total}} = \frac{1}{\sqrt{1+\frac{\lambda^2 \times z^2}{\delta^2} \times \frac{^1\sigma^2_{v,total}}{^2\sigma^2_{v,col}} \times \frac{1}{{C_F}^2}}} \quad \text{Eq. 2}$$

avec $^2\sigma_{v,\,col}$ l'écart type du pic en unité de volume résultant de l'élargissement de bande sur la colonne ^{2}D, $^2\sigma_{v,\,total}$ l'écart type total du pic en ^{2}D, δ^2 qui dépend du processus d'injection (égal à 3-4 en pratique), z le ratio de split réduisant le débit au niveau de l'interface ($0 \leq z \leq 1$), C_F le facteur de compression et λ qui correspond à un multiple de l'écart type d'un pic de ^{1}D de telle sorte à ce que le temps d'échantillonnage de la ^{1}D, t_s, soit égal à $t_s = \lambda * {}^1\sigma_{t,total}$.

Le facteur de compression peut s'écrire dans le cas de gradient très rapide ($^2k_{e,2}$ très faible) et/ou de solvant d'injection fortement éluant ($^2k_{e,1}$ élevé) [23,24]

$$C_F = \frac{^2k_{e,1}}{^2k_{e,2}} \quad \text{Eq. 3}$$

avec $^2k_{e,1}$ et $^2k_{e,2}$ le facteur de rétention d'un soluté sur la ^{2}D dans le solvant d'injection et dans les conditions de gradients respectivement.

Différentes stratégies peuvent être employées (et combinées) pour obtenir β proche de 1 :

(i) Réduire z entre les deux dimensions [25–29]. Cette option présente l'inconvénient d'augmenter le facteur de dilution diminuant ainsi la sensibilité de la méthode. De plus, il a été montré que l'utilisation d'un té afin d'obtenir le ratio de split désiré pouvait générer de la dispersion et par conséquent diminuer la capacité de pics de ^{1}D [30].

(ii) Réduire λ et donc augmenter le nombre de fraction en ^{1}D (^2V_i diminue) grâce à une approche dite « stop flow » LCxLC, qui consiste à stopper ^{1}F le temps nécessaire à l'analyse de ^{2}D [31], ou en utilisant plusieurs boucles de stockage par position [32,33]. L'utilisation de deux colonnes en parallèle en ^{2}D présente également cet avantage [34,35]. Ces solutions entraînent une augmentation du

temps d'analyse notamment le mode « stop flow » et peuvent conduire à une augmentation du facteur de dilution.

(iii) Minimiser $\frac{^1\sigma^2_{v,total}}{^2\sigma^2_{v,col}}$ et donc le $^1V_0/^2V_0$ et en particulier le rapport $\frac{^1d_c}{^2d_c}$ [16,20,29,36]. Ici encore, le facteur de dilution augmente.

(iv) Augmenter le facteur de compression en utilisant le phénomène de concentration du créneau d'injection en tête de colonne. En RPLCxRPLC, ce phénomène peut être obtenu en utilisant une colonne plus rétentive en seconde dimension [13] et/ou lorsque la pente normalisée de ^{1}D est faible par rapport à celle de ^{2}D.
Un autre moyen pour augmenter C_F consiste à utiliser un liquide additionnel peu éluant [37] afin de diminuer le pouvoir éluant de la phase mobile de ^{1}D et augmenter $^2k_{e,1}$. Des colonnes de trapping sont également montées à la place des boucles vides pour piéger les solutés avant leur élution vers la ^{2}D [38]. Ces deux approches sont souvent associées afin de favoriser le piégeage des composés [17,39,40].
Très récemment, Van de Ven et coll. ont développé une interface constituée d'une colonne monolithique capillaire qui est chauffée lors du remplissage puis refroidie avant l'élution afin de permettre une concentration des analytes et leurs transfert dans le solvant d'élution [41].

De toutes les solutions proposées pour limiter l'impact des effets à l'injection, il est important de noter que seules celles menant à l'augmentation du facteur de compression ne présentent que des avantages. En effet, en plus de limiter les problèmes à l'injection, il permet une augmentation de la sensibilité globale de la méthode comme l'illustre clairement la Fig. 4 de l'article 1. L'optimisation de ce paramètre sera donc particulièrement importante.

La diversité des stratégies employées par différents groupes de recherche illustre le fait que la maîtrise des effets à l'injection en ^{2}D représente un enjeu central lors du développement d'une méthode LCxLC. Ces effets à l'injection doivent donc absolument être pris en compte lors de l'optimisation.

CONCLUSIONS

L'optimisation des conditions en LCxLC en ligne doit tenir compte d'un grand nombre de paramètres liés aux conditions opératoires ainsi qu'aux contraintes instrumentales. Les conditions optimales résultent d'un compromis permettant de maximiser la capacité de pics tout en minimisant le temps d'analyse et le facteur de dilution.

Dans cette quête, seules quelques tendances « universelles » semblent émerger pour l'optimisation :

- un pic de ^{1}D doit être fractionné entre 1.7 et 3 fois pour conserver une majeure partie de la séparation en ^{1}D sans trop limiter le temps d'analyse en ^{2}D
- l'emploi de conditions HT-UHPLC en ^{2}D doit être privilégié pour générer des capacités de pics importantes lors d'analyses très rapides
- la mise en œuvre de moyens permettant d'augmenter le facteur de compression ne présente que des avantages

Finalement très peu de stratégies d'optimisation tenant compte simultanément des trois objectifs (capacité de pics, temps d'analyse et facteur de dilution) ont été proposées. La plus intéressante est basée sur la méthode « Pareto-optimal ». Cependant, seuls des résultats théoriques ont été présentés. Par ailleurs des paramètres importants ont parfois été fixés arbitrairement (par exemple t_G/t_0) et certaines grandeurs instrumentales (volume de délai, temps d'équilibrage, rapport de split) n'ont pas été prises en compte. Une amélioration des techniques d'optimisation doit passer par la prise en compte de ces aspects importants. D'autre part, la comparaison entre les valeurs prédites et les valeurs expérimentales est absolument nécessaire.

RÉFÉRENCES

[1] J.M. Davis, D.R. Stoll, P.W. Carr, Effect of First-Dimension Undersampling on Effective Peak Capacity in Comprehensive Two-Dimensional Separations, Anal. Chem. 80 (2008) 461–473. doi:10.1021/ac071504j.

[2] X. Li, D.R. Stoll, P.W. Carr, Equation for Peak Capacity Estimation in Two-Dimensional Liquid Chromatography, Anal. Chem. 81 (2009) 845–850. doi:10.1021/ac801772u.

[3] H. Gu, Y. Huang, P.W. Carr, Peak capacity optimization in comprehensive two dimensional liquid chromatography: A practical approach, J. Chromatogr. A. 1218 (2011) 64–73. doi:10.1016/j.chroma.2010.10.096.

[4] P.J. Schoenmakers, G. Vivó-Truyols, W.M.C. Decrop, A protocol for designing comprehensive two-dimensional liquid chromatography separation systems, J. Chromatogr. A. 1120 (2006) 282–290. doi:10.1016/j.chroma.2005.11.039.

[5] K. Horie, H. Kimura, T. Ikegami, A. Iwatsuka, N. Saad, O. Fiehn, N. Tanaka, Calculating Optimal Modulation Periods to Maximize the Peak Capacity in Two-Dimensional HPLC, Anal. Chem. 79 (2007) 3764–3770. doi:10.1021/ac062002t.

[6] F. Bedani, P.J. Schoenmakers, H.-G. Janssen, Theories to support method development in comprehensive two-dimensional liquid chromatography – A review, J. Sep. Sci. 35 (2012) 1697–1711. doi:10.1002/jssc.201200070.

[7] M. Sarrut, G. Crétier, S. Heinisch, Theoretical and practical interest in UHPLC technology for 2D-LC, TrAC Trends Anal. Chem. 63 (2014) 104–112. doi:10.1016/j.trac.2014.08.005.

[8] G. Vivó-Truyols, S. van der Wal, P.J. Schoenmakers, Comprehensive Study on the Optimization of Online Two-Dimensional Liquid Chromatographic Systems Considering Losses in Theoretical Peak Capacity in First- and Second-Dimensions: A Pareto-Optimality Approach, Anal. Chem. 82 (2010) 8525–8536. doi:10.1021/ac101420f.

[9] B.G.M.V. D.L. Massart L.M.C. Buydens, S. De Jong, P.J. Lewi and J. Smeyers-Verbeke, Chapter 26 Other optimization methods, in: Data Handl. Sci. Technol., Elsevier, 1998: pp. 771–804. http://www.sciencedirect.com/science/article/pii/S0922348797800561 (accessed July 10, 2015).

[10] B.W.J. Pirok, S. Pous-Torres, C. Ortiz-Bolsico, G. Vivó-Truyols, P.J. Schoenmakers, Program for the interpretive optimization of two-dimensional resolution, J. Chromatogr. A. 1450 (2016) 29–37. doi:10.1016/j.chroma.2016.04.061.

[11] M.R. Schure, Quantification of resolution for two-dimensional separations, J. Microcolumn Sep. 9 (1997) 169–176. doi:10.1002/(SICI)1520-667X(1997)9:3<169::AID-MCS5>3.0.CO;2-#.

[12] D.R. Stoll, X. Wang, P.W. Carr, Comparison of the Practical Resolving Power of One- and Two-Dimensional High-Performance Liquid Chromatography Analysis of Metabolomic Samples, Anal. Chem. 80 (2008) 268–278. doi:10.1021/ac701676b.

[13] Y. Huang, H. Gu, M. Filgueira, P.W. Carr, An experimental study of sampling time effects on the resolving power of on-line two-dimensional high performance

liquid chromatography, J. Chromatogr. A. 1218 (2011) 2984–2994. doi:10.1016/j.chroma.2011.03.032.
[14] L.W. Potts, P.W. Carr, Analysis of the temporal performance of one versus on-line comprehensive two-dimensional liquid chromatography, J. Chromatogr. A. 1310 (2013) 37–44. doi:10.1016/j.chroma.2013.07.102.
[15] X. Wang, D.R. Stoll, P.W. Carr, P.J. Schoenmakers, A graphical method for understanding the kinetics of peak capacity production in gradient elution liquid chromatography, J. Chromatogr. A. 1125 (2006) 177–181. doi:10.1016/j.chroma.2006.05.048.
[16] A. D'Attoma, S. Heinisch, On-line comprehensive two dimensional separations of charged compounds using reversed-phase high performance liquid chromatography and hydrophilic interaction chromatography. Part II: Application to the separation of peptides, J. Chromatogr. A. 1306 (2013) 27–36. doi:10.1016/j.chroma.2013.07.048.
[17] Q. Li, F. Lynen, J. Wang, H. Li, G. Xu, P. Sandra, Comprehensive hydrophilic interaction and ion-pair reversed-phase liquid chromatography for analysis of di- to deca-oligonucleotides, J. Chromatogr. A. 1255 (2012) 237–243. doi:10.1016/j.chroma.2011.11.062.
[18] P. Jandera, T. Hájek, P. Česla, Effects of the gradient profile, sample volume and solvent on the separation in very fast gradients, with special attention to the second-dimension gradient in comprehensive two-dimensional liquid chromatography, J. Chromatogr. A. 1218 (2011) 1995–2006. doi:10.1016/j.chroma.2010.10.095.
[19] A. Medvedovici, V. David, V. David, C. Georgita, Retention Phenomena Induced by Large Volume Injection of Solvents Non-Miscible with the Mobile Phase in Reversed-Phase Liquid Chromatography, J. Liq. Chromatogr. Relat. Technol. 30 (2007) 199–213. doi:10.1080/10826070601064201.
[20] I. François, A. De Villiers, P. Sandra, Considerations on the possibilities and limitations of comprehensive normal phase–reversed phase liquid chromatography (NPLC×RPLC), J. Sep. Sci. 29 (2006) 492–498. doi:10.1002/jssc.200500451.
[21] K.J. Mayfield, R.A. Shalliker, H.J. Catchpoole, A.P. Sweeney, V. Wong, G. Guiochon, Viscous fingering induced flow instability in multidimensional liquid chromatography, J. Chromatogr. A. 1080 (2005) 124–131. doi:10.1016/j.chroma.2005.04.093.
[22] R.A. Shalliker, G. Guiochon, Understanding the importance of the viscosity contrast between the sample solvent plug and the mobile phase and its potential consequence in two-dimensional high-performance liquid chromatography, J. Chromatogr. A. 1216 (2009) 787–793. doi:10.1016/j.chroma.2008.11.067.
[23] M. Martin, M. Mishra, A. De Wit, C. Grivel, S. Heinisch, 28th International Symposium on Chromatography ISC, in: Valencia, 2010.
[24] F. Rouvière, C. Grivel, M. Martin, S. Heinisch, F. Rouviere; C.Grivel; M. Martin; S. Heinisch; J. Chromatogr.A to be submitted, Journal of Chromatography A. (n.d.).
[25] M.R. Filgueira, Y. Huang, K. Witt, C. Castells, P.W. Carr, Improving Peak Capacity in Fast Online Comprehensive Two-Dimensional Liquid Chromatography with Post-First-Dimension Flow Splitting, Anal. Chem. 83 (2011) 9531–9539. doi:10.1021/ac202317m.
[26] T. Beelders, K.M. Kalili, E. Joubert, D. de Beer, A. de Villiers, Comprehensive two-dimensional liquid chromatographic analysis of rooibos (Aspalathus linearis) phenolics, J. Sep. Sci. 35 (2012) 1808–1820. doi:10.1002/jssc.201200060.

[27] K.M. Kalili, A. de Villiers, Systematic optimisation and evaluation of on-line, off-line and stop-flow comprehensive hydrophilic interaction chromatography × reversed phase liquid chromatographic analysis of procyanidins, Part I: Theoretical considerations, J. Chromatogr. A. 1289 (2013) 58–68. doi:10.1016/j.chroma.2013.03.008.
[28] A. Le Masle, D. Angot, C. Gouin, A. D'Attoma, J. Ponthus, A. Quignard, S. Heinisch, Development of on-line comprehensive two-dimensional liquid chromatography method for the separation of biomass compounds, J. Chromatogr. A. 1340 (2014) 90–98. doi:10.1016/j.chroma.2014.03.020.
[29] C.M. Willemse, M.A. Stander, J. Vestner, A.G.J. Tredoux, A. de Villiers, Comprehensive Two-Dimensional Hydrophilic Interaction Chromatography (HILIC) × Reversed-Phase Liquid Chromatography Coupled to High-Resolution Mass Spectrometry (RP-LC-UV-MS) Analysis of Anthocyanins and Derived Pigments in Red Wine, Anal. Chem. 87 (2015) 12006–12015. doi:10.1021/acs.analchem.5b03615.
[30] A. D'Attoma, Développement de méthodes bidimensionnelles en ligne LCxLC-MS pour l'analyse de composés chargés, Lyon 1, 2013. http://www.theses.fr/2013LYO10214 (accessed April 28, 2016).
[31] F. Bedani, W.T. Kok, H.-G. Janssen, A theoretical basis for parameter selection and instrument design in comprehensive size-exclusion chromatography × liquid chromatography, J. Chromatogr. A. 1133 (2006) 126–134. doi:10.1016/j.chroma.2006.08.048.
[32] S.R. Groskreutz, M.M. Swenson, L.B. Secor, D.R. Stoll, Selective comprehensive multi-dimensional separation for resolution enhancement in high performance liquid chromatography. Part I: Principles and instrumentation, J. Chromatogr. A. 1228 (2012) 31–40. doi:10.1016/j.chroma.2011.06.035.
[33] S.R. Groskreutz, M.M. Swenson, L.B. Secor, D.R. Stoll, Selective comprehensive multidimensional separation for resolution enhancement in high performance liquid chromatography. Part II: Applications, J. Chromatogr. A. 1228 (2012) 41–50. doi:10.1016/j.chroma.2011.06.038.
[34] I. François, A. de Villiers, B. Tienpont, F. David, P. Sandra, Comprehensive two-dimensional liquid chromatography applying two parallel columns in the second dimension, J. Chromatogr. A. 1178 (2008) 33–42. doi:10.1016/j.chroma.2007.11.032.
[35] I. François, D. Cabooter, K. Sandra, F. Lynen, G. Desmet, P. Sandra, Tryptic digest analysis by comprehensive reversed phase×two reversed phase liquid chromatography (RP-LC×2RP-LC) at different pH's, J. Sep. Sci. 32 (2009) 1137–1144. doi:10.1002/jssc.200800578.
[36] L. Mondello, P. Donato, F. Cacciola, C. Fanali, P. Dugo, RP-LC×RP-LC analysis of a tryptic digest using a combination of totally porous and partially porous stationary phases, J. Sep. Sci. 33 (2010) 1454–1461. doi:10.1002/jssc.200900816.
[37] D.R. Stoll, E.S. Talus, D.C. Harmes, K. Zhang, Evaluation of detection sensitivity in comprehensive two-dimensional liquid chromatography separations of an active pharmaceutical ingredient and its degradants, Anal. Bioanal. Chem. 407 (2014) 265–277. doi:10.1007/s00216-014-8036-9.
[38] F. Cacciola, P. Jandera, Z. Hajdú, P. Česla, L. Mondello, Comprehensive two-dimensional liquid chromatography with parallel gradients for separation of phenolic and flavone antioxidants, J. Chromatogr. A. 1149 (2007) 73–87. doi:10.1016/j.chroma.2007.01.119.

[39] R.J. Vonk, A.F.G. Gargano, E. Davydova, H.L. Dekker, S. Eeltink, L.J. de Koning, P.J. Schoenmakers, Comprehensive Two-Dimensional Liquid Chromatography with Stationary-Phase-Assisted Modulation Coupled to High-Resolution Mass Spectrometry Applied to Proteome Analysis of Saccharomyces cerevisiae, Anal. Chem. 87 (2015) 5387–5394. doi:10.1021/acs.analchem.5b00708.
[40] A.F.G. Gargano, M. Duffin, P. Navarro, P.J. Schoenmakers, Reducing Dilution and Analysis Time in Online Comprehensive Two-Dimensional Liquid Chromatography by Active Modulation, Anal. Chem. 88 (2016) 1785–1793. doi:10.1021/acs.analchem.5b04051.
[41] H.C. van de Ven, A.F.G. Gargano, S. van der Wal, P.J. Schoenmakers, Switching solvent and enhancing analyte concentrations in small effluent fractions using in-column focusing, J. Chromatogr. A. 1427 (2016) 90–95. doi:10.1016/j.chroma.2015.11.082.

CHAPITRE 2 – CONDITIONS EXPÉRIMENTALES

INTRODUCTION

Ce chapitre décrit l'appareillage, la nature des échantillons ainsi que les méthodologies employées pour le traitement des données dans les différentes études.

La section A détaille les différents instruments employés à savoir deux systèmes bidimensionnels de chromatographie en phase liquide et un système de chromatographie en phase supercritique. Les différents couplages étudiés ont été réalisés à l'aide de trois interfaces qui sont également décrites. En plus de la détection UV, deux types de spectromètre de masse ont été employés : un simple quadripôle et un appareil Q-TOF (un quadripôle associé à un temps de vol).

Les sections B et C décrivent les phases stationnaires et mobiles utilisées lors des différentes études.

La section D détaille la nature et les caractéristiques des échantillons utilisés au cours des différents travaux. Des mélanges complexes de peptides sont issus de la digestion tryptique de six ou trois protéines (chapitre 3). Des anticorps monoclonaux (mAbs) et anticorps conjugués (ADCs), fournis par les Laboratoires Pierre Fabre, ont fait l'objet d'une étude approfondie (chapitre 4). Des composés aromatiques et la partie aqueuse d'une bio-huile, fournie par l'IFPEN, ont également été analysés (chapitre 5).

Enfin, la section E aborde le traitement et la gestion des données LCxLC-UV et LCxLC-MS.

Nous remercions Waters pour le prêt puis le don du système bidimensionnel 2D I-Class, pour le prêt de l'UPC² et des colonnes dédiées ainsi que pour le prêt du logiciel de retraitement MaxEnt. Nous remercions les Laboratoires Pierre Fabre, l'Université de Genève et l'IFPEN pour le don d'échantillons d'ADC, de colonnes et de l'échantillon de bio-huile respectivement. Nous remercions l'Irstea Villeurbanne pour le prêt du système Q-TOF.

A. INSTRUMENTATION

1. Appareillages de chromatographie

1.1. 2D I-Class (Waters)

Ce système de chromatographie en phase liquide bidimensionnelle inclut deux systèmes de pompage binaires ultra haute pression identiques (un pour chaque dimension), un passeur d'échantillon, deux fours colonnes identiques (un pour chaque dimension), une interface composée de deux vannes hautes pressions 6 ports 2-positions, un détecteur UV mono longueur d'onde (1ère dimension, ^{1}D) et un détecteur à barrette de diodes ou DAD (2ème dimension, ^{2}D). Le système de pompage peut délivrer jusqu'à 2 mL/min. Le maximum de pression autorisée est 1285 bar mais décroît à partir de 1 mL/min en fonction du débit et de la composition de phase mobile. Le système d'injection n'utilise pas de boucle d'injection, l'aiguille de prélèvement de 15 µL permet également de stocker l'échantillon avant d'être balayé par la phase mobile vers la colonne (« flow-through needle », FTN). Une boucle d'extension optionnelle permet d'augmenter le volume injecté à 50 µL. La température maximale du four colonne est de 90°C. L'interface est détaillée dans la partie 3. Les cellules de détection ont un volume de 0.5 µL, chemin optique de 10 mm et supportent une pression de 70 bar maximum.

Le système 2D I-Class est piloté par le logiciel Masslynx qui permet également l'acquisition des données.

Ce système est également utilisé pour des analyses unidimensionnelles. Dans ce cas, seule la pompe ^{1}D, le passeur d'échantillon, un des deux fours colonnes et le DAD sont utilisés.

1.2. 1290 Infinity 2D-LC (Agilent)

Ce système de chromatographie en phase liquide bidimensionnelle inclut deux systèmes de pompage binaires haute pression identiques (un pour chaque dimension), un passeur d'échantillon, deux fours colonnes identiques (un pour chaque dimension), une interface composée d'une vanne double 4 ports 2 positions résistante aux hautes pressions, un détecteur UV mono longueur d'onde (^{1}D) et un DAD (^{2}D). Le système de pompage peut délivrer jusqu'à 5 mL/min. Le maximum de pression autorisée est 1200 bar. Le système d'injection est un FTN et permet l'injection de volume jusqu'à 20 µL. Pour injecter des volumes jusqu'à 100 µL, il est nécessaire d'ajouter un tube dimensionné selon le volume souhaité. La température maximale du four colonne est de 100°C. L'interface est détaillée dans la partie 3 de ce chapitre. Le détecteur UV possède une cellule de 2 µL, un chemin optique de 3 mm et supporte une pression de 60 bar maximum. Le détecteur DAD possède une cellule de 0.6 µL, un chemin optique de 10 mm et supporte une pression de 120 bar maximum.

Le système 2D-LC est piloté par le logiciel OpenLab CDS qui permet également l'acquisition des données.

Ce système est également utilisé pour des analyses unidimensionnelles. Dans ce cas, seule la pompe de première dimension, le passeur d'échantillon, un des deux fours colonnes et le DAD sont utilisés.

1.3. UPC² (Waters)

Ce système de chromatographie en phase supercritique (SFC) inclut un système de pompage binaire haute pression, un passeur d'échantillon, deux fours colonnes identiques avec deux vannes de sélection de colonne 6 ports 2 positions, un détecteur DAD et un module permettant la régulation de la contre pression. Le système de pompage peut délivrer jusqu'à 4 mL/min. Le maximum de pression autorisée est de 414 bar pour des débits inférieurs à 3.25 mL/min et décroît linéairement à 293 bar à 4 mL/min. Le volume de la boucle d'injection est de 10 µL. La température maximale du four colonne est de 90°C. Le détecteur DAD possède une cellule 8 µL, un chemin optique de 10 mm et supporte une pression de 414 bar maximum.

Le système UPC² est piloté par le logiciel Empower qui permet également l'acquisition des données.

1.4. Couplage LCxSFC

Contrairement aux couplages LCxLC qui ont été réalisés à l'aide d'instruments commerciaux, le couplage LCxSFC nécessite de relier deux instruments différents.

La première dimension est composée de différents modules du 2D I-Class à savoir le système de pompage de première dimension, le passeur d'échantillon, les fours colonnes et le détecteur DAD. La deuxième dimension est constituée du système de pompage, du détecteur DAD et du régulateur de contre pression de l'UPC². Les fours colonnes du 2D I-Class abritent donc les colonnes de première et deuxième dimension. Une vanne 10 ports 2 positions équipée de boucles identiques de 3 et 5 µL selon les expériences est utilisée comme interface entre les deux instruments. Celle-ci est détaillée dans la partie 3 de ce chapitre.

Le logiciel Masslynx permet le pilotage de la première dimension et celui de l'interface ainsi que l'acquisition des données de première dimension. Le logiciel Empower permet le pilotage et l'acquisition des données de l'UPC². La synchronisation entre les systèmes est réalisée en connectant électriquement les deux systèmes et en programmant des évènements externes à partir de la première dimension sous Masslynx.

2. Caractéristiques des systèmes

Le tableau 1 recense le volume de délai et le volume externe des différents systèmes chromatographiques utilisés. La mesure du volume externe a été réalisée en considérant le moment statistique centré d'ordre 1 par injection d'1 µL d'ethyl-parabène, une union à zéro volume mort remplaçant la colonne. Le volume de délai a été calculé après l'enchainement de montée linéaire–palier isocratique–descente linéaire rapide [1].

		$V_{délai}$ (µL)	Volume externe (µL)
2D I-Class	1ère dimension	110	12
	2ème dimension	120	6.5*
1290 Infinity 2D-LC	1ère dimension	140	22
	2ème dimension	65	8.5*
UPC²	Appareillage unidimensionnel	300	83
UPC²	2ème dimension	300	57

Tableau 1 : Caractéristiques des différents systèmes et couplages utilisés. * Le volume indiqué ne tient pas compte du volume des boucles d'échantillonnages situées au niveau de l'interface

Les variances extra-colonnes ont été mesurées selon la méthode des moments statistiques centrés d'ordre 2 [2] et sont présentées Fig. 3.

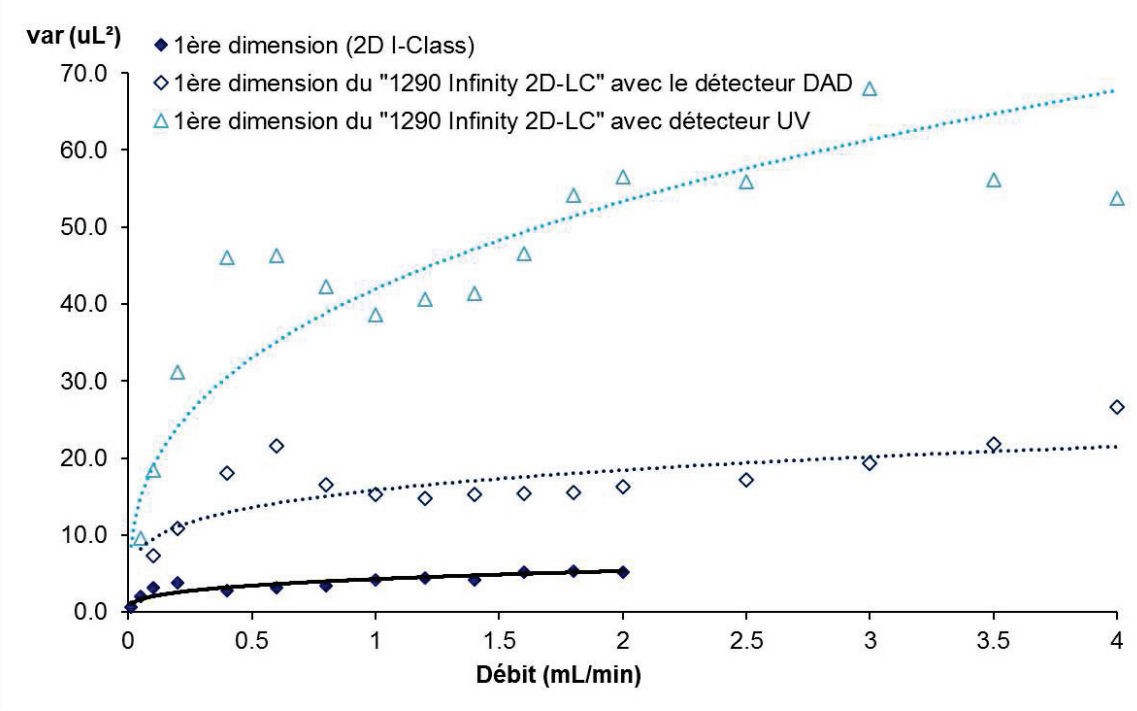

Figure 3 : Évolution de la variance extra-colonne en fonction du débit pour les systèmes 2D I-Class et 1290 Infinity 2D-LC utilisant les pompes de 1ère dimension. Injection de 1 µL d'ethylparabène dans 50/50 eau/acétonitrile

Lorsqu'ils sont utilisés comme système unidimensionnel, le 2D I-Class génère une variance environ 4 fois moins importante que le système 1290 Infinity 2D-LC. Ceci étant dû en majeure partie au tubing utilisé (65 µm vs 127 µm de diamètre interne pour le 2D I-Class et 1290 Infinity 2D-LC respectivement) et à la cellule de détection (0.5 µL pour le 2D-IClass *versus* 2 µL pour le 1290 Infinity 2D-LC). De plus, tandis que les deux cellules de détection sont identiques sur le 2D I-Class et génèrent donc la même variance, celles qui équipent le 1290 Infinity 2D-LC n'ont pas le même volume (2 µL et 0.6 µL pour l'UV et le DAD respectivement) générant des dispersions différentes. Ceci explique l'écart entre les variances mesurées en 1D-LC avec le DAD par rapport à une utilisation 2D pour laquelle le DAD sera utilisé comme détecteur de 2ème dimension pendant que l'UV sera utilisé comme détecteur de 1ère dimension.

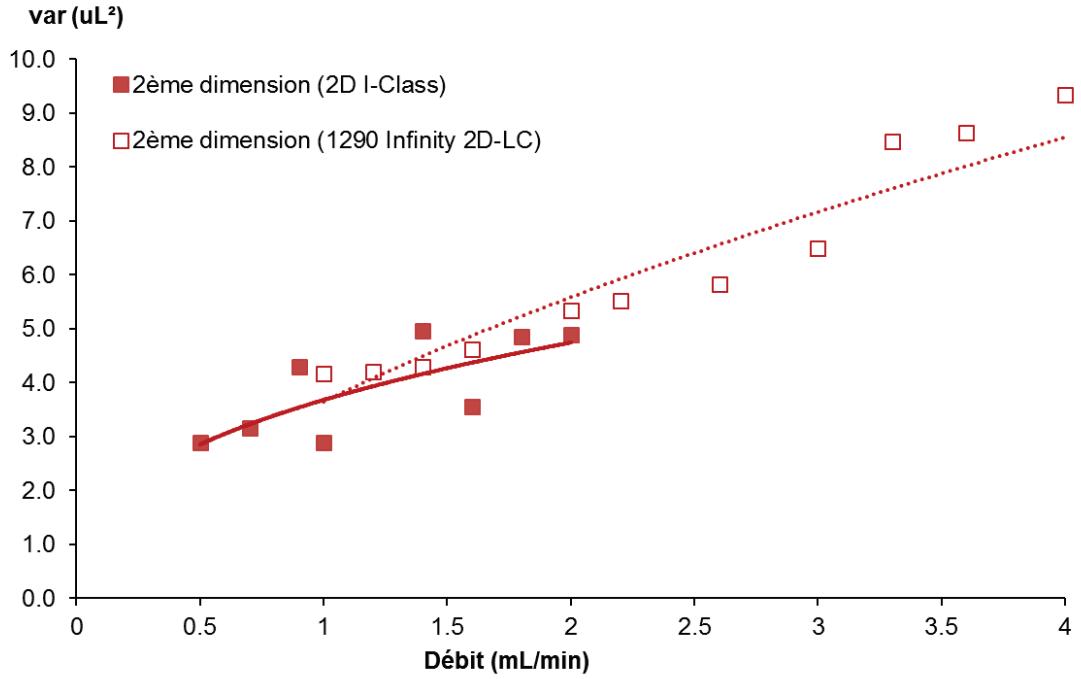

Figure 4 : Évolution de la variance extra-colonne en fonction du débit pour les systèmes 2D I-Class et 1290 Infinity 2D-LC utilisée en 2ème dimension. Injection de 3 µL d'ethylparabène dans 50/50 eau/acétonitrile. Boucles de 20 µL (125 µm de diamètre interne) à l'interface.

Les variances mesurées en 2ème dimension (Fig. 4) sont de l'ordre de 4-5 µL² pour les deux appareillages pour des débits ≤ à 2 mL.min^{-1}. Ces valeurs permettent de travailler avec des colonnes de faibles volumes morts (≤ 110 µL) et très efficaces (sub-2µm) qui seront nécessaires pour des analyses en 2ème dimension.

3. Interfaces

Le rôle de l'interface est primordial pour la bonne conduite d'une analyse bidimensionnelle « comprehensive ». Chaque interface est composée de deux boucles identiques dont les volumes varient en fonction du dimensionnement de l'analyse. Pendant que l'une des boucles échantillonne la séparation issue de la première dimension, le contenu de la seconde est analysé en deuxième dimension, chacune des boucles remplissant les deux rôles alternativement. Les boucles sont remplies et vidées en sens inverse (« back-flush ») ce qui permet de diminuer la dispersion du créneau d'injection par rapport à une approche « même sens » (« forward-flush »).

3.1. Deux vannes 6 ports 2 positions (2D-IClass)

Une interface composée de deux vannes 6 ports 2 positions (Fig. 5) est utilisé sur le système 2D I-Class commercial. Cette interface est symétrique. Cela signifie que le trajet des composés est le même (boucle 1 et boucle 2) ce qui permet d'éviter les décalages d'une fraction à l'autre [3]. La symétrie est obtenue grâce à deux raccords de 2 µL reliant les ports 1-5 (vanne de gauche) et 2-4 (vanne de droite). Une

bonne synchronisation entre les deux vannes lors de la rotation est indispensable pour obtenir des analyses ^{2}D répétables.

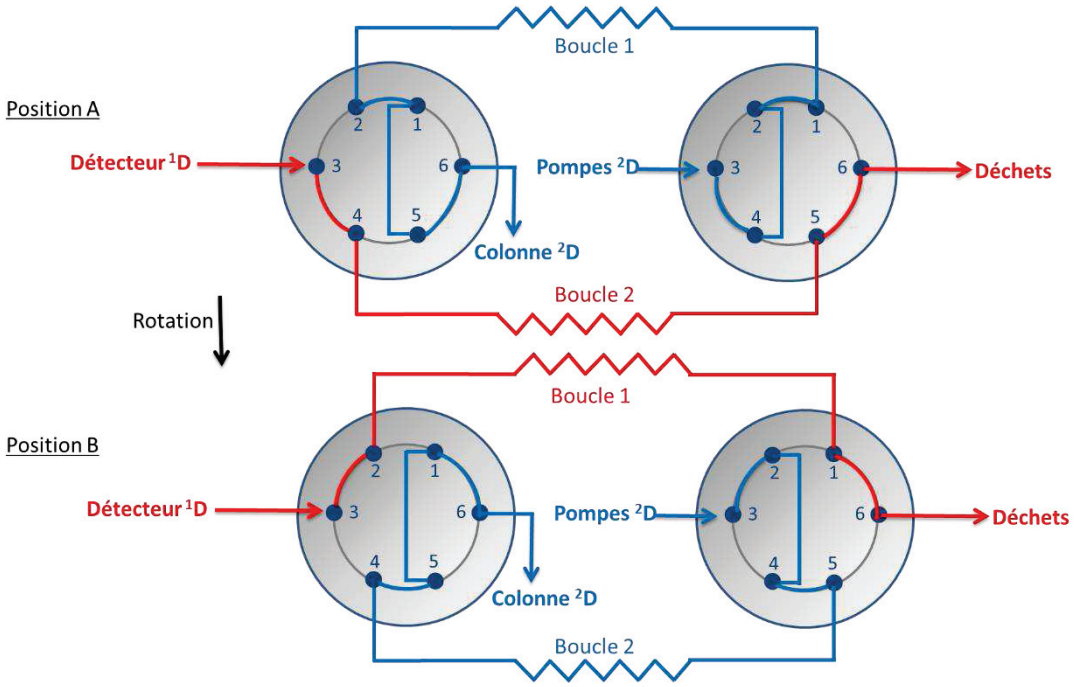

Figure 5 : Deux vannes 6 ports 2 positions

3.2. Une vanne double 4 ports 2 positions (1290 Infinity 2D-LC)

Cette interface, présentée Fig. 6, permet de travailler dans une configuration symétrique sans avoir besoin de chemins additionnels et aucun problème de synchronisation n'est à craindre entre les deux positions puisqu'elle n'est composée que d'une seule vanne.

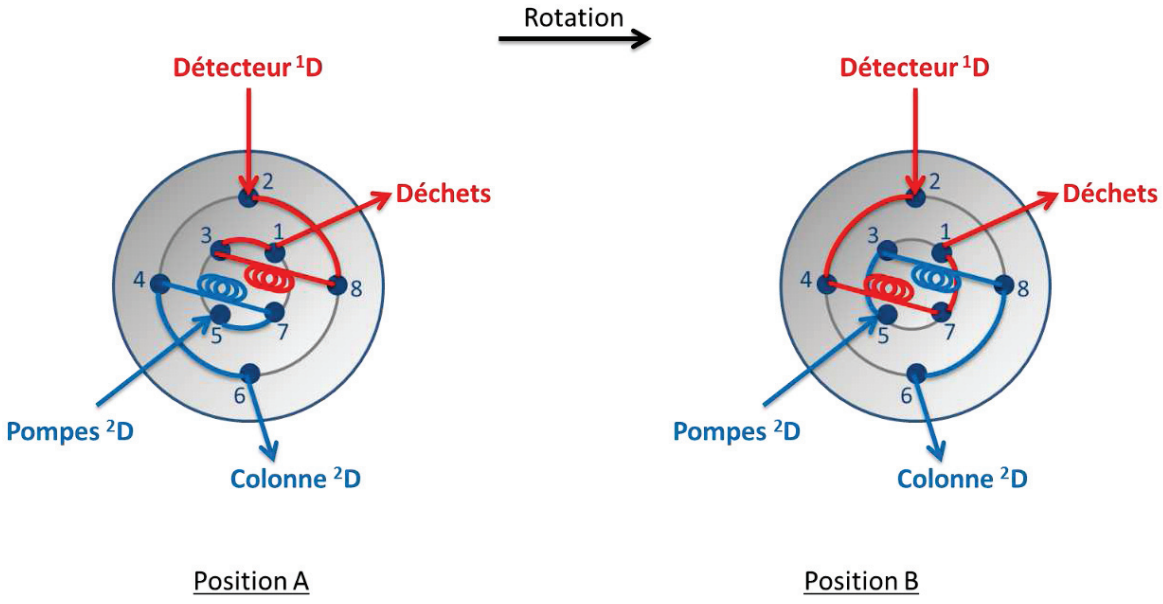

Figure 6 : Une vanne double 4 ports 2 positions

3.3. Une vanne 10 ports 2 positions (LCxSFC)

Cette interface a été utilisée pour le couplage LCxSFC. À la différence des deux précédentes, lors de l'injection en ^{2}D, l'échantillon ne parcourt pas le même trajet en position A et en position B. Ceci s'explique par la présence d'un raccord, entre les positions 4 et 9. En seconde dimension, le chemin parcouru est plus important pour la position A, en bleu, que pour la position B, en rouge (Fig. 7). En effet, dans le premier cas, le raccord intervient après la boucle, contrairement à la position B où il intervient avant la boucle. Pour tenir compte de ce décalage, il sera donc nécessaire de réaligner les pics des fractions paires et impaires. D'autre part, en position A, le raccord engendre une augmentation du volume externe alors qu'il engendre une augmentation du volume de délai en position B. Cet aspect peut également contribuer à un décalage des pics sur la ^{2}D.

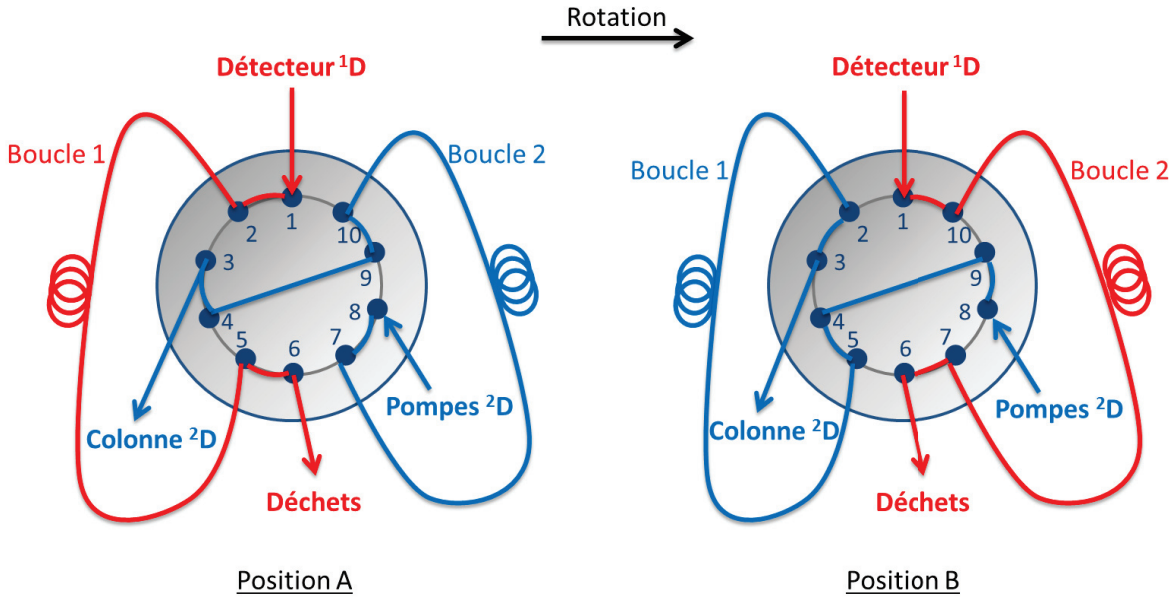

Figure 7 : Vanne 10 ports 2 positions

4. Spectromètres de masse

Deux spectromètres de masses couplés aux systèmes unidimensionnels et bidimensionnels ont été utilisés.

4.1. QDa (Waters)

Le QDa est un simple quadripôle équipé d'une source electrospray (ESI) possédant une gamme dynamique de 50 à 1250 Th. Il est piloté par le logiciel Masslynx. Les réglages de sources sont listés dans le tableau 2. Les conditions spécifiques à chaque composé sont mentionnées dans le chapitre concerné. Les acquisitions ont été réalisées en mode SIM (« Single Ion Monitoring ») qui permet de sélectionner une ou plusieurs masses à suivre spécifiquement.

Polarité	ESI +
Mode d'acquisition	SIM
Tension du capillaire (kV)	1.5
Température de désolvatation (°C)	650

Tableau 2 : Réglages du spectromètre de masse QDa pour l'analyse de peptides

Ce détecteur a été couplé au 1290 Infinity 2D-LC utilisé en 1D-LC-MS et 2D-LC-MS.

4.2. G2-S QTOF (Waters)

Ce spectromètre de masse est composé d'un simple quadripôle associé à un analyseur à temps de vol par l'intermédiaire d'une cellule de collision. L'instrument est équipé d'une source ESI. Le temps de vol permet l'obtention de spectre de masse haute résolution (≈ 40 000). Le pilotage est réalisé via le logiciel Masslynx. Les acquisitions ont été enregistrées en mode scan qui permet de balayer une gamme de m/z choisie. Le signal enregistré représente alors la somme de toutes les masses ou courant ionique total (TIC). Il est alors possible de connaître les m/z qui constituent ce signal ou d'extraire spécifiquement une ou plusieurs m/z (EIC).

Le G2-S QTOF a été couplé au 2D I-Class pour l'analyse de protéines à très hauts poids moléculaires (entre 25 et 150 kDa) présentées au chapitre 4. Les réglages utilisés sont listés ci-dessous dans le tableau 3 :

Format des données	Continuum
Polarité	ESI +
Analyseur	Mode sensibilité
Gamme de masse (m/z)	500-3500
Tension du capillaire (kV)	3.2
Tension du cône d'échantillonnage (V)	120
Température de la source (°C)	110
Température de désolvatation (°C)	500
Débit de gaz du cône (L/Hr)	50
Débit de gaz de désolvatation (L/Hr)	950
Composé lock spray	Leucine enkephaline
Calibrant	NaI

Tableau 3 : Réglages du spectromètre de masse G2-S QTOF pour l'analyse de protéines

B. PHASES STATIONNAIRES

Les différentes phases stationnaires à base silice ou à support carbone graphite (colonne Hypercarb) utilisées au cours de ce travail sont listées dans le tableau 4

	Nom	Type	Fournisseur	L (mm)	d_i (mm)	d_p (µm)	d_{pores} (Å)	Chap.
RPLC	Ascentis Express C18	SP	Supelco	100	2.1	5	NR	3
	Xbridge C18	TP	Waters	50	2.1	5	100	
	Ascentis Express C18	SP	Supelco	50	2.1	2.7	NR	
	Kinetex C18	SP	Phenomenex	30	2.1	1.3	100	
HIC	MabPac HIC-10	TP	Thermo Scientific	100	4.6	5	1000	4
RPLC	Acquity UPLC BEH C4	TP	Waters	50	2.1	1.7	300	
RPLC	Hypercarb	TP	Thermo Scientific	100	1.0	5	250	5
	Xbridge C18	TP	Waters	50	1.0	3.5	100	
	Acquity CSH PH	TP	Waters	50	2.1	1.7	130	
SFC	Acquity UPC² BEH-2EP	TP	Waters	50	2.1	1.7	100	
	Acquity UPC² BEH	TP	Waters	50	2.1	1.7	100	
	Acquity UPC² HSS C18	TP	Waters	50	2.1	1.7	130	
	Acquity UPC² CSH FP	TP	Waters	50	2.1	1.7	100	

Tableau 4 : Phases stationnaires utilisées pour les différentes études. Séparations de peptides, protéines et molécules issues de la biomasse dans les chapitres 3, 4 et 5 respectivement. TP : Totalement poreuse ; SP : Superficiellement poreuse

C. PHASES MOBILES

1. Phase inverse (RPLC)

L'eau utilisée pour la préparation des phases mobiles provient d'un système de purification à eau Elga. La conductivité obtenue est supérieure 18 MΩ.cm. Les bactéries présentes dans l'eau sont détruites par rayonnement UV. Les phases mobiles organiques sont préparées à partir d'acétonitrile et de méthanol qualité LC-MS ou HPLC fournis par Sigma Aldrich.

Divers additifs (qualité MS) sont ajoutés dans les phases mobiles aqueuses et organiques. Ces additifs sont l'acide formique (FA), l'acide trifluoroacétique (TFA) et l'acétate d'ammonium (AA). Ces additifs sont introduits dans les phases mobiles aqueuses et organiques sauf l'acétate d'ammonium. Les phases mobiles aqueuses préparées à base de sels sont filtrées sur 0.22 µm avec un système de filtration Millipore afin de garantir l'absence de particules.

2. Chromatographie d'interactions hydrophobes (HIC)

Pour réaliser la séparation d'un ADC, une phase mobile constituée de (A) 2.5 M AA + 0.1 M Na_2HPO_4 ajusté à pH=7 (acide phosphorique) et (B) 0.1 M de tampon phosphate (Na_2HPO_4 et NaH_2PO_4) ajusté à pH=7 avec de l'hydroxyde de sodium a été utilisée.

3. Chromatographie en phase supercritique (SFC)

Dans l'étude développée au chapitre 5, des mélanges 1:1 (v/v) d'ACN et de MeOH ont été employés avec le CO_2 en mode d'élution isocratique et gradient.

D. ÉCHANTILLONS

1. Peptides

1.1. Composés standards

Six peptides ont été sélectionnés de manière à être représentatif de peptides issus de digestion tryptiques de protéines. Ils sont extraits d'une liste de peptides utilisés lors de la thèse d'A. d'Attoma [1]. Les peptides ont été fournis par Sigma Aldrich et stockés à -20°C une fois solubilisés dans l'eau. Le tableau 5 récapitule les caractéristiques des six peptides.

Peptide	Masse exacte(Da)	Point isoéléctrique
Influenza Hemagglutinin	1101.5	3.5
leucine enkephalin	555.3	6.0
bombesin	1618.8	7.6
[arg8]-vasopressin	1083.4	8.2
[ile]-angiotensin	896.5	9.4
bradykinin fragment 1-5	572.3	10.6

Tableau 5 : Caractéristiques des peptides étudiés

1.2. Peptides issus de digestions tryptiques de protéines

Des mélanges complexes de peptides ont été obtenus après digestion enzymatique de protéines à l'aide de la trypsine. L'albumine de sérum bovin (BSA), le lysozyme et la myoglobine ont été mélangées (noté mélange de 3 protéines) afin d'obtenir après digestion un mélange de 115 peptides [4]. Un mélange de 6 protéines comprenant la BSA, l'HSA, le lysozyme, la myoglobine, le cytochrome C et la β-caséine a aussi fait l'objet d'une digestion. Celle-ci conduit à un mélange de 196 peptides [4].

Les différentes étapes de la digestion sont présentées Fig. 8. Les réactifs ont tous été fournis par Sigma Aldrich.

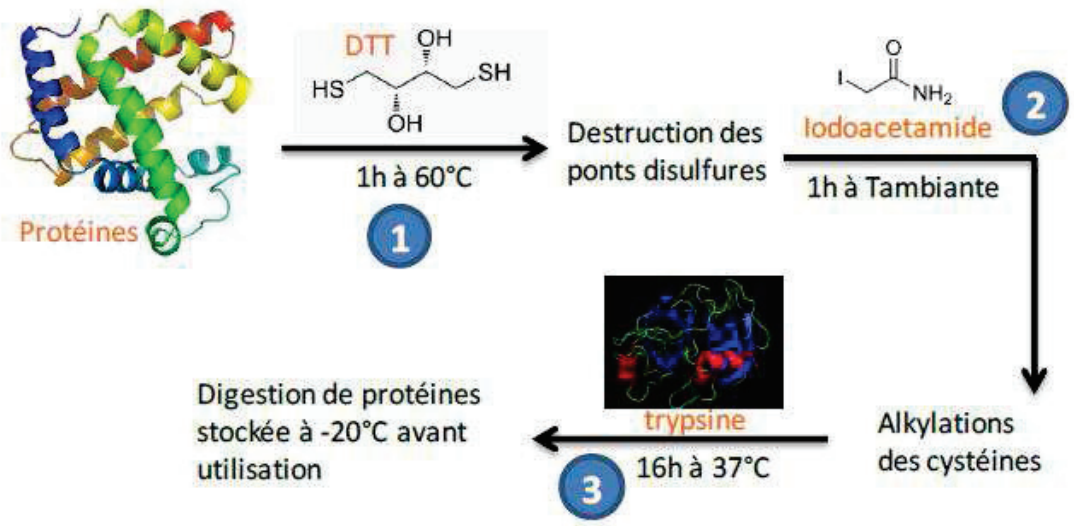

Figure 8 : Procédure de digestion tryptique de protéines [1]

Le protocole complet est le suivant [1] : 35 mg de protéines sont mis à réagir avec 0.5 mL d'une solution de dithiothréitol (DTT) dans l'eau à 20 mM. Pour la deuxième étape, 0.5 mL d'une solution d'iodoacétamide à 20 mM est ajouté. La trypsine est solubilisée dans une solution de HCA (hydrogénocarbonate d'ammonium) à 20 mM à la teneur de 1 mg/mL. 0.5 mL de cette solution est ajouté au milieu réactionnel. Un volume total de digestion de 1.5 mL est ainsi obtenu. Le milieu réactionnel est chauffé dans un système thermomixer (Eppendorf) lors des étapes 1 et 3.

Des aliquots sont ensuite conservés au congélateur à -20°C dans des tubes coniques en plastique. Les aliquots sont ensuite décongelés selon le besoin, filtrés sur 0.22 µm et les solutions diluées sont préparées dans des flacons HPLC en plastiques pour éviter les adsorptions sur le verre. Ces solutions sont ensuite conservées à 4°C dans le passeur du système chromatographique ou au réfrigérateur. La longueur d'onde de détection UV est de 210 nm.

2. Biomolécules

2.1. Anticorps monoclonal (mAb)

Le Brentuximab B, a été fourni par les Laboratoires Pierre Fabre. Sa concentration est de 2 mg/mL. Il est stocké à 4 °C. La longueur d'onde de détection est 280 nm.

2.2. Anticorps conjugué (ADC)

Un ADC à cystéine, le Brentuximab Vedotin (Adcetris®), commercialisé par Seattle Genetics et fourni par les Laboratoires Pierre Fabre à une concentration de 5 mg/mL a été analysé. La longueur d'onde de détection est 280 nm.

3. Molécules neutres

3.1. Composés standards

12 composés ont été sélectionnés à partir des travaux de Le Masle et al. [5] afin d'être représentatif d'un échantillon complexe de bio-huile.

	Composé	Famille chimique	Formule brute	MW (g/mol)	log P
1	α-angelica lactone	lactone	$C_5H_6O_2$	98.10	0.236
2	2-phenylethanol	alcohol	$C_8H_{10}O$	122.16	1.504
3	5-methylfurfural	furane	$C_6H_6O_2$	110.11	0.670
4	phenol	phenol	C_6H_6O	94.11	1.50
5	o-cresol	phenol	C_7H_8O	108.14	1.962
6	m-cresol	phenol	C_7H_8O	108.14	2.043
7	2,4,6-trimethylphenol	phenol	$C_9H_{12}O$	136.19	2.935
8	α-hydroxycumene	phenol	$C_9H_{12}O$	136.19	2.861
9	guaiacol	guaiacol	$C_7H_8O_2$	124.14	1.341
10	syringol	syringol	$C_8H_{10}O_3$	154.16	1.218
11	1-indanone	enone	C_9H_8O	132.16	1.419
12	anisole	éther aromatique	C_7H_8O	108.14	2.170

Tableau 6 : Propriétés physico-chimiques de composés représentatifs de la bio-huile

3.2. Bio-huile

La partie aqueuse d'une bio-huile a été fournie par l'IFPEN et analysée tel quel.

E. OUTILS DE CALCULS ET DE TRAITEMENT DES DONNÉES

1. Optimisation de méthodes LCxLC

Les calculs effectués dans le cadre de l'optimisation de méthodes RPLCxRPLC pour la séparation de peptides (chapitre 3) sont réalisés à l'aide d'une feuille de calcul Excel développée au laboratoire.

2. Données 1D

Les données acquises en 1D-LC ou 1D-SFC ont été traitées sur le logiciel dédié à l'instrument ou sur Excel après exportation des données brutes.

3. Données 2D

Une analyse bidimensionnelle génère un nombre très important de données. En effet, leur représentation s'effectue selon trois dimensions, le temps de rétention

dans chacune des dimensions et le signal du détecteur, mais les données sont obtenues sous forme matricielle. Le traitement de ces données est donc complexe.

- Généralement, le détecteur en sortie de seconde dimension enregistre le signal en continu pendant toute la durée de l'analyse (temps de séparation de la première dimension). Le chromatogramme de deuxième dimension correspond ainsi à la succession de toutes les injections envoyées en seconde dimension (à chaque rotation de vanne). Ce chromatogramme peut alors être fractionné. Les fractions sont réalignées si besoin et superposées pour permettre l'interprétation des résultats (Fig. 9). Une macro Excel développée au laboratoire réalise ces différentes étapes.

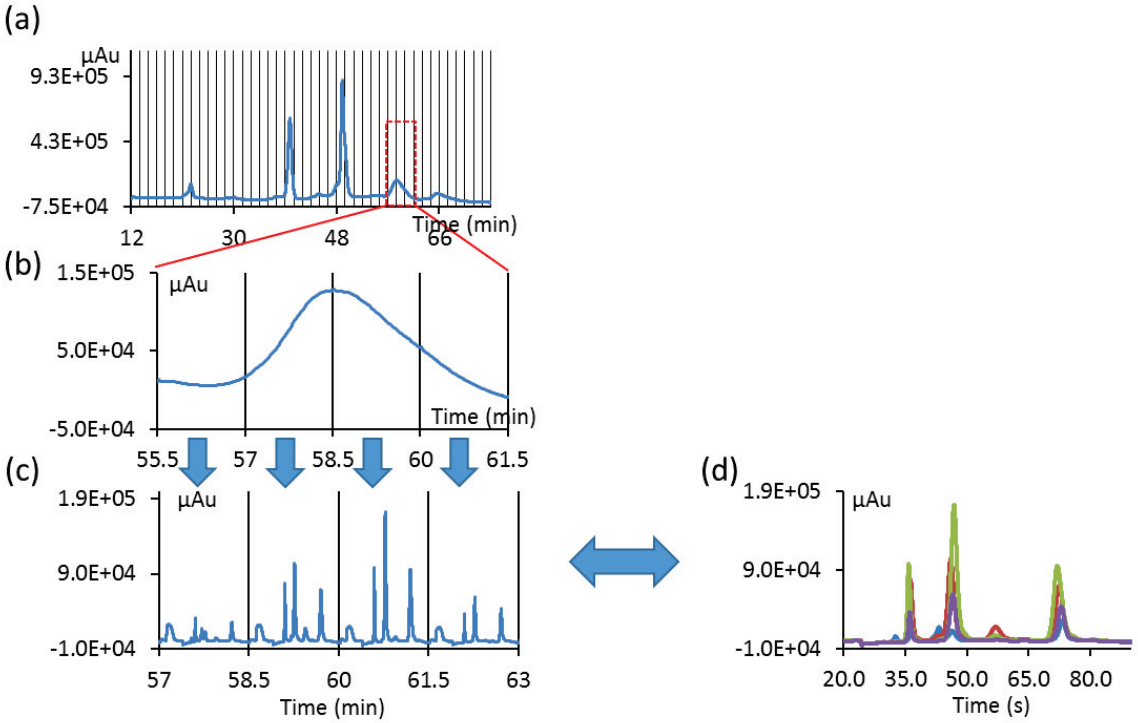

Figure 9 : Illustration du traitement des données 2D. Chaque fraction du chromatogramme ^{1}D (a,b) est analysée générant un chromatogramme unique de ^{2}D (c) dont les fractions sont ensuite superposées (d).

- Les données peuvent être visualisées sous forme de « contour plot » ou de représentation 3D (Fig. 10). Ces types de représentations sont réalisés sous Matlab grâce à un programme développé au laboratoire.

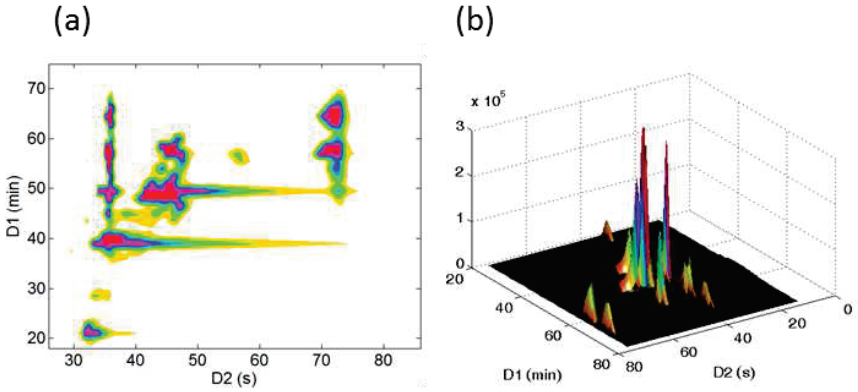

Figure 10 : Représentation d'une analyse 2D par (a) un contour plot et (b) 3D-plot

Bien que des logiciels de représentation de données LCxLC soient commercialement disponibles, des progrès restent nécessaires pour une utilisation plus routinière de l'exploitation des données. De plus, leur utilisation quels que soient les formats de données générées selon les différents fournisseurs reste problématique.

4. Analyse des biomolécules

Le logiciel MaxEnt® (Waters) permettant l'obtention de la masse monoisotopique d'une protéine après déconvolution des spectres MS a été utilisé. En effet, une protéine de plusieurs dizaines de kDa peut générer une série de 10-20 pics correspondants à différents états de charge. Un outil d'aide pour le calcul de la masse d'une telle molécule est donc intéressant. La Figure 11 décrit de façon simplifiée le travail de l'algorithme et le résultat obtenu.

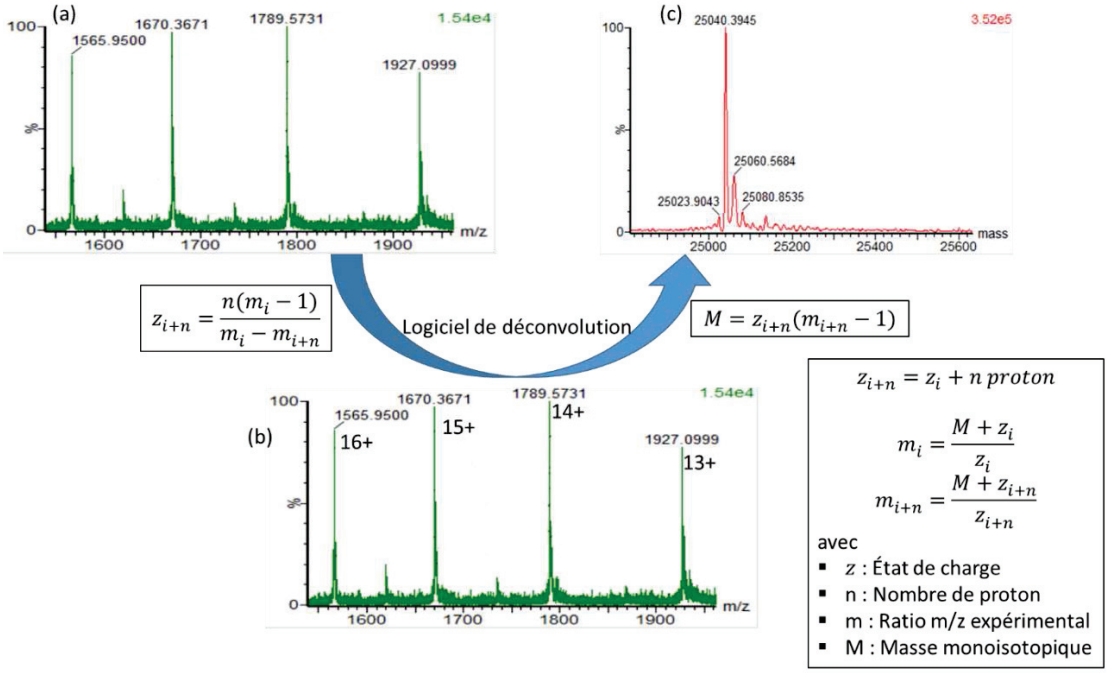

Figure 11 : Obtention de la masse monoisotopique d'une protéine à partir du calcul de ses états de charges. (a) le spectre de masse, (b) l'obtention du nombre d'états de charges et (c) le calcul de la masse monoisotopique

RÉFÉRENCES

[1] A. D'Attoma, Thesis, University of Lyon, 2013.

[2] F. Gritti, G. Guiochon, Accurate measurements of peak variances: Importance of this accuracy in the determination of the true corrected plate heights of chromatographic columns, J. Chromatogr. A. 1218 (2011) 4452–4461. doi:10.1016/j.chroma.2011.05.035.

[3] A. van der Horst, P.J. Schoenmakers, Comprehensive two-dimensional liquid chromatography of polymers, J. Chromatogr. A. 1000 (2003) 693–709. doi:10.1016/S0021-9673(03)00495-3.

[4] PeptideCutter, (n.d.). http://web.expasy.org/peptide_cutter/ (accessed April 6, 2016).

[5] A. Le Masle, D. Angot, C. Gouin, A. D'Attoma, J. Ponthus, A. Quignard, S. Heinisch, Development of on-line comprehensive two-dimensional liquid chromatography method for the separation of biomass compounds, J. Chromatogr. A. 1340 (2014) 90–98. doi:10.1016/j.chroma.2014.03.020.

CHAPITRE 3 – OPTIMISATION DE MÉTHODES RPLCXRPLC EN LIGNE : APPLICATION À UN MÉLANGE COMPLEXE DE PEPTIDES

Ce chapitre a fait l'objet de deux publications :

Article 2

"Optimization of conditions in on-line comprehensive two-dimensional reversed phase liquid chromatography. Experimental comparison with one-dimensional reversed phase liquid chromatography for the separation of peptides";

M. Sarrut, A. D'Attoma, S. Heinisch, J. Chromatogr. A. 1421 (2015) 48–59. doi:10.1016/j.chroma.2015.08.052.

Article 3

"Comparison of optimized sub-one hour separations between one dimensional and on-line comprehensive two-dimensional liquid chromatography for peptide mapping";

M. Sarrut, F. Rouvière, S. Heinisch, J. Chromatogr. A, (2016), to be submitted

INTRODUCTION

Une méthode de chromatographie en phase liquide se doit de répondre à plusieurs critères. Le chromatographiste doit trouver le meilleur compromis entre des objectifs contradictoires que sont (i) maximiser la capacité de pics, (ii) minimiser le temps d'analyse et (iii) maximiser la sensibilité de la méthode. En 1D-LC, et plus particulièrement en RPLC, il existe des logiciels d'aide au développement qui permettent de modéliser le comportement des molécules pour finalement définir les meilleures conditions de séparations.

En LCxLC, le nombre de paramètres influençant la qualité de la séparation, le temps d'analyse et le facteur de dilution de la méthode augmente considérablement. Trouver le meilleur compromis entre ces différents objectifs ne peut pas s'effectuer sans utiliser des modèles prédictifs afin de tenir compte de toutes les répercussions possibles provenant de la modification d'un ou plusieurs paramètres (pente du gradient, temps de délai, volume injecté, etc…).

La section A de ce chapitre propose, sous forme d'article, une approche pour l'optimisation de séparations RPLCxRPLC en ligne basée sur le modèle LSS (Linear Solvent Strength) et une méthode Pareto-optimale. Cette méthodologie est ensuite appliquée à un échantillon complexe de peptides. Les performances obtenues en RPLCxRPLC pour trois temps d'analyses (60, 120 et 200 min) sont comparées avec les meilleures performances connues en 1D-RPLC.

La section B approfondit la comparaison entre 1D-RPLC et RPLCxRPLC pour la séparation de mélanges complexes de peptides pour des temps d'analyses inférieurs à 60 min tout en affinant la méthodologie d'optimisation. Le temps au bout duquel une analyse 2D surpasse une analyse 1D d'un point de vue de la capacité de pics est discuté. Une comparaison entre ces deux techniques couplées à la spectrométrie de masse est effectuée.

A. OPTIMISATION DE MÉTHODES RPLCXRPLC EN LIGNE. COMPARAISON DES PERFORMANCES EXPÉRIMENTALES AVEC LA 1D-RPLC POUR LA SÉPARATIONS DE MÉLANGES COMPLEXES DE PEPTIDES

Article 2

"Optimization of conditions in on-line comprehensive two-dimensional reversed phase liquid chromatography. Experimental comparison with one-dimensional reversed phase liquid chromatography for the separation of peptides";

M. Sarrut, A. D'Attoma, S. Heinisch, J. Chromatogr. A. 1421 (2015) 48–59. doi:10.1016/j.chroma.2015.08.052.

Journal of Chromatography A, 1421 (2015) 48–59

Contents lists available at ScienceDirect

Journal of Chromatography A

journal homepage: www.elsevier.com/locate/chroma

Optimization of conditions in on-line comprehensive two-dimensional reversed phase liquid chromatography. Experimental comparison with one-dimensional reversed phase liquid chromatography for the separation of peptides

Morgan Sarrut, Amélie D'Attoma, Sabine Heinisch*

Université de Lyon, Institut des Sciences Analytiques, UMR CNRS UCBL ENS 5280, 5 rue de la Doua, 69100 Villeurbanne, France

ARTICLE INFO

Article history:
Received 15 July 2015
Received in revised form 24 August 2015
Accepted 25 August 2015
Available online 29 August 2015

Keywords:
Comprehensive two-dimensional liquid chromatography
2D-LC
RPLC × RPLC
Peptides
Protein digest
LC × LC optimization

ABSTRACT

Comprehensive on-line two-dimensional liquid chromatography is an attractive technique to enhance peak capacity and deal with complex samples. Yet, its optimization is not straightforward and requires to take into account a huge number of parameters to finally obtain a good compromise between different criteria which are often conflicting. In this study, we propose a procedure for RPLC × RPLC separations able to define, for a given analysis time, the optimized LC × LC parameters for achieving the best compromise between high peak capacity and low dilution. This procedure makes use of both a prediction tool based on theoretical relationships and a Pareto-optimality approach to optimize these two criteria. The possibility to split the flow-rate of the first dimension before the interface is taken into account as well as the focusing effect in the second dimension. This optimization procedure is applied to the prediction of optimized conditions for the separation of peptides. The need for very short and efficient columns (typically 30 mm as column length and 1.3 μm as particle diameter) in the second dimension is clearly established whatever the geometry of the first dimension column. Furthermore it is shown that several sets of quite different conditions in the first dimension can lead to similar results and hence that additional quality descriptors are required to make a decision. RPLC × RPLC separations of a protein digest were carried out and the obtained results were found in very good accordance with the predicted ones. Our results were compared to the top results reported in the literature for 1D-RPLC separations of peptides. More than 4-fold increase in peak capacity (5100 vs 1150) at 200 min has been obtained. Furthermore a 40-fold gain in analysis time (1 h vs 40 h) was obtained for achieving 1800 as effective peak capacity which is close to the highest peak capacity reported in 1D-RPLC for the separation of peptides.

1. Introduction

On-line comprehensive two-dimensional liquid chromatography (LC × LC) is a powerful technique to achieve very high peak capacity. Its great advantage over conventional one-dimensional techniques for separating very complex samples such as protein digests has been highlighted by a large amount of papers and very recent reviews continue to deal with this topic [1–3]. Despite its great potential, the optimization of LC × LC conditions is not straightforward. It requires to take into account a huge amount of parameters while considering (i) conflicting goals (enhancing peak capacity while reducing both analysis time and sample dilution) (ii) instrumental limits in term of pressure, flow-rate, column length, column temperature and dwell time and (iii) mobile phase compatibility since a weak solvent in ^{1}D could become a strong solvent in ^{2}D, thereby leading to serious deterioration of peak shapes. It is therefore of major importance to find a way to make the situation less complex.

When a few compounds are to be separated, optimization software based on either theoretical or empirical relationships can be used by the analyst to optimize simultaneously different parameters while considering quality descriptors such as the resolution between the different pairs of compounds and the analysis time. Yet additional quality descriptors such as robustness and/or sensitivity and/or analysis cost can be considered. In this case, in addition to reliable relationships able to relate retention to chromatographic conditions, the optimization methodology requires suitable multi criteria decision making approach [4]. Pareto-optimality approach

* Corresponding author. Tel.: +33 437 423 551.
E-mail address: sabine.heinisch@univ-lyon1.fr (S. Heinisch).

http://dx.doi.org/10.1016/j.chroma.2015.08.052
0021-9673/

is an interesting method to optimize two different conflicting criteria [5]. As underlined by Vanbel and Schoenmakers [4], the key advantage of the Pareto approach is that it provides the chromatographer with multiple sets of conditions leading to the same results so that he can decide which of the Pareto-optimal points is the best. For complex samples, a gradient elution is used and the separation power is usually assessed by the peak capacity [6] while the analysis time can be described by the gradient time. The separation system (mobile phase and stationary phase) must be first properly selected in term of selectivity. Peak capacity and analysis time can then be optimized by means of the so-called Kinetic Plot Method (KPM) [7,8] applied to gradient elution [9,10]. KPM which is also a Pareto-optimality method in its concept requires reliable relationships to describe the two quality descriptors as a function of the chromatographic parameters.

In LC × LC, the problem is far more complex since, in addition to thermodynamic parameters (stationary phase, mobile phase and temperature in both dimensions) a huge number of kinetic parameters affect the quality of the analysis, including gradient conditions, sampling rate, column dimensions, flow splitting, etc. All these parameters are interconnected and are likely to affect significantly the quality of the 2D-separation. The difficulty of on-line LC × LC optimization is highlighted in Fig. 1 with all LC × LC conditions related to the main quality descriptors via intermediate parameters. This graphic which represents the multiple interactions between the different parameters, points out at a glance the complexity of the problem and the difficulty to take into account all these interactions simultaneously. It can be compared to the famous circle of interactions proposed by Bounine for 1D-LC separations [11]. The different relationships involved in Fig. 1 are more detailed in next theoretical section. Obviously, in LC × LC the problem has to be simplified and some parameters must be defined at first. Methods dealing with multiple criteria and supporting LC × LC optimization have been recently reviewed [12]. Two studies using KPM were reported [13,14]. As highlighted [12], the dilution factor has been often ignored whereas its increase during the separation process can be tremendous. Pareto-optimality approach was recently applied for the first time by Vivo-Truyols et al. [15,16] to the optimization of LC × LC separations. They considered both analysis time and effective peak capacity as criteria. They also proposed an extension of this approach with a view to find a good compromise between short analysis time, low dilution and high effective peak capacity. To achieve this, they used theoretical equations relating the peak capacity, the analysis time and the dilution factor to the considered LC × LC parameters. Whereas many theoretical studies have pointed out some guidelines to achieve correct LC × LC separations [14,17,18], no study has so far confirmed the theoretical approach by experimental results.

In this study, we propose a procedure that optimizes all the kinetic parameters arranged on the circumference of the circle presented in Fig. 1 except (i) the thermodynamic ones (stationary phases and mobile phases) which determines the degree of orthogonality of the 2D-system and (ii) the sampling rate which can be defined prior to optimizing. In particular, the optimized parameters include the flow-rate in the first dimension and the split ratio. The thermodynamic parameters (i.e. LC-systems for both dimensions) were defined in previous studies for the separation of peptides [19,20]. The Pareto-optimality approach was applied to define optimized sets of conditions considering both effective peak capacity and dilution factor as quality descriptors at three different analysis times (60 min, 120 min and 200 min). The objectives of this study were (i) to determine the most relevant parameters in RPLC × RPLC for the separation of peptides (ii) to validate our predicted optimized results by means of experimental RPLC × RPLC separations; (iii) to emphasize the advantage of very short and very efficient columns for performing 2D-LC within a relatively short analysis time (≤200 min); (iv) to compare our optimized 2D-LC separations to the top published 1D-LC separations of peptides.

2. Theoretical considerations

2.1. Effective peak capacity

The effective peak capacity in RPLC × RPLC can be predicted using the theoretical relationships [15] listed below

$$n_{2D,effective} = \alpha \cdot \beta \cdot \gamma \cdot {}^1n \cdot {}^2n \tag{1}$$

where ${}^1n$ and ${}^2n$ are the peak capacities in the first and second dimension, respectively. In RPLC, the peak capacity, n, can be calculated according to [6]

$$n = 1 + \frac{\sqrt{N}}{4} \cdot \frac{1}{2.3b+1} \ln\left(\frac{2.3b+1}{2.3b} e^{2.3S\cdot\Delta c_e} - \frac{1}{2.3b}\right) \tag{2}$$

As shown by Eq. (2), the peak capacity calculation requires the knowledge of (i) ΔC_e, the range of compositions at elution covered by the sample); (ii) S, the average value of the slope of the relationship between the logarithm of the retention factor and the solvent composition; (iii) N, the column plate number and (iv) b, the Linear Solvent Strength (LSS) gradient steepness ($S\,\Delta C(t_0/t_G)$ [21], t_0 and t_G being the column dead time and the gradient time respectively).

In Eq. (1), α, β and γ are coefficient factors lower than 1. They operate as follows:

α corrects ${}^1n$ due to undersampling. It is calculated from [22]

$$\alpha = \frac{1}{\sqrt{1 + 0.21(6/\tau)^2}} \tag{3}$$

where τ is the sampling rate (number of fractions sent to ^{2}D per 6σ peak width in ^{1}D).

γ takes into account the retention surface coverage which depends on the degree of orthogonality between both RPLC systems. Its value can be determined according to preliminary studies on the degree of orthogonality [19].

β corrects ${}^2n$ due to non-ideal transfer of the sample fraction from ^{1}D to ^{2}D. Indeed, there may be significant peak distortion if large fractions of ^{1}D are injected in ^{2}D. The effect of large injection volumes on peak variance has been studied for a long time [23]. β, can be expressed as:

$$\beta = \frac{1}{\sqrt{1 + (1/\delta_i^2) \times ({}^2V_i^2/{}^2\sigma_{v,col}^2) \times (1/C_F^2)}} \tag{4}$$

where δ_i^2 is dependent on the injection process (equal to 12 for plug injection and close to 3–4 in practice). ${}^2\sigma_{v,col}^2$ is the peak variance in volume units resulting from peak band broadening in the ^{2}D column and ${}^2V_i$ is the injected volume in ^{2}D and C_F is the so-called compression factor [24] or focusing factor [15]. In Eq. (4), the contribution of other extra-column volumes to peak dispersion was neglected. This omission is correct as long as the contribution of the injection process is predominant.

C_F is related to the two solute retention factors in ^{2}D, ${}^2k_{e,1}$ with ^{1}D mobile phase at elution and ${}^2k_{e,2}$ with ^{2}D mobile phase at elution [15,24,25]. The compression factor is high (>1) if the injection solvent in the transferred fraction is weaker than the mobile phase at peak elution and low otherwise (<1). It is equal to unity if the eluent strength of injection solvent and mobile phase are the same. The most usual equation for C_F is given by [15,24,26,27]

$$C_F = \frac{1 + {}^2k_{e,1}}{1 + {}^2k_{e,2}} \tag{5}$$

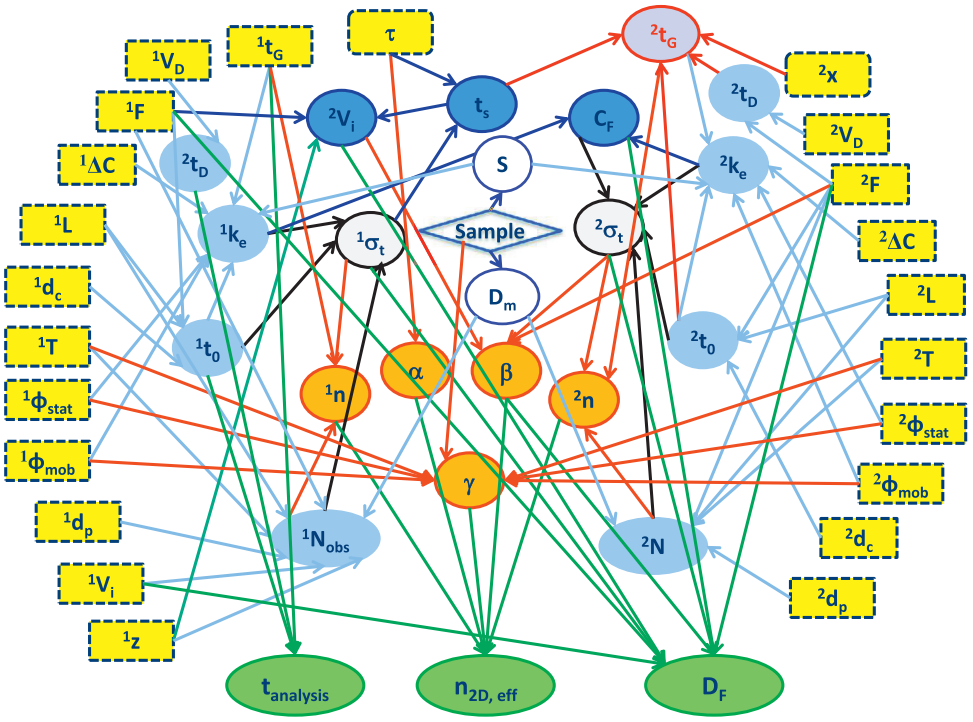

Fig. 1. Schematic representation of the complex interactions between conditions, intermediate parameters and criteria in on-line LC × LC. A glossary of abbreviations is given in Table 1. Parameters (with ^{1} and ^{2} corresponding to first and second dimension, respectively): V_D: System dwell volume; t_G: Gradient time; t_D: Column dwell time; $t_{analysis}$: Analysis time; t_s: Sampling time; t_0: Column dead time; F: Flow rate; ΔC: Gradient composition range; φ_{stat}: Stationary phase; φ_{mob}: Mobile phase; T: Column temperature; d_c: Column internal diameter; d_p: Particle diameter; D_m: Diffusion coefficient; V_i: Injection Volume; τ: Sampling rate; ^2x: number of column volumes for equilibration; k_e: Retention factor at elution; n: One-dimensional peak capacity; $n_{2D,eff}$: Two-dimensional effective peak capacity; N_{obs}: Observed column plate number; N: Column plate number; σ_t: Peak width in time unit; C_F: Compression factor; S: Average slope of the relatonship between the logarithm of the retention factor and the stronger solvent composition; α, β and γ: Correction factors due to undersampling, non ideal transfer from the 1st to the 2nd dimension and retention surface coverage, respectively; D_F: Dilution factor; z: Split ratio.

However, it was recently shown that, for very steep gradients (very low $^2k_{e,2}$ values) and/or very strong injection solvent (very low $^2k_{e,1}$ values), C_F was more correctly described by [21,22]

$$C_F = \frac{^2k_{e,1}}{^2k_{e,2}} \tag{6}$$

In RPLC × RPLC, assuming a LSS behavior [21] and similar retention in both systems (i.e. $^2k_{e,1}$ close to $^1k_{e,1}$), the compression factor can be approximated by

$$C_F = \frac{^2S}{^1S} \tag{7}$$

where ^1s and ^2s are the normalized gradient slopes in ^{1}D and ^{2}D, respectively.

^2V_i is related to the total peak standard deviation (in volume units) in ^{1}D, $^1\sigma_{v,total}$, the sampling rate, t_s, and the split ratio, ^1z, potentially designed for reducing the flow-rate entering ^{2}D ($0 < {}^1z \leq 1$) [30]:

$$^2V_i = \frac{6 \cdot {}^1\sigma_{v,total}}{\tau} \cdot {}^1z = t_s \cdot {}^1F \cdot {}^1z \tag{8}$$

The combination of Eqs. (4) and (8) yields:

$$\beta = \frac{1}{\sqrt{1 + (36 \cdot {}^1z^2/\tau^2 \cdot \delta_i^2) \times ({}^1\sigma^2_{v,total}/{}^2\sigma^2_{v,col}) \times (1/C_F^2)}} \tag{9}$$

From Eq. (9), it clearly appears that β can be tuned or maintained to an acceptable value (for example > 0.9 which means that less than 10% of the peak capacity is lost in ^{2}D as a result of injection effect) by various means. For a given sampling rate and a given ^1t_G, increasing β can be achieved by

(i) increasing the compression factor. In RPLC × RPLC, this can be obtained with relative smooth gradient in ^{1}D (by increasing ^1F) and much steeper gradient in ^{2}D and/or with more retentive stationary phase in ^{2}D than that in ^{1}D.
(ii) decreasing the ratio $^1\sigma_{v,total}/{}^2\sigma_{v,col}$ ($^1d_c < {}^2d_c$).
(iii) decreasing $^1\sigma_{v,total}$, (by decreasing ^1F).
(iv) increasing $^2\sigma_{v,col}$ (by increasing ^2L and/or by using less steep gradients).
(v) decreasing the split ratio ($^1z < 1$) which may lead to additional extra-column band broadening.

2.2. Dilution factor

The dilution factor is often considered as the product of the dilution factors in both dimensions [31]. The dilution factor in ^{2}D can be expressed as

$$^2D_F = \frac{\sqrt{2\pi}}{\beta} \times \frac{^2\sigma_{v,col}}{^2V_i} \tag{10}$$

Combining Eqs. (4) and (8) yields

$$^2D_F = \frac{\sqrt{2\pi}}{\delta_i \cdot \sqrt{1-\beta^2}} \times \frac{1}{C_F} \tag{11}$$

Maximizing peak capacity (β close to 1) is conflicting with minimizing dilution (β close to 0) as pointed out by Eqs. (1) and (11), respectively. However for a given β value, Eq. (11) shows that ^2D_F becomes dependent on the compression factor only. An additional pump can be used in order to dilute the ^{1}D mobile phase with water thereby increasing the compression factor in RPLC [32].

It is clear from the theoretical discussion above that some decisions may have opposite effects and that a good compromise has

to be found which must be supported by an accurate knowledge of the impact of LC × LC conditions on the intermediate parameters shown in Fig. 1.

2.3. Analysis time

The analysis time in ^{1}D represents the total analysis time of the 2D-separation. It can be approximated by the gradient time in ^{1}D, assuming that both dwell time and column dead time to be negligible.

The analysis time in ^{2}D is the sampling time, t_s. It can be calculated via Eq. (8):

$$t_s = \frac{6 \cdot {}^1\sigma_{v,total}}{\tau \cdot {}^1F} \quad (12)$$

The gradient time in ^{2}D can be deduced from the sampling time with

$${}^2t_G = t_s - {}^2t_0 \times \left(\frac{{}^2V_{D,total}}{{}^2V_0} + (1+x) \right) \quad (13)$$

where x is the number of column volume required for column equilibration and $^2V_{D,total}$ is the total dwell volume, dependent on the loop volume and hence on the injected volume in ^{2}D. It can be expressed as

$${}^2V_{D,total} = {}^2V_{D,instrument} + \lambda \cdot t_s \cdot {}^1F \cdot {}^1z \quad (14)$$

where $^2V_{D,instrument}$ is the specific instrument dwell volume and λ, a factor which defined the volume of the required sample loop in view of the injected volume (see Eq. (8)). A value from 1.5 to 2 is sufficient to avoid sample loss during the sample loop filling time.

The peak capacity ^2n increases with $^2t_G/^2t_0$. As a consequence of Eq. (12), $^2t_G/^2t_0$ is positive and hence the related optimized conditions are realistic provided that

$$\frac{t_s}{{}^2t_0} \gg \frac{{}^2V_{D,total}}{{}^2V_0} + 1 + x \quad (15)$$

Eq. (15) emphasizes the absolute necessity of considering both column equilibration and total dwell volume in the optimization strategy.

3. Experimental

3.1. Material and reagents

The gradient runs were performed with different mixtures of water and acetonitrile (ACN). Acetonitrile was HPLC grade from Sigma Aldrich (Steinheim, Germany). Water was obtained from an Elga water purification system (Veolia water STI, Le Plessis Robinson, France). Two types of pH additive were used, formic acid 0.1% (FA) and ammonium acetate 10 mM (AA), both from Sigma Aldrich (Steinheim, Germany). Formic acid was added to both water and ACN. Ammonium acetate was added to water only due to the lack of solubility in organic solvent. Aqueous phases with ammonium acetate were filtered on 0.22 μm nylon filter before use. The six proteins (BSA, HSA, lysozyme, cytochrome C, beta-casein and myoglobin) were purchased from Sigma Aldrich (Steinheim, Germany). A tryptic digest was prepared according to a protocol including denaturation with dithiothreitol (DTT), alkylation with iodoacetamide and digestion with trypsin (mass ratio protein/trypsin of 70). The concentration in each protein was 4 mg/mL. The aliquots were stored at −20 °C. The sample was filtered on 0.22 μm before injection. All reagents for the tryptic digest were obtained from Sigma Aldrich (Steinheim, Germany).

3.2. Columns

Different columns were used in the first dimension (^{1}D): X-Bridge C18 (50 mm × 2.1 mm, 5 μm) from Waters (Milford, MA, USA), Ascentis Express C18 (100 mm × 2.1 mm, 5 μm) and Ascentis Express C18 (50 mm × 2.1 mm, 2.7 μm) both from Sigma-Aldrich (Saint-Louis, MO, USA). The second dimension (^{2}D) column was a Kinetex C18 (30 mm × 2.1 mm, 1.3 μm) from Phenomenex (Torrence, CA, USA).

3.3. Apparatus

The LC × LC system was a 1290 Infinity 2D-LC from Agilent Technologies (Waldbronn, Germany). This instrument includes two high-pressure binary solvent delivery pumps, an autosampler with a flow-through needle of 20 μL, a column oven with an allowed maximum temperature of 100 °C, a UV detector and a diode array detector equipped with 2 μL and 0.6 μL flow-cells respectively. A 2-position/4-port duo valve was used as interface between the two dimensions. The measured dwell volume was 140 μL and 65 μL for the first and second dimension respectively. It should be noted here that the given dwell volume value of the second dimension does not take into account the size of the loops used between the two dimensions (20, 40 and 80 μL according to the experiments). A total extra-column volume of 22 μL and 8.5 μL and an extra-column variance of 12 μL^2 and 4.5 μL^2 were determined for the first and the second dimension respectively. Dwell volumes, extra-column volumes and extra-column variances were determined using a zero dead volume union connector in place of the column. The methods are described elsewhere [33].

Several parameters were kept identical for all LC × LC experiments. They are listed below:

- The mobile phase in the first dimension was composed of ammonium acetate 10 mM and ACN. The mobile phase in the second dimension was composed of water and ACN both with 0.1% FA.
- The temperature was set at 30 °C and 90 °C for the first and the second dimension, respectively.
- For detection, both detector wavelengths were set at 210 nm. The acquisition rate was set at 5 Hz and 80 Hz for the first and the second dimension, respectively.

Data acquisition and instrumental control were performed by OpenLab software (Agilent). 2D-data were exported to Microsoft Excel and Matlab V7.12.0635 to construct a matrix via calculation tool enabling the construction of 2D-contour plots.

3.4. Calculations

The chosen values used in this study are summarized in Table 1. All optimization calculations were performed using an Excel spreadsheet and appropriate home-made routines.

Predicted effective peak capacities were calculated according to Eqs. (1)–(9) with a value of 0.6 for γ. β was allowed to vary down to 0.5. Below this value strong peak distortion may occur according to our own results. Column plate heights, ^iH, retention factors at elution, ^ik_e, peak standard deviations, $^i\sigma_{v,col}$, and column pressure drop were calculated from Eqs. (16), (17), (18) and (19):

$${}^iH = a \cdot {}^id_p + \frac{b \cdot {}^iD_m}{{}^iu} + c \cdot \frac{{}^id_p^2}{{}^iD_m} \cdot {}^iu \quad (16)$$

$${}^ik_e = \frac{1}{2.3 \cdot S \cdot {}^is} \quad (17)$$

$${}^i\sigma_{v,col} = \frac{{}^iV_0 \cdot (1 + {}^ik_e)}{\sqrt{{}^iL}} \times \sqrt{{}^iH} \quad (18)$$

Table 1
Chosen values for the optimization procedure.

Name	Symbol	Values	Equation
H coefficients (porous)	(a, b, c)	(0.6; 7.0; 0.15)	16
H coefficients (superficially porous)	(a, b, c)	(0.5; 3.2; 0.05)	16
Diffusion coefficient at 25 °C in water	D_m	2×10^{-10} m^2/s	16
Total column porosity (for V_0 calculation)	ε_t	0.6 (porous); 0.5 (superficially porous)	
Factor due to the injection process	δ_i^2	3	4; 9; 11
Flow resistance factor	Φ	800	19
Multiplying factor for loop volume	λ	2	14
Number of column volumes for equilibration	X	2.5	13; 15
Gradient steepness	S	0.2	2; 17
Sampling rate	τ	2.5	3; 8; 9; 12
Ratio $^1V_i/^1V_0$	q	0.1	
Maximum pressure in ^{1}D and ^{2}D	ΔP_{max}	900 bar	
Correction factor for surface coverage	γ	0.6	1
Maximum Flow-rate in ^{2}D	$^2F_{max}$	2 mL/min	
Column temperature in ^{1}D	^1T	30 °C	
Column temperature in ^{2}D	^2T	90 °C	
Gradient time in ^{1}D	^1t_G	60 min; 120 min; 200 min	
Range of compositions in ^{1}D	$^1\Delta C_e$	30% (1–31%)	2
Range of compositions in ^{2}D	$^2\Delta C_e$	43% (1–44%)	2
Column diameter in ^{1}D	^1d_c	1 mm; 2.1 mm	
Column diameter in ^{2}D	^2d_c	2.1 mm	
Column length in ^{1}D	^1L	5 cm; 10 cm	
Column length in ^{2}D	^2L	3 cm; 5 cm	
Particle size in ^{1}D	^1d_p	2.7 μm; 5 μm	16; 19
Particle size in ^{2}D	^2d_p	1.3 μm; 1.7 μm	16; 19

$$^i\Delta P_{col} = \phi \frac{^iL \cdot {}^i\eta \cdot {}^iu}{^id_p^2} \quad (19)$$

"i", standing for the dimension number, ^iu, being the linear velocity (L/t_0) and ^is being the normalized gradient slope. Some parameters cannot be controlled. Those include the flow resistance, Φ, the diffusion coefficients, D_m, the gradient steepness, S, assuming a LSS behavior for the gradients in both dimensions, the mobile phase viscosities, η, the coefficients for the plate height equation and the dwell volume in the second dimension. 0.2 as S value and 2×10^{-10} m^2/s as D_m value at 25 °C were found to be average values for peptides with molar weights in the range 500–2000 Da [19,34]. Mobile phase viscosities, were calculated according to a method described elsewhere [35]; (a, b, c) values came from our own results obtained on the selected columns with neutral compounds. They are given in Table 1 for porous and superficially porous stationary phases. The total dwell volume being dependent on the injected volume as discussed in the theoretical section, it was calculated according to Eq. (14). Finally, the dilution factors were calculated according to Eq. (10).

Experimental effective peak capacities were measured according to

$$n_{2D,effective,\exp} = \alpha \cdot \gamma \cdot \frac{^1t_G}{^1w} \cdot \frac{^2t_G}{^2w} \quad (20)$$

with ^1w and ^2w being the average 4σ peak widths in ^{1}D and ^{2}D, respectively, obtained from at least 10 individual peaks. α was calculated according to Eq. (3) and γ was graphically measured according to a method described elsewhere [36].

4. Results and discussion

4.1. Optimization procedure

Whereas the Pareto-optimality approach can provide the analyst with a useful procedure for finding the best compromise between relevant criteria, it is a graphical tool and hence, it is not easy for the chromatographer to handle more than two criteria. Additional criteria must either be fixed before following the optimization procedure or be optimized after the different sets of conditions, located on the same point of the Pareto front, have been established. In the proposed procedure shown in Fig. 2, the analysis time is fixed at first before finding the good compromise between low dilution and high peak capacity. Thus, for given analysis time, the conditions are optimized in such a way that the maximum peak capacity is achieved with the minimum sample dilution. The optimization problem can become very complex when the number of parameters to be optimized increases. As was underlined [15], the number of sets of conditions grows exponentially with the number of conditions. Such a complex situation can give rise to some difficulties to find the good solution. With a view to simplifying the problem, three input levels are suggested in Fig. 2. The chromatographer can choose the level he prefers depending on both available instrumentation and available columns. As a result, at each input level the corresponding parameters and those at the preceding levels are fixed prior to optimization. In our opinion, first parameters should be fixed while second and third parameters can be optimized. First parameters include column temperatures in both dimensions, the column diameter in ^{2}D and the sampling rate. The sampling rate should be between 2 and 3 since it was shown that 2–3 cuts per ^{1}D peak permit a good compromise between the decrease in ^1n_c due to ^{1}D undersampling and the decrease in ^2n_c due to ^{2}D fast gradients [37,38]. The temperature in the second dimension should be as high as possible in order to perform very fast efficient separation in the second dimension. Finally, the column diameter in ^{2}D should be chosen according to the available instrumentation.

Second parameters include column length and particle size in ^{2}D. These parameters are not continuous. Thus, only realistic values should be considered. At this second input level where the ^{2}D-column dimensions are selected, the ^{2}D-flow-rate is fixed in such a way that the maximum allowable pressure can be reached. At the third input level, column dimensions in ^{1}D (column length, particle size and column diameter) are optimized. As stated above, only realistic values are considered. The ratio of the injected volume to the column dead volume (parameter q) can be fixed with a value adapted to the injection solvent conditions. The fourth optimized parameters are continuous and are allowed to vary within a specified range. They include the flow-rate in the first dimension and the split ratio. Whatever the input level, a full Pareto plot

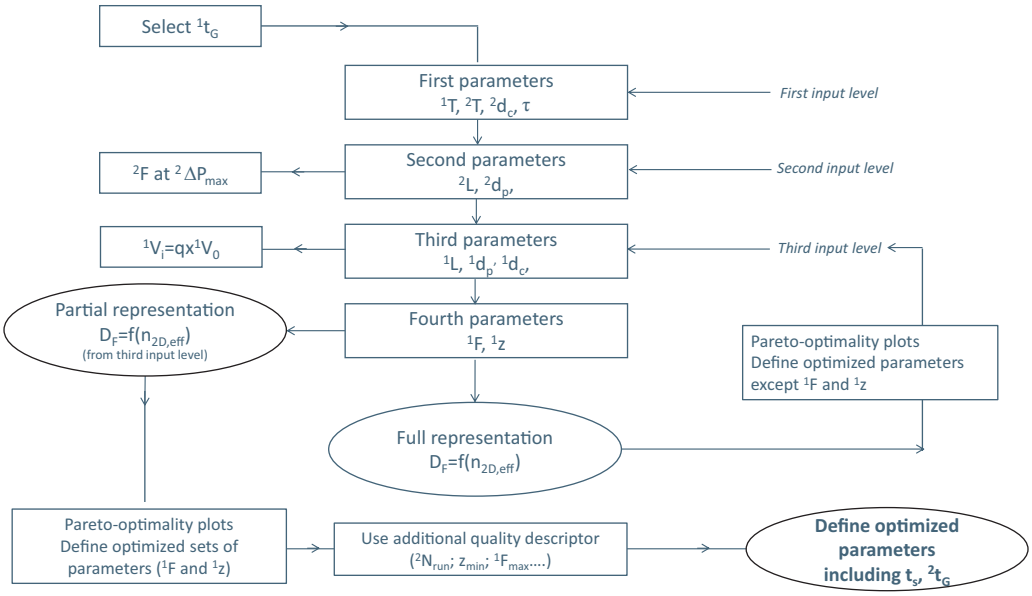

Fig. 2. Procedure for optimizing LC × LC conditions. A glossary of abbreviations is given in Table 1.

can be proposed leading to a preselection of all parameters except ^1F and ^1z. The further construction of a partial Pareto plot with these two continuous parameters is expected to improve the optimization procedure. Finally, additional goals and hence additional quality descriptors may be required to establish a clear difference between the numerous sets of conditions obtained after the Pareto-optimality procedure. The additional goal can be either (i) to minimize the number of runs in the second dimension in order to preserve the column or (ii) to maximize the split ratio thereby avoiding too much dispersion into the split unit or (iii) to prioritize high flow-rates in the first dimension in order to properly meet the gradient specifications of the instrument. At the end of the procedure, a unique set of conditions is established, yielding the sampling time and the gradient time in the second dimension.

It should be noted that although our proposed optimization strategy is quite close to that developed by Vivo-Truyols et al. [15], it differs in several main respects listed below:

(i) The conditions were optimized at fixed analysis time in such a way that the maximum peak capacity was achieved with the minimum sample dilution.
(ii) The sampling rate was fixed prior to optimizing and hence not allowed to vary [16,28,29].
(iii) Splitting of the ^{1}D mobile phase before entering the sample loop of the interface was considered.
(iv) The variation of the total dwell volume in ^{2}D which is dependent on the injection volume and hence on the required loop was taken into account. Similarly, the re-equilibration time depending on the column dead time was also taken into account.
(v) Additional band broadening due to strong injection solvent ($C_F < 1$) as well as focusing effect due to weak injection solvent ($C_F > 1$) were taken into account using Eq. (6) for the compression factor calculation.

4.2. Full Pareto representation

Our objective was to separate peptides in less than 200 min as is mostly requested in on-line LC × LC. All values used for the different parameters are listed in Table 1.

The following conditions were chosen prior to optimizing: (i) fully porous and superficially porous stationary phases were considered in ^{1}D and ^{2}D, respectively; (ii) the temperature in ^{2}D was at the maximum value recommended by the column supplier (i.e. 90 °C) while the temperature in ^{1}D was fixed at 30 °C; (iii) the column internal diameter in ^{2}D was 2.1 mm which is a standard value for current UHPLC instruments; (iv) the sampling rate was fixed at 2.5. As a result, the optimization procedure started at the second input level. The injected volume in the first dimension, ^1V_i, was fixed at 10% of the column dead volume ($^1V_i = 0.1\,^1V_0$) which was found to be appropriate for injected mixtures of peptides containing no organic solvent. The analysis time was assumed to be the gradient time, ^1t_G, in the first dimension (both column dead time and dwell volume in ^{1}D were considered as negligible). The second dimension flow-rate, ^2F was fixed at the maximum allowable column pressure drop (i.e. 900 bar). ^1F and ^1z were allowed to vary within 2 μL/min and 2000 μL/min and within 0.1 and 1, respectively. It is important to note that 0.1 as minimum z value means that the first dimension flow-rate cannot be split more than 10 times. Beyond 10, it was found that the dispersion into the splitting unit might be significant [39].

Three full Pareto-representations were constructed for three different analysis times (60 min, 120 min and 200 min) in such a way that the maximum peak capacity for the separation of peptides was achieved with the minimum sample dilution. The full representations are given in Fig. 3. For sake of clarity, the full representations for the two studied column diameters in ^{1}D (2.1 mm and 1 mm) are displayed separately. Optimum conditions are related to both effective peak capacity and dilution factor values located along the Pareto front. Some instructive conclusions can be raised from Fig. 3. Firstly, as could be expected, an increase in effective peak capacity may be achieved at the expense of longer analysis times and/or higher dilution. For example, considering unity as dilution factor, the optimized effective peak capacity is about 4000, 9000 and 17,000 in 60, 120 and 200 min, respectively. Thus, it seems that, for a given dilution, the effective peak capacity should be doubled if one accept to double the analysis time. Secondly, it appears that 2.1 mm as column diameter in ^{1}D is more attractive than 1 mm since it allows to achieve quite similar effective peak capacities with less dilution thanks to the possibility of flow splitting in ^{1}D and furthermore to peak focusing in ^{2}D. Thirdly, the shortest ^{2}D column lengths (i.e. 30 mm, open symbols in Fig. 3) lead always to the best results. This last result is in very good agreement with numerous studies [13,40,41]. For more convenience, Fig. 4 presents less complex Pareto plots. They were extracted from those

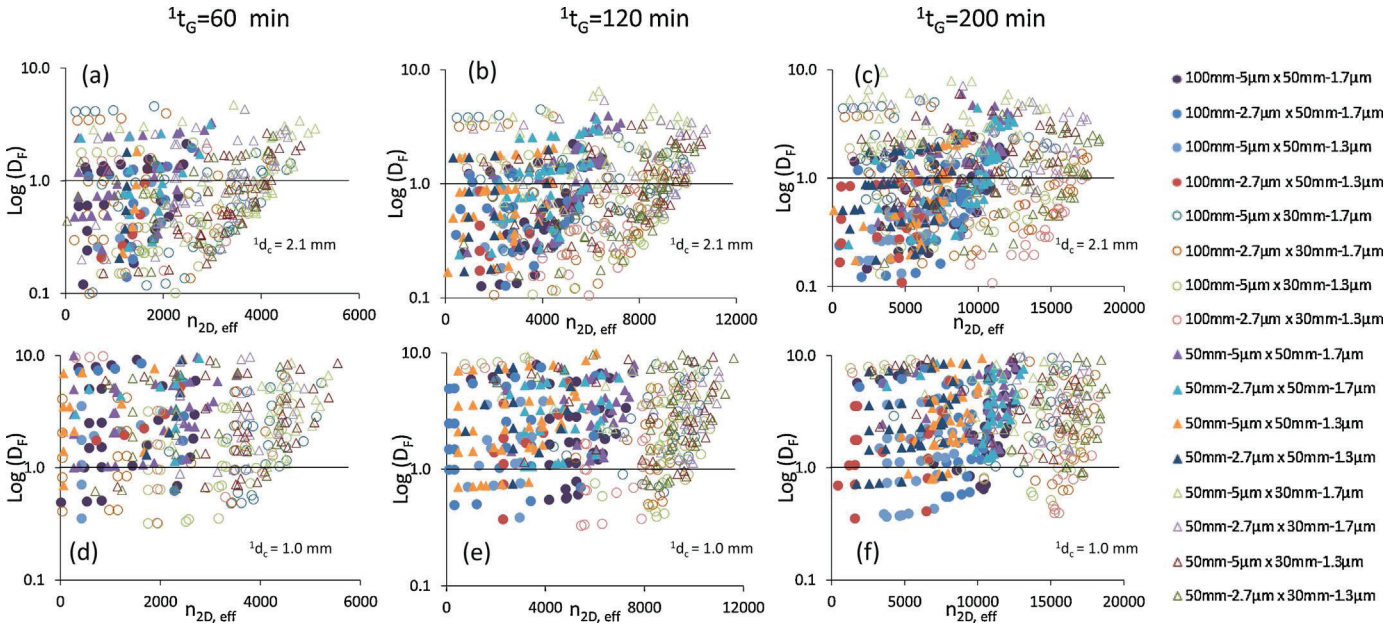

Fig. 3. Full Pareto plots of the predicted dilution factor (D_F) as a function of effective peak capacity ($n_{2D,eff}$) for three gradient times in ^{1}D: (a,d) 60 min, (b,e) 120 min and (c,f) 200 min with two different column diameters in ^{1}D: (a, b, c) 2.1 mm and (d, e, f) 1.0 mm; ^2d_c = 2.1 mm. Circle and triangle correspond to ^1L = 100 mm and ^1L = 50 mm, respectively. Full and open symbols correspond to ^2L = 50 mm and ^2L = 30 mm respectively. The legend is given as ^1L (mm) – $^1d_p \times {}^2L$ (mm) – ^2d_p. For other conditions, see Table 1.

of Fig. 3a–c, with the choice of 2.1 mm as column diameter in ^{1}D and 30 mm as column length in ^{2}D. Fig. 4 highlights the effect of the particle size in ^{2}D (all figures), of the particle size in ^{1}D (Fig. 4a–c vs Fig. 4d–f) and of the column length in ^{1}D (Fig. 4d–f vs Fig. 4g–i). As regards the particle size in ^{2}D, 1.3 µm particles seem to be better than 1.7 µm in most cases in term of both effective peak capacity and dilution, in particular when a 50 mm–5 µm column is used in the first dimension (Fig. 4b and c). 1.7 µm particles allow to reach higher flow-rates and hence higher $^2t_G/^2t_0$ which should lead to higher peak capacities. However, 1.3 µm particles compensate by a better efficiency which yields finally a better peak capacity. Yet, the performance in 60 min is quite similar for both particle sizes

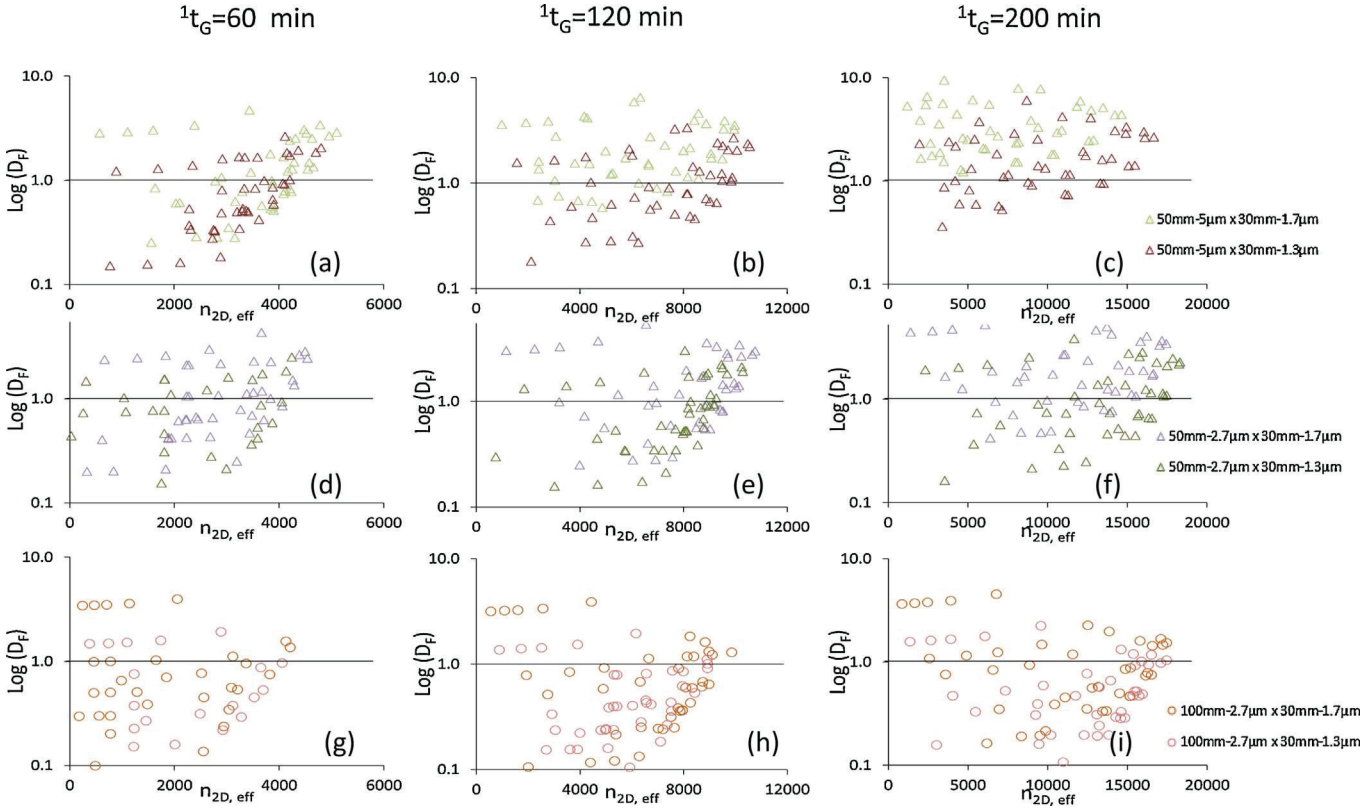

Fig. 4. Simplified representation of the Pareto plots shown in Fig. 3a, b and c with ^1d_c = 2.1 mm and ^2L = 30 mm.

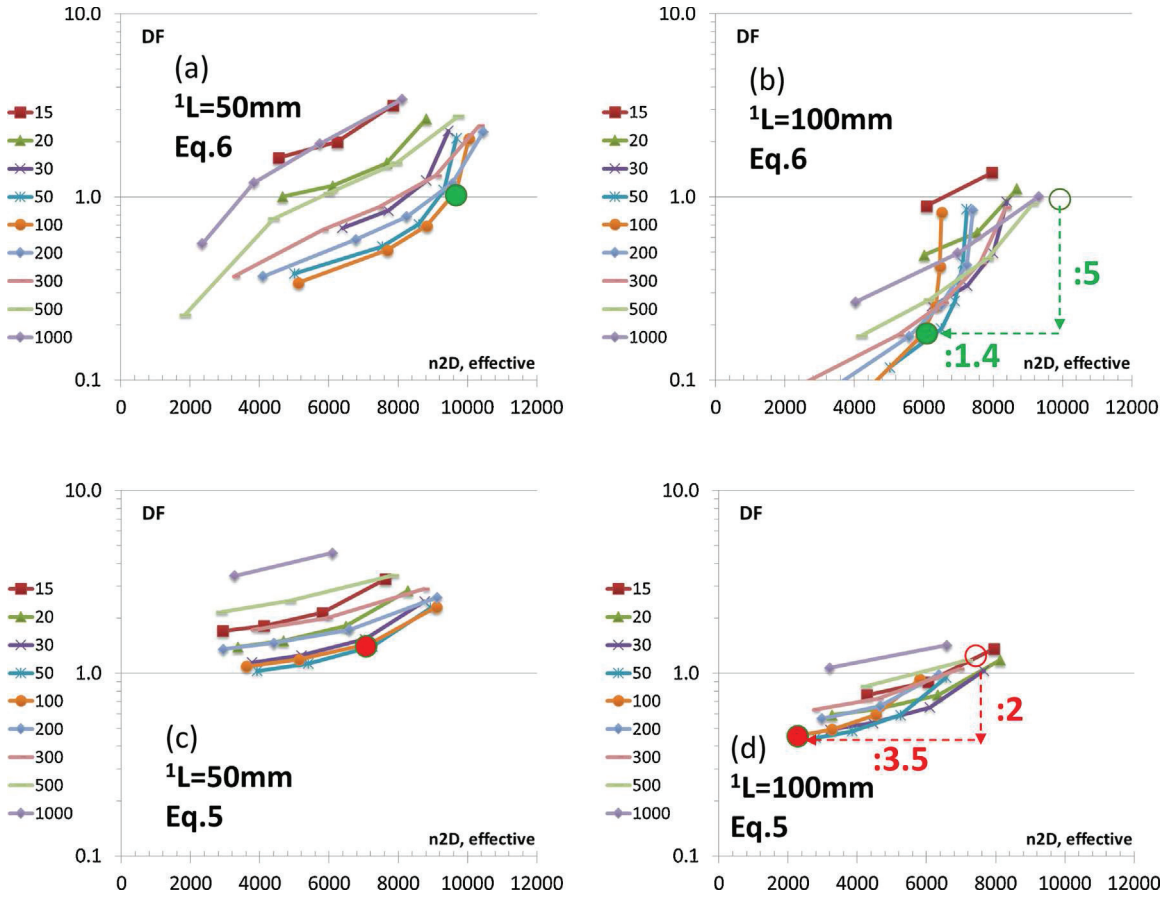

Fig. 5. Partial Pareto curves for different values of z and ${}^{1}F$, obtained for an analysis time of 120 min, with 50 mm (a, c) and 100 mm (b, d) as column length in ^{1}D. Eq. (6) (a, b) and Eq. (5) (c, d) were used for the estimation of the compression factor. The legend is given for different ${}^{1}F$ values in μL/min. Other conditions: ${}^{2}L = 30$ mm; ${}^{2}d_p = 1.3$ μm; ${}^{1}d_p = 5$ μm; ${}^{1}d_c = {}^{2}d_c = 2.1$ mm.

(Fig. 4a, d, g). The use of 5 μm as particle size in ^{1}D does not reduce the ultimate effective peak capacity that can be achieved compared to the use of 2.7 μm but it seems that the dilution is higher in this case, especially for long analysis time (i.e. 200 min). Finally, increasing the column length in ^{1}D is not advantageous in term of peak capacity. However the plots are shifted from top to bottom yielding higher sensitivity (lower dilution) on the Pareto front.

4.3. Application to the experimental RPLC × RPLC separation of peptides

In the light of the above results, it seems that a good choice in ^{2}D for on-line RPLC × RPLC separations of peptides consists in using very short columns packed with very small particles (e.g. ${}^{2}L = 30$ mm and ${}^{2}d_p = 1.3$ μm). In ^{1}D, a column packed with 5 μm particles will be suitable for short analysis times. For longer analysis times (e.g. >120 min), sub-3 μm particles should be preferred. The choice of the column dimensions in ^{1}D depends on whether or not sensitivity is essential. If it is the case, columns with 100 mm as length and 2.1 mm as diameter should be chosen rather than shorter columns and/or thinner columns. It is important to note that this recommendation regarding the column diameter is given by considering 2.1 mm as column diameter in ^{2}D. In any case the column diameter in ^{1}D must be adapted to the column diameter in ^{2}D. However the conclusions could be somewhat different considering another instrument

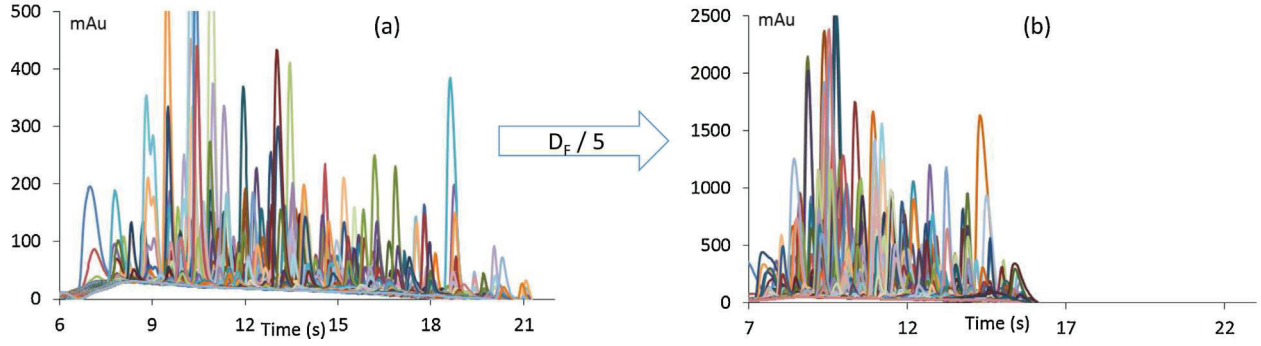

Fig. 6. Overlay of the chromatograms of the second dimension obtained with two on-line RPLC × RPLC separations of peptides performed in 120 min with Pareto-optimum conditions indicated by full circles in Fig. 5. The column lengths in ^{1}D were (a) ${}^{1}L = 50$ mm (b) ${}^{1}L = 100$ mm. Other conditions are given in Table 3 (RPLC × RPLC #3 and RPLC × RPLC #4, respectively).

Table 2
Experimental conditions for the LC × LC separations of a tryptic digest of proteins. Other conditions are given in the text.

	1st dimension (^{1}D)	2nd dimension (^{2}D)	1st dimension (^{1}D)	2nd dimension (^{2}D)
^1t_G = 60 min	#1		#2	
Stationary phase	XBridge C18	Kinetex C18	XBridge C18	Kinetex C18
Column geometry	50 × 2.1 mm, 5 μm	30 × 2.1 mm, 1.3 μm	50 × 2.1 mm, 5 μm	30 × 2.1 mm, 1.3 μm
Flow rate	30 μL/min	1.5 mL/min	500 μL/min	1.5 mL/min
Gradient	1–31% (B) in 60 min	1–44% (B) in 0.17 min	1–31% (B) in 60 min	1–44% (B) in 0.15 min
Split ratio	1:5		1:5	
Sampling time	0.33 min		0.31 min	
Injected volume (%V_0)	10 μL (10% $^1V_0$)	2 μL (4% $^2V_0$)	10 μL (10% $^1V_0$)	36 μL (69% $^2V_0$)
^1t_G = 120 min	#3		#4	
Stationary phase	XBridge C18	Kinetex C18	Ascentis Express C18	Kinetex C18
Column geometry	50 × 2.1 mm, 5 μm	30 × 2.1 mm, 1.3 μm	100 × 2.1 mm, 5 μm	30 × 2.1 mm, 1.3 μm
Flow rate	100 μL/min	1.5 mL/min	100 μL/min	1.5 mL/min
Gradient	1–31% (B) in 120 min	1–44% (B) in 0.26 min	1–31% (B) in 120 min	1–44% (B) in 0.15 min
Split ratio	1:5		1:2	
Sampling time	0.43 min		0.32 min	
Injected volume (%V_0)	10 μL (10% $^1V_0$)	9 μL (17% $^2V_0$)	20 μL (10% $^1V_0$)	17 μL (33% $^2V_0$)
^1t_G = 200 min	#5			
Stationary phase	Ascentis Express C18	Kinetex C18		
Column geometry	50 × 2.1 mm, 2.7 μm	30 × 2.1 mm, 1.3 μm		
Flow rate	100 μL/min	1.5 mL/min		
Gradient	1–31% (B) in 200 min	1–44% (B) in 0.31 min		
Split ratio	1:5			
Sampling time	0.48 min			
Injected volume (%V_0)	10 μL (10% $^1V_0$)	20 μL (39% $^2V_0$)		

with different maximum values for both pressure and flow-rate.

The selection of both ^1F and ^1z can be done by considering partial Pareto plots, as shown in Fig. 5 for an analysis time of 120 min. Two different column lengths in ^{1}D were considered: 50 mm fully porous stationary phase (Fig. 5a and c) and 100 mm superficially porous stationary phase (Fig. 5b and d). As previously shown, a longer column allows to reduce dilution. Furthermore, depending on the conditions it might enhance the focusing effect as can be expected from the dilution factors lower than unity observed in Fig. 4. The calculations were operated by using Eq. (6) (Fig. 5a and b) and Eq. (5) (Fig. 5c and d) for the estimation of the compression factor. It is clear that the obtained results are quite different. With Eq. (6), the focusing effect which happens with low ^2k_e and high ^2k_s is emphasized resulting in a significant shift of the curves towards lower dilution factors compared to Pareto curves calculated using Eq. (5). The considered conditions are indicated by a full circle in Fig. 5. The first set of conditions (^1L = 50 mm, ^1F = 100 μL/min and $1/^1z$ = 5) is located on the Pareto front and corresponds to D_F = 1 (Fig. 5a) while the second set of conditions (^1L = 100 mm, ^1F = 100 μL/min and $1/^1z$ = 2) is also located on the Pareto front but corresponds to D_F = 0.2 (Fig. 5b). As a result, according to Eq. (6) and in view of Fig. 5b, a 5-fold gain in sensitivity was expected from the first to the second set of conditions with a slight decrease in the effective peak capacity (about 40%). On the other hand, with Eq. (5) and the same conditions, only a 2-fold gain in sensitivity might be expected whereas the predicted peak capacity might be divided by a factor 3.5 (Fig. 5e). Overlays of the ^{2}D separations obtained with these two sets of conditions are shown in Fig. 6a and b for the first and the second set of conditions respectively. The conditions used are given in Table 2 (as RPLC #3 and RPLC #4, respectively). As expected from predictions with Eq. (6), peak heights are about 5-fold higher in Fig. 6b. The results in terms of peak capacity are reported in Table 3 and as also predicted, the loss in effective peak capacity is of around 40% thereby showing the reliability of the method. It is important to note that, as can be seen in Table 3, measured effective peak capacities are about 2–3 times lower than those calculated. The significant discrepancy between predicted and experimental effective peak capacity values is not surprising and can be well explained. Firstly, the volumes behind the ^{2}D-column might substantially contribute to the total band broadening given the very low predicted peak widths in the second dimension (about 0.07s predicted while 0.16s obtained). Secondly, predicted effective peak capacities were calculated from Eqs. (1) and (2) while experimental peak capacities were calculated from Eq. (20) which is known to yield underestimated values especially in the range of low gradient slopes as in ^{1}D [6]. Thirdly Van Deemter coefficients were determined from a neutral solute. However it was shown that the Van Deemter curves of charged compounds, especially at acidic pH, are shifted towards higher plate heights thereby leading to a decrease in column efficiency [42]. Yet, it is noteworthy that an experimental effective peak capacity of nearly 3500 was achieved in two hours without dilution (D_F = 1). RPLC × RPLC separations were performed in 60 min with two different flow-rates (30 μL and 500 μL/min), 120 min and 200 min. In the four cases, the sets of conditions were located on the Pareto front and corresponded to D_F = 1. The conditions are reported in Table 2 (conditions #1, #2, #3 and #5, respectively) and the results in Table 3. The resulting chromatograms can be seen in Fig. 7. Once again there is a factor of around 3 between predicted and experimental peak capacity values as explained above (see Table 3). The observed errors between predicted and experimental values do not affect the reliability of the optimization procedure to deliver good LC × LC conditions but underline the fact that predicted tools in LC × LC can significantly overestimate effective peak capacities. Indeed, as predicted, the peak heights were quite similar in the three chromatograms which confirms the reliability of this approach. Furthermore, two sets of conditions, both corresponding to a point of the Pareto front were applied with the analysis time of 60 min and D_F = 1 (#1 and #2 in Tables 2 and 3). These two sets differ by the flow-rate in the first dimension (30 vs 500 μL/min). Both led to similar experimental effective peak capacities as predicted. Whereas it is often stated that ^{1}D-gradient should be slowed down with sub-optimum flow-rates [12], this study shows that high flow-rates can also be very attractive in RPLC × RPLC provided that other conditions were fully optimized.

The obtained results with D_F = 1 are compared in Fig. 8 to the Pareto-front in 1D-RPLC obtained from the best results found in the literature for the separation of peptides. As can be observed, a 40-fold decrease in analysis time can be obtained in RPLC × RPLC

Table 3
Comparison of on-line RPLC × RPLC experimental results with predicted values.

RPLC × RPLC[a] conditions	^1t_G (min)	γ	^{1}D peak width (min)[b]			^{2}D peak width (s)[b]			$n_{2D,effective}$		
			Predicted	Experimental	Error (%)	Predicted	Experimental	Error (%)	Predicted	Experimental	Error (%)
#1	60	0.56	0.34	0.48	+41%	0.07	0.16	+129%	4000	1300	−68%
#2	60	0.61	0.35	0.25	−29%	0.06	0.16	+167%	4100	1800	−56%
#3	120	0.50	0.45	0.4	−7%	0.07	0.16	+129%	9600	3400	−65%
#4	120	0.52	0.34	0.36	+6%	0.07	0.18	+160%	6500	2300	−65%
#5	200	0.45	0.5	0.4	−20%	0.08	0.18	+125%	17000	5100	−70%

[a] Refers to Table 2.
[b] Measured at half peak height.

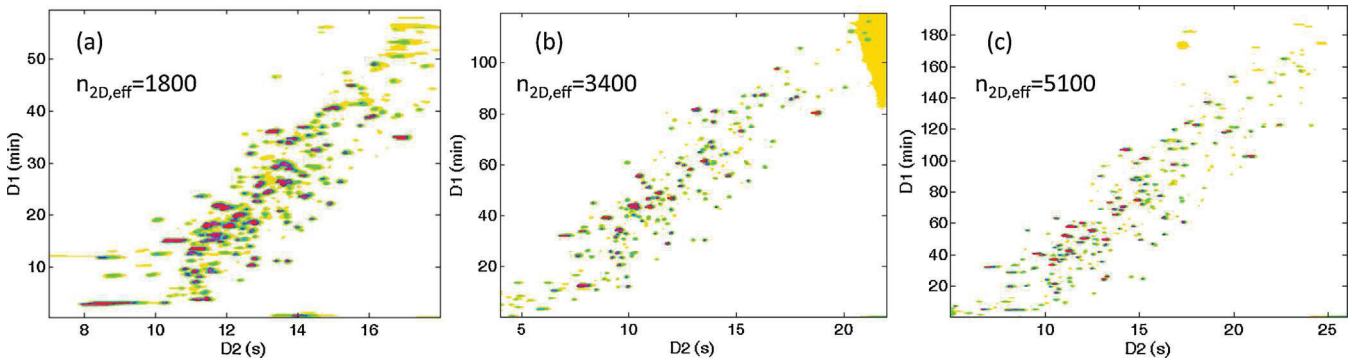

Fig. 7. Contour plots of the experimental on-line RPLC × RPLC separations performed in (a) 60, (b) 120 and (c) 200 min with D_F = 1.0. RPLC × RPLC conditions are given in Table 2 as #2, #4 and #5. The baseline has been subtracted.

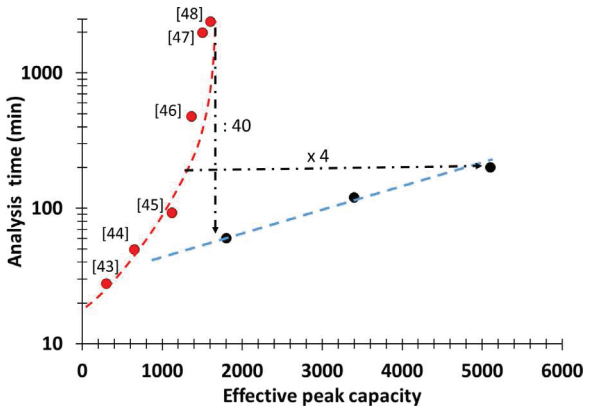

Fig. 8. Comparison between 1D-RPLC and on-line RPLC × RPLC for the separation of peptides. Red circles represent the best reported separations of peptides in 1D-RPLC [43–48]. Blue circles correspond to experimental on-line RPLC × RPLC separations (#1, #3 and #5 in Table 2). (For interpretation of the references to color in this figure legend, the reader is referred to the web version of the article.)

compared to 1D-RPLC to achieve 1600 as effective peak capacity which is the maximum value that has ever been reached for the separation of peptides. Furthermore for an analysis time of 200 min, it was shown in the present study that the effective peak capacity can be multiplied by a factor 4.

For given column formats, increasing peak capacity in 1D-separations is always achieved at the cost of higher gradient time but also of higher dilution. However, in case of RPLC × RPLC separations, it is very interesting to notice that whereas a peak capacity increase is accompanied by a longer analysis time, it is possible not to increase dilution as highlighted by the limit curve in Fig. 8, obtained while keeping the same column geometry and the same dilution (D_F = 1) all over the curve. That is likely to be due to very fast gradients in ^{2}D and hence strong focusing effect.

5. Conclusions

Predictive calculation tools allowed the simultaneous optimization of several parameters and the set-up of relevant conditions for on-line RPLC × RPLC separations of peptides, considering both effective peak capacity and dilution factor for a given analysis time. To our knowledge, it is the first time that optimized parameters obtained from predictive tools are applied to real separations in LC × LC and that predicted and experimental results are successfully compared. Thanks to this approach, an experimental peak capacity of 5100 was obtained in 200 min only. This result is far better than the best published results in 1D-RPLC (i.e. 1600 in 40 h). Furthermore, the optimization procedure was able to define different sets of best conditions for three different analysis times and hence, to experimentally delimit the current ultimate performance of on-line RPLC × RPLC for the separation of peptides. The resulting Pareto curve shows that on-line RPLC × RPLC performance greatly exceeds 1D-RPLC one when the analysis time is 60 min or more.

From predictive calculations and after experimental verification, the following recommendations can be stated:

- Very short and very efficient columns are required in the second dimension whatever the first dimension column geometry. For this purpose, columns such as the Kinetex C18 column (30 mm × 2.1 mm, 1.3 μm) used in this study are suitable.
- The use of the same column diameters in both dimensions is a good choice to find conditions that minimize sample dilution. It is indeed shown in this study that very large volumes can be injected in the second dimension (up to 70% of the dead volume) without peak shape deterioration thereby underlining the importance of considering the focusing effect when optimizing on-line RPLC × RPLC.
- The same set of columns (same column dimensions) can be kept for increasing analysis time and hence effective peak capacity while maintaining same sensitivity (same dilution factor). This is quite impossible in 1D-LC.

- Numerous sets of conditions can achieve the same chromatographic performance in LC × LC, in terms of analysis time, peak capacity and sensitivity. It is of prime importance to choose additional goal to select the appropriate conditions.

Acknowledgements

Tivadar Farkas is greatly acknowledged for the gift of the Kinetex column and for his stimulating advices.

References

[1] P.Q. Tranchida, P. Donato, F. Cacciola, M. Beccaria, P. Dugo, L. Mondello, Potential of comprehensive chromatography in food analysis, TrAC Trends Anal. Chem. 52 (2013) 186–205, http://dx.doi.org/10.1016/j.trac.2013.07.008.
[2] M. Sarrut, G. Crétier, S. Heinisch, Theoretical and practical interest in UHPLC technology for 2D-LC, TrAC Trends Anal. Chem. 63 (2014) 104–112, http://dx.doi.org/10.1016/j.trac.2014.08.005.
[3] D. Li, C. Jakob, O. Schmitz, Practical considerations in comprehensive two-dimensional liquid chromatography systems (LC × LC) with reversed-phases in both dimensions, Anal. Bioanal. Chem. 407 (2014) 153–167, http://dx.doi.org/10.1007/s00216-014-8179-8.
[4] P.F. Vanbel, P.J. Schoenmakers, Selection of adequate optimization criteria in chromatographic separations, Anal. Bioanal. Chem. 394 (2009) 1283–1289, http://dx.doi.org/10.1007/s00216-009-2709-9.
[5] Chapter 26, Other optimization methods, in: B.G.M. Vandeginste, L.M.C. Buydens, S. De Jong, P.J. Lewi, J. Smeyers-Verbeke, D.L. Massart (eds.), Data Handl. Sci. Technol., Elsevier, 1998, pp. 771–804, http://www.sciencedirect.com/science/article/pii/S0922348797800561 (accessed July 10, 2015).
[6] U.D. Neue, Theory of peak capacity in gradient elution, J. Chromatogr. A 1079 (2005) 153–161, http://dx.doi.org/10.1016/j.chroma.2005.03.008.
[7] H. Poppe, Some reflections on speed and efficiency of modern chromatographic methods, J. Chromatogr. A 778 (1997) 3–21, http://dx.doi.org/10.1016/S0021-9673(97)00376-2.
[8] G. Desmet, D. Clicq, P. Gzil, Geometry-independent plate height representation methods for the direct comparison of the kinetic performance of lc supports with a different size or morphology, Anal. Chem. 77 (2005) 4058–4070, http://dx.doi.org/10.1021/ac050160z.
[9] X. Wang, D.R. Stoll, P.W. Carr, P.J. Schoenmakers, A graphical method for understanding the kinetics of peak capacity production in gradient elution liquid chromatography, J. Chromatogr. A 1125 (2006) 177–181, http://dx.doi.org/10.1016/j.chroma.2006.05.048.
[10] M. Sarrut, N. Marchetti, S. Heinisch, Two dimensional Liquid Chromatography, in: J. Anderson, A. Berthod, V. Pino, A.A. Stalcup, (eds.), Anal. Sep. Sci., vol. 2, Ch. 6, 2015, in press.
[11] J.P. Bounine, G. Guiochon, H. Colin, A simple pragmatic optimization procedurer for some parameters involved in high-performance liquisd chromatographic matographic separations: column design, temperature, solvent flow-rate and composition, J. Chromatogr. 298 (1984) 1–20, http://dx.doi.org/10.1016/S0021-9673(01)92691-3.
[12] F. Bedani, P.J. Schoenmakers, H.-G. Janssen, Theories to support method development in comprehensive two-dimensional liquid chromatography—a review, J. Sep. Sci. 35 (2012) 1697–1711, http://dx.doi.org/10.1002/jssc.201200070.
[13] P.J. Schoenmakers, G. Vivó-Truyols, W.M.C. Decrop, A protocol for designing comprehensive two-dimensional liquid chromatography separation systems, J. Chromatogr. A 1120 (2006) 282–290, http://dx.doi.org/10.1016/j.chroma.2005.11.039.
[14] H. Gu, Y. Huang, P.W. Carr, Peak capacity optimization in comprehensive two dimensional liquid chromatography: a practical approach, J. Chromatogr. A 1218 (2011) 64–73, http://dx.doi.org/10.1016/j.chroma.2010.10.096.
[15] G. Vivoí-Truyols, S. van der Wal, P.J. Schoenmakers, Comprehensive study on the optimization of online two-dimensional liquid chromatographic systems considering losses in theoretical peak capacity in first- and second-dimensions: a pareto-optimality approach, Anal. Chem. 82 (2010) 8525–8536, http://dx.doi.org/10.1021/ac101420f.
[16] D.J.D. Vanhoutte, G. Vivó-Truyols, P.J. Schoenmakers, Pareto-optimality study into the comparison of the separation potential of comprehensive two-dimensional liquid chromatography in the column and spatial modes, J. Chromatogr. A 1235 (2012) 39–48, http://dx.doi.org/10.1016/j.chroma.2012.01.059.
[17] K. Horváth, J.N. Fairchild, G. Guiochon, Generation and limitations of peak capacity in online two-dimensional liquid chromatography, Anal. Chem. 81 (2009) 3879–3888, http://dx.doi.org/10.1021/ac802694c.
[18] X. Li, D.R. Stoll, P.W. Carr, Equation for peak capacity estimation in two-dimensional liquid chromatography, Anal. Chem. 81 (2009) 845–850, http://dx.doi.org/10.1021/ac801772u.
[19] A. D'Attoma, C. Grivel, S. Heinisch, On-line comprehensive two-dimensional separations of charged compounds using reversed-phase high performance liquid chromatography and hydrophilic interaction chromatography. Part I: Orthogonality and practical peak capacity considerations, J. Chromatogr. A 1262 (2012) 148–159, http://dx.doi.org/10.1016/j.chroma.2012.09.028.
[20] A. D'Attoma, S. Heinisch, On-line comprehensive two dimensional separations of charged compounds using reversed-phase high performance liquid chromatography and hydrophilic interaction chromatography. Part II: Application to the separation of peptides, J. Chromatogr. A 1306 (2013) 27–36, http://dx.doi.org/10.1016/j.chroma.2013.07.048.
[21] L.R. Snyder, J.W. Dolan, J.R. Gant, Gradient elution in high-performance liquid chromatography: I. Theoretical basis for reversed-phase systems, J. Chromatogr. 165 (1979) 3–30, http://dx.doi.org/10.1016/S0021-9673(00)85726-X.
[22] J.M. Davis, D.R. Stoll, P.W. Carr, Effect of first-dimension undersampling on effective peak capacity in comprehensive two-dimensional separations, Anal. Chem. 80 (2008) 461–473, http://dx.doi.org/10.1021/ac071504j.
[23] J.C. Sternberg, in: J.C. Giddings, R.A. Keller (Eds.), Advances in Chromatography, vol. 2, Dekker, New York, 1966, p. 205.
[24] P. Jandera, P. Česla, T. Hájek, G. Vohralík, K. Vyňuchalová, J. Fischer, Optimization of separation in two-dimensional high-performance liquid chromatography by adjusting phase system selectivity and using programmed elution techniques, J. Chromatogr. A 1189 (2008) 207–220, http://dx.doi.org/10.1016/j.chroma.2007.11.053.
[25] J. Lankelma, H. Poppe, Determination of methotrexate in plasma by on-column concentration and ion-exchange chromatography, J. Chromatogr. 149 (1978) 587–598, http://dx.doi.org/10.1016/S0021-9673(00)81013-4.
[26] F. Gritti, C.A. Sanchez, T. Farkas, G. Guiochon, Achieving the full performance of highly efficient columns by optimizing conventional benchmark high-performance liquid chromatography instruments, J. Chromatogr. A 1217 (2010) 3000–3012, http://dx.doi.org/10.1016/j.chroma.2010.02.044.
[27] A.C. Sanchez, J.A. Anspach, T. Farkas, Performance optimizing injection sequence for minimizing injection band broadening contributions in high efficiency liquid chromatographic separations, J. Chromatogr. A 1228 (2012) 338–348, http://dx.doi.org/10.1016/j.chroma.2012.01.038.
[28] M. Martin, M. Mishra, A. De Wit, C. Grivel, S. Heinisch, in:28th International Symposium on Chromatography ISC, Valencia, 2010.
[29] S. Heinisch, F. Rouviere, C. Grivel, M. Martin, J. Chromatogr. A, submitted for publication.
[30] M.R. Filgueira, Y. Huang, K. Witt, C. Castells, P.W. Carr, Improving peak capacity in fast online comprehensive two-dimensional liquid chromatography with post-first-dimension flow splitting, Anal. Chem. 83 (2011) 9531–9539, http://dx.doi.org/10.1021/ac202317m.
[31] M.R. Schure, Limit of detection, dilution factors, and technique compatibility in multidimensional separations utilizing chromatography, capillary electrophoresis, and field-flow fractionation, Anal. Chem. 71 (1999) 1645–1657, http://dx.doi.org/10.1021/ac981128q.
[32] D.R. Stoll, E.S. Talus, D.C. Harmes, K. Zhang, Evaluation of detection sensitivity in comprehensive two-dimensional liquid chromatography separations of an active pharmaceutical ingredient and its degradants, Anal. Bioanal. Chem. 407 (2014) 265–277, http://dx.doi.org/10.1007/s00216-014-8036-9.
[33] S. Heinisch, G. Desmet, D. Clicq, J.-L. Rocca, Kinetic plot equations for evaluating the real performance of the combined use of high temperature and ultra-high pressure in liquid chromatography: application to commercial instruments and 2.1 and 1 mm I.D. columns, J. Chromatogr. A. 1203 (2008) 124–136, http://dx.doi.org/10.1016/j.chroma.2008.07.039.
[34] M.A. Stadalius, H.S. Gold, L.R. Snyder, Optimization model for the gradient elution separation of peptide mixtures by reversed-phase high-performance liquid chromatography: verification of retention relationships, J. Chromatogr. 296 (1984) 31–59, http://dx.doi.org/10.1016/S0021-9673(01)96400-3.
[35] D. Guillarme, S. Heinisch, J.L. Rocca, Effect of temperature in reversed phase liquid chromatography, J. Chromatogr. A 1052 (2004) 39–51, http://dx.doi.org/10.1016/j.chroma.2004.08.052.
[36] A. Le Masle, D. Angot, C. Gouin, A. D'Attoma, J. Ponthus, A. Quignard, et al., Development of on-line comprehensive two-dimensional liquid chromatography method for the separation of biomass compounds, J. Chromatogr. A 1340 (2014) 90–98, http://dx.doi.org/10.1016/j.chroma.2014.03.020.
[37] R.E. Murphy, M.R. Schure, J.P. Foley, Effect of sampling rate on resolution in comprehensive two-dimensional liquid chromatography, Anal. Chem. 70 (1998) 1585–1594, http://dx.doi.org/10.1021/ac971184b.
[38] K. Horie, H. Kimura, T. Ikegami, A. Iwatsuka, N. Saad, O. Fiehn, et al., calculating optimal modulation periods to maximize the peak capacity in two-dimensional HPLC, Anal. Chem. 79 (2007) 3764–3770, http://dx.doi.org/10.1021/ac062002t.
[39] A. D'Attoma, Thesis, University of Lyon, 2013.
[40] S. Heinisch, in: D. Guillarme, J.-L. Veuthey (Eds.), UHPLC in Life Sciences (Chapter 4), Royal Society of Chemistry, London, 2012.
[41] M. Gilar, A.E. Daly, M. Kele, U.D. Neue, J.C. Gebler, Implications of column peak capacity on the separation of complex peptide mixtures in single- and two-dimensional high-performance liquid chromatography, J. Chromatogr. A 1061 (2004) 183–192, http://dx.doi.org/10.1016/j.chroma.2004.10.092.
[42] S. Heinisch, A. D'Attoma, C. Grivel, Effect of pH additive and column temperature on kinetic performance of two different sub-2 μm stationary phases for ultrafast separation of charged analytes, J. Chromatogr. A 1228 (2012) 135–147, http://dx.doi.org/10.1016/j.chroma.2011.08.041.
[43] J.E. MacNair, K.D. Patel, J.W. Jorgenson, Ultrahigh-pressure reversed-phase capillary liquid chromatography: isocratic and gradient elution using columns packed with 1.0-μm particles, Anal. Chem. 71 (1999) 700–708, http://dx.doi.org/10.1021/ac9807013.
[44] J. Ruta, D. Guillarme, S. Rudaz, J.-L. Veuthey, Comparison of columns packed with porous sub-2 μm particles and superficially porous sub-3 μm particles for peptide analysis at ambient and high temperature, J. Sep. Sci. 33 (2010) 2465–2477, http://dx.doi.org/10.1002/jssc.201000023.

[45] P.J. Eugster, D. Biass, D. Guillarme, P. Favreau, R. Stöcklin, J.-L. Wolfender, Peak capacity optimisation for high resolution peptide profiling in complex mixtures by liquid chromatography coupled to time-of-flight mass spectrometry: application to the Conus consors cone snail venom, J. Chromatogr. A 1259 (2012) 187–199, http://dx.doi.org/10.1016/j.chroma.2012.05.033.
[46] J. De Vos, C. Stassen, A. Vaast, G. Desmet, S. Eeltink, High-resolution separations of tryptic digest mixtures using core–shell particulate columns operated at 1200 bar, J. Chromatogr. A 1264 (2012) 57–62, http://dx.doi.org/10.1016/j.chroma.2012.09.065.
[47] Y. Shen, R. Zhang, R.J. Moore, J. Kim, T.O. Metz, K.K. Hixson, et al., Automated 20 kpsi RPLC-MS and MS/MS with chromatographic peak capacities of 1000-1500 and capabilities in proteomics and metabolomics, Anal. Chem. 77 (2005) 3090–3100, http://dx.doi.org/10.1021/ac0483062.
[48] K. Horie, Y. Sato, T. Kimura, T. Nakamura, Y. Ishihama, Y. Oda, et al., Estimation and optimization of the peak capacity of one-dimensional gradient high performance liquid chromatography using a long monolithic silica capillary column, J. Chromatogr. A 1228 (2012) 283–291, http://dx.doi.org/10.1016/j.chroma.2011.12.088.

B. RPLCXRPLC VS 1D-RPLC POUR LA SÉPARATION DE MÉLANGES COMPLEXES DE PEPTIDES POUR DES TEMPS D'ANALYSES INFÉRIEURS À 60 MIN

Article 3

"Theoretical and experimental comparison of one dimensional versus on-line comprehensive two dimensional liquid chromatography for optimized sub-hour separations of complex peptide samples";

M. Sarrut, F. Rouvière, S. Heinisch, J. Chromatogr. A, (2017), In press

Journal of Chromatography A, xxx (2017) xxx–xxx

Contents lists available at ScienceDirect

Journal of Chromatography A

journal homepage: www.elsevier.com/locate/chroma

Theoretical and experimental comparison of one dimensional versus on-line comprehensive two dimensional liquid chromatography for optimized sub-hour separations of complex peptide samples

Morgan Sarrut, Florent Rouvière, Sabine Heinisch*

Université de Lyon, Institut des Sciences Analytiques, UMR 5280, CNRS, Université Lyon 1, ENS Lyon, 5 rue de la Doua, 69100 Villeurbanne, France

ARTICLE INFO

Article history:
Received 31 July 2016
Received in revised form 11 January 2017
Accepted 22 January 2017
Available online xxx

Keywords:
Fast 2D-LC
On-line LCxLC–MS
Peptide mapping
Mass spectrometry
Optimization
Pareto-optimal approach

ABSTRACT

This study was devoted to the search for conditions leading to highly efficient sub-hour separations of complex peptide samples with the objective of coupling to mass spectrometry. In this context, conditions for one dimensional reversed phase liquid chromatography (1D-RPLC) were optimized on the basis of a kinetic approach while conditions for on-line comprehensive two-dimensional liquid chromatography using reversed phase in both dimensions (on-line RPLCxRPLC) were optimized on the basis of a Pareto-optimal approach. Maximizing the peak capacity while minimizing the dilution factor for different analysis times (down to 5 min) were the two objectives under consideration. For gradient times between 5 and 60 min, 15 cm was found to be the best column length in RPLC with sub–2 μm particles under 800 bar as system pressure. In RPLCxRPLC, for less than one hour as first dimension gradient time, the sampling rate was found to be a key parameter in addition to conventional parameters including column dimension, particle size, flow-rate and gradient conditions in both dimensions. It was shown that the optimum sampling rate was as low as one fraction per peak for very short gradient times (i.e. below 10 min). The quality descriptors obtained under optimized RPLCxRPLC conditions were compared to those obtained under optimized RPLC conditions. Our experimental results for peptides, obtained with state of the art instrumentation, showed that RPLCxRPLC could outperform 1D-RPLC for gradient times longer than 5 min. In 60 min, the same peak intensity (same dilution) was observed with both techniques but with a 3-fold lower injected amount in RPLCxRPLC. A significant increase of the signal-to-noise ratio mainly due to a strong noise reduction was observed in RPLCxRPLC–MS compared to the one in 1D-RPLC–MS making RPLCxRPLC–MS a promising technique for peptide identification in complex matrices.

1. Introduction

On-line two-dimensional comprehensive liquid chromatography is a powerful separation technique for the characterization of complex samples in numerous application fields [1–3]. However due to the large number of parameters involved in the separation process [4], the approach for optimizing such methods is not straightforward. Accordingly, prediction tools are of prime importance to find out a good trade-off between three important but conflictual objectives: (i) maximizing the peak capacity (ii) minimizing the dilution factor and (iii) minimizing the analysis time [5]. A protocol was proposed for the first time by Schoenmakers et al. [6] to simultaneously optimize peak capacity, analysis time and dilution factor. Based on a Poppe approach [7], the authors selected a set of first dimension conditions (particle diameter, column length) from a given gradient time fixed as ten times the column dead time and could thus determine the first dimension peak capacity. The sampling time was set as the first dimension peak standard deviation. The same Poppe plot approach was applied to the second dimension, thereby yielding the second dimension peak capacity. A proper column diameter ratio between first and second dimension was chosen to avoid band broadening resulting from large injection volumes and the dilution factor could be estimated. The authors highlighted the fact that, unless using on-column focusing in the second dimension (not considered in this study), the column diameter ratio had to be high enough to avoid any injection effect and hence significant dilution. This approach is attractive because it is easily implemented. However, based on the Poppe plot approach, it was assumed that the best conditions in both dimensions were those related to the maximum allowable pressure. Furthermore,

* Corresponding author.
E-mail address: sabine.heinisch@univ-lyon1.fr (S. Heinisch).

http://dx.doi.org/10.1016/j.chroma.2017.01.054
0021-9673/

many conditions (sampling time, gradient times etc. . .) were fixed and hence not optimized [8].

Gu et al. [9] proposed two optimization protocols for maximizing the peak capacity while taking into account undersampling effects in the first dimension. In their two-step protocol, first dimension conditions were also firstly optimized for a given analysis time according to the Poppe plot method. The gradient time of the second dimension and hence the sampling time were further optimized to obtain the highest effective peak capacity in LCxLC. The second proposed protocol is a one-step protocol where the first dimension flow-rate, the first dimension column length and the second dimension gradient time, were simultaneously optimized. All other parameters including column diameters, particle sizes in both dimensions and column length in the second dimension were fixed in both protocols. As expected, the results showed the importance of the sampling rate to avoid undersampling. A more important result was that, the highest value for the effective peak capacity could be obtained with sub-optimum values for the first dimension peak capacity, highlighting the need for optimizing both dimensions simultaneously. Yet, these optimization procedures did not take into account the dilution factors in both dimensions which could have led to an estimation of the dilution factor in 2DLC. Furthermore, additional band broadening due to injection effects was not considered despite very high injection volumes in the second dimension.

An elegant approach to optimize on-line LCxLC separations was developed by Vivo-Truyols et al. [10] using a Pareto-optimal approach. The advantage of this approach is its capability to optimize simultaneously several conflictual objectives [11]. The maximum allowable pressure was taken into account. Column diameters, injection volume in the first dimension and sampling time were chosen prior to optimizing. From specific data related to the chromatographic system (Van Deemter coefficient, diffusion coefficient, mobile phase viscosity, column flow-resistance and porosity) an algorithm generated the optimum values for column lengths and flow-rates in both dimensions. The final conditions could be selected among these optimum conditions according to desired values for peak capacity, dilution factor and/or analysis time. As previously, the gradient time in both dimensions was fixed as 10 times the column dead time thereby limiting the sets of optimum conditions and probably missing some more attractive conditions. This theoretical study clearly showed the importance of considering focusing effect during the optimization process.

Some alternative studies evaluated the so-called "crossover time". At longer analysis times LCxLC provides higher peak capacity while at shorter analysis times 1D-LC is more successful [12]. A theoretical study predicted a crossover time between 3 and 8 min for the separation of low molecular weight compounds ranging in molecular mass from 181 to 376 Da [13]. This study was in good accordance with previous experimental works [12,14]. The gradient time in the second dimension was dependent on both chosen sampling time and re-equilibration time. The 33 × 2.1 mm, 3 μm column used in the second dimension was operated at 400 bar under high temperature conditions (110 °C). By extrapolating the number of observed peaks obtained in 15, 30 and 60 min, in both optimized LCxLC and optimized 1D-LC conditions, it was possible to estimate a crossover time of about 5 min for the specific case of a maize extract [12]. These different studies pointed out the strong impact of sampling time [13–15] and retention space coverage on the crossover time [12,13].

We recently developed a Pareto-optimal approach to optimize both peak capacity and dilution factor for analysis times ranging from 60 to 200 min [4]. With a view to apply the theoretical results to real separations, flow-splitting between the two-dimensions was also considered. Furthermore, important instrumental parameters including the re-equilibration time (depending on second dimension column dead time) and the total loop volume (depending on the injection volume and therefore strongly impacting on the total dwell volume), were considered for calculations. The compression factor, C_F, was also considered in order to take into account both additional band broadening ($C_F < 1$) and focusing effect ($C_F > 1$). As was highlighted, very steep gradients in the second dimension made it possible to inject very large volumes (up to seventy per cent of the column dead volume) without any additional band broadening thereby enhancing sensitivity (dilution factor <1). Optimized conditions were applied to the on-line RPLC × RPLC separation of a complex peptide sample and the resulting peak capacities were compared to the best reported peak capacities in one-dimensional liquid chromatography. In particular, optimized RPLCxRPLC conditions allowed to achieve an effective peak capacity of 1800 in one hour only, without sample dilution (dilution factor = 1) whereas such a value was attained in more than 40 h in 1D-LC [16]. This study yielded a figure showing two curves both representing the analysis time as a function of the peak capacity. The first one fitted the best reported 1D-LC results and the second one fitted our obtained results in RPLC × RPLC. The extrapolation of these curves to very short analysis times yields a crossover time of about 20 min, much higher than that found by Stoll et al. [12] for maize extract. However, the reported 1D-LC results originated from different studies involving various conditions (pressure, mobile phase additive), various protein digests and various methods for determining peak capacities, thereby making the extrapolation value quite unreliable.

The objective of the present study was to pursue our previous one [4] and to extend it to sub-one hour separations in order to experimentally find out the crossover time for larger molecules such as peptides, considering both the best current column format in 1D-RPLC under optimized HT-UHPLC conditions and fully optimized parameters in RPLC × RPLC. Predicted and experimental results in optimized 1D-RPLC and optimized RPLC × RPLC conditions were compared for different analysis times (down to 5 min), considering the same peptide sample, the same mobile phase additive and the same procedure for peak capacity assessment in order to ensure unbiased conclusions. Finally the potential interest of on-line RPLCxRPLC–MS for the separation of complex peptide samples is presented from the coupling with a mass detector operated in single ion monitoring mode. The results in terms of signal-to-noise ratio are compared with those obtained in 1D-RPLC for different peptides spiked in a tryptic digest of three proteins.

2. Experimental section

2.1. Material and reagents

The gradient runs were performed with different mixtures of water and acetonitrile (ACN). Acetonitrile was MS grade from Sigma Aldrich (Steinheim, Germany). Water was obtained from an Elga water purification system (Veolia water STI, Le Plessis Robinson, France). Two different pH additives were used, formic acid 0.1% (FA) (pH = 2.8) and ammonium acetate 10 mM (AA) (pH = 6.8), both from Sigma Aldrich (Steinheim, Germany). Formic acid was added to both water and ACN. Ammonium acetate was added to water only due to the lack of solubility in organic solvent. Aqueous phases with ammonium acetate were filtered on 0.22 μm nylon filter before use. The three proteins (BSA, lysozyme, myoglobin) were purchased from Sigma Aldrich (Steinheim, Germany). A tryptic digest was prepared according to a protocol including denaturation with dithiothreitol (DTT), alkylation with iodoacetamide and digestion with trypsin (mass ratio protein/trypsin of 70). The concentration in each protein was 4 mg/mL. The aliquots were stored at −20 °C. The sample was filtered on 0.22 μm before injection. All reagents

Please cite this article in press as: M. Sarrut, et al., Theoretical and experimental comparison of one dimensional versus on-line comprehensive two dimensional liquid chromatography for optimized sub-hour separations of complex peptide samples, J. Chromatogr. A (2017), http://dx.doi.org/10.1016/j.chroma.2017.01.054

for the tryptic digest were obtained from Sigma Aldrich. Three peptides from Sigma Aldrich were used for this study. [ile]-angiotensin was used as reference compound for obtaining the experimental kinetic plots while leucine enkephalin and bradykinin fragment 1–5 were used for the comparison between 1D-RPLC–MS and RPLCxRPLC–MS.

2.2. Columns

For 1D-RPLC experiments two Acquity CSH C18 columns (50 mm × 2.1 mm 1.7 μm and 150 mm × 2.1 mm 1.7 μm) from Waters (Milford, MA, USA) were used.

For RPLCxRPLC experiments, ^{1}D columns were an Ascentis Express C18 (50 mm × 2.1 mm, 2.7 μm) from Sigma-Aldrich (Saint-Louis, MO, USA) and a Xbridge C18 (50 mm × 2.1 mm 5 μm) from Waters depending on the experiments. The second dimension (^{2}D) column was a Kinetex C18 (30 mm × 2.1 mm, 1.3 μm) from Phenomenex (Torrence, CA, USA).

2.3. Apparatus

All 1D-LC experiments were carried out with an I-Class system from Waters (Instrument 1). This instrument includes a high-pressure binary solvent delivery pumps, an autosampler with a flow-through needle of 15 μL, a column manager composed of two column ovens with an allowed maximum temperature of 90 °C and a diode array detector (DAD) equipped with 500 nL flow-cell. The upper maximum allowable pressure is 1285 bar for the two pumps. Beyond a flow-rate of 1 mL/min, the upper limit decreases depending on both flow-rate and mobile phase composition. The measured dwell volume was 110 μL. A total extra-column volume of 12 μL and an extra-column variance of about 4 μL^2 were determined. Data acquisition and instrument control were performed by Masslynx software (Waters).

The LCxLC system (Instrument 2) was a 1290 Infinity 2D-LC from Agilent Technologies (Waldbronn, Germany). This instrument includes two high-pressure binary solvent delivery pumps, an autosampler with a flow-through needle of 20 μL, a column oven with an allowed maximum temperature of 100 °C, a UV detector and a diode array detector (DAD) equipped with 2 μL and 0.6 μL flow-cells respectively. A 2-position/4-port duo valve was used as interface between the two dimensions. The measured dwell volume was 140 μL and 65 μL for the first and second dimension respectively. It should be noted that the given dwell volume value of the second dimension does not take into account the size of the loops used between the two dimensions (20 μL). For 1D-LC experiment, a total extra-column volume of 22 μL and an extra-column variance of 15 μL^2 (DAD detector) were measured. For LCxLC experiments, a total extra-column volume of 22 μL and 8.5 μL and an extra-column variance of 30 μL^2 (UV detector) and 4.5 μL^2 (DAD detector) were determined for the first and the second dimension respectively. The estimated value of the extra-column variance related to extra-column volumes located after the column outlet was 2 μL^2. It is important to note that the UV detector was not used as ^{1}D detection since its contribution to extra-column dispersion was significant. Accordingly the peak capacity in the first dimension was measured by injecting representative peptides [17] in 1D-LC using the DAD detector.

A mass detector, QDa from Waters, was coupled to the 1290 2D-LC and used in Single Ion Monitoring mode (SIM). 1D-RPLC–MS separations were carried out with the first dimension of the 2D-LC system.

Data acquisition and instrument control were performed by OpenLab software (Agilent) for the chromatographic process. 2D-data were exported to Microsoft Excel and Matlab V7.12.0635 to construct a matrix via calculation tools enabling the construction of 2D-contour plots. MS acquisition and instrument control were performed by Masslynx software (Waters).

Table 1
Characteristics of the two peptides injected alone and spiked in the tryptic digest of proteins at a concentration of 1 mg/L for comparison between 1D-RPLC–MS and RPLCxRPLC–MS separations. The source temperature, the capillary voltage, the dwell time and the acquisition rate were 600 °C, 1.5 kV, 5 ms and 16.7 Hz respectively both for RPLC–MS and RPLCxRPLC–MS experiments.

Peptide	M (Da)	*m/z* (Th)	Cone voltage (V)
Leucine enkephalin	555.3	556.3	10
Bradykinin fragment 1–5	572.3	573.3	20

2.4. Chromatographic conditions

For 1D-LC separations with 5 and 15 cm columns, the mobile phase was composed of Water (A) and ACN (B) both with 0.1% FA, the temperature was set at 60 °C, the composition range was from 1 to 31% B and the flow-rate was adjusted so that the total system pressure attained 800 bar. The acquisition rate was 40 Hz. 1D-RPLC–MS separation was carried out on the 150 × 2.1 mm 1.7 μm Acquity CSH C18 column. 30 μL (10% V_0) were injected. The flow rate was 800 μL/min and the gradient time was 60 min. The acquisition rate was 80 Hz. For RPLCxRPLC separations, the mobile phase of the first dimension was composed of ammonium acetate 10 mM (A) (pH = 6.8) and ACN (B) while the mobile phase of second dimension was composed of Water with 0.1% FA (A) (pH = 2.8) and ACN with 0.1% FA (B). The temperature was set at 30 °C and 90 °C for the first and the second dimension respectively for all LCxLC experiments. The acquisition rate was 80 Hz. Other conditions are detailed in Table 2. The wavelength was set at 210 nm for UV detection for all the experiments presented in this work. For MS detection, Single Ion Monitoring mode (SIM) was used. A capillary voltage of 1.5 kV and a source temperature of 600 °C were found as the best values for all the peptides in term of sensitivity both in 1D-RPLC–MS and RPLCxRPLC–MS. The acquisition rate was 16.7 Hz and the dwell time was 5 ms for all separations. The MS settings are given in Table 1. No flow splitting was used prior to MS.

Other conditions (gradient time, flow-rate, sampling time…) are subjected to optimization and are therefore given throughout this paper.

2.5. Calculations

All calculations including Pareto curves were performed using an Excel spreadsheet and appropriate home-made routines.

Predicted peak capacities were calculated according to the equation developed by Neue [18] with respect to the Linear Solvent Strength Theory (LSST) [19]:

$$ {}^{i}n = 1 + \frac{\sqrt{{}^{i}N_{col}}}{4} \times \frac{1}{1+2.3^{i}b} \ln\left(\frac{1+2.3^{i}b}{2.3^{i}b} e^{2.3^{i}S^{i}\Delta\varphi_B} - \frac{1}{2.3^{i}b} \right) \quad (1) $$

where the superscript "i" refers to first or second dimension N_{col} is the column plate number, $\Delta\varphi_B$ is the gradient range expressed in volume fraction, S is the slope of the relationship between the logarithm of the retention factor and the volume fraction of the strong solvent, B. S value was estimated from 3 peptides (see next section). b is the gradient steepness given by

$$ b = S \times \Delta\varphi_B \times \left(\frac{t_O}{t_G} \right) \quad (2) $$

Where t_0 and t_G are the column dead time and the gradient time respectively.

Please cite this article in press as: M. Sarrut, et al., Theoretical and experimental comparison of one dimensional versus on-line comprehensive two dimensional liquid chromatography for optimized sub-hour separations of complex peptide samples, J. Chromatogr. A (2017), http://dx.doi.org/10.1016/j.chroma.2017.01.054

Table 2
Experimental conditions for the RPLCxRPLC separations of a tryptic digest of proteins. Other conditions are given in the experimental section.

	1st dimension (^{1}D)	2nd dimension (^{2}D)	1st dimension (^{1}D)	2nd dimension (^{2}D)
	^1t_G = 5 min – # 1		^1t_G = 10 min – # 2	
Stationary phase	Ascentis Express C18	Kinetex C18	Ascentis Express C18	Kinetex C18
Column geometry	50 × 2.1 mm, 2.7 μm	30 × 2.1 mm, 1.3 μm	50 × 2.1 mm, 2.7 μm	30 × 2.1 mm, 1.3 μm
Flow rate	30 μL/min	1.5 mL/min	30 μL/min	1.5 mL/min
Gradient	1–36% (B) in 5 min	1–47% (B) in 0.08 min	1–34% (B) in 10 min	1–45% (B) in 0.1 min
Temperature	30 °C	90 °C	30 °C	90 °C
Split ratio	1:10		1:10	
Sampling time	0.21 min		0.26 min	
Injected volume (%V_0)	10 μL (10% $^1V_0$)	0.7 μL (1.4% $^2V_0$)	10 μL (10% $^1V_0$)	0.8 μL (1.5% $^2V_0$)
	^1t_G = 30 min – # 3		^1t_G = 60 min – # 4	
Stationary phase	Ascentis Express C18	Kinetex C18	X Bridge C18	Kinetex C18
Column geometry	50 × 2.1 mm, 2.7 μm	30 × 2.1 mm, 1.3 μm	50 × 2.1 mm, 5 μm	30 × 2.1 mm, 1.3 μm
Flow rate	50 μL/min	1.5 mL/min	500 μL/min	1.5 mL/min
Gradient	1–31% (B) in 30 min	1–44% (B) in 0.18 min	1–31% (B) in 60 min	1–44% (B) in 0.17 min
Temperature	30 °C	90 °C	30 °C	90 °C
Split ratio	1:10		1:5	
Sampling time	0.34 min		0.36 min	
Injected volume (%V_0)	10 μL (10% $^1V_0$)	1.7 μL (3.3% $^2V_0$)	10 μL (10% $^1V_0$)	36 μL (69% $^2V_0$)

For predictive purpose, the peak standard deviation due to solute dispersion in the column was calculated according to LSST as

$$\sigma_{col} = \frac{t_0\,(2.3b+1)}{2.3b\sqrt{N_{col}}} \tag{3}$$

The predicted dilution factor in dimension "i" can be expressed as

$${}^iD_F = \frac{\sqrt{2\pi}}{{}^i\beta} \times \frac{{}^i\sigma_{v,col}}{{}^iV_{inj}} \tag{4}$$

where $^i\sigma_{v,col}$ is the peak standard deviation in volume unit. $^i\beta$ corrects for $^i\sigma_{v,col}$ by considering extra-column band broadening. In this study, no extra-column band broadening was assumed in the first dimension ($^1\beta = 1$) while only injection effects were considered in the second dimension as discussed below. $^iV_{inj}$ is the injection volume. $^1V_{inj}$ was set at 10% of the first dimension column dead volume ($^1V_{inj} = 0.1\,^1V_0$) while $^2V_{inj}$ was given by

$${}^2V_{inj} = t_s \times {}^1F \times z \tag{5}$$

Where t_s is the sampling time, ^1F, the first dimension flow-rate and z, the split ratio, potentially designed to reduce the flow-rate entering the interface ($0 < z \leq 1$). The sampling rate, τ, is related to the sampling time by

$$\tau = \frac{6\,{}^1\sigma_{col}}{t_s} \tag{6}$$

where $^1\sigma_{col}$ being the first dimension peak standard deviation in time unit.

In 2D-LC the total dilution factor was considered as the product of the dilution factors in both dimensions (Eq. (4)).

N_{col} was estimated from the coefficients (a,b and c) of the Knox equation:

$$N_{col} = \frac{L_c}{d_p} \times \frac{1}{\left(au^{0.33} + b\frac{D_m}{ud_p} + c\frac{ud_p}{D_m}\right)} \tag{7}$$

Where L_c is the column length, u, the linear velocity (L_c/t_0), d_p, the particle size and D_m, the diffusion coefficient. The values for the coefficients (a–c) came from our own results obtained on the selected columns with neutral compounds: (0.57, 7.22, 0.14) and (0.5, 3.2, 0.05) for porous and superficially porous stationary phases respectively. The calculation for diffusion coefficients is based on a value of 2.10^{-10} m^2/s in water at 25 °C. It is more detailed in a previous study [17].

Experimental peak capacities in dimension "i", both in 1D-LC and 2D-LC were estimated according to

$${}^in = \frac{{}^it_G}{4{}^i\sigma_{tot}} \tag{8}$$

Where σ_{tot} is the total peak standard deviation in time units calculated from the Dorsey Foley equation [20] which was shown to be well correlated to the true peak standard deviation for small peak asymmetry (i.e. As <2.5):

$$\sigma_{tot} = \frac{w_{10\%}\sqrt{As + 1.25}}{6.46} \tag{9}$$

$w_{10\%}$ being the measured peak width at 10% of the peak height and As, the peak asymmetry (ratio of the right half peak width to the left half peak width, measured at 10% of the peak height).

Effective peak capacities in RPLCxRPLC were calculated from the following relationship [10]:

$$n_{2D,effective} = {}^1\alpha \times {}^1n \times {}^2\beta \times {}^2n \times \gamma \tag{10}$$

where ^{1}n and ^{2}n are the peak capacities in first and second dimensions respectively, calculated with Eq. (1) for predicted values. Experimental ones were calculated according to Eq. (8), thereby leading to ^{1}n and $^2\beta\,^2$n. $^1\alpha$, $^2\beta$ and γ are correction coefficients lower than 1. $^1\alpha$ corrects for ^{1}n values by considering undersampling [21]. $^2\beta$ corrects for predicted ^{2}n values by taking into account additional band broadening due to injection effects. It is dependent on the compression factor, C_F and calculated for optimization purpose by the following equation:

$${}^2\beta = \frac{1}{\sqrt{1 + \frac{1}{4} \times \frac{{}^2V_{inj}^2}{{}^2\sigma_{col}^2} \times \frac{1}{C_F^2}}} \tag{11}$$

For additional details about the calculations of $^1\alpha$, $^2\beta$ and C_F, it is recommended to refer to our previous study [4]. γ corrects for partial retention surface coverage [17]. For predicted peak capacities, γ was set at 0.6 according to preceding 2D-results obtained by changing the mobile phase pH between the two dimensions [4] while for experimental ones, γ was graphically measured according to a method described elsewhere [22].

3. Results and discussion

The objective of this work was to assess and to compare the chromatographic performance of 1D-RPLC and on-line RPLC × RPLC for the separation of peptides with a view to coupling to MS detection

Please cite this article in press as: M. Sarrut, et al., Theoretical and experimental comparison of one dimensional versus on-line comprehensive two dimensional liquid chromatography for optimized sub-hour separations of complex peptide samples, J. Chromatogr. A (2017), http://dx.doi.org/10.1016/j.chroma.2017.01.054

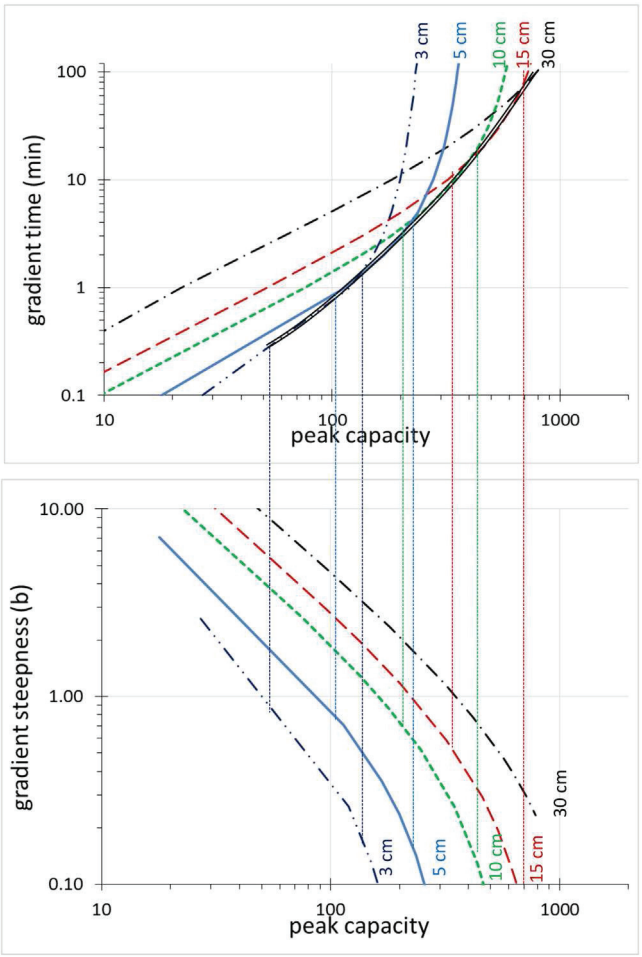

Fig. 1. Predicted variation of the gradient time vs peak capacity (top) and predicted variation of gradient steepness vs peak capacity (bottom) at 800 bar for column lengths ranging from 3 to 30 cm. Coefficients of reduced Knox equation were measured on a 50 × 2.1 mm, 1.7 μm Acquity CSH-C18 column using Ethylparaben in 30% Acetonitrile at 30 °C (k = 4): A = 0.24; B = 5.25; C = 0.21; n = 0.33; S = 25 and Dm = 0.58 10^{-9} m^2 s (calculated for [ile]-angiotensin at 60 °C). Composition range=30%. Flow-rate: 1800 μL/min for 3 cm; 1100 μL/min for 5 cm; 600 μL/min for 10 cm; 400 μL/min for 15 cm and 200 μL/min for 30 cm. The double line, in the top figure, joins data corresponding to the lowest gradient time for a given peak capacity and hence delimit the area of interest in 1D-RPLC. Vertical lines delimit the area of interest for each column length.

and further performing peptide mapping. Only gradient times of one hour or less were considered for that purpose.

3.1. Optimization of 1D-RPLC separations

According to LSST, the logarithm of the retention factor is assumed to be a linear function of the volume fraction of the strong solvent B, φ_B:

$$\log(k) = \log(k_0) - S\varphi_B \quad (12)$$

where S is the solvent strength parameter and k_0 is the extrapolated retention factor in the weak solvent. The two coefficients of Eq. (12) were calculated with HPLC modeling software (Osiris 4.1.1.2, Datalys, Grenoble, France) [23], from three peptides ([ile]-angiotensin, leucine enkephalin and bradykinin fragment 1–5) by running two gradients with two different slopes. An average value of 25 was obtained for S.

For a linear gradient elution, the retention time can be given by

$$t_r = t_0\left(1 + \frac{t_D}{t_0} + \frac{1}{b}log(2.3bk_i + 1)\right) \quad (13)$$

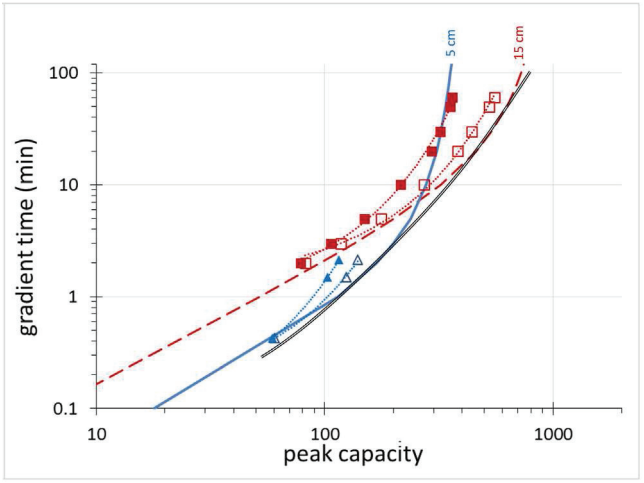

Fig. 2. Variation of gradient time vs peak capacity at 800 bar in optimized 1D-RPLC conditions. Theoretical data with 15 (-----) and 5 cm (——) Acquity CSH-C18 columns (S = 25 and Dm = 0.58 10^{-9} m^2 s). Experimental data obtained with [ile]-angiotensin with two different concentrations, 50 ppm (■) with 15 or (▲) with 5 cm and 5 ppm (□) with 15 or (Δ) with 5 cm. Conditions for experimental data are the same as those given in Fig. 1 for 5 and 10 cm columns. V_i = 0.5 and 1.5 μL for 5 and 15 cm columns respectively (0.5% V_0). Detection at 210 nm.

t_D being the dwell time. Eq. (13) is true provided that the retention factor, k_i, in initial gradient conditions is high enough. In these conditions, the retention factor at elution is

$$k_e = \frac{1}{2.3b} \quad (14)$$

For a given sample, it is assumed via Eq. (1) that the variation of the retention window (i.e. ΔC) with t_G and hence b, is not significant enough to affect the peak capacity value. As a matter of fact, it was found, for large molecules, that the error on peak capacity did not exceed 10% for b values between 0.02 and 3 (results not presented here).

According to the kinetic plot method discussed for isocratic elution in many seminal papers [7,24,25], the highest plate number, for a given particle diameter, a given column temperature and a given column dead time, can be obtained at the highest allowable pressure, thus determining both column length and flow-rate. On the basis of the Linear Solvent Strength Theory (LSST) [19], kinetic curves in gradient elution can be calculated as well [26,27].

Similarly to the kinetic curves in isocratic elution, those in gradient elution permit to know the highest peak capacity that can be obtained for a given gradient time. For highly efficient 1D-RPLC separations, HT-UHPLC is the technique of choice [28]. We have therefore chosen a 1.7 μm Acquity CSH-C18 column which is expected to work well at acidic pH for the separation of peptides, thanks to positive charges on the surface of the stationary phase [29]. The column temperature was fixed at the maximum recommended temperature (i.e. 60 °C). Kinetic curves are usually calculated for a given value of the gradient steepness, b, by keeping the ratio of the gradient time to the column dead time (t_G/t_0) constant [26,30]. However there are as many curves as there are gradient steepness values and it is necessary to consider all the curves to find optimum conditions. Top Fig. 1 shows the variation of gradient time with peak capacity at 800 bar for different column lengths. Bottom Fig. 1 shows the corresponding variation of gradient steepness with peak capacity. The curves were calculated for a peptide ([ile]-angiotensin) with a molecular weight of 800 Da (D_m = 0.6 10^{-9} m^2 s^{-1} in these conditions) and a calculated S value of 25. According to this representation, the column length is constant for a given curve while the column dead time varies as the flow-rate varies. As a result, the gradient steepness varies as shown

Please cite this article in press as: M. Sarrut, et al., Theoretical and experimental comparison of one dimensional versus on-line comprehensive two dimensional liquid chromatography for optimized sub-hour separations of complex peptide samples, J. Chromatogr. A (2017), http://dx.doi.org/10.1016/j.chroma.2017.01.054

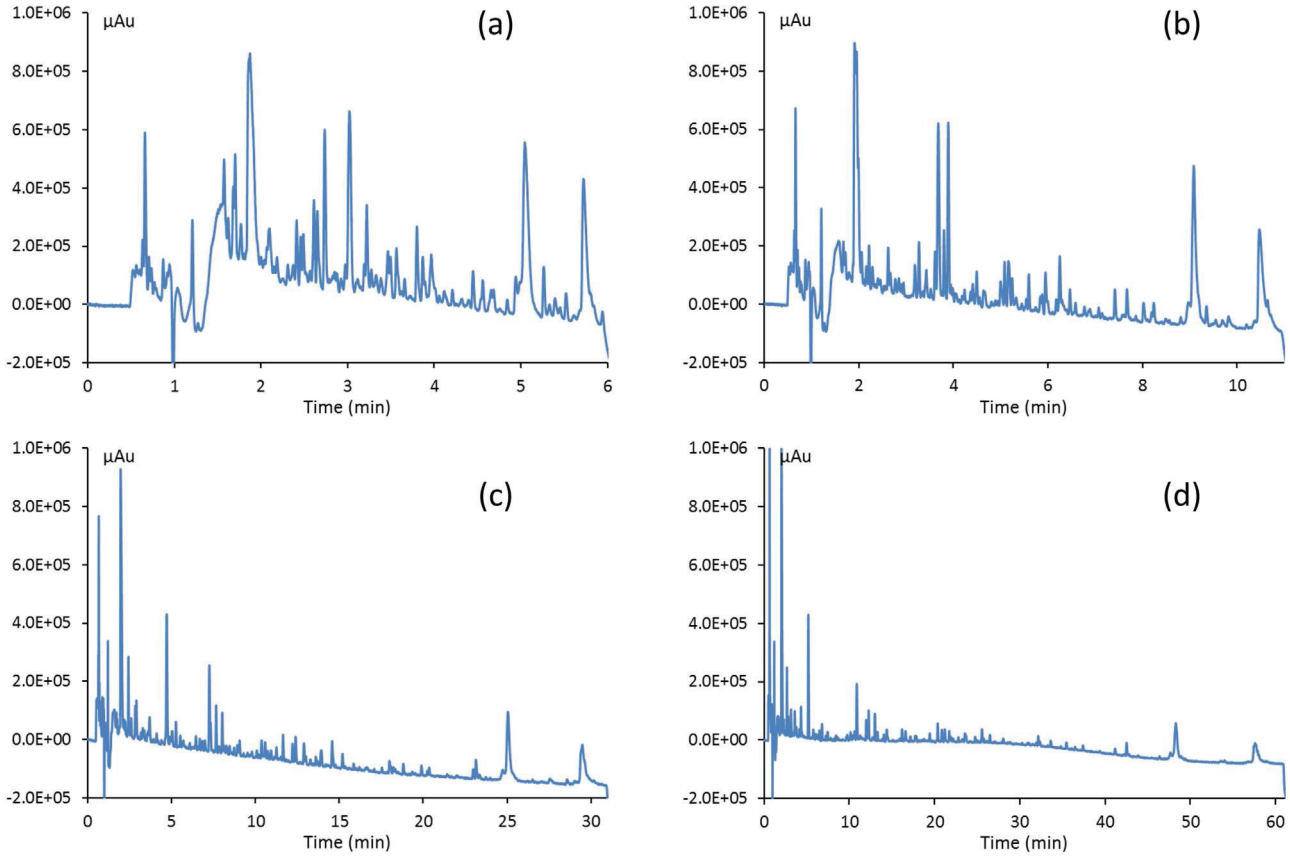

Fig. 3. Separations of a tryptic digest of 3 proteins under optimized 1D-gradient conditions (see text for explanation). Acquity CSH-C18 column (150 × 2.1 mm; 1.7 µm); 400 µL/min; 60 °C; A: water + 0.1% formic acid; B: ACN + 0.1% formic acid; 1%B–31%B in (a) 5 min; (b) 10 min; (c) 30 min and (d) 60 min. V_i = 1.5 µL. Detection at 210 nm.

in the bottom figure. The double line in top Fig. 1 joins values corresponding to the highest peak capacity for a given gradient time and therefore represents the limit curve that defines optimum conditions. It can be therefore considered as the final kinetic curve in gradient elution. As can be observed in Fig. 1, for gradient times ranging from 10 to 60 min, a 15 cm column is adequate. For lower gradient times, shorter columns seem to be necessary. A column length of 3 cm becomes advantageous for gradient times below 1 min and should be therefore highly recommended for the second dimension of comprehensive on-line LCxLC. It is interesting to notice that the same performance can be obtained with different column lengths as pointed out by the straight vertical lines delimiting the areas of interest for each column length. For a given gradient time, the required gradient steepness increases as the chosen column length decreases. As an example, for a gradient time of about 4 min, it is possible to reach 200 as peak capacity with either 15, 10 or 5 cm columns, the corresponding gradient steepness being 0.1, 0.7 and 1 respectively. It also appears that the range of optimum gradient steepness is between 0.1 and 0.8 and is slightly shifted toward higher values for shorter columns.

Experimental results obtained in optimum conditions for 5 and 15 cm columns with [ile]-angiotensin, at two different concentrations (50 ppm and 5 ppm), are shown in Fig. 2. It appears that experimental data drift away from theoretical curves and that the resulting gap increases with the gradient time and hence with the solute retention. As a result, while the theoretical peak capacity was expected to reach 600 with a gradient time of 60 min, only half that value could be experimentally achieved. It is also highlighted that the shift towards lower peak capacities is less significant for lower peptide concentrations. Both observations suggest the existence of an overloading effect which appears at very low concentrations as pointed out in earlier studies [31–33] when formic acid is used as additive. For a given peak capacity, this effect is more pronounced with a 5 cm than with a 15 cm column. This can be explained by the fact that the column dead time of a 5 cm column being 10-fold shorter for a given gradient time, the column gradient steepness is 10-fold lower, resulting in a 10-fold increase in the retention factor at elution (Eq. (13)). As a result, the extrapolation of the experimental curve to a gradient time of 5 min suggests that a 5 cm column should be worse (50 ppm) or similar (5 ppm) to a 15 cm one in these gradient conditions.

According to the above results, a 15 cm column was selected for comparison with on-line RPLC x RPLC separations. Fig. 3 shows the separations of a tryptic digest of 3 proteins performed with four different gradient times under the best conditions established in the preceding discussion. The peak capacity was calculated from Eq. (8) considering the average peak width of 5 well separated peaks that were well distributed among the separation space. The resulting values were 135, 214, 291 and 377 for gradient times of 5, 10, 30 and 60 min respectively. These results were in very good accordance with those experimentally obtained for [ile]-angiotensin injected with a concentration of 50 ppm (see Fig. 2), thereby definitely validating our preliminary selection of ^{1}D conditions.

3.2. Optimization of RPLC × RPLC separations

For RPLC x RPLC separations, the optimization procedure was based on predictive calculation tools [4]. This procedure made use of a Pareto-optimality approach to define, for a given analysis time, the best set of conditions, considering simultaneously the effective peak capacity and the dilution factor. In this predictive approach, injection effects in the second dimension were taken into account. It

Please cite this article in press as: M. Sarrut, et al., Theoretical and experimental comparison of one dimensional versus on-line comprehensive two dimensional liquid chromatography for optimized sub-hour separations of complex peptide samples, J. Chromatogr. A (2017), http://dx.doi.org/10.1016/j.chroma.2017.01.054

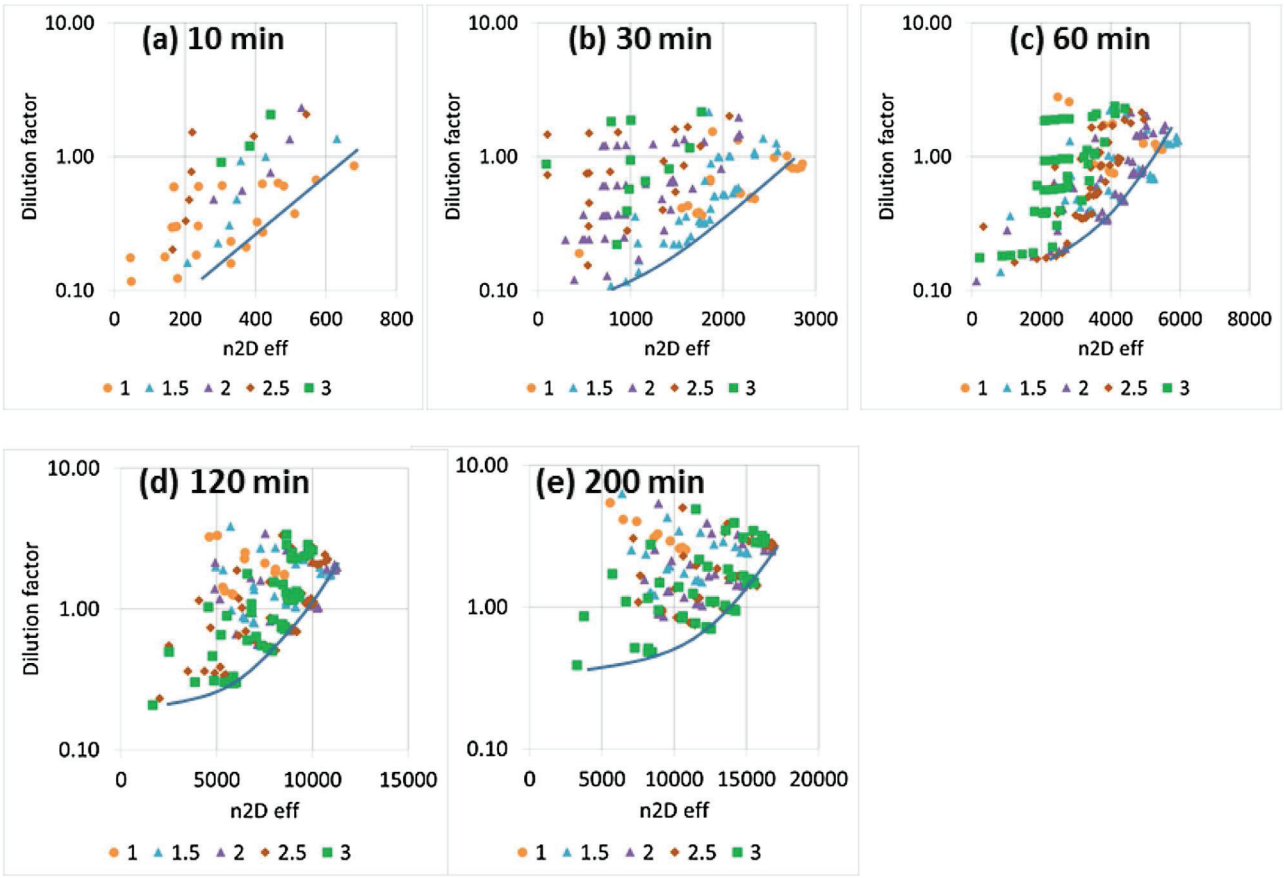

Fig. 4. Pareto plots of the predicted dilution factor (D_F) as a function of effective peak capacity ($n_{2D,eff}$) for 5 different ^1t_G values: (a) 10 min; (b) 30 min; (c) 60 min; (d) 120 min and (e) 200 min and 5 different sampling rates: 1 (●); 1.5 (▲); 2 (▲); 2.5 (◆); and 3 (■). ^1F and z were allowed to vary within 20 μL/min and 1000 μL/min and within 0.1 and 1, respectively. All other 2D-conditions were fixed (see text for explanation). Pareto fronts are represented by curved lines.

is indeed of prime importance to predict additional band broadening which results in a decrease of both sensitivity and peak capacity. It can also be helpful to predict on-column focusing in order to improve sensitivity in the second dimension by injecting larger volumes while keeping the same peak width.

In our previous study [4], the first dimension gradient time varied from 60 to 200 min. Since the number of sets of conditions can dramatically increase with the number of parameters to be optimized, we proposed a flexible optimization procedure, allowing to proceed at three different input levels. Depending on the input level, a more or less extensive preselection of conditions can be done. Thus, the user can choose the level he wants depending on both available instrumentation and available columns. It was recommended in usual cases to fix the parameters of the first input level which includes column temperatures in both dimensions, second dimension column diameter and the sampling rate. This latter was fixed at 2.5 fractions per peak as recommended in several studies [8,34]. This sampling rate was found to be suitable for ^1D gradient times longer than one hour. Accordingly, optimized parameters included ^1L_c, ^2L_c, ^1d_p, ^2d_p, ^1F and the split ratio, z, between the two dimensions. In the present study, shorter analysis times were investigated and the sampling rate was found to be also a key parameter in these conditions as shown in Fig. 4 where Pareto plots as well as Pareto fronts are given for different ^1t_G values. The pareto-front represents the performance limit with respect to the objectives (i.e. minimizing the dilution factor and maximizing the peak capacity) within the specified set of fixed conditions. Each symbol is related to a set of three changing conditions (^1F, split ratio and sampling rate), all other conditions being fixed. Optimum conditions are related to the data located along the Pareto front. As expected, Fig. 4d and e shows that sampling rate values between 2 and 3 are well adapted to long 2D-separations (>60 min) with corresponding data located close to the Pareto front. Conversely, Figs. 4a and 4b clearly show that such values are no longer suitable for rapid separations and that lower values should be used which is in good accordance with a previous study [14]. For a gradient time of 60 min, 2 fractions per peak seem to be more appropriate than 2.5, especially in the range of very high effective peak capacities (high dilution)

We therefore applied the optimization procedure to different gradient times, starting from the first input level of the procedure. The second dimension temperature was preselected so that it was as high as possible for the selected column, considering the supplier recommendations (i.e. 90 °C). Furthermore column diameters in both dimensions were fixed at 2.1 mm in view of the available instrumentation. It was previously shown for large analysis times (i.e. >60 min) that a 30 × 2.1 mm, 1.3 μm Kinetex C18 column used at 90 °C in the second dimension outperformed other column conditions [4]. Considering the very short investigated analysis times, we also included, in the present optimization procedure, column length and particle diameter in the second dimension. The flow-rate in the second dimension was set at its maximum value considering the available maximum column pressure drop of 800 bar. To sum up, the conditions that were considered in this optimization procedure included τ, ^1T, ^1L, ^2L, ^1d_p, ^2d_p, ^1F and z. A representation of Pareto fronts obtained in different fixed conditions are given in Fig. 5 for a first dimension gradient time of 10 min. The Pareto fronts delimit optimum conditions for ^1F, z and

Please cite this article in press as: M. Sarrut, et al., Theoretical and experimental comparison of one dimensional versus on-line comprehensive two dimensional liquid chromatography for optimized sub-hour separations of complex peptide samples, J. Chromatogr. A (2017), http://dx.doi.org/10.1016/j.chroma.2017.01.054

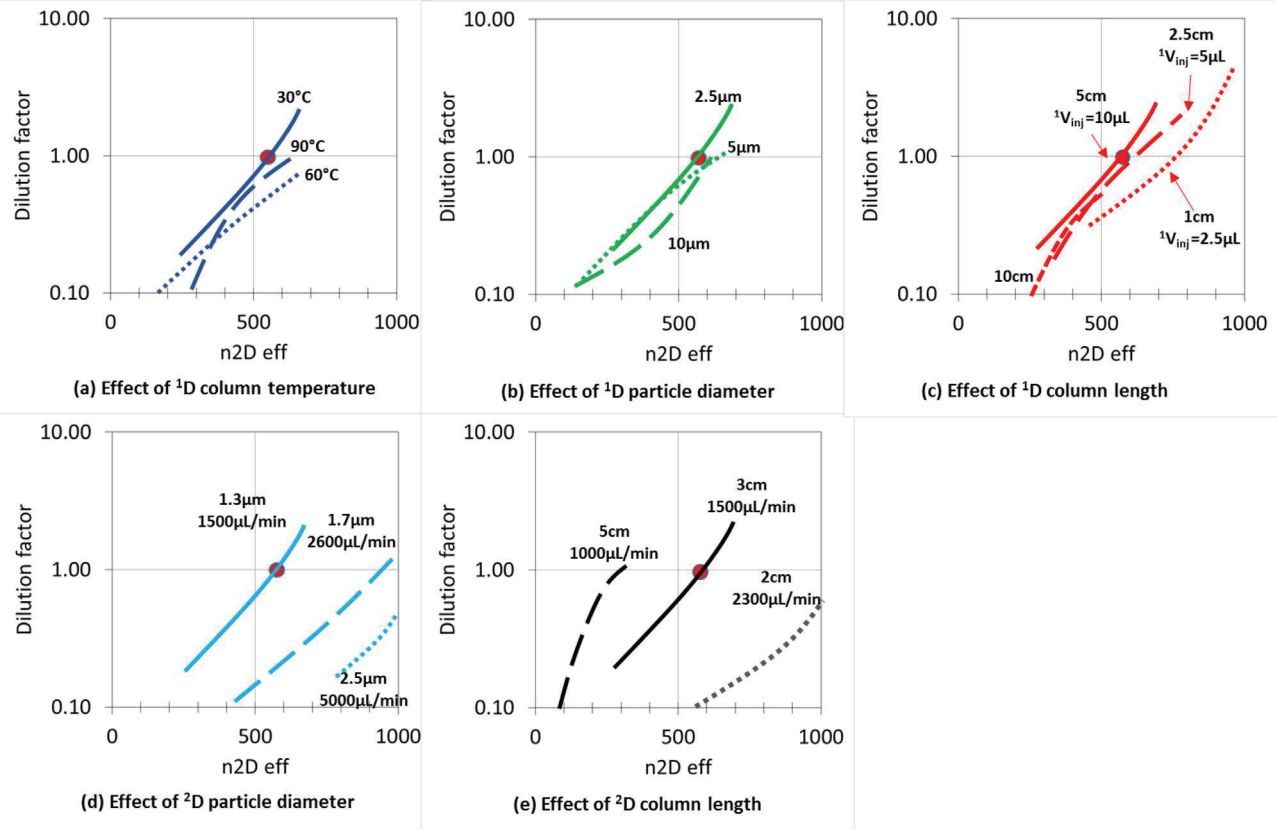

Fig. 5. Pareto fronts for ^{1}D gradient time of 10 min, delimiting optimum conditions for ^{1}F, z and τ in different fixed conditions (a) effect of ^{1}T: 30 °C (——), 60 °C (·····), 90 °C (– – –); (b) effect of ^1d_p: 10 µm (– – –), 5 µm (·····), 2.5 µm (——); (c) effect of ^{1}L: 5 cm (——), 2.5 cm (– – –), 1 cm (·····); (d) effect of ^2d_p: 2.5 µm (·····), 1.7 µm (– – –), 1.3 µm (——); (e) effect of ^{2}L: 5 cm (– – –), 3 cm (—), 2 cm (···). ^{2}F was adjusted to the maximum allowed pressure of 800 bar. $^1V_{inj}/^1V_0$ was kept constant. The calculations were carried out with a γ value of 0.6. Other conditions are those selected in this study and indicated by the red circle. They are listed in Table 2. (For interpretation of the references to colour in this figure legend, the reader is referred to the web version of this article.)

τ, other conditions being fixed, except ^{2}F which was adjusted to the maximum allowed pressure and the injection volume in the first dimension, $^1V_{inj}$, which was adjusted to the column dead volume $^1V_0$ (i.e. $^1V_{inj}/^1V_0$ kept constant). Some instructive conclusions can be drawn:

(i) The gain obtained by elevating column temperature in the first dimension is not significant and may even be counterproductive (Fig. 5a).
(ii) Surprisingly, the first dimension particle diameter has little effect on the pareto front (Fig. 5b).
(iii) Very short columns (i.e. 1 cm) in the first dimension should permit to achieve larger effective peak capacities (Fig. 5c). This could be surprising but can be easily explained by the much higher compression factor in case of 1 cm column. Indeed, for a given flow-rate, the column dead time and hence the gradient steepness is 5 times higher with a 5 cm compared to a 1 cm column. As a result, the compression factor which is related to the ratio of the gradient steepness between both dimensions is expected to be 5 times lower [4]. This underlines the great interest in considering the compression factor for an optimization approach. However, considering the current column availability and furthermore the difficulty to pack very short columns, a 5 cm column with either 5 or 2.5 µm particles seemed to be a good choice. It is interesting to note that RPLCxRPLC with longer columns (e.g. 10 cm) can be an attractive option for on-column focusing, and hence for enhancing sensitivity. Of course that would be done at the cost of lower peak capacities.
(iv) The flow-rate in the second dimension can be increased by increasing the particle diameter while maintaining the same column pressure drop (800 bar), thereby reducing the column dead time, $^2t_0$ and hence the gradient steepness. The gain observed by increasing ^{2}F and hence decreasing $^2t_0$ is significant (see Fig. 5d). Despite a decrease in the plate number (8600–1600), the peak capacity is two-fold higher for 2.5 µm compared to 1.3 µm, the corresponding column dead times being 0.6 s and 2.1 s respectively.
(v) Similarly, due to lower flow-rate and hence longer dead time, a 5 cm column is less attractive than a 3 cm or even a 2 cm column despite a plate number four times lower in the latter case (Fig. 5e). However, a major issue in case of very short column dead times arises from the detector whose response time and acquisition rate are often not suitable for very thin peaks, especially MS-detectors as discussed below.

Considering the available instrumentation, we chose a 50 × 2.1 mm, 2.7 µm column at 30 °C for the first dimension and a 30 × 2.1 mm; 1.3 µm column at 90 °C for the second dimension. From the preceding observations, it is clear that very short columns (<3 cm), both in ^{1}D and ^{2}D should be more attractive for very fast 2D-separations and should permit to double the peak capacity for a first dimension gradient time of 10 min. A larger particle size in the second dimension should be also advantageous. However these conditions are not currently easy to handle considering (i) the pump limits at both high flow-rate and high pressure, (ii) the limited number of columns withstanding temperatures as high as 90 °C, (iii) the low MS-acquisition rate, usually not suitable for very thin peaks and

Please cite this article in press as: M. Sarrut, et al., Theoretical and experimental comparison of one dimensional versus on-line comprehensive two dimensional liquid chromatography for optimized sub-hour separations of complex peptide samples, J. Chromatogr. A (2017), http://dx.doi.org/10.1016/j.chroma.2017.01.054

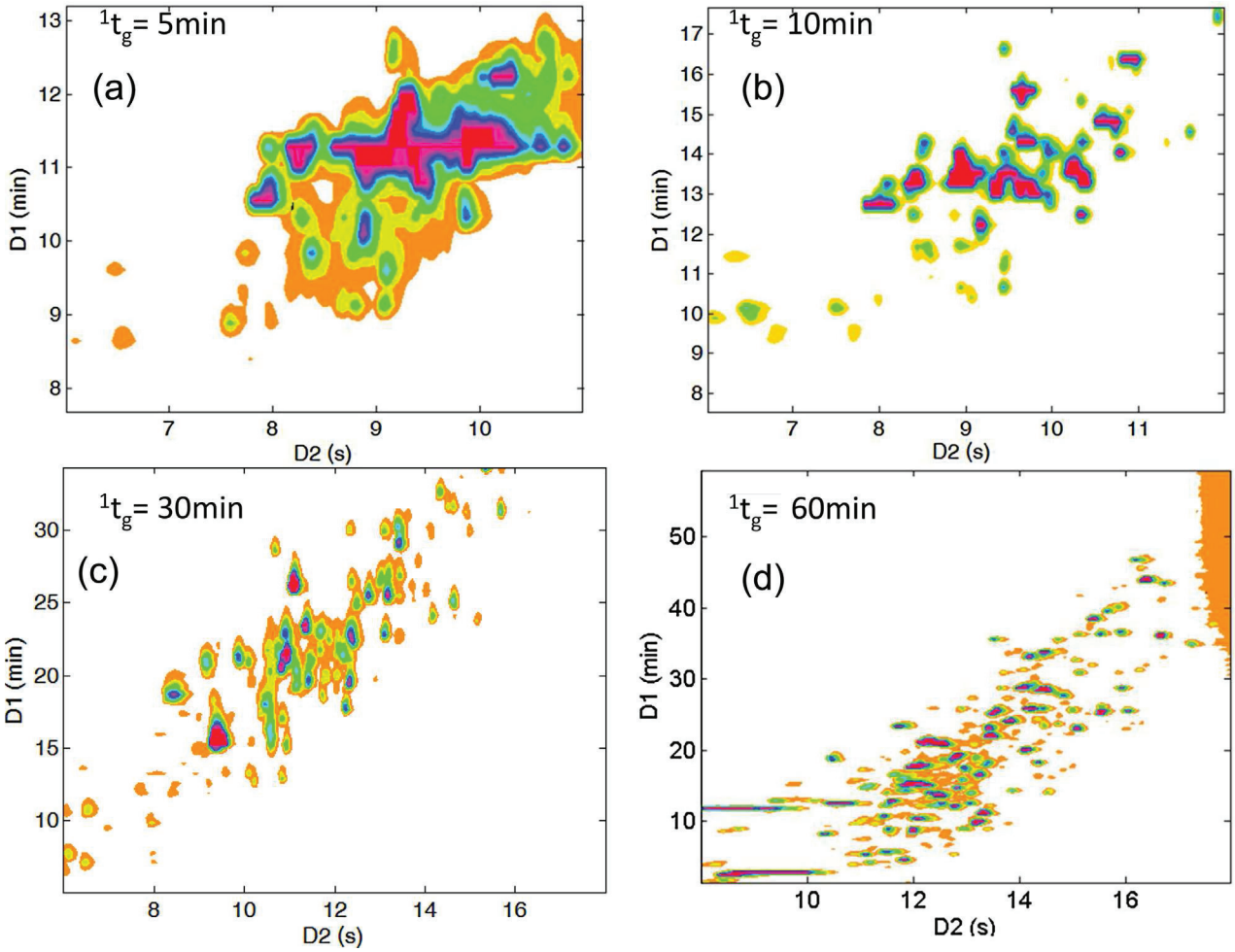

Fig. 6. Contour plots of optimized on-line RPLCxRPLC separations of a tryptic digest of three proteins for different first dimension gradient times: (a) 5 min; (b) 10 min; (c) 30 min; (d) 60 min. Conditions given in Table 2.

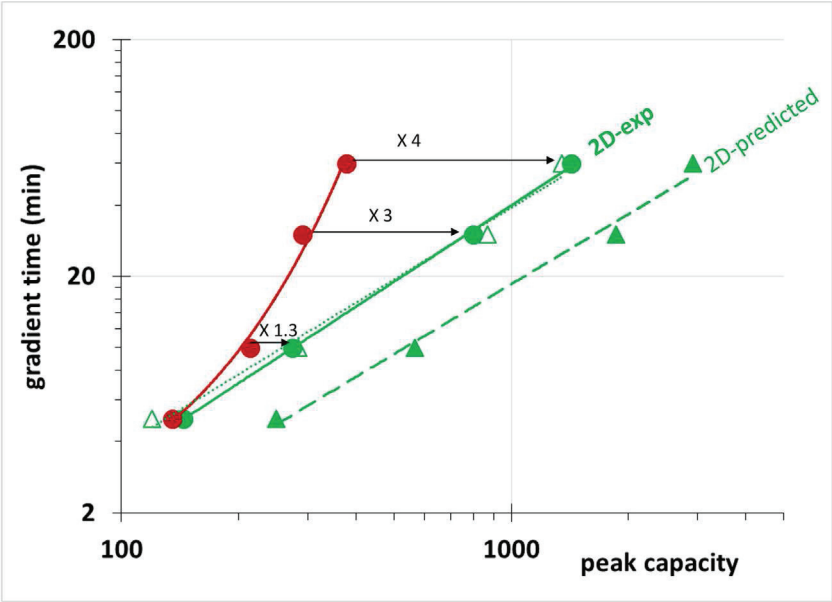

Fig. 7. Gradient time versus effective peak capacity. Experimental data in optimized 1D-RPLC (●); Experimental data in optimized RPLC x RPLC (●); Predicted data in optimized RPLC x RPLC (▲) and Corrected predicted data in optimized RPLC x RPLC taking into account the extra-column variance (Δ) (see text for explanations). The experimental gain in peak capacity for a given gradient time is specified in the figure as "x1.3", "x3" and "x4". 1-D conditions as in Fig. 3. 2D-Conditions given in Table 2.

Please cite this article in press as: M. Sarrut, et al., Theoretical and experimental comparison of one dimensional versus on-line comprehensive two dimensional liquid chromatography for optimized sub-hour separations of complex peptide samples, J. Chromatogr. A (2017), http://dx.doi.org/10.1016/j.chroma.2017.01.054

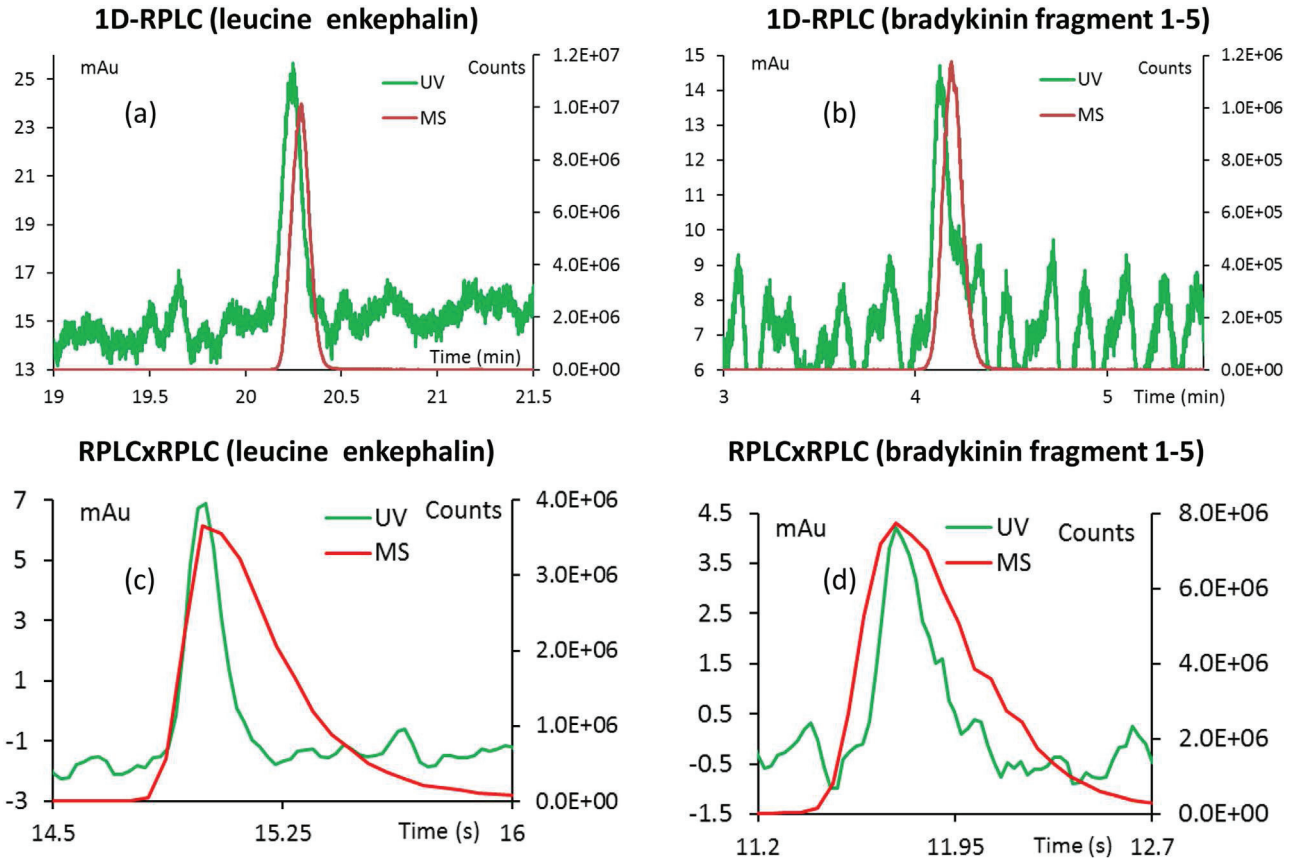

Fig. 8. Peaks of leucine enkephalin and bradykinin fragment 1–5 in 1D-RPLC (a, b) and RPLCxRPLC (c, d) with UV detection (green chromatograms) and MS detection (red chromatograms). ^{1}D dimension conditions: XBridge C18 column (50 × 2.1 mm 5 μm); 500 μL/min; A:10 mM AA and B: ACN; $^{1}t_G$ = 60 min 1–31%B; 30 °C, $^{1}V_i$ = 10 μL. Split ratio = 5. ^{2}D dimension conditions: Kinetex C18 column (30 × 2.1 mm 1.3 μm); 1500 μL/min; A: Water + 0.1%FA and B: ACN + 0.1%FA; $^{2}t_G$ = 0.17 min 1–44%B; 80 °C, Sampling time = 0.36 min. MS conditions: The source temperature, capillary voltage, dwell time and acquisition rate were 600 °C, 1.5 kV, 5 ms and 16.7 Hz for the two targeted compounds. The cone voltage optimized at 10 V and 20 V for Leucine enkephalin and Bradykinin fragment 1–5 respectively both for 1D-RPLC and RPLCxRPLC experiments. For more information, see Tables 1 and 2 for chromatographic and MS conditions respectively. (For interpretation of the references to colour in this figure legend, the reader is referred to the web version of this article.)

(iv) the fact that very high flow rates are often not compatible with MS, thus requiring flow splitting prior to MS.

The contour plots of on-line RPLC × RPLC separations of a tryptic digest of 3 proteins, obtained with optimized sets of 2D-conditions and a predicted dilution factor equal to 1 (i.e. no dilution during the separation process) are shown in Fig. 6 for four different gradient times, 5, 10, 30 and 60 min. A sufficient degree of orthogonality was ensured by changing the mobile phase pH between the two dimensions, namely 6.8 and 2.8 in first and second dimension respectively as earlier recommended [17]. Other conditions are reported in Table 2. 2D-contour plots can be compared to the optimized 1D-separations shown in Fig. 3 for the same gradient times. It is important to note that the peak width cannot be evaluated from the 2D-contour plot since the observed spots depends on the peak intensity but also on the chosen Z-scale. As a result, very intense peaks look much larger. Furthermore, some poorly retained peaks eluted together in the second dimension (see $^{1}t_G$ = 60 min) thereby leading to very large spots. The obtained results in terms of peak capacities can be compared between both techniques in Fig. 7. Experimental data are represented by red and green circles for 1D-RPLC and RPLC x RPLC respectively. The advantage of RPLC x RPLC can be assessed by the gain in peak capacity which increases with the analysis time up to a factor 4 for a gradient time of 60 min. It can be observed that the corresponding curves intersect at about 5 min suggesting that, by using cutting edge instruments and cutting edge columns in both techniques, the crossover time for peptides is similar to that obtained by Huang et al. [14] for small molecules (i.e. between 5 and 7 min). Predicted effective peak capacities (see green triangles in Fig. 7) were calculated from Eq. (10) with experimentally determined γ value (0.6; 0.6; 0.42 and 0.41 for 5; 10; 30 and 60 min respectively). As can be observed in Fig. 7, predicted data are shifted towards higher peak capacities with a crossover time that could be expected to be much shorter. It is important to note that predicted data were obtained by assuming that the contribution of extra-column volumes to the total peak variance was not significant. In case of the 2D-Agilent instrument, the estimated value for the extra-column variance (resulting from both the cell volume and the tubing located between the column outlet and the detector) was estimated at 2 μL^2. Considering ^{2}D peak thinness (in volume units), this value may be quite significant. Eq. (11) was therefore modified in order to take into account the extra column variance in the second dimension, yielding for $^{2}\beta$ calculation:

$$ {}^{2}\beta = \frac{1}{\sqrt{1 + \frac{1}{4} \times \frac{{}^{2}V_{inj}^{2}}{{}^{2}\sigma_{col}^{2}} \times \frac{1}{C_F^2} + \frac{{}^{2}\sigma_{ext}^{2}}{{}^{2}\sigma_{col}^{2}}}} \quad (15) $$

Where σ^2_{ext} is the extra column variance in the second dimension.

Resulting corrected predicted data are represented by green empty triangles in Fig. 7. As can be seen, the predicted corrected curve is very close to the experimental one. In our previous study [4], we suggested that the observed error between experimental and predicted data could be derived from different issues, the main one being related to the fact that Van Deemter coefficients

Please cite this article in press as: M. Sarrut, et al., Theoretical and experimental comparison of one dimensional versus on-line comprehensive two dimensional liquid chromatography for optimized sub-hour separations of complex peptide samples, J. Chromatogr. A (2017), http://dx.doi.org/10.1016/j.chroma.2017.01.054

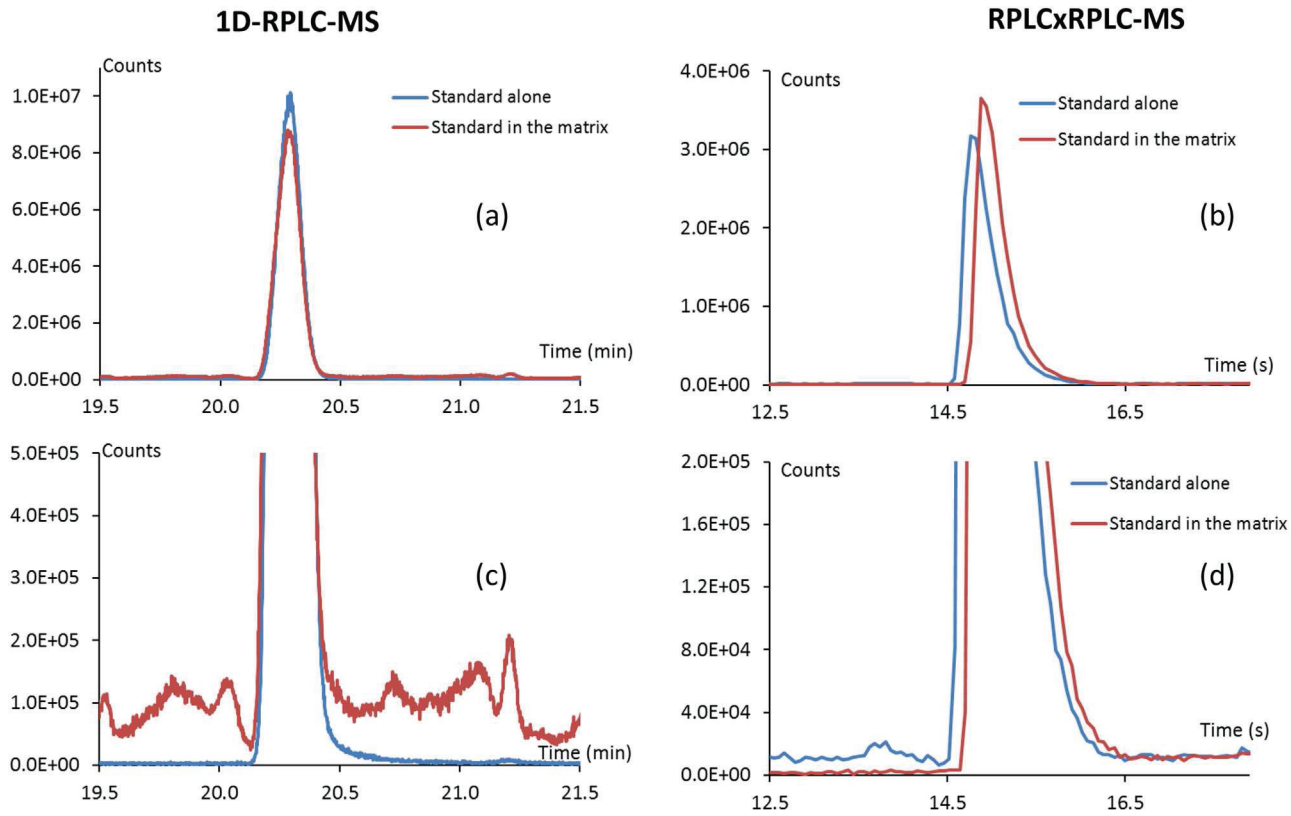

Fig. 9. MS-signal of leucine enkephalin injected alone (blue signal) and spiked in the matrix (red signal) in (a, c) RPLC–MS and (b, d) RPLCxRPLC–MS (main fraction). Bottom chromatograms represent zoom of upper chromatograms for comparison of short-term noiseSame conditions as in Fig. 8. (For interpretation of the references to colour in this figure legend, the reader is referred to the web version of this article.)

were calculated from a neutral solute and hence could significantly overestimate the column plate value for charged compounds with formic acid as additive [31]. From the present results, it appears that Van Deemter coefficients obtained with neutral solutes are quite reliable for the prediction of RPLC x RPLC separations of peptides. Unlike in 1D-RPLC, very steep gradients are used in the second dimension of RPLC x RPLC, resulting in much lower retention and hence little or no overloading effect. This is not true in 1D-RPLC as discussed above (Fig. 2). It can be concluded from these results that the main reason for the observed discrepancy between predicted and experimental data in RPLCxRPLC is the significant extra-column band broadening which occurs in spite of very small extra-column volumes proposed by current 2D-UHPLC instruments. In light of these results, this optimization approach appears to be quite reliable with predicted values matching experimental ones provided that the extra column variance, in addition to the injection effects are considered. Furthermore this suggests that optimization results, and in particular the crossover time should strongly differ from one 2D-instrument to another. As a consequence of the above, decreasing extra-column volumes and especially those located after the column outlet should permit to further decrease the crossover time.

3.3. Comparison of mass spectrometry detection capability between 1D-RPLC–MS and RPLCxRPLC–MS

In addition to UV detection, a mass spectrometry detector (single quadrupole) was hyphenated to the 1D-instrument and to the 2D-instrument for comparing RPLC and RPLCxRPLC signal intensities in optimized conditions for a gradient time of 60 min. In order to further increase the peak capacity in 1D-LC, another 1D-instrument (Instrument 2) was used. The advantage of Instrument 2 consisted in its larger tubing, thus allowing higher flow-rates. It is important to note that the contribution of larger tubing to the total peak dispersion was not significant due to high $^1\sigma_{col}$ values in 1D-conditions. 1D-separations of peptides could be carried out with a higher flow-rate, thereby further enhancing the experimental peak capacity (close to 400 with the 15 cm Acquity CSH-C18 column). Two peptides were followed in Single Ion Monitoring mode (SIM) with characteristics and MS conditions listed in Table 1. The two peptides were analyzed alone and spiked in a tryptic digest of three proteins (matrix), each at a concentration of 1 mg/L. The peaks of the peptides obtained alone under RPLC–MS and RPLCxRPLC–MS conditions are shown in Fig. 8. For both techniques, the injected volume (30 μL in 1D-RPLC and 10 μL in RPLC x RPLC) represented 10% of the column dead volume. It is very interesting to notice that, for both peptides, UV-signal intensities (green chromatograms in Fig. 8) in RPLC-UV (Fig. 8a and b) and in RPLCxRPLC-UV (Fig. 8c and d) are quite similar which means that the same sensitivity level (same dilution factor) was reached in both techniques while the injected amount was three times smaller and the peak capacity four times higher in case of RPLC x RPLC, thereby emphasizing the advantage of 2D-LC compared to 1D-LC. In 1D-LC (Fig. 8a and b), peak widths with MS detection are similar to those obtained with UV detection. This is not the case in 2D-LC for which peaks are much larger with MS detection (Fig. 8c and d) suggesting a much stronger contribution of MS-instrument (tubing, capillary and MS parameters) to extra-column band broadening in 2D-LC–MS compared to 1D-LC–MS. The estimated value for the extra-column variance with MS detection was 8 μL^2, four times higher than the estimated value of the extra-column variance with UV detection. As discussed above, such value cannot be compatible with the remarkable thinness of the peaks in 2D, both in time unit (0.2–0.5 s) and in volume unit (5–12 μL). As a consequence, the coupling with MS

Please cite this article in press as: M. Sarrut, et al., Theoretical and experimental comparison of one dimensional versus on-line comprehensive two dimensional liquid chromatography for optimized sub-hour separations of complex peptide samples, J. Chromatogr. A (2017), http://dx.doi.org/10.1016/j.chroma.2017.01.054

detection generates a significant additional band broadening in 2D-LC–MS thereby leading to both a reduction of signal intensity and a decrease in peak capacity, thus spoiling the separation power achieved in optimized RPLCxRPLC conditions.

A major advantage of 2D-LC is clearly pointed out in Fig. 9 which compares the baseline noise between 1D-LC and 2D-LC. In 1D-LC, the noise is significantly increased when the peptide is spiked in the matrix (red signal) compared to when it is alone (blue signal) (Fig. 9a and c) whereas in 2D-LC the noise intensity is the same in both cases (Fig. 9b and d). The origin of the noise in 1D-LC may stem from the complexity of the matrix resulting in numerous species with close m/z values coming simultaneously in the MS-source. From the comparison of MS-signals between the two techniques (two-fold lower in RPLCxRPLC for leucine enkephalin as shown in Fig. 9. It results that the signal-to-noise ratio (S/N) is dramatically improved in RPLCxRPLC–MS compared to 1D-RPLC–MS (i.e. by a factor 15). As a consequence, the lower noise generated in 2D-LC may compensate a lower signal in MS due to the use of higher acquisition rates which are mandatory for untargeted applications considering the very narrow peaks that are obtained in RPLCxRPLC.

4. Conclusions

This study was devoted to the optimization of both 1D-RPLC and on-line RPLCxRPLC conditions for the separations of complex samples of peptides with gradient times of one hour or less.

In 1D-RPLC, despite the use of a stationary phase dedicated to the separation of charged compounds, a strong overloading effect was highlighted, in acidic medium, which significantly reduced the experimental peak capacity compared to the predicted one, especially in the range of very low gradient steepness values as those obtained with both short columns and high flow-rates. This issue is not at stake in RPLCxRPLC due to very steep gradients used in the second dimension.

In RPLCxRPLC, the peak capacity and the dilution factor were considered together, at a given first dimension gradient time, for the optimization of numerous parameters. It was shown that the sampling rate has to be decreased down to one fraction per peak for very short first dimension gradient times (below 10 min). Our experimental results show that the experimental effective peak capacity in RPLC × RPLC outperforms that in 1D-RPLC when the analysis time is longer than 5 min. Furthermore, the experimental RPLCxRPLC separation, performed in optimized conditions with a gradient time of 60 min, led to a 4-fold gain in peak capacity compared to the optimized 1D-RPLC separation. At the same time, peak heights with UV detection were exactly the same in spite of an injected volume divided by 3 in RPLCxRPLC.

An important discrepancy was found between predicted and experimental data which was proved to be mainly due to extra-column band broadening occurring between column outlet and detection. By considering this issue, we obtained that predicted and experimental data match very well, thereby emphasizing the reliability of our optimization approach.

Despite a lower peak capacity with MS detection than with UV detection, resulting from a greater contribution of extra column volumes to extra-column band broadening, the somewhat higher peak capacity in 2D-LC compared to 1D-LC allowed a drastic decrease of baseline noise thereby significantly increasing the signal-to-noise ratio (by 15–20 times).

As a consequence of the results detailed in this study (lower amount of sample required, higher peak capacity and lower noise), optimized on-line RPLCxRPLC hyphenated to mass spectrometry seems to be very promising for the fast analysis of complex peptide samples.

References

[1] P.Q. Tranchida, P. Donato, F. Cacciola, M. Beccaria, P. Dugo, L. Mondello, Potential of comprehensive chromatography in food analysis, TrAC Trends Anal. Chem. 52 (2013) 186–205, http://dx.doi.org/10.1016/j.trac.2013.07.008.
[2] M. Sarrut, G. Crétier, S. Heinisch, Theoretical and practical interest in UHPLC technology for 2D-LC, TrAC Trends Anal. Chem. 63 (2014) 104–112, http://dx.doi.org/10.1016/j.trac.2014.08.005.
[3] D.R. Stoll, J. Danforth, K. Zhang, A. Beck, Characterization of therapeutic antibodies and related products by two-dimensional liquid chromatography coupled with UV absorbance and mass spectrometric detection, J. Chromatogr. B 1032 (2016) 51–60, http://dx.doi.org/10.1016/j.jchromb.2016.05.029.
[4] M. Sarrut, A. D'Attoma, S. Heinisch, Optimization of conditions in on-line comprehensive two-dimensional reversed phase liquid chromatography. Experimental comparison with one-dimensional reversed phase liquid chromatography for the separation of peptides, J. Chromatogr. A 1421 (2015) 48–59, http://dx.doi.org/10.1016/j.chroma.2015.08.052.
[5] F. Bedani, P.J. Schoenmakers, H.-G. Janssen, Theories to support method development in comprehensive two-dimensional liquid chromatography–a review, J. Sep. Sci. 35 (2012) 1697–1711, http://dx.doi.org/10.1002/jssc.201200070.
[6] P.J. Schoenmakers, G. Vivó-Truyols, W.M.C. Decrop, A protocol for designing comprehensive two-dimensional liquid chromatography separation systems, J. Chromatogr. A 1120 (2006) 282–290, http://dx.doi.org/10.1016/j.chroma.2005.11.039.
[7] H. Poppe, Some reflections on speed and efficiency of modern chromatographic methods, J. Chromatogr. A 778 (1997) 3–21, http://dx.doi.org/10.1016/S0021-9673(97)00376-2.
[8] K. Horie, H. Kimura, T. Ikegami, A. Iwatsuka, N. Saad, O. Fiehn, N. Tanaka, Calculating optimal modulation periods to maximize the peak capacity in two-dimensional HPLC, Anal. Chem. 79 (2007) 3764–3770, http://dx.doi.org/10.1021/ac062002t.
[9] H. Gu, Y. Huang, P.W. Carr, Peak capacity optimization in comprehensive two dimensional liquid chromatography: a practical approach, J. Chromatogr. A 1218 (2011) 64–73, http://dx.doi.org/10.1016/j.chroma.2010.10.096.
[10] G. Vivoí-Truyols, S. van der Wal, P.J. Schoenmakers, Comprehensive study on the optimization of online two-dimensional liquid chromatographic systems considering losses in theoretical peak capacity in first- and second-dimensions: a pareto-optimality approach, Anal. Chem. 82 (2010) 8525–8536, http://dx.doi.org/10.1021/ac101420f.
[11] Chapter 26 other optimization methods, in: D.L. Massart, B.G.M. Vandeginste, L.M.C. Buydens, S. De Jong, P.J. Lewi, J. Smeyers-Verbeke (Eds.), Data Handl. Sci. Technol., Elsevier, 1998, pp. 771–804, http://www.sciencedirect.com/science/article/pii/S0922348797800561 (Accessed 10 July 2015).
[12] D.R. Stoll, X. Wang, P.W. Carr, Comparison of the practical resolving power of one- and two-dimensional high-performance liquid chromatography analysis of metabolomic samples, Anal. Chem. 80 (2008) 268–278, http://dx.doi.org/10.1021/ac701676b.
[13] L.W. Potts, P.W. Carr, Analysis of the temporal performance of one versus on-line comprehensive two-dimensional liquid chromatography, J. Chromatogr. A 1310 (2013) 37–44, http://dx.doi.org/10.1016/j.chroma.2013.07.102.
[14] Y. Huang, H. Gu, M. Filgueira, P.W. Carr, An experimental study of sampling time effects on the resolving power of on-line two-dimensional high performance liquid chromatography, J. Chromatogr. A 1218 (2011) 2984–2994, http://dx.doi.org/10.1016/j.chroma.2011.03.032.
[15] L.W. Potts, D.R. Stoll, X. Li, P.W. Carr, The impact of sampling time on peak capacity and analysis speed in on-line comprehensive two-dimensional liquid chromatography, J. Chromatogr. A 1217 (2010) 5700–5709, http://dx.doi.org/10.1016/j.chroma.2010.07.009.
[16] K. Horie, Y. Sato, T. Kimura, T. Nakamura, Y. Ishihama, Y. Oda, T. Ikegami, N. Tanaka, Estimation and optimization of the peak capacity of one-dimensional gradient high performance liquid chromatography using a long monolithic silica capillary column, J. Chromatogr. A 1228 (2012) 283–291, http://dx.doi.org/10.1016/j.chroma.2011.12.088.
[17] A. D'Attoma, C. Grivel, S. Heinisch, On-line comprehensive two-dimensional separations of charged compounds using reversed-phase high performance liquid chromatography and hydrophilic interaction chromatography. Part I: orthogonality and practical peak capacity considerations, J. Chromatogr. A 1262 (2012) 148–159, http://dx.doi.org/10.1016/j.chroma.2012.09.028.
[18] U.D. Neue, Theory of peak capacity in gradient elution, J. Chromatogr. A 1079 (2005) 153–161, http://dx.doi.org/10.1016/j.chroma.2005.03.008.
[19] L.R. Snyder, J.W. Dolan, J.R. Gant, Gradient elution in high-performance liquid chromatography: I. Theoretical basis for reversed-phase systems, J. Chromatogr. A 165 (1979) 3–30, http://dx.doi.org/10.1016/S0021-9673(00)85726-X.
[20] J.P. Foley, J.G. Dorsey, Equations for calculation of chromatographic figures of merit for ideal and skewed peaks, Anal. Chem. 55 (1983) 730–737, http://dx.doi.org/10.1021/ac00255a033.
[21] J.M. Davis, D.R. Stoll, P.W. Carr, Effect of first-dimension undersampling on effective peak capacity in comprehensive two-dimensional separations, Anal. Chem. 80 (2008) 461–473, http://dx.doi.org/10.1021/ac071504j.
[22] A. Le Masle, D. Angot, C. Gouin, A. D'Attoma, J. Ponthus, A. Quignard, S. Heinisch, Development of on-line comprehensive two-dimensional liquid chromatography method for the separation of biomass compounds, J.

Please cite this article in press as: M. Sarrut, et al., Theoretical and experimental comparison of one dimensional versus on-line comprehensive two dimensional liquid chromatography for optimized sub-hour separations of complex peptide samples, J. Chromatogr. A (2017), http://dx.doi.org/10.1016/j.chroma.2017.01.054

Chromatogr. A 1340 (2014) 90–98, http://dx.doi.org/10.1016/j.chroma.2014.03.020.
[23] S. Heinisch, J.-L. Rocca, M. Feinberg, Optimization of a chromatographic analysis in reversed phase liquid chromatography, J. Chemom. 3 (1989) 127–137, http://dx.doi.org/10.1002/cem.1180030505.
[24] J.C. Giddings, Comparison of theoretical limit of separating speed in gas and liquid chromatography, Anal. Chem. 37 (1965) 60–63, http://dx.doi.org/10.1021/ac60220a012.
[25] G. Desmet, D. Clicq, P. Gzil, Geometry-Independent plate height representation methods for the direct comparison of the kinetic performance of LC supports with a different size or morphology, Anal. Chem. 77 (2005) 4058–4070, http://dx.doi.org/10.1021/ac050160z.
[26] Y. Zhang, X. Wang, P. Mukherjee, P. Petersson, Critical comparison of performances of superficially porous particles and sub-2 μm particles under optimized ultra-high pressure conditions, J. Chromatogr. A 1216 (2009) 4597–4605, http://dx.doi.org/10.1016/j.chroma.2009.03.071.
[27] K. Broeckhoven, D. Cabooter, F. Lynen, P. Sandra, G. Desmet, The kinetic plot method applied to gradient chromatography: theoretical framework and experimental validation, J. Chromatogr. A 1217 (2010) 2787–2795, http://dx.doi.org/10.1016/j.chroma.2010.02.023.
[28] S. Heinisch, J.-L. Rocca, Sense and nonsense of high-temperature liquid chromatography, J. Chromatogr. A 1216 (2009) 642–658, http://dx.doi.org/10.1016/j.chroma.2008.11.079.
[29] F. Gritti, G. Guiochon, Separation of peptides and intact proteins by electrostatic repulsion reversed phase liquid chromatography, J. Chromatogr. A 1374 (2014) 112–121, http://dx.doi.org/10.1016/j.chroma.2014.11.036.
[30] S. Heinisch, Using elevated temperature in UHPLC: interest and limitations, in: D. Guillarme, J.-L. Veuthey (Eds.), UHPLC in Life Sciences, Royal Society of Chemistry, London, 2012, pp. 102–130.
[31] S. Heinisch, A. D'Attoma, C. Grivel, Effect of pH additive and column temperature on kinetic performance of two different sub-2 μm stationary phases for ultrafast separation of charged analytes, J. Chromatogr. A 1228 (2012) 135–147, http://dx.doi.org/10.1016/j.chroma.2011.08.041.
[32] J. Ruta, D. Zurlino, C. Grivel, S. Heinisch, J.-L. Veuthey, D. Guillarme, Evaluation of columns packed with shell particles with compounds of pharmaceutical interest, J. Chromatogr. A 1228 (2012) 221–231, http://dx.doi.org/10.1016/j.chroma.2011.09.013.
[33] A. D'Attoma, S. Heinisch, On-line comprehensive two dimensional separations of charged compounds using reversed-phase high performance liquid chromatography and hydrophilic interaction chromatography. Part II: application to the separation of peptides, J. Chromatogr. A 1306 (2013) 27–36, http://dx.doi.org/10.1016/j.chroma.2013.07.048.
[34] R.E. Murphy, M.R. Schure, J.P. Foley, Effect of sampling rate on resolution in comprehensive two-dimensional liquid chromatography, Anal. Chem. 70 (1998) 1585–1594, http://dx.doi.org/10.1021/ac971184b.

Glossary

Exponents [1] and [2] correspond to first and second dimension respectively:

As: Peak asymmetry
b: Gradient steepness
φ_B*:* Volume fraction of the strong solvent B
C_F*:* Compression factor
d_c*:* Column diameter
D_F*:* Dilution factor
D_m*:* Diffusion coefficient
d_p*:* Particle diameter
F: Flow rate
k_0*:* Extrapolated retention factor in the weak solvent
N_{col}*:* Column plate number
n: One-dimensional peak capacity
$n_{2D,eff}$*:* Two-dimensional effective peak capacity
S: Solvent strength parameter
T: Column temperature
t_0*:* Column dead time
t_D*:* System dwell time
t_G*:* Gradient time
t_s*:* Sampling time
V_D*:* System dwell volume
V_{inj}*:* Injection volume
$w_{10\%}$*:* Peak width at 10%
α*:* Correction factor due to undersampling effect
β*:* Correction factor due to non ideal transfer from the 1st to the 2nd dimension
γ*:* Correction factor due to retention surface coverage
$\Delta\varphi$*:* Gradient range in volume fraction
σ_{col}*:* Peak standard deviation due to solute dispersion in the column
σ_{tot}*:* Peak standard deviation due to solute dispersion in column and extra-column units
σ^2_{col}*:* Peak variation due to extra column dispersion
τ*:* Sampling rate

Please cite this article in press as: M. Sarrut, et al., Theoretical and experimental comparison of one dimensional versus on-line comprehensive two dimensional liquid chromatography for optimized sub-hour separations of complex peptide samples, J. Chromatogr. A (2017), http://dx.doi.org/10.1016/j.chroma.2017.01.054

CONCLUSIONS

L'optimisation simultanée de la capacité de pics, du temps d'analyse et du facteur de dilution a été réalisée à l'aide d'outils prédictifs puis appliquée à un échantillon réel de peptides. L'intérêt d'utiliser des colonnes très courtes (30 mm) et très efficaces en ^{2}D mais également de même diamètre qu'en ^{1}D pour respectivement maximiser la capacité de pics et la sensibilité est clairement montré. Cela est notamment rendu possible par le $^{2}C_{F}$ qui permet de larges volumes injectés en ^{2}D (70 $\%V_{0}$).

La capacité de pics maximale atteinte en 1D-RPLC est obtenue en divisant le temps d'analyse par 40 en RPLCxRPLC (1h vs 40h). De plus, une séparation RPLCxRPLC génère une capacité de pics supérieure à celle obtenue en 1D-RPLC dès l'utilisation de temps de gradient d'environ 3-4 min.

D'autres parts il est intéressant de noter que plusieurs sets de conditions conduisent au même résultat et que des critères supplémentaires doivent être considérés pour finalement choisir les meilleures conditions.

Enfin, les résultats obtenus en 2D pour un même set de colonnes à différents temps d'analyse l'ont été à sensibilité équivalente ce qui est impossible en 1D-LC.

CHAPITRE 4 – LA CHROMATOGRAPHIE EN PHASE LIQUIDE BIDIMENSIONNELLE « COMPREHENSIVE » EN LIGNE COUPLÉE À LA SPECTROMÉTRIE DE MASSE POUR LA CARACTÉRISATION D'ANTICORPS CONJUGUÉS : OPTIMISATION ET APPLICATION

Ce chapitre a fait l'objet de deux publications :

Article 4

"Analysis of antibody-drug conjugates by comprehensive on-line two-dimensional hydrophobic interaction chromatography x reversed phase liquid chromatography hyphenated to high resolution mass spectrometry. I- Optimization of chromatographic conditions";

M. Sarrut, A. Corgier, S. Fekete, D. Guillarme, D. Lascoux, M-C. Janin-Bussat, A. Beck, S. Heinisch, J. Chromatogr. B, 1032 (2016), 103-111

Article 5

"Analysis of antibody-drug conjugates by comprehensive on-line twodimensional hydrophobic interaction chromatography x reversed phase liquid chromatography hyphenated to high resolution mass spectrometry. II- Identification of sub-units for the characterization of even and odd load drug species";

M. Sarrut, S. Fekete, M-C. Janin-Bussat, D. Guillarme, O. Colas, D. Guillarme, A. Beck, S. Heinisch, J. Chromatogr. B, 1032 (2016), 91-102

INTRODUCTION

Les anticorps conjugués (ADCs) représentent l'une des classes de molécules thérapeutiques les plus prometteuses pour le traitement du cancer [1]. Ces biomolécules combinent la spécificité d'un anticorps monoclonal (mAb) avec la présence de puissantes molécules cytotoxiques liées de façon covalentes au mAb par le biais de linkers. Les cellules cancéreuses sont alors sélectivement détruites tout en limitant les effets secondaires.

Ces protéines sont des macromolécules d'environ 150 kDa (environ 1300 acides aminés) qui peuvent générer des milliers de variants différents (charges, taille, oxydation, deamidation, glycosylation…) [2]. Le nombre moyen de molécules cytotoxiques conjuguées sur un mAb (DAR moyen) est également une donnée majeure puisqu'il influence les paramètres pharmacocinétiques, toxicologiques mais aussi la dissipation et l'index thérapeutique de l'ADC dans l'organisme [3–5].

La complexité de telles structures requiert de multiples approches analytiques complémentaires pour leur caractérisation telles que la chromatographie (IEX, SEC, HIC, HILIC, RPLC), les techniques électrophorétiques (CZE, cIEF, CGE) et la spectrométrie de masse (MS native, approches top-down, middle-up, bottom-up, peptide mapping…) [6]. La possibilité de coupler ces techniques en ligne, particulièrement en mode « comprehensive », présente donc un intérêt indéniable puisqu'il sera possible de recueillir des données orthogonales en une seule injection tout en limitant la consommation d'échantillon ou des problèmes de contaminations [7]. Le développement et l'optimisation de telles méthodes bidimensionnelles représentent toutefois un challenge analytique important aussi bien du point de vue instrumental que du traitement des données.

La section A de ce chapitre détaille, sous la forme d'un article, l'intérêt et l'optimisation d'une méthode HICxRPLC-UV/MS en ligne pour la caractérisation d'un ADC commercial à cystéine, le Brentuximab Vedotin (Adcetris©).

La section B est dédiée au traitement des données UV et MS de la méthode développée dans la section A dans le but d'obtenir à la fois le DAR moyen (i.e. le nombre moyen de molécules cytotoxiques liées au mAb) ainsi que des informations structurales sur l'ADC. L'analyse d'échantillons d'ADCs stressés a également été réalisée afin d'étudier la dégradation de ces biomolécules. Cette partie est présentée sous la forme d'un second article.

A. OPTIMISATION DES CONDITIONS CHROMATOGRAPHIQUES

Article 4

“Analysis of antibody-drug conjugates by comprehensive on-line two-dimensional hydrophobic interaction chromatography x reversed phase liquid chromatography hyphenated to high resolution mass spectrometry. I- Optimization of chromatographic conditions”;

M. Sarrut, A. Corgier, S. Fekete, D. Guillarme, D. Lascoux, M-C. Janin-Bussat, A. Beck, S. Heinisch, J. Chromatogr. B, 1032 (2016), 103-111

Journal of Chromatography B, 1032 (2016) 103–111

Contents lists available at ScienceDirect

Journal of Chromatography B

journal homepage: www.elsevier.com/locate/chromb

Analysis of antibody-drug conjugates by comprehensive on-line two-dimensional hydrophobic interaction chromatography x reversed phase liquid chromatography hyphenated to high resolution mass spectrometry. I – Optimization of separation conditions

Morgan Sarrut[a], Amélie Corgier[a], Szabolcs Fekete[b], Davy Guillarme[b], David Lascoux[d], Marie-Claire Janin-Bussat[c], Alain Beck[c], Sabine Heinisch[a,*]

[a] Univ Lyon, CNRS, Université Claude Bernard Lyon 1, Ens de Lyon, Institut des Sciences Analytiques, UMR 5280, 5 rue de la Doua, F-69100 VILLEURBANNE, France
[b] School of Pharmaceutical Sciences, University of Geneva, University of Lausanne, Bd d'Yvoy 20, 1211 Geneva 4, Switzerland
[c] Center of Immunology Pierre Fabre, 5 Avenue Napoléon III, BP 60497, 74160 Saint-Julien-en-Genevois, France
[d] Waters SAS, BP 608, 78056 St Quentin en Yvelines, France

ARTICLE INFO

Article history:
Received 15 January 2016
Received in revised form 19 May 2016
Accepted 27 June 2016
Available online 28 June 2016

Keywords:
On-line comprehensive 2D-LC
HICxRPLC-QTOF-MS
Antibody-drug conjugate
ADC
Brentuximab vedotin
Adcetris®

ABSTRACT

Antibody-drug-conjugates (ADCs) manufacturing leads to a mixture of species which needs to be characterized during development and for further quality control. The coupling of on-line HIC x RPLC to high resolution mass spectrometry can be considered as a very efficient analytical method, providing extensive information on ADC sample, within a reduced time scale. Our intention in this first paper is to present the approach used to rationally optimize the numerous conditions that can affect the quality of the 2D-separation. HIC and RPLC conditions were therefore optimized to prevent salt precipitation due to solvent mixing and to enhance sensitivity, while limiting the total analysis time. We demonstrated that adding salt in the sample solvent before HIC injection allows a significant peak shape improvement. The gradient profile was also carefully optimized in both dimensions, leading to a two-step gradient in HIC and bracketed gradient in RPLC. This study shows that on-line HIC x RPLC hyphenated to high resolution mass spectrometry is a useful method to obtain rapid and extensive structural information on the peaks observed in the first HIC dimension, thereby leading, in a single step requiring 75 min, to the precise determination of the average drug-to-antibody ratio (DAR) by HIC as well as the knowledge of the drug load distribution for a particular DAR. The structural characterization of ADC fragments by RPLC-QTOF will be discussed in the second part of this two-part series.

1. Introduction

Monoclonal antibodies (mAbs) and their related products such as antibody-drug-conjugates (ADCs), bispecific antibodies, Fab fragments, Fc-fusion proteins and radio-immunoconjugates are the fastest growing class of human therapeutics [1]. Even if numerous mAbs and derivatives have been approved, the first generation mAbs often suffers from a limited efficacy. ADC technology combines the specificity of a monoclonal antibody (mAb) together with a potent cytotoxic drug covalently bounded via a linker to the antibody, allowing an efficacy improvement. There are two main types of ADC technology based either on cysteine or lysine linked conjugations and currently – as a third class – the so-called engineered ADCs (cysteine residues are engineered on the surface of the mAb) are often mentioned as a promising technology. Cysteine linked ADCs are made by the chemical conjugation of cytotoxins to mAbs, by first reducing inter-chain disulfide bonds, followed by the conjugation of the resulting free thiols with drugs. This process yields a controlled, but heterogeneous population of conjugated products that contains species with various numbers of drugs linked to different former inter-chain disulfide cysteine residues on the antibodies [2]. This process results in conjugates with a distribution of 0, 2, 4, 6 and 8 drugs incorporated per antibody and an average DAR of around 3–4 drugs/mAb which seems to be optimal in clinical trials [3,4]. Fig. 1 shows the possible positional isomers of DAR species of a cysteine conjugated ADC. In ADC products, the DAR0

* Corresponding author.
E-mail address: sabine.heinisch@univ-lyon1.fr (S. Heinisch).

http://dx.doi.org/10.1016/j.jchromb.2016.06.048
1570-0232/

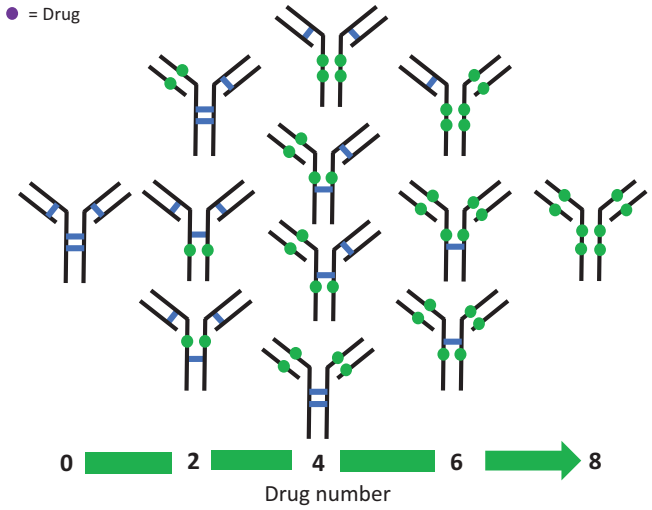

Fig. 1. Representation of positional isomers for the different even DARs of a cysteine conjugated ADC.

is considered as an impurity while DAR species with odd numbers (DAR1 or DAR3) are degradation products.

Among the several liquid chromatographic (LC) modes applied for the analysis of ADCs, hydrophobic interaction chromatography (HIC) is the reference technique to separate the different populations of DARs. The main advantage of HIC compared to other LC modes (reversed phase (RP) particularly) is that it is non-denaturating, so the native forms of the proteins are expected to be maintained. HIC allows the separation of the different DARs of native cysteine conjugated IgG1 type ADCs such as DAR0, DAR2, DAR4, DAR6 and DAR8 under their physiological-like conformation [5–7]. In an orthogonal way, DAR species can also be separated by RPLC under reducing conditions as well as capillary electrophoresis sodium dodecyl sulfate (CE-SDS) under both non-reducing and reducing conditions [2]. Finally, mass spectrometry (MS) is ultimately used for structural assessment [8,9].

MAbs are heterogeneous and possess several microvariants including glyco variants, charge variants and size variants [10]. In addition, the conjugation of payloads to mAb further increases the structural complexity, and requires improved methods for the characterization of drug loading, distribution, average DAR, size and charge variants or unconjugated drug linkers [11]. State-of-the-art structural characterization methods of ADCs were recently reviewed by Beck and Cianferani and case studies of cysteine-linked Brentuximab vedotin (Adcetris®) and lysine-linked Trastuzumab emtansine (Kadcyla®) were also discussed [12,13]. ADC analysis and characterization can be performed at different levels such as top-down, middle-down and bottom-up levels. Coupling of different techniques such as LC–MS or multidimensional LC separations may offer additional benefits over one-dimensional methods [14,15].

Recently, Debaene et al. applied HIC and off-line ion mobility native mass spectrometry (IM-MS) for the detailed characterization of Brentuximab vedotin [16]. The main advantage of using native MS for exact mass measurements of ADCs with inter-chain cysteine-linked drugs, lies in its ability to detect non-covalent associations of light and heavy chains that cannot be detected directly with classical denaturating LC–MS methods. This methodology resulted in a fast determination of DAR ratio, average DAR and naked mAb, but provided no information about the drug loading position.

An improved LC–MS peptide mapping protocol to characterize the drug loaded peptides was reported by Janin-Bussat et al. [17]. This protocol was developed for the commercially available Brentuximab vedotin. Because of the drug hydrophobicity, all the steps (including enzymatic digestion) were improved to maintain the hydrophobic drug-loaded peptides in solution, allowing their unambiguous identification by LC–MS. For the first time, the payloads positional isomers observed by RP-LC after IdeS-digestion and reduction of the ADC were also characterized.

Recently, an interesting work showed that multi-dimensional (2D) chromatography could be a powerful technique for ADC analysis and characterization, since it allows the hyphenation of non-compatible MS chromatographic method (i.e. HIC as the first dimension) to MS instrumentation via a suitable interface (involving the use of RPLC as the second dimension) [18]. Informative data could be obtained with intact ADC injected in non-denaturing medium in first dimension. Even DARs were separated and injected in the second dimension leading to the separation of sub-units resulting from denaturing RPLC conditions. Although this approach was efficient, this 2D-LC method, based on heart-cuts of the first dimension peaks, requires as many injections as peaks to be analyzed, which makes this strategy sample-consuming and hence less attractive when only a limited sample amount is available. Moreover, this approach may be time consuming and requires 3 pumps, including first and second dimension pumps as well as a regenerating pump. On-line comprehensive two-dimensional liquid chromatography could therefore be an attractive alternative for reducing both sample consumption and analysis time. In addition, in on-line LCxLC, the entire first dimension separation is subjected to the second separation. As a result, the risk of missing peaks of interest which in turn may lead to lose essential information is avoided. However, it was recently shown that the optimization of on-line LCxLC conditions may turn out to be a tedious task without an efficient method development, able to find the best trade-off between peak capacity, sensitivity and analysis time [19]. The purpose of the present study is therefore to develop a straightforward on-line HICxRPLC–MS method. In the first part of this study, the conditions of the two-dimensional separation were rationally optimized to gain information that would help in enlarging the current knowledge on ADCs. Our objective is to obtain in one single injection, both average DAR determination and comprehensive identification of positional isomers, thereby allowing the characterization of both even and odd DARs. This second aspect will be extensively discussed in the second part of this study.

2. Experimental section

2.1. Material and reagents

Acetonitrile (ACN), methanol (MeOH), formic acid (FA) and trifluoroacetic acid (TFA) all LC–MS grade were purchased from Sigma-Aldrich (Steinheim, Germany). Ultra-pure water was obtained from an Elga water purification system (Veolia water STI, Le Plessis Robinson, France). For HIC mobile phase, ammonium-sulfate, ammonium-acetate (AA), ammonium-formate and sodium-chloride were purchased from Sigma Aldrich (Steinheim, Germany). Disodium-hydrogen-phosphate dodecahydrate, sodium-dihydrogen-phosphate (anhydrous), phosphoric acid and sodium hydroxide were purchased from Acros Organic (New Jersey, USA). Brentuximab Vedotin (Adcetris©) and Brentuximab B were kindly provided by the Center of Immunology Pierre Fabre (Saint-Julien en Genevois, France). Brentuximab B is a mAb differing from naked Brentuximab in three amino acids. Their concentrations were 5 mg/mL and 2 mg/mL respectively. The pH values were measured with a Standard pH meter (Radiometer analytical, Villeurbanne, France).

2.2. Columns

The HIC column was a MabPac HIC-10 (100 mm × 4.6 mm, 5 μm, 1000 Å) from Thermo Scientific (Cheshire, UK). The RPLC column was an Acquity UPLC Protein BEH C4 (50 mm x 2.1 mm, 1.7 μm, 300 Å) from Waters (Milford, MA, USA).

2.3. Instrumentation

The LCxLC–MS system is presented in Fig. 2. It consists in a 2D-IClass liquid chromatograph hyphenated to a quadrupole time-of-flight Xevo G2-S Q-Tof, both from Waters (Milford, MA, USA). The 2D-IClass instrument includes two high-pressure binary solvent delivery pumps, an autosampler with a flow-through needle of 15 μL equipped with an extension loop of 50 μL, a column manager composed of two independent column ovens with a maximum temperature of 90 °C and two 6-port high pressure two-position valves acting as interface between the two separation dimensions. A single wavelength UV detector and a diode array detector both equipped with 500 nL flow-cell withstanding pressure up to 70 bar were used for the first and second dimension respectively. The maximum pressure capability is 1285 bar for both pumps. Beyond a flow-rate of 1 mL/min, the upper pressure limit decreases depending on both flow-rate and mobile phase composition. The measured dwell volumes were 160 μL and 100 μL for the first and the second dimensions, respectively. It should be noted that the dwell volume of the second dimension does not take into account the volume of the sample loops used at the interface. The measured extra-volumes were 12 μL and 17 μL for the first and second dimensions, respectively. The volume of the sample loops used for interfacing both dimensions was 200 μL. 1D-LC experiments were carried out with the first dimension instrument. For the LCxLC–MS experiments, an external 10-port high pressure 2-positions valve (Vici Valco Instruments, Houston, USA) was placed before the MS to avoid any salt contamination due to the injection plug. A flow splitter was also used to reduce the flow rate before entering MS.

Data acquisition and instrument controlling were performed with Masslynx software (Waters). 2D-data were exported to Microsoft Excel and Matlab V7.12.0635 was used to construct a matrix via house-made calculation tools enabling the construction of 2D-contour plots.

2.4. Experimental conditions

2.4.1. Sample preparation

Both Brentuximab Vedotin and Brentuximab B were injected as intact proteins.

2.4.2. Chromatographic conditions

Three ammonium acetate (AA) concentrations were considered to optimize the HIC separation, namely 2.5, 3 and 3.5 M. The mobile phase A was composed of the desired concentration of AA and 0.1 M phosphate buffer (Na_2HPO_4) with pH adjusted to 7 with phosphoric acid. The mobile phase B was composed of 0.1 M phosphate (Na_2HPO_4 and NaH_2PO_4) with pH adjusted to 7 with sodium hydroxide solution. For this optimization, the gradient conditions were 0–100% B in 10 min at a flow-rate of 800 μL/min. Column temperature, wavelength and acquisition rate were set at 30 °C, 280 nm and 10 Hz respectively.

The acquisition rates for UV detection were set at 10 Hz and 40 Hz for the first and second dimensions respectively. The wavelength was set at 280 nm for both dimensions. The conditions in HICxRPLC result from specific development discussed in this work.

2.4.3. Mass spectrometry conditions

Continuous data were acquired in sensitivity mode with positive polarity. A mass to charge ratio (m/z) from 500 to 3500 was used for data collection. Other mass spectrometer settings were 3.20 kV and 120 V as capillary and sample cone voltage, respectively. Source and desolvation temperature were equal to 110 and 500 °C, respectively. Gas flow for desolvation and cone were set at 900 and 50 L/Hr, respectively. The scan time was set at 0.5 s.

3. Results and discussion

3.1. Optimization of HICxRPLC–MS separation

3.1.1. Optimization of ^{1}D HIC conditions

3.1.1.1. Phase system optimization in HIC. Ammonium sulfate is the most widely used salt for HIC, as it often leads to an efficient separation of the different DARs [5–7,20]. However, it is not a good candidate for on-line HICxRPLC, as it may precipitate with organic solvent in the second RP dimension, even at very low salt concentrations, resulting in pressure elevation and risk of clogging. Thus, different combination of stationary phases and salts were evaluated.

First, the stationary phase was selected on the basis of DARs retention (elution) window and achievable peak capacity (efficiency). Among the six tested columns at disposal (i.e. Thermo MAbPac HIC-10, Thermo MAbPac HIC-20, Thermo MAbPac HIC-butyl, Thermo ProPac HIC-10, Waters Protein-Pak Hi Res HIC and Tosoh TSKgel Ether-5PW), the Thermo Mab-Pac HIC-10 was selected since it provided appropriate retention, selectivity and peak capacity. Some of the columns (Thermo MAbPac HIC-20 and Thermo MAbPac HIC-butyl) did not allowed the elution of the most hydrophobic DAR species (DAR6 and DAR8) of brentuximab-vedotin [21].

Then, the mobile phase salt concentration and type (lyotropic strength) were optimized, since these variables are highly relevant for tuning HIC retention and selectivity. Generally, the influence of different salts on hydrophobic interactions follows the Hoffmeister (lyotropic) series for the precipitation of proteins from aqueous solutions [22]. Not only the effect of salt concentration on ADC DARs retention was evaluated, but the impact of different salts on selectivity was also studied.

First, the solubility of 1–4 M ammonium-sulfate, ammonium-acetate, ammonium-formate and sodium-chloride was assessed in 10, 30, 50% and 100% methanol and acetonitrile. Based on the results, ammonium-sulfate was found to be the less appropriate salt, while ammonium-acetate and ammonium-formate showed acceptable solubility in all organic mixtures. The solubility was found to be somewhat lower in neat acetonitrile than in methanol.

Ammonium-acetate and ammonium-formate were then compared. Ammonium-formate showed somewhat lower elution-strength than ammonium-acetate and therefore required higher salt concentration to sufficiently retain the DAR0 and DAR2 species. Higher salt concentration is not recommended, because of the high organic modifier content in the second RP dimension. Therefore, taking the solubility and elution strength of the four salts into account, ammonium-acetate was selected for the HIC separation.

Finally, the salt concentration was optimized. Based on the preliminary results, 2.5, 3.0 and 3.5 M ammonium-acetate were tested when applying a linear salt gradient from 100 to 0% salt concentration. To keep sufficient retention for the least retained compounds, while minimizing the analysis time, 2.5 M was found to be the optimum concentration (see Supplementary Fig. S1).

3.1.1.2. Optimization of ^{1}D-Gradient conditions in HIC. The analysis time in the first dimension separation has to be minimized, since

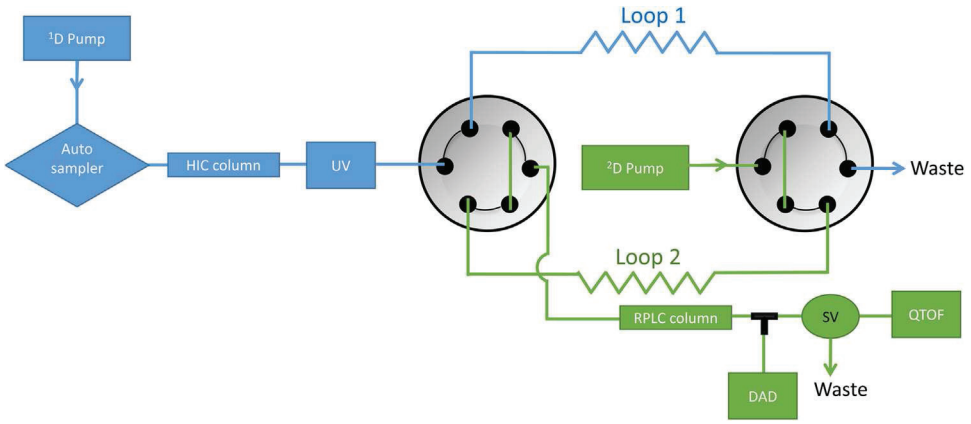

Fig. 2. HICxRPLC set-up. The eluent of the first dimension is stored in the loop 1, while the content of loop 2 is injected in the second dimension. Abbreviations are defined as SV: switching valve; UV: UV detector; DAD: diode array detector; QTOF: quadrupole time-of-flight mass spectrometer.

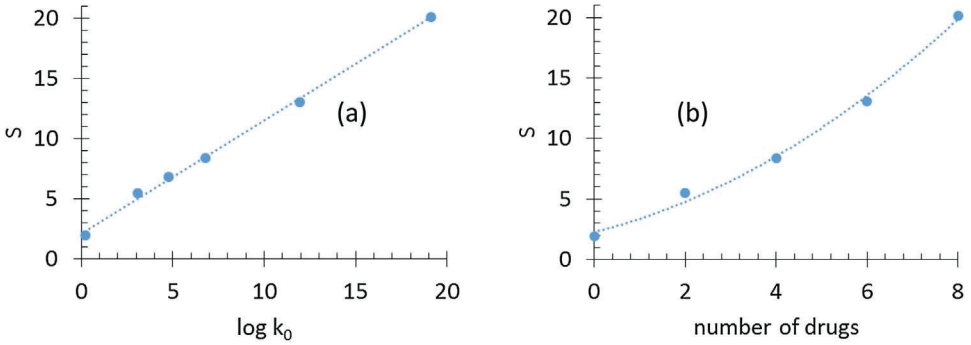

Fig. 3. Variation in HIC, of the coefficient S in Eq. 1 with (a) the calculated log(k_0) and (b) the number of drugs. Conditions: Mobile phase A: 2.5 M ammonium acetate + 0.1 M phosphate and B: 0.1 M phosphate; 800 μL/min, gradient from 0 to 100% B in 24.9 min (5%), 8.3 min (15%) and 5 min (25%). 20 μL injected; 30 °C. S and log k_0 were calculated from Osiris software.

it represents the analysis time of the whole LCxLC separation. In the meantime, the separation power has to be maximized. Furthermore, with the objective to send in ^{2}D, a constant number of fractions per peak of first dimension, gradient conditions must be carefully chosen, so that the widths can be kept constant for all peaks. To achieve these conflicting objectives, HIC gradient conditions were optimized using computer assisted optimization (Osiris software). Three preliminary experiments were performed under linear gradient conditions with three different normalized gradient slopes (5%, 15% and 25%), the normalized gradient slope being the product of the gradient slope and the column dead time. It was shown that the Linear Solvent Strength model (LSS) [23] was accurate enough to describe the retention behavior of DAR species in HIC. The corresponding retention model (log k) can be written as:

$$\log k = \log k_0 - S.C \quad (1)$$

where log k_0 is the extrapolation of the retention model to a null value of the salt concentration, C is the salt concentration and S is the slope. S and log k_0 can be determined from two gradient runs. As shown in Fig. 3a, the variation of S with log k_0 for the different peaks is linear which is in good accordance with the fact that only one mechanism is involved in the HIC separation process (i.e. hydrophobic interaction mechanism). The strong increase in S value with the number of drugs and hence with the hydrophobicity of DAR species (Fig. 3b) suggests that a linear gradient cannot be suitable for the purpose of keeping both the same peak width and the same peak spacing all over the separation and that a concave profile should be much more appropriate. The optimum predicted gradient separation is given in Fig. 4a, while the experimental one is shown in Fig. 4b. A first normalized gradient slope of 25% was first applied followed by a second normalized gradient slope of 5%. As expected, the predicted separation is in good agreement with the experimental one. However, it can be observed that the least retained peaks (e.g. DAR 0) are strongly distorted. This is mainly due to injection effects produced by the combination of large injection volume (20 μL) and strong injection solvent (no salt).

3.1.1.3. Effect of salt addition in the sample solvent in HIC. To enhance sensitivity in HICxRPLC–MS, large injection volumes are mandatory. However, strong injection effects such as peak distortions and breakthrough phenomena may occur as above highlighted, particularly for the least retained compound (i.e. DAR 0 and DAR 2). Decreasing the eluent strength of the sample solvent is a good way to improve the peak shape. In HIC, the eluent strength can be decreased by increasing the ionic strength. The effect of different AA concentrations in the sample solvent on Brentuximab B (homemade naked brentuximab) peak shape can be observed in Fig. 5 for different injection volumes. As observed, the phenomenon of breakthrough appears for salt concentrations lower than 1.5 M even for very low injection volumes. On the contrary, this phenomenon no longer exists at higher salt concentrations. The obtained results clearly point out that a volume as high as 40 μL can be injected onto the column without peak distortions, provided that the concentration of ammonium acetate in the injection solvent is 2.5 M or more.

As highlighted in this study, the addition of AA into the sample solvent is very efficient to improve mAbs peak shape in HIC. Such ionic strength conditions were further applied to the ADC sample. The obtained separations for different injection volumes with 2.5 M AA added to the sample solvent are shown in Fig. 6. As expected,

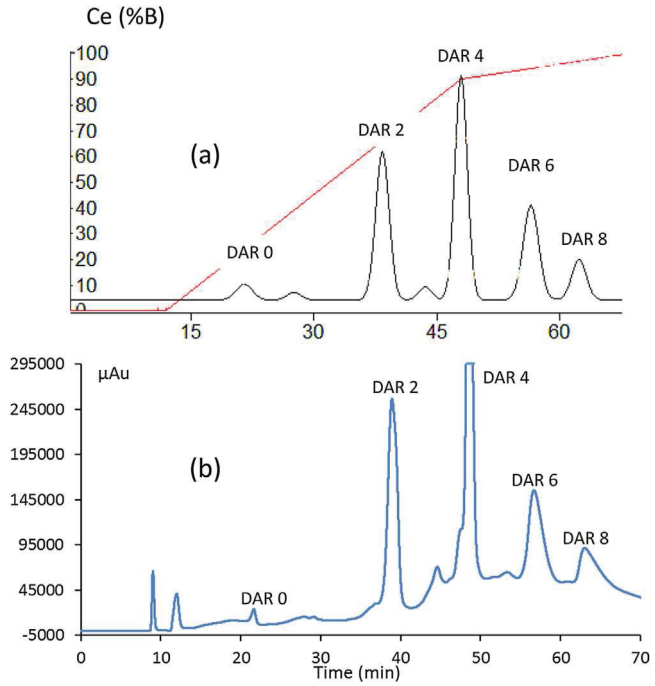

Fig. 4. Comparison between (a) predicted and (b) experimental [1]D HIC separations of Brentuximab Vedotin. Mobile phase A: 2.5 M ammonium acetate + 0.1 M phosphate and B: 0.1 M phosphate; 100 µL/min, gradient from 0 to 90% B in 36 min and 90–100% B in 21 min 20 µL injected; 30 °C. The straight lines represent the gradient profile (Ce is the eluent composition at the column exit). See experimental section for other conditions.

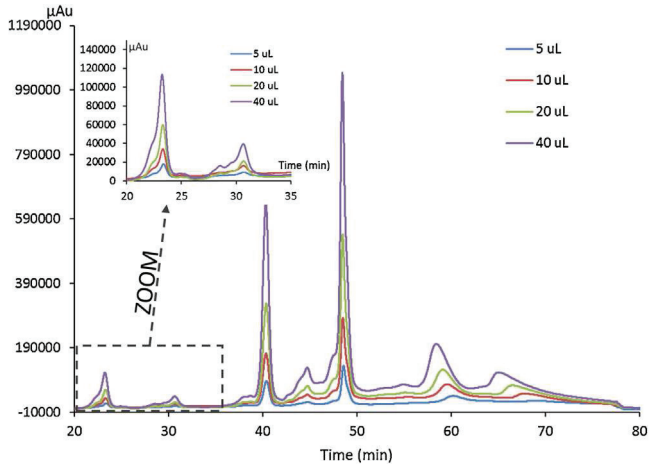

Fig. 6. Effect of different injection volumes on the HIC separation of ADC. 2.5 M as ammonium concentration in the sample. Optimized HIC conditions as in Fig. 4.

neither peak distortion nor peak broadening can be observed with injection volumes as high as 40 µL. Thus, these conditions (2.5 M AA in injection solvent and 40 µL as injected volume) were further selected for 2D experiments with the goal to significantly enhance sensitivity of least retained compounds.

3.1.2. Optimization of RPLC–MS conditions

3.1.2.1. Selection of organic modifier in RPLC. To avoid a potential precipitation issue when the injection plug coming from the first HIC dimension is diluted in the second RPLC mobile phase, methanol was first preferred to acetonitrile. However, with very short gradient times, the optimal flow-rate to achieve the highest possible peak capacity is much higher than the one to achieve the best plate number (van Deemter curve), thereby leading to the need for very high flow-rates in the second dimension [24] to maximize peak capacity. In this context, acetonitrile (ACN) is expected to be more attractive than methanol (MeOH) due to its lower viscosity. The two organic modifiers were therefore compared at the highest possible flow-rate compatible with the instrumentation, namely 1.2 and 1.4 mL/min for MeOH and ACN, respectively. The comparison was based on the achievable peak capacity obtained in the second RPLC dimension for a given sampling time (i.e. 1 min), considering the separation of the fractions of DAR 6. Fig. 7 illustrates the overlaid separations of the different sub-units of DAR 6 resulting from disruption of non-covalent bonds in RPLC denaturing conditions. It can be observed that the retention space was larger when acetonitrile was used as organic modifier. For a more reliable assessment of the separation power, the experimental peak

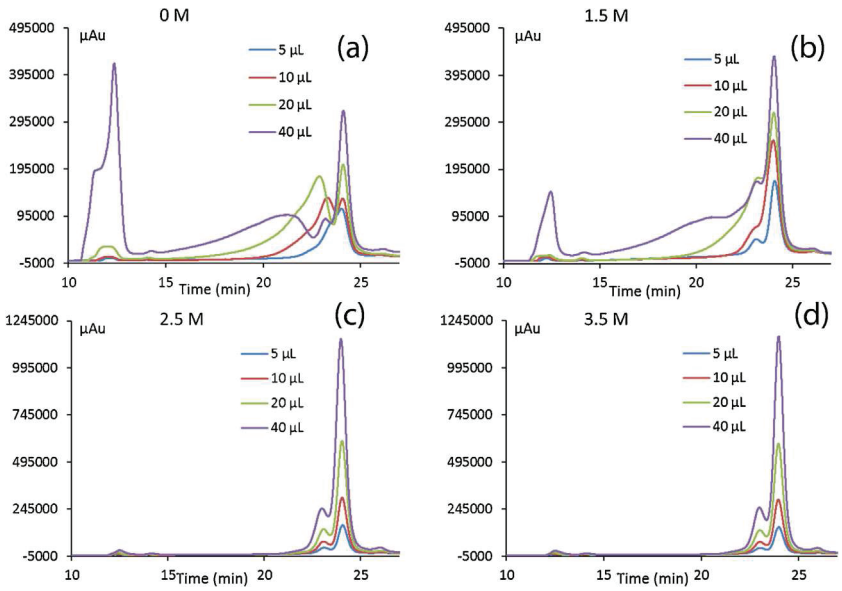

Fig. 5. Effect of different concentrations of ammonium acetate in the sample solvent on the peak shape of Brentuximab B for different injection volumes. (a) 0 M; (b) 1.5 M; (c) 2.5 M and (d) 3.5 M. Optimized HIC conditions as in Fig. 4.

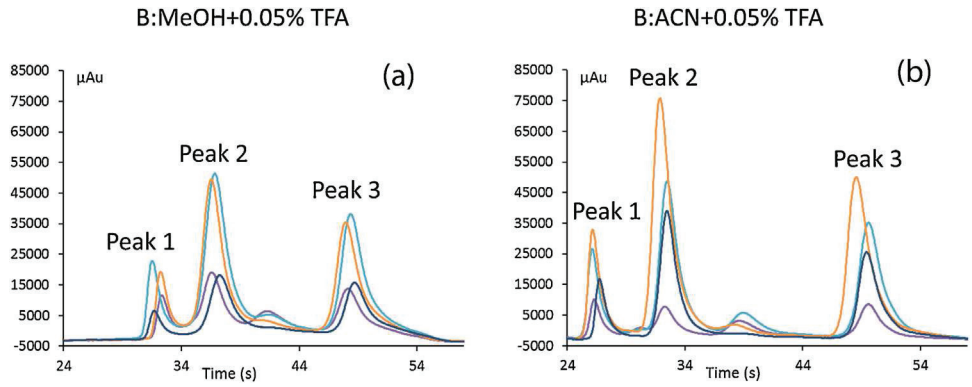

Fig. 7. Overlay of ^{2}D RPLC separations of fractions of DAR 6 with (a) MeOH; 1.2 mL/min; 50–58% in 0.6 min and (b) ACN; 1.4 mL/min; 42–50% B in 0.7 min. Sampling time: 1 min; 80 °C; 280 nm as wavelength. Fig. 8: Optimized ^{1}D HIC separation. The successive fractions of 1.5 min sent in the second dimension are delimited from vertical lines. Conditions as in Fig. 4.

Table 1
Comparison of the peak capacities obtained in Fig. 8 for the separation of the fractions of DAR 6. MeOH and ACN as organic modifier. Conditions given in Fig. 8.

	MeOH (Δt=17s)		ACN (Δt=23s)	
	$w_{4\sigma}$ (s)	$^{2}n_c$	$w_{4\sigma}$ (s)	$^{2}n_c$
Peak 1	1.9	8.9	1.8	12.8
Peak 2	3.2	5.3	2.7	8.5
Peak 3	3.4	5	3.4	6.8
Average value	2.8	6	2.6	9

Table 2
^{2}D RPLC method with bracketing water steps.

Time (min)	%B (ACN + 0.05%TFA + 0.1%FA)
0	1
0.14	1
0.15	32
1.21	40
1.22	1
1.5	1

capacity, ^{2}n, was calculated in both cases according to the following relationship:

$$^{2}n = 1 + \Delta t/^{2}w$$

Where Δt is the retention space represented by the difference in retention times between the last and the first eluted compounds and ^{2}w is the average peak width at 4.$^{2}\sigma$.

The results listed in Table 1, point out a 1.5-fold gain in peak capacity when using acetonitrile rather than methanol. As a result, acetonitrile was chosen for the rest of the study.

3.1.2.2. Optimization of gradient conditions in RPLC. The ^{2}D RPLC method has to fulfill two major objectives: (i) minimizing the risk of precipitation which could result from the large amount of salt injected from the first dimension to the hydro-organic media of the second dimension has to be avoided and (ii) maximizing the peak capacity in order to facilitate MS spectra deconvolution.

To avoid precipitation, an easy solution may consist in injecting a very low sample volume in the second dimension. This can be done either by setting a short sampling time or by using a flow splitter to reduce the flow-rate entering the interface. However, shortening the sampling time results in decreasing the peak capacity, while increasing sample dilution. On the other hand, flow splitting allows to keep an acceptable peak capacity but also leads to high dilution and hence low sensitivity. An alternative solution consists in using a gradient elution bracketed by two water steps so that the contact of the injection plug, rich in salt, with the mobile phase of the second dimension, rich in organic solvent, can be minimized. According to this idea, the second dimension RPLC gradient conditions were modified by programming an isocratic hold (99% water) at the beginning and at the end of the gradient method, to complete the elimination of the salt in both the loop and the column before the organic solvent was in contact with the injection plug.

To maximize the peak capacity, we took into account the strong focusing power of water as injection solvent in RPLC, thereby allowing the injection of large volumes without the occurrence of peak distortion. As a result, sampling times and hence peak capacities could be maximized. To keep an acceptable sampling rate (2–3 fractions *per* peak), the sampling time was set at 1.5 min, corresponding to an injection volume of 150 μL. Accordingly, two identical sample loops of 200 μL were selected for the interface. Their volume was slightly higher than the injection volume to prevent any sample loss. It should be underlined that the sampling time must include the bracketing times in addition to the gradient time. Once again, it was of prime importance to work at the highest possible flow-rate so that the column dead time was as low as possible. The use of high column temperature in the second dimension was therefore mandatory.

Instrumental dwell volume (100 μL), loop volume (200 μL) and column dead volume (about 100 μL) were carefully considered to determine the duration of the isocratic hold, which has to be long enough to avoid any salt precipitation and as short as possible to maximize peak capacity. Considering these two conflicting objectives, the duration of the first and the second isocratic holds were set at 0.14 min and 0.28 min respectively, corresponding to solvent volumes of 200 μL and 400 μL, respectively for a second dimension flow-rate of 1.4 mL/min. In these conditions, the injection plug was therefore washed out with 350 μL of water-rich solvent (99% water). Such a volume corresponds to more than two injection volumes (350 μL vs 150 μL). At the end of the analysis run, the column was filled with the same solvent, thereby bracketing the next injection plug. Considering the duration of the two isocratic holds, the time available for the gradient was 1.06 min which led to a reasonable normalized gradient slope of 0.56% with 8% as composition range. The gradient conditions for the ^{2}D RPLC separation are given in Table 2.

3.1.2.3. Further RPLC optimization designed to enhance MS detection. To increase sensitivity, 0.1% FA was added to the mobile phase in addition to 0.05% TFA [25]. To prevent any salt contamination in the MS source resulting from the very high salt concentration in the injection plug, the ^{2}D-mobile phase coming from the UV-detector was sent to the waste, thanks to a two-positions switching valve. This was done for a period which depends on the width of the sol-

Table 3
HICxRPLC conditions.

Chromatographic conditions	1st dimension (^{1}D)		2nd dimension (^{2}D)
Stationary phase	MabPac HIC-10		Acquity Protein BEH C4
Column geometry	100 x 4.6 mm, 5 μm 1000 Å		50 x 2.1 mm, 1.7 μm 300 Å
Mobile phase	A : 2.5 M AA (pH = 7) B : 0.1 M Phosphate (pH = 7)		A : Water + 0.05%TFA + 0.1%FA B : ACN +0.05%TFA + 0.1%FA
Flow rate	100 μL/min		1.4 mL/min
Gradient	0 to 90% (B) in 36 min, 90 to 100% (B) in 21 min, 100% (B) for 11 min		1 % (B) for 0.14 min, 1 to 32% (B) in 0.01 min, 32 to 40% (B) in 1.06 min, 40 to 1% (B) in 0.01 min,
Temperature	30 °C		80 °C
Sampling time		1.5 min	
Injected volume (%V_0)	40 μL (4% $^1V_0$)		150 μL (150% $^2V_0$)
UV detection	280 nm (10 Hz)		280 nm (40 Hz)
MS conditions (ESI+)			
Scan range			500–3500 *m/z*
Scan time			0.5 s
Capillary / Sample cone voltage			3.20 kV / 120 V
Desolvation temperature			500 °C
Desolvation / Cone gas flow			900 L/Hr / 50 L/Hr
Source temperature			110 °C

vent peak. The time required for the salt peak to fully return to the baseline corresponds to about 0.4 min after the injection time, thereby fixing the time required to eliminate the whole amount of salt (see Supplementary Fig. S2). It should be noticed that this time is more than two-fold higher than the time required for on-column injecting and column travelling (i.e. about 0.18 min) as a result of the high dilution of the injection plug in the mobile phase. PolyEthylene Glycol (PEG) was also detected from the Total Ion Current signal (MS-TIC-signal) at the beginning of the gradient run due to its presence in the ADC formulation. However, the most intense signal for PEG was found within 500–800 *m/z* as mass range which did not constitute a barrier for the MS-detection of ADC sub-units considering their higher expected mass-to-charge values. Furthermore, the flow was split post-column so that the flow-rate entering MS was 750 μL/min only to enhance ionization, while 650 μL/min were directed to UV detection.

3.2. HICxRPLC–MS results

The above optimized conditions were applied to the HIC x RPLC–MS separation of brentuximab vedotin®. All operating conditions were summarized in Table 3. The obtained first dimension HIC separation is shown in Fig. 8. The successive fractions sent to the second dimension are delimited from vertical lines. As expected by our optimization approach above discussed, two to three fractions per peak could be analyzed in the second RPLC-dimension, ensuring a comprehensive on-line 2D-LC separation. The integration of the peak areas of the different even DARs allowed to determine the average DAR (avDAR) value according to the following relationship [2,26]:

$$avDAR = \frac{\sum_0^8 nA_{DAR_n}}{\sum_0^8 A_{DAR_n}} \quad (2)$$

where n correspond to the number of loaded drug and A_{DARn} corresponds to the peak area of DAR n, n being the DAR number.

The results are shown in Table 4. The obtained value of 3.9 ± 0.1 is in good agreement with those found in the literature [16,27]. Furthermore, the reliability of this measure seems to be very good, considering the obtained relative standard deviation of 1.5% calculated from 3 replicate injections (Table 4). These results demonstrate the ability of the ^{1}D HIC method to provide an accurate determination of the average DAR.

The 2D-colour plots are shown in Fig. 9a and b for UV and MS-signal, respectively. Each horizontal dotted line shown in Fig. 9b,

Table 4
Average DAR calculation.

Number of drug load	HIC peak area (%) (average on 3 injections)
DAR 0	6.0
DAR 2	26.1
DAR 4	42.6
DAR 6	17.2
DAR 8	8.1
Average DAR	3.9
RSD (%)	1.5

passes through the peak apex of the different sub-units obtained from the dissociation of a given species. Horizontal black dotted lines allow to locate the separations of the 5 fractions corresponding to the peak apex of the 5 even DARs in 1D- HIC (see also Fig. 8). As shown by the black spots in Fig. 9b, 17 peaks were found in this 2D-map. Some of them are vertically aligned suggesting that the corresponding sub-units are the same. The vertical alignment of these colored spots is noteworthy. This observation highlights the very good run-to-run repeatability of retention times and as a result, the ability of this ^{2}D RPLC method to discriminate between the different spots. Here, the three vertical lines in Fig. 9b indicate three series of identical sub-units. However, it appears that 6 spots are not aligned with the others thereby suggesting that the corresponding sub-units are quite different. Similarly, some horizontal dotted lines (highlighted in red in Fig. 9b) do not correspond to any peak apex of even DARs. They suggest that some additional species, unknown so far, are also separated to some extent in ^{1}D HIC. It can be concluded that 2D-maps can be very helpful for further MS identification of sub-units and beyond sub-units, for identification of the different species present in the ADC product. This will be discussed in more details in the second part of this study.

Finally, it is very interesting to notice the excellent similarity between two 2D-UV-colour-plots obtained from the same brentuximab vedotin, but analyzed with four days between injections (Fig. 9a and c). This result points out that, in addition to good run-to-run repeatability of ^{2}D separations, as above discussed, the variability of the whole developed 2D-separation method is very low. The perfect similarity between the two 2D-separations is attested by the excellent correspondence between ^{2}D-retention times as emphasizes by the vertical dotted lines joining the spots in Fig. 9a to those in Fig. 9c. The low variability of this comprehensive 2D-separation method can further be assessed by observing the similar intensity of UV-signals between the two successive sepa-

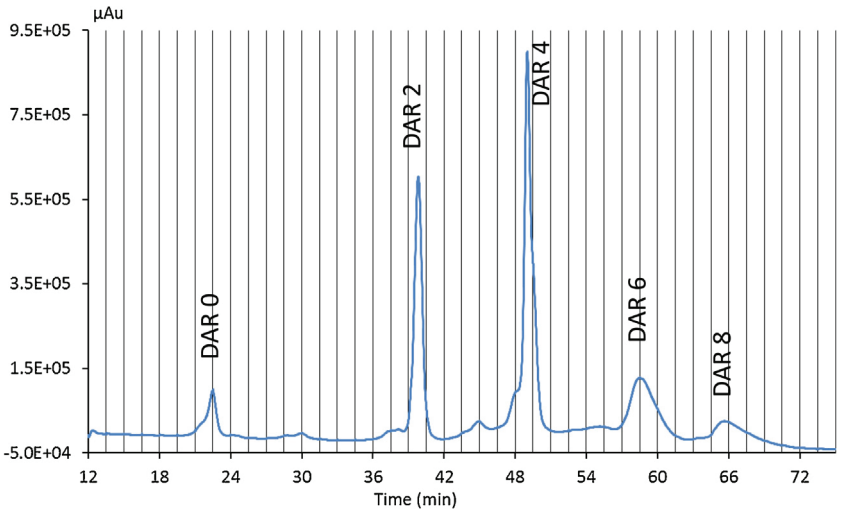

Fig. 8. Optimized [1]D HIC separation. The successive fractions of 1.5 min sent in the second dimension are delimited fromby vertical lines. Conditions as in Fig. 4.

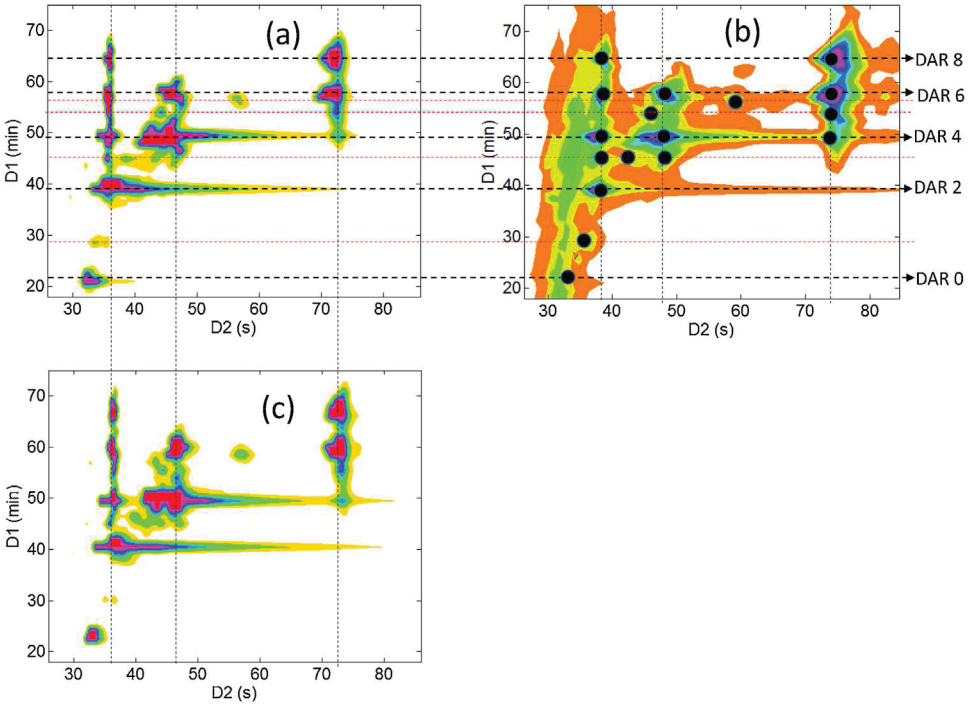

Fig. 9. 2D-colour plots of the HIC x RPLC separation of Brentuximab Vedotin using optimized conditions displayed in Table 3. (a) first UV-signal, (b) Total Ion Current MS signal and (c) second-UV-signal obtained four days after the first one.

rations. The high reliability of this comprehensive 2D-separation method associated to the versatile information it can provide, suggests that such 2D-colour plots, obtained from either UV or MS signal or from both, might constitute a very convenient tool to quickly evaluate the quality of a given ADC. Knowing that two different ADCs can still deliver similar HIC profiles, 2D-plots could be indeed very useful for gathering extensive information within a single run. This feature will be more extensively discussed in the second part of this study wherein 2D-colour plots of stressed ADCs will be compared to that of the original one.

4. Conclusion

The comprehensive characterization of ADCs is a challenging task due to their high complexity. In this work, an on-line HICxRPLC–MS method was successfully developed leading to an informative 2D-separation requiring 75 min only. The objective was to get relevant information on both drug loaded profile (average DAR) and structural information on positional isomers of each DAR of a cysteine-linked commercial ADC (brentuximab vedotin, Adcetris®).

To achieve this goal, several optimization steps were tackled. [1]D HIC conditions were carefully optimized by (i) replacing the usual salts employed in the mobile phase with ammonium acetate to improve the solubility of the salt in the hydro-organic media of the second dimension and MS hyphenation (ii) using a concave gradient thanks to a computer assisted method based on LSS model, which was found to accurately predict the retention behavior of different DARs and (iii) adding a sufficient amount of salt in the sample before injection to reduce the injection solvent strength

thereby allowing to increase the injected amount and hence sensitivity. ^{2}D RPLC gradient conditions were also carefully optimized. Furthermore, the gradient profile was bracketed by two water steps to prevent any salt precipitation at the injection time and both very high flow-rate and high temperature were used to maximize peak capacity. Peak capacity was also enhanced thanks to the strong column focusing effect in the second dimension, allowing a sampling time of 1.5 min and therefore very large injection volume (150% of the second dimension column dead volume). Finally, the flow-rate coming from the second dimension was first diverted to discard the salt plug coming from ^{1}D fractions to preserve MS detector and then decreased to ensure a sufficient sensitivity.

The obtained average DAR value was found in very good accordance with those reported in the literature. In addition, the LCxLC-UV method was found to be highly reproducible and very informative and could therefore be used for a rapid characterization of ADCs. We demonstrated that the precise determination of the average drug-to-antibody ratio (DAR) and an extensive knowledge of the drug load distribution could be obtained in a single step method. The identification of the different sub-units related to their specific DAR will be discussed in the second part of this series.

Acknowledgments

Sabine Heinisch and Morgan Sarrut are deeply grateful to Christelle Margoum and Philippe Bados from IRSTEA laboratory for the loan of the Q-Tof instrument.

Davy Guillarme wishes to thank the Swiss National Science Foundation for support through a fellowship to Szabolcs Fekete (31003A_159494).

Appendix A. Supplementary data

Supplementary data associated with this article can be found, in the online version, at http://dx.doi.org/10.1016/j.jchromb.2016.06.048.

References

[1] A. Beck, T. Wurch, C. Bailly, N. Corvaia, Strategies and challenges for the next generation of therapeutic antibodies, Nat. Rev. Immunol. 10 (2010) 345–352, http://dx.doi.org/10.1038/nri2747.
[2] L.N. Le, J.M.R. Moore, J. Ouyang, X. Chen, M.D.H. Nguyen, W.J. Galush, Profiling antibody drug conjugate positional isomers: a system-of-equations approach, Anal. Chem. 84 (2012) 7479–7486, http://dx.doi.org/10.1021/ac301568f.
[3] P.D. Senter, E.L. Sievers, The discovery and development of brentuximab vedotin for use in relapsed Hodgkin lymphoma and systemic anaplastic large cell lymphoma, Nat. Biotechnol. 30 (2012) 631–637, http://dx.doi.org/10.1038/nbt.2289.
[4] B.A. Teicher, R.V.J. Chari, Antibody conjugate therapeutics: challenges and potential, Clin. Cancer Res. Off. J. Am. Assoc. Cancer Res. 17 (2011) 6389–6397, http://dx.doi.org/10.1158/1078-0432.CCR-11-1417.
[5] B. Wiggins, L. Liu-Shin, H. Yamaguchi, G. Ratnaswamy, Characterization of cysteine-linked conjugation profiles of immunoglobulin G1 and immunoglobulin G2 antibody–drug conjugates, J. Pharm. Sci. 104 (2015) 1362–1372, http://dx.doi.org/10.1002/jps.24338.
[6] M. Haverick, S. Mengisen, M. Shameem, A. Ambrogelly, Separation of mAbs molecular variants by analytical hydrophobic interaction chromatography HPLC: overview and applications, mAbs 6 (2014) 852–858, http://dx.doi.org/10.4161/mabs.28693.
[7] J. Ouyang, Drug-to-antibody ratio (DAR) and drug load distribution by hydrophobic interaction chromatography and reversed phase high-Performance liquid chromatography, in: L. Ducry (Ed.), Antib.-Drug Conjug., Humana Press, Totowa, NJ, 2013, pp. 275–283, http://link.springer.com/10.1007/978-1-62703-541-5_17 (accessed 10.30.15.).
[8] J.F. Valliere-Douglass, S.M. Hengel, L.Y. Pan, Approaches to interchain cysteine-linked ADC characterization by mass spectrometry, Mol. Pharm. 12 (2015) 1774–1783, http://dx.doi.org/10.1021/mp500614p.
[9] L.Y. Pan, O. Salas-Solano, J.F. Valliere-Douglass, Conformation and dynamics of interchain cysteine-linked antibody-drug conjugates as revealed by hydrogen/deuterium exchange mass spectrometry, Anal. Chem. 86 (2014) 2657–2664, http://dx.doi.org/10.1021/ac404003q.
[10] A. Beck, E. Wagner-Rousset, D. Ayoub, A. Van Dorsselaer, S. Sanglier-Cianférani, Characterization of therapeutic antibodies and related products, Anal. Chem. 85 (2013) 715–736, http://dx.doi.org/10.1021/ac3032355.
[11] A. Wakankar, Y. Chen, Y. Gokarn, F.S. Jacobson, Analytical methods for physicochemical characterization of antibody drug conjugates, mAbs 3 (2011) 161–172, http://dx.doi.org/10.4161/mabs.3.2.14960.
[12] A. Beck, S. Cianferani, Harnessing the benefits of mass spectrometry for in-depth antibody drug conjugates analytical characterization, LC-GC, Eur. Adv. Biopharm. Anal. 2 (2015) 24–30.
[13] A. Beck, G. Terral, F. Debaene, J. Wagner-Rousset, O. Janin-Bussat, A.V. Dorsselaer, S. Cianférani, Cutting-edge mass spectrometry methods for the multi-level structural characterization of antibody-drug conjugates, Expert Rev. Proteomics (2015), http://dx.doi.org/10.1586/14789450.2016.1132167 (Epub ahead of print).
[14] R.E. Birdsall, S.M. McCarthy, M.C. Janin-Bussat, M. Perez, J.-F. Haeuw, W. Chen, A. Beck, A sensitive multidimensional method for the detection, characterization, and quantification of trace free drug species in antibody-drug conjugate samples using mass spectral detection, mAbs 8 (2016) 306–317, http://dx.doi.org/10.1080/19420862.2015.1116659.
[15] K. Sandra, G. Vanhoenacker, I. Vandenheede, M. Steenbeke, M. Joseph, P. Sandra, Multiple heart-cutting and comprehensive two-dimensional liquid chromatography hyphenated to mass spectrometry for the characterization of the antibody-drug conjugate ado-trastuzumab emtansine, J. Chromatogr. B (n.d.). 10.1016/j.jchromb.2016.04.040.
[16] F. Debaene, A. Bœuf, E. Wagner-Rousset, O. Colas, D. Ayoub, N. Corvaïa, A. Van Dorsselaer, A. Beck, S. Cianférani, Innovative native MS methodologies for antibody drug conjugate characterization: high resolution native MS and IM-MS for average DAR and DAR distribution assessment, Anal. Chem. 86 (2014) 10674–10683, http://dx.doi.org/10.1021/ac502593n.
[17] M.-C. Janin-Bussat, M. Dillenbourg, N. Corvaia, A. Beck, C. Klinguer-Hamour, Characterization of antibody drug conjugate positional isomers at cysteine residues by peptide mapping LC–MS analysis, J. Chromatogr. B 981–982 (2015) 9–13, http://dx.doi.org/10.1016/j.jchromb.2014.12.017.
[18] R.E. Birdsall, H. Shion, F.W. Kotch, A. Xu, T.J. Porter, W. Chen, A rapid on-line method for mass spectrometric confirmation of a cysteine-conjugated antibody-drug-conjugate structure using multidimensional chromatography, mAbs 7 (2015) 1036–1044, http://dx.doi.org/10.1080/19420862.2015.1083665.
[19] M. Sarrut, A. D'Attoma, S. Heinisch, Optimization of conditions in on-line comprehensive two-dimensional reversed phase liquid chromatography. Experimental comparison with one-dimensional reversed phase liquid chromatography for the separation of peptides, J. Chromatogr. A 1421 (2015) 48–59, http://dx.doi.org/10.1016/j.chroma.2015.08.052.
[20] J.L. Fausnaugh, L.A. Kennedy, F.E. Regnier, Comparison of hydrophobic-interaction and reversed-phase chromatography of proteins, J. Chromatogr. 317 (1984) 141–155, http://dx.doi.org/10.1016/S0021-9673(01)91654-1.
[21] A. Cusumano, D. Guillarme, A. Beck, S. Fekete, Practical method development for the separation of monoclonal antibodies and antibody-drug-conjugate species in hydotphobic interaction chromatography, Part 2: Optimization of the phase sytem, J. Pharm. Biomed. Anal. (2016) (submitted for publication).
[22] S. Pahlman, J. Rosengren, S. Hjertén, Hydrophobic interaction chromatography on uncharged sepharose® derivatives: effects of neutral salts on the adsorption of proteins, J. Chromatogr. 131 (1977) 99–108, http://dx.doi.org/10.1016/S0021-9673(00)80924-3.
[23] L.R. Snyder, J.W. Dolan, J.R. Gant, Gradient elution in high-performance liquid chromatography: i. Theoretical basis for reversed-phase systems, J. Chromatogr. A 165 (1979) 3–30, http://dx.doi.org/10.1016/S0021-9673(00)85726-X.
[24] M. Sarrut, G. Crétier, S. Heinisch, Theoretical and practical interest in UHPLC technology for 2D-LC, TrAC Trends Anal. Chem. 63 (2014) 104–112, http://dx.doi.org/10.1016/j.trac.2014.08.005.
[25] B. Bobály, A. Beck, J. Fekete, D. Guillarme, S. Fekete, Systematic evaluation of mobile phase additives for the LC–MS characterization of therapeutic proteins, Talanta 136 (2015) 60–67, http://dx.doi.org/10.1016/j.talanta.2014.12.006.
[26] K.J. Hamblett, P.D. Senter, D.F. Chace, M.M.C. Sun, J. Lenox, C.G. Cerveny, K.M. Kissler, S.X. Bernhardt, A.K. Kopcha, R.F. Zabinski, D.L. Meyer, J.A. Francisco, Effects of drug loading on the antitumor activity of a monoclonal antibody drug conjugate, Clin. Cancer Res. 10 (2004) 7063–7070, http://dx.doi.org/10.1158/1078-0432.CCR-04-0789.
[27] E.L. Sievers, P.D. Senter, Antibody-Drug conjugates in cancer therapy, Annu. Rev. Med. 64 (2013) 15–29, http://dx.doi.org/10.1146/annurev-med-050311-201823.

B. ELUCIDATION STRUCTURALE DES SOUS UNITÉS DES DARS PAIRS ET IMPAIRS

Article 5

"Analysis of antibody-drug conjugates by comprehensive on-line twodimensional hydrophobic interaction chromatography x reversed phase liquid chromatography hyphenated to high resolution mass spectrometry. II- Identification of sub-units for the characterization of even and odd load drug species";

M. Sarrut, S. Fekete, M-C. Janin-Bussat, D. Guillarme, O. Colas, D. Guillarme, A. Beck, S. Heinisch, J. Chromatogr. B, 1032 (2016), 91-102

Journal of Chromatography B, 1032 (2016) 91–102

Contents lists available at ScienceDirect

Journal of Chromatography B

journal homepage: www.elsevier.com/locate/chromb

Analysis of antibody-drug conjugates by comprehensive on-line two-dimensional hydrophobic interaction chromatography x reversed phase liquid chromatography hyphenated to high resolution mass spectrometry. II- Identification of sub-units for the characterization of even and odd load drug species

Morgan Sarrut[a], Szabolcs Fekete[b], Marie-Claire Janin-Bussat[c], Olivier Colas[c], Davy Guillarme[b], Alain Beck[c], Sabine Heinisch[a,*]

[a] Univ Lyon, CNRS, Université Claude Bernard Lyon 1, Ens de Lyon, Institut des Sciences Analytiques, UMR 5280, 5 rue de la Doua, F-69100 VILLEURBANNE, France
[b] School of Pharmaceutical Sciences, University of Geneva, University of Lausanne, Bd d'Yvoy 20, 1211 Geneva 4, Switzerland
[c] Center of Immunology Pierre Fabre, 5 Avenue Napoléon III, BP 60497, 74160 Saint-Julien-en-Genevois, France

ARTICLE INFO

Article history:
Received 22 February 2016
Received in revised form 20 June 2016
Accepted 27 June 2016
Available online 28 June 2016

Keywords:
On-line comprehensive 2DLC
HICxRPLC-QTOF-MS
Quadrupole time-of-flight
Antibody-drug conjugate
ADCs
Odd DARs

ABSTRACT

This paper is the second part of a two-part series dedicated to the development of an on-line comprehensive HICxRPLC-UV/MS method for the characterization of a commercial inter-chain cysteine-linked ADC (brentuximab vedotin, Adcetris®). The first part focused on the optimization of the chromatographic conditions. In the second part of this series of papers, the structural characterization of the Brentuximab Vedotin was extensively discussed. With the combination of HIC and RPLC–MS data, the average DAR was easily measured in HIC and, at the same time, the predominant positional isomers were identified in RPLC–MS in one single injection. It was also demonstrated that the retention data obtained in the first and second dimensions was particularly useful to assist ADC characterization through the identification of sub-units. Using this methodology, the presence of odd DARs (1, 3 and 5) and their relative abundance was assessed by a systematic evaluation of HIC x RPLC-UV/MS data for both commercial and stressed ADC samples. Finally, once the exhaustive characterization of ADC was completed, MS could be conveniently replaced by UV detection to quickly assess the conformity of different ADCs batches.

1. Introduction

Hydrophobic interaction chromatography (HIC) is one of the most popular modes of chromatography that is widely applied for the characterization of antibody-drug conjugates (ADCs). This reference technique enables the separation of the different populations of ADC molecules that differ in their number of drugs *per* antibody which are often known as DAR (drug-to-antibody ratio) species [1,2]. For cysteine linked ADCs, thiol conjugates are produced by the partial reduction of disulphide bridges and followed by the conjugation with a drug linker, resulting in a heterogeneous population that differs with respect to the site of conjugation and the number of drugs *per* antibody (DAR) [1].

The drug-loading distribution and conjugation sites of ADCs have been reported to influence pharmacokinetic, toxicity, clearance and therapeutic index [3–5], therefore it is important to determine the average DAR and distribution of the different populations. One of the most important quality attributes of an ADC is the average number of drugs that are conjugated, because this determines the amount of "payload" that can be delivered to the tumor cell. A fully conjugated IgG1 ADC has a maximum DAR of 8 and is composed of a heterogeneous mixture of 0, 2, 4, 6, and 8 DARs [6]. An odd number (e.g. DAR 1 or DAR 3) of conjugated drug is typically indicative of incomplete conjugation or degradation, and odd DARs are therefore mostly observed in very small amount [1].

Obviously, other techniques than HIC can also be used to determine the average DAR and DAR distribution [7]. UV–vis spectrophotometry, reversed-phase liquid chromatography (RPLC) or sodium-dodecyl-sulfate capillary gel electrophoresis (CGE-SDS) are often used for cysteine linked ADCs, while ion-exchange

* Corresponding author.
E-mail address: sabine.heinisch@univ-lyon1.fr (S. Heinisch).

http://dx.doi.org/10.1016/j.jchromb.2016.06.049
1570-0232/

chromatography (IEX) or capillary isoelectric focusing (cIEF) are routinely used for lysine conjugations [6,7]. With RPLC, not only the average DAR, but also the amount of each positional isomer can be determined. Native mass spectrometry (MS) is also an important tool for the determination of average DAR and DAR distribution [8].

Multi-dimensional (2D) chromatography could be a powerful technique for ADC characterization, since it allows the hyphenation of MS incompatible chromatographic modes to MS instrumentation. Three approaches are applied for multi-dimensional separations of ADC samples: (i) off-line sample collection (LC–MS), (ii) heart-cutting approach (LC–LC–MS) and (iii) fully comprehensive on-line approach (LCxLC–MS). Debaene et al. applied HIC for off-line native MS characterization of ADC (brentuximab vedotin) [9]. HIC fractions were collected and then analyzed by ion mobility (IMS) combined with native MS. On-line multi-dimensional LC of HIC and MS using an RPLC desalting step prior to MS was applied by Birdsall et al. [10]. Their heart-cutting setup provided the identification of positional isomers and the drug conjugation site confirmation. This approach however requires as many injections as peaks to be analyzed. On-line comprehensive two-dimensional liquid chromatography could therefore be an attractive alternative for reducing both sample consumption and analysis time.

It has been shown in the first part of this study that combining HIC in the first dimension of an on-line comprehensive 2D-separations and RPLC in the second dimension was a promising solution for MS-coupling, given the fact that the salt can be completely eliminated in the second dimension [11]. In addition, the whole sample is subjected to two different separation modes in comprehensive 2D-LC which dramatically increases the separation power provided of course that the degree of orthogonality of the combination is sufficient. Indeed, we demonstrated that the second RPLC-dimension permitted to obtain a good separation of the different sub-units of the DAR positional isomers. It was also shown that 2D retention times were highly repeatable and hence able to provide useful additional information for completing MS identification. As a result, an extensive information on the peaks observed in the first HIC-dimension can be expected from 2D-data. The objective of this second study was therefore to cross information from retention and MS data to clearly identify the peaks obtained in the second dimension, thus tracking the ADC structure. Non-stressed and stressed brentuximab vedotin samples were analyzed to assist the ADC characterization. The final objective was to demonstrate that, once the characterization was completed, MS could be conveniently replaced by UV detection to quickly assess the conformity of different ADC batches.

2. Experimental section

For detailed explanations, the reader is kindly referred to Part I [11] of the present study, in particular to Table 3 for the description of the HIC x RPLC-UV/MS method and to Fig. 2 for instrumental set-up.

2.1. MS-data processing

Mass spectra were deconvoluted using the MaxEnt 3 algorithm of Waters MassLynx.

2.2. Protocol to obtain stressed ADC samples

The Brentuximab vedotin ADC sample was analyzed as soon as received (non-stressed sample) and after having been subjected at 40 °C during one month (one-month stressed sample) and two months (two-month stressed sample).

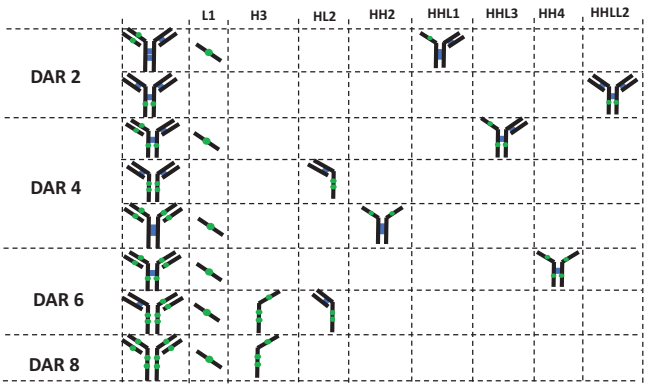

Fig. 1. Expected sub-units for the positional isomers of even DARs resulting from denaturing conditions in RPLC. Abbreviations are defined as "L" for light chain; "H" for heavy chain with numbers 1, 2, 3 and 4 referring to the number of drugs.

3. Results and discussion

3.1. Structural elucidation of even DAR positional isomers by on-line HICxRPLC–MS

Brentuximab vedotin is a cysteine-conjugated ADC. The conjugation of drugs to the antibody results in a heterogeneous population of DARs. Drug loads are usually expected in even intervals (2, 4, 6 and 8). The positional isomers of even DARs are shown in Fig. 1 as well as the expected sub-units resulting from disruption of non-covalent interaction in a denaturing medium such as RPLC hydro-organic mobile phase. For sake of convenience, abbreviations for the different sub-units have been used all along this paper in the following way: "L" and "H" refer to light and heavy chains respectively; a combination of "L" and "H" is used when several chains are present; the number at the end of the abbreviation indicates the number of payloads without specification of their location in the sub-unit. For example, HHL1 refers to two heavy chains, one light chain and one drug. HHL1 corresponds to a theoretical mass of 125675 Da, as calculated from the work of Janin-Bussat et al. [12]. Theoretical masses for both sub-units and even DARs are given in Table 1.

The different steps leading to identification of the different peaks obtained in the second RPLC dimension have been reported in Fig. 2 for the particular case of DAR 6, whose peak apex was located at a retention time of 58.5 min in HIC (Fig. 2a). The fraction between 58.5 and 60 min was sent to the second RPLC-dimension and led to the separation of four major sub-units, as highlighted by MS-Total Ion Current (MS-TIC) chromatogram (Fig. 2b). Sub-units could be identified after deconvolution of mass spectra (Fig. 2c), leading to measured masses of 25040.4 Da (peak 1) matching with L1, 76676.4 Da (peak 2) matching with HL2, 105915 Da (peak 3) matching with HH4 and 54271.3 Da (peak 4) matching with H3. In the cases of HL2 and H3, two masses differing by 162 Da were observed as a result of microheterogeneity in the sub-units (difference in glycoforms G1F/G0F). MS-sensitivity was limited for HH4 and prevented from unambiguously identifying glycosylation (G1F). Measured masses can be compared to theoretical ones in Table 1 for all the identified sub-units. The observed errors were 24, 26, 63 and 123 ppm for L1, HL2, H3 and HH4, respectively. The increase in error with the mass of the sub-unit is likely to be due to a lower sensitivity for larger sub-units. Increase in error on measured masses may also be the result of less efficient de-adducting of the higher loaded species [9]. Fig. 3 shows the HICxRPLC-UV analysis of brentuximab vedotin. Even DARs are given on the left side of the 1D-HIC separation. The corresponding sub-units that were further identified by mass spectra deconvolution are indicated at the top of

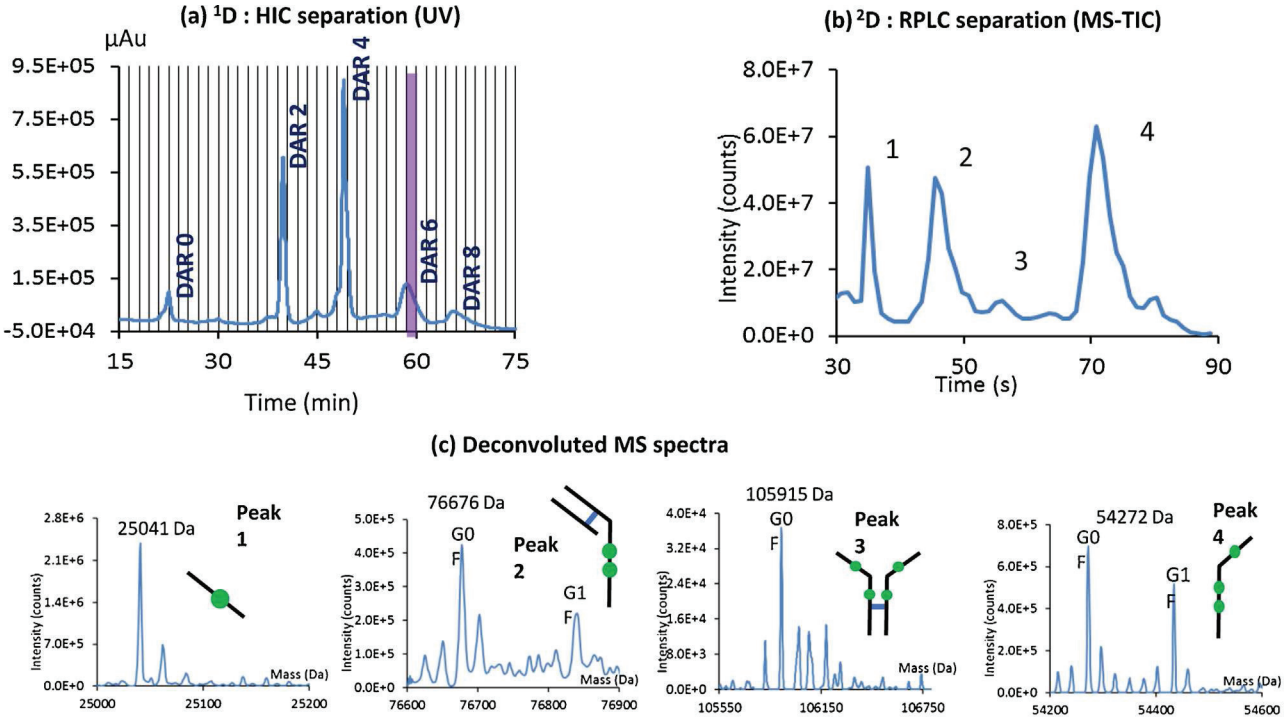

Fig. 2. Successive steps leading to the identification of sub-units by HICxRPLC–MS. This example illustrates the identification of DAR 6 sub-units: (a) 1D-HIC separation; the fraction at 58 min (colored vertical line) was sent to 2D; (b) 2D-RPLC separation of the fraction at 58 min (TIC chromatogram); (c) Identification of the 4 sub-units, corresponding to the 4 peaks observed on MS-TIC chromatogram, by deconvolution of MS signal. Experimental conditions were given in the experimental section of part 1 [11].

the contour-plot. Measured sub-unit masses found for each DAR as well as average mass values are listed in Table 1. The error between average measured masses and calculated theoretical masses, was in the range 24–155 ppm. This error is strongly dependent on the sub-unit mass, due to potential difficulty in detecting large masses. Sub-units are ranked in the ascending order of their retention times in Table 1. The number of identified sub-units was 6, out of a total of 8 that were expected (see Fig. 1). As above mentioned, HHL3 (for DAR 4) or HHLL2 (for DAR 2) were more difficult to detect by MS, probably due to their size. According to the data set including all ^{2}D-retention times for detected sub-units (discussed below), the retention time of HHL3 should be close to 54s. Yet, UV detection

Table 1
Summary of experimental values for the different sub-units identified for even DARs: retention times in the second dimension and molecular weights obtained from deconvoluted mass spectra. Abbreviations are defined as "L" for light chain; "H" for heavy chain with numbers 1, 2, 3 and 4 referring to the number of drugs. The retention time (RT), the standard deviation of the RT and the MW of each detected sub-units is indicated. Grey cells mean that the related sub-unit was not expected with the corresponding positional isomer. Theoretical masses of sub-units were compared to the experimental ones at the bottom. Similarly, theoretical masses of DARs were compared to the experimental ones on the right hand.

Sub-units	L1	HHL1	HH2	HL2	HH4	H3				
^{2}D retention time (s)	36.3	40.5	43.3	46.7	57.1	73.1				
Standard deviation (s)	0.4	/	0.9	0.4	0.4	0.5				
	MW (Da)						Sum (Da)	Theoretical mass (Da)	Δ mass (Da)	Error (ppm)
DAR 2	25040.8	125690					150731	150715	16	106
DAR 4	25040.8 (x2)		103284				153365	153349	16	104
				76676.9 (x2)			153354	153349	5	33
DAR 6	25040.7 (x2)				105915		155996	155982	14	90
	25040.7			76675.8		54271.9	155988	155982	6	38
DAR 8	25040.5 (x2)					54270.6 (x2)	158622	158616	6	38
Experimental MW (Da) (average value)	25040.7	125690	103284	76676.4	105915	54271.3				
Theoretical MW[a] (Da)	25040.1	125675	103268	76674.4	105902	54267.9				
Δ mass (Da)	0.6	15.0	16.0	2.0	13.0	3.4				
Error (ppm)	24	119	155	26	123	63				

[a] obtained or calculated from [12].

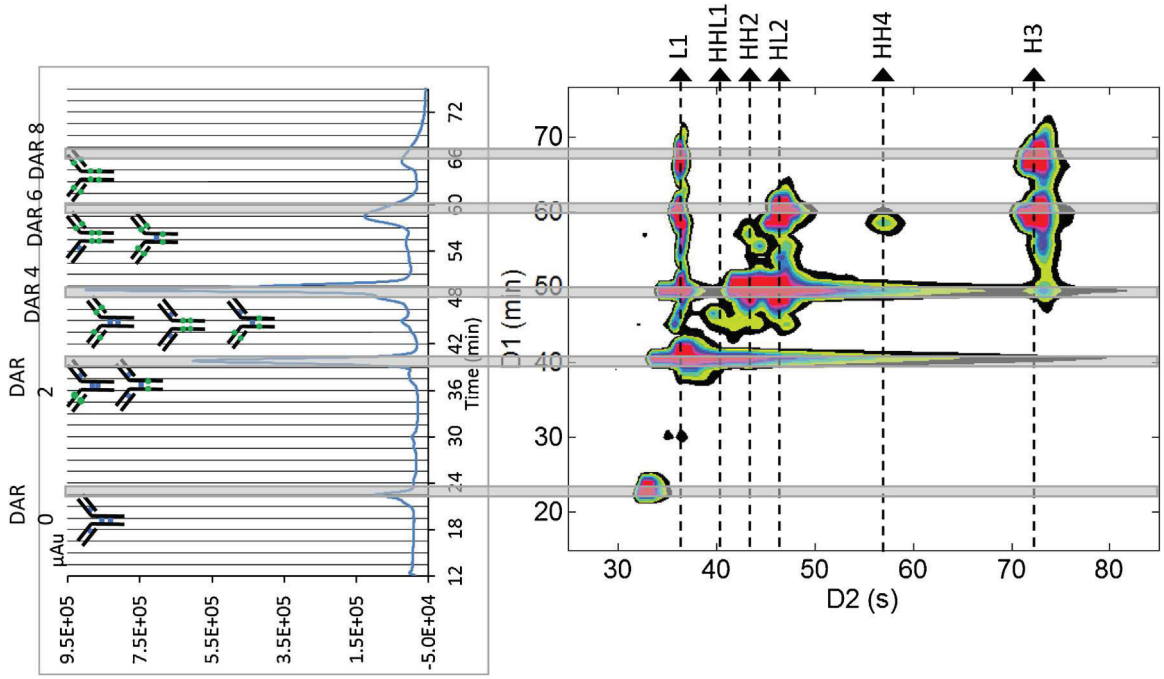

Fig. 3. HICxRPLC separation of Brentuximab Vedotin. [1]D HIC separation is on the left side. The different positional isomers for each DAR are specified. The 2D-contour plot was on the right side. The grey grid delimits the different [1]D fractions sent to [2]D. The sub-units identified after MS deconvolution were specified according to the abbreviations given in Fig. 2. Horizontal thick grey lines correspond to the most concentrated fractions of DAR 0, 2, 4, 6 and 8. UV detection at 210 nm was used in both dimensions. Other experimental conditions were given in the experimental section of part 1.

also failed to detect a peak at this time. It is therefore likely that the corresponding positional isomers were either not present or be present in the ADC sample in very small amount. Despite these two non-detected species, the clear and unambiguous identification of the four even DARs (2, 4, 6 and 8) was made possible with a reasonable error on the total mass (33–106 ppm), as shown in Table 1. DAR 0 (i.e. mAb) was poorly detected by mass spectrometry due to its large mass, and the signal was too low for an accurate deconvolution. Of course, this information is not of prime importance since the relative DAR 0 abundance can be directly assessed from [1]D HIC separation, its structure being generally known before ADC synthesis.

The separations of the most concentrated fractions of even DARs, indicated as horizontal grey lines in Fig. 3, are shown in Fig. 4. As shown, the peaks are located within a narrow retention range (36–73 s). However, as reported in Table 1, the standard deviation of retention times (in the order of 0.5 s) is low compared to the average peak width at half peak height (from 1 s for L1 to 2.5 s for H3). As a result the 2D-retention times of sub-units can be considered as helpful data (in addition to those provided by MS) for completing the identification of sub-units. In this way, it was surprising to observe a small peak corresponding to HL2 in the separation of the DAR 8 fraction (Fig. 4e). The presence of this sub-unit is likely to be due to the peak tailing of DAR 6 in HIC (Fig. 1a), both DARs being not baseline resolved in HIC. More surprisingly, a small peak of H3 can be observed in the chromatogram of the fraction of DAR 4 (Fig. 4c) whereas this sub-unit is expected to be present in the fractions of DAR 6 and DAR 8 only, as highlighted in Fig. 1.

The observation of the contour plot shown in Fig. 3 provides some relevant information summarized below:

As highlighted by the large spot of DAR 0, UV detection seems to be more sensitive than MS detection for such very large proteins.

For a given sub-unit, the corresponding plots are well aligned along a vertical line whatever the [2]D-run. In the light of this, it is clear that some spots cannot correspond to any of the sub-units related to even DARs as listed in Fig. 1. Some of these spots could be also identified by MS and suggested that odd DARs were also present in this ADC sample. This issue will be addressed in the next section.

The spot corresponding to HH4 appears to be slightly offset from the other spots of the DAR 6 sub-units (i.e. L1, HL2, H3). This can be more easily observed in Fig. 5, showing the [2]D-separations of two successive fractions, the most concentrated fraction of DAR 6 at 60 min and the preceding fraction at 58.5 min (Fig. 5). As expected from the observation of the contour plot, the peak heights of both HL2 and H3 increase between the fraction at 58.5 min and that at 60 min while it decreases for HH4. This suggests that the positional isomer of DAR 6 with the six drugs uniformly distributed over the mAb, thereby leading to a symmetrical structure, was slightly less retained in HIC than the second positional isomer. Furthermore, the comparison of peak intensities between both separations suggests that the first positional isomer was far less abundant. That is not in agreement with the results obtained by Birdsall et al. in 2D-heart cutting [10]. However, their results were not obtained with Brentuximab Vedotin, but with an ADC synthetized from a non-cytotoxic-drug-mimic.

As expected from the results presented in the first part of this study, the present results confirm that on-line HICxRPLC-UV/MS can be a powerful technique to obtain, in a single step method of 75 min, an extensive information on both the drug loaded distribution (HIC separation) and the drug loaded position (RPLC–MS), making this method very attractive for the characterization of ADCs.

3.2. Structural elucidation of odd DAR positional isomers by on-line HICxRPLC-UV/MS

In the previous section, it was suggested that some peaks obtained in the second dimension could correspond to sub-units that were different from those coming from even DARs in denaturing conditions. The deconvolution of mass spectra for these peaks pointed out the existence of sub-units specific of odd drug loads. In

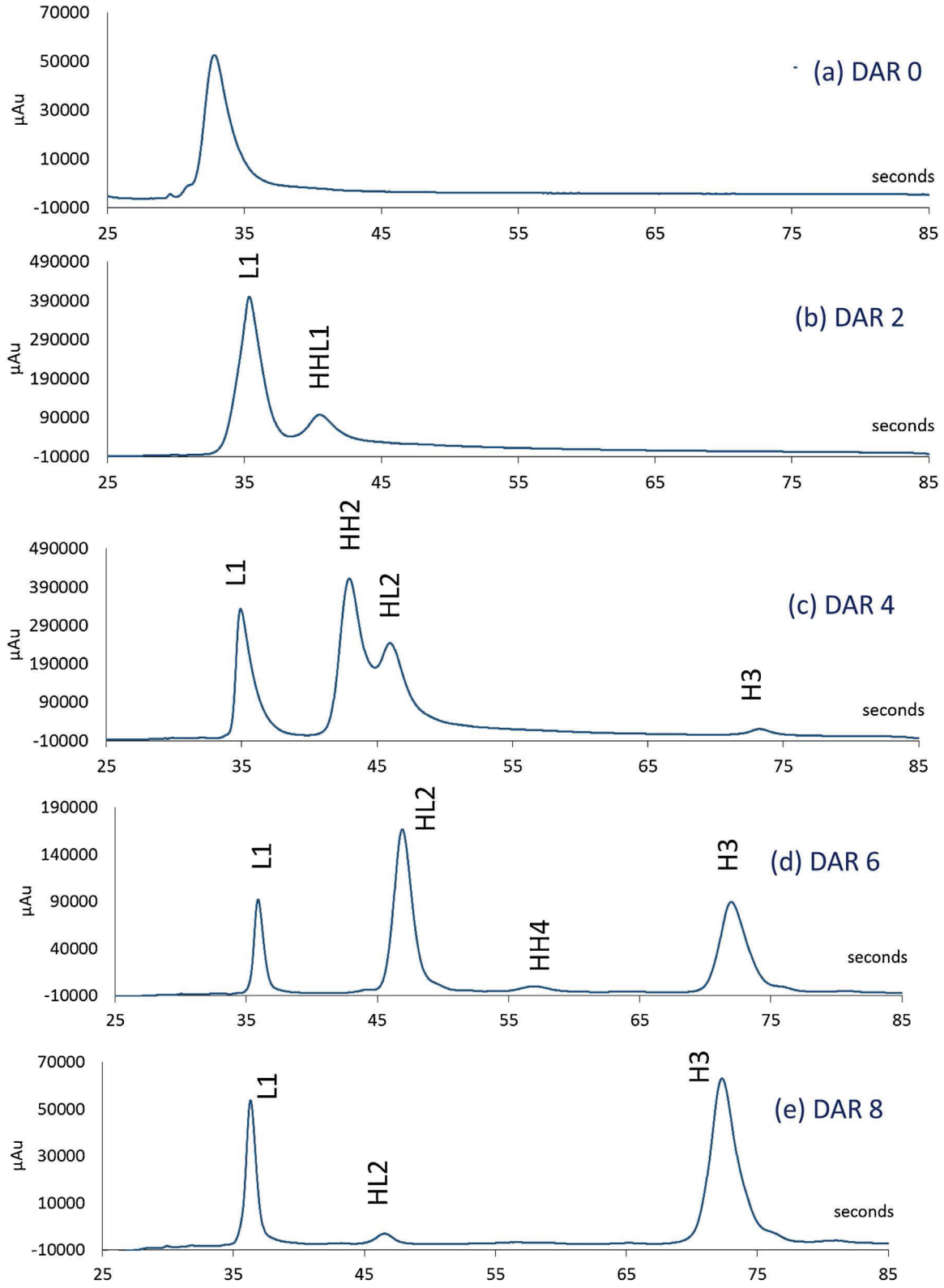

Fig. 4. [2]D RPLC-separations of the most concentrated fractions of DAR 0, 2, 4, 6 and 8 (indicated as horizontal grey lines in Fig. 3). The subunits that could be identified by deconvolution of mass spectra were specified above the corresponding peak apex.

a recent work of Debaene et al. [9], the unexpected presence of odd drug load species was highlighted by off-line combination of HIC and native MS in the case of an in-house produced ADC. For Brentuximab Vedotin, this analytical approach was not able to identify odd-numbered DARs. It should be noted that, whereas the presence of odd drug load is usually observed in lysine ADCs, it is rather unexpected in the case of cysteine conjugated ADCs [8] and may result from an incomplete conjugation.

In the present study, most of the sub-units that could be related to odd DARs were not sufficiently concentrated to be unambigu-

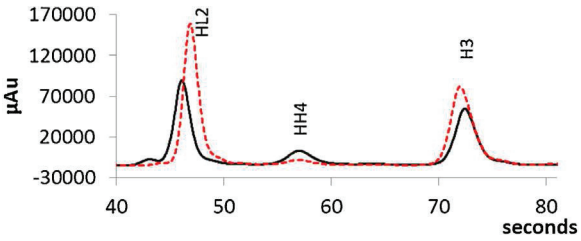

Fig. 5. ^{2}D RPLC-separations of two successive fractions of DAR 6 illustrating the partial separation in HIC of the two positional isomers of DAR 6. Fractions at 58.5 min (–) and 60 min (–).

ously identified. The DAR distribution may change over time under stress conditions, with an occurrence of odd load drug species. Then, we decided to stress the ADC sample, which would subsequently lead to a decrease of the drug load level, and hence an increase in the concentration of odd DARs. The ADC sample was subjected to one-month and two-month stress procedure, according to a protocol described in the experimental section. An overlay of the three resulting HIC separations is shown in Fig. 6.

As observed, the HIC distribution profile of a stressed ADC sample is quite different from that of a non-stressed one. In particular, the peak intensities of even DARs decreased when the stress duration is increased while, at the same time, the intensities of two unidentified peaks (indicated by arrows in Fig. 6) increase, suggesting a potential degradation of the product. In view of their respective location in the chromatogram, these peaks could correspond to odd-numbered conjugated species, namely DAR 1 and DAR 3 respectively. DAR 0 (i.e. mAb) also seems to have been impacted by the stress procedure since the emergence of several peaks can be seen at its retention time. In the light of the peak intensities, the sample was particularly degraded during the first month. HICxRPLC-UV contour plots of the three ADC samples are shown in Fig. 7. This representation gives a more thorough comparison thanks to the additional RPLC dimension which allows the separation of the different sub-units for each DAR specie. Here, the color scale (indicated on the left side of the figure) was the same for the three 2D-separations. The decrease in drug load level when the stress duration was increased was reflected by the lower intensities of the spots corresponding to all sub-units of DAR 8 and DAR 6 and to a lesser extent, of DAR 4 and DAR 2. As an example, the HH4 spot (specific sub-unit of DAR 6) disappeared in the contour plots of the stressed samples (Fig. 7), meaning that the corresponding positional isomer of DAR 6 has probably been degraded. As expected from ^{1}D HIC separations (Fig. 6), the contour plots also point out significant intensity increase for spots corresponding to ^{1}D-retention times of about 30 and 45 min, which do not match with ^{1}D-retention times of even DARs. Moreover, some new spots were clearly observed in the case of stressed samples, while they were hardly visible in the case of non-stressed sample at the same time coordinates (e.g. at 30 and 32 s in ^{2}D). Accordingly, the methodology involving mass spectra deconvolution, as previously described in Fig. 2, was applied to identify unknown species. Fig. 8a lists the three hypothetical positional isomers of DAR 1 (labeled 1A, 1B and 1C) along with their related sub-units in a denaturing medium. Apart from L1 (found in all DARs) and HHL1 (also found in DAR 2), the other ones (L0, HHL0 and HHLL1) are not related to even DARs (see Fig. 1). In particular, HHL0 is a specific sub-unit of DAR 1. Fig. 8b shows the overlay of ^{2}D RPLC chromatograms obtained for both non-stressed and stressed samples. As expected from the contour plots in Fig. 7, the peak intensities were strongly increased for stressed ADC samples, thereby allowing to clearly identify two sub-units on the basis of their deconvoluted masses, corresponding to L0 and L1 respectively. While difficult to unambiguously identify by mass deconvolution, the presence of HHL0 was highly suspected. This idea is supported by (i) the obtained charge distribution which was very close to that of HHL1 previously identified in case of DAR 2 and (ii) the presence of L1 which is associated to HHL0 for the positional isomer 1A. Sub-unit retention

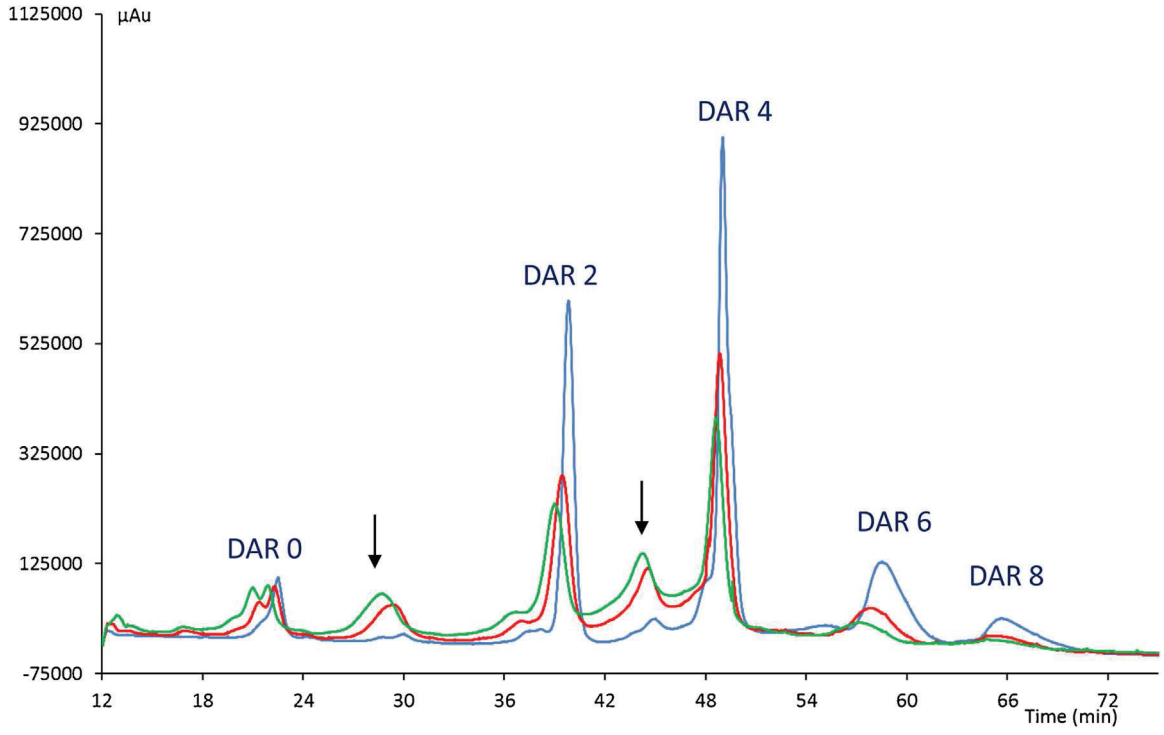

Fig. 6. Overlay of HIC-separations of non-stressed (blue), one-month stressed (red) and two-month stressed (green) ADC samples. The two arrows indicate unidentified peaks in HIC, for which intensities increase with stress conditions. Experimental conditions were given in the experimental section of part 1 (for interpretation of the references to colour in this figure legend, the reader is referred to the web version of this article)..

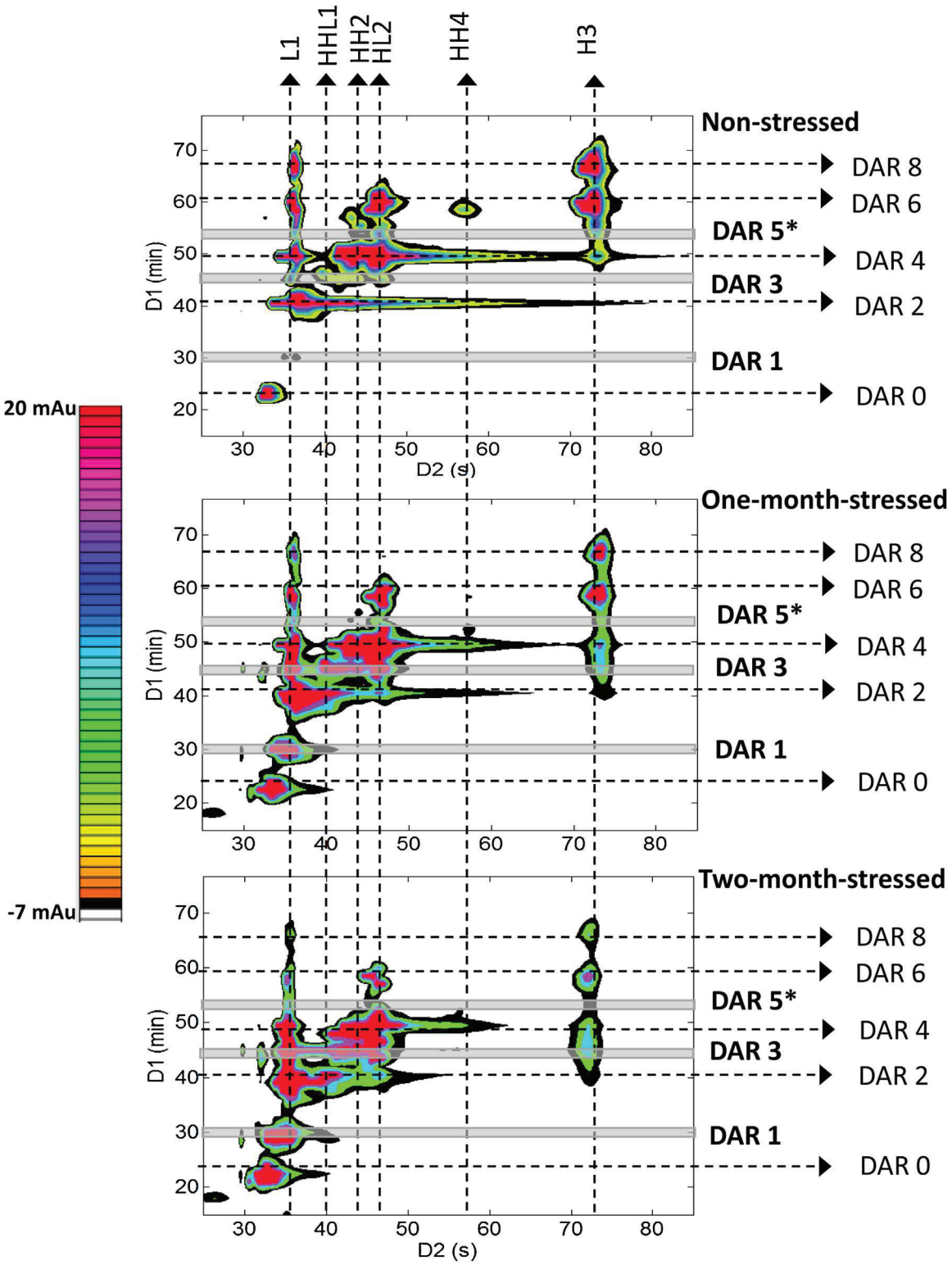

Fig. 7. Comparison of the contour plots of HIC x RPLC-UV 210 nm separations of non-stressed (top), one-month stressed (middle) and two-months stressed (bottom) ADC sample. The sub-units identified after MS deconvolution for even DARs were specified at the top of the figure according to the abbreviations given in Fig. 2. Horizontal thick grey lines correspond to the most concentrated fractions of possible odd DARs. Color scale (on the left side) was the same for the three separations. Experimental conditions were given in the experimental section of part 1."*" indicates that the presence of DAR 5 remains hypothetical.

times and mass data were listed in Table 2. Both L1 and HHL0 are sub-units of positional isomer 1A, thereby clearly highlighting the presence of this isoform. HHL1 could not be clearly identified by MS although a peak was observed in Fig. 8b with ^{2}D-retention time corresponding exactly to the expected one for HHL1 (i.e. 40.5 s as given in Table 1). It can be concluded that, isomer 1B is likely to be present but in much lower abundance than isomer 1A. Similarly to HHLL2 for DAR 2, HHLL1 and hence its corresponding isomer 1C, could not be detected, either due to its large mass or just because it is not present. The addition of salt in the sample solvent in HIC, as

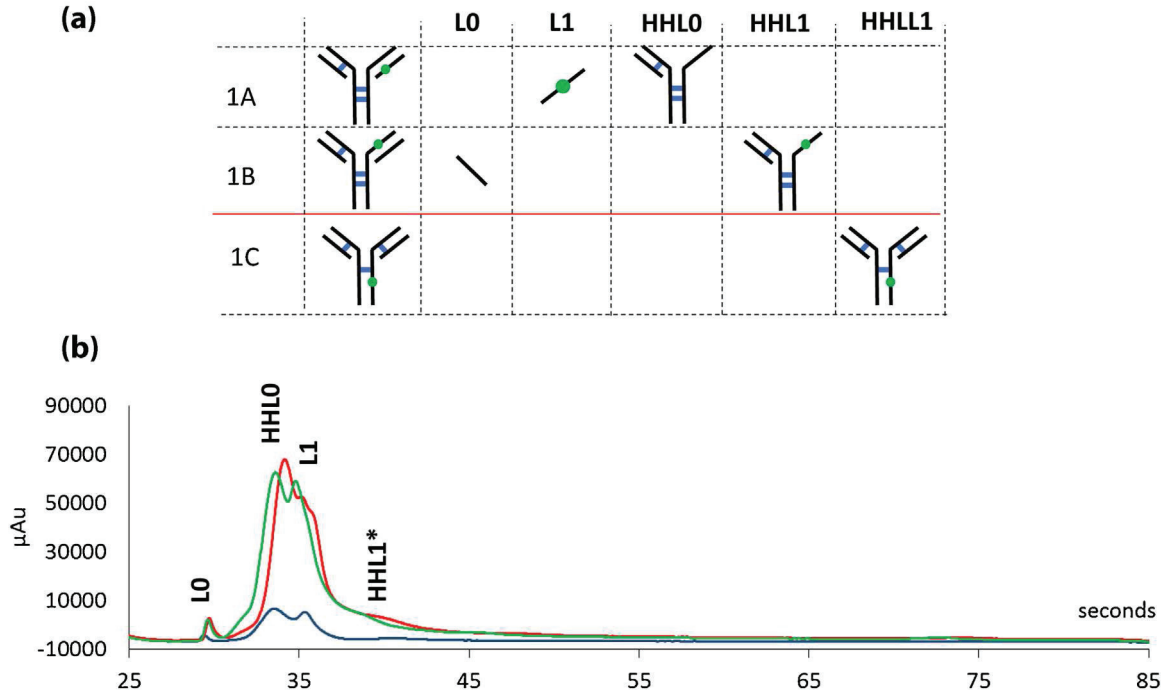

Fig. 8. (a) Possible positional isomers of DAR 1 and their expected sub-units resulting from denaturing conditions in RPLC (hinge region-isomers were not represented) and (b) overlay of the ^{2}D RPLC-separations of sub-units corresponding to the most concentrated fractions in ^{1}D for DAR1 (indicated as horizontal grey lines at 30 min in Fig. 7), for non-stressed (blue), one-month stressed (red) and two-months stressed (green) ADC samples. The full red line delimits the positional isomers (above) that could be unambiguously identified. Abbreviations are defined as "L" for light chain; "H" for heavy chain, with numbers 1, 2, 3 and 4 referring to the number of drugs (for interpretation of the references to colour in this figure legend, the reader is referred to the web version of this article).

described in the first part of this study, was likely to be a valuable asset for sample focusing and hence fraction concentration enhancing. This was important to help for identifying both isomers 1A and 1B, thereby confirming the presence of DAR 1 in stressed samples, but also in non-stressed one. Finally, it is important to underline the high complementarity between UV and MS detection in association with retention times in both dimensions for sub-unit identification.

Similarly to DAR 1, the fraction obtained in HIC at 45 min was investigated with the goal to identify most of the sub-units among the large number of DAR3 positional isomers, as listed in Fig. 9a. As shown in Fig. 7, the spot intensity of H3 significantly increases at this ^{1}D time, suggesting the presence of 3A positional isomer (H3 was indeed specific of isomer 3A). In addition, the intensity of two other spots (i.e. at 29.8 and 32.4 s) also increases for stressed sample. Those spots do not correspond to any sub-unit related to even DARs. The ^{2}D-separation of the fraction at 45 min with UV detection is shown in Fig. 9b revealing seven well separated peaks in spite of the narrow retention range in the second dimension (<1 min). Mass spectra deconvolution permitted the identification of seven sub-units, indicated at peak apex. Among them, L0, HL0, HL1 and H1 do not belong to the list of sub-units related to even DARs (Table 1) and hence were not detected before. Table 2 shows the corresponding masses for these new species. As shown, they were very close to the theoretical ones, with mass error ranging from 2 to 38 ppm. The presence of HL1 at 39.8 s could not be unambiguously ensured by deconvoluted mass spectra, but the obtained charge distribution was very close to that obtained for both HL0 and HL2, making the presence of this sub-unit very likely. According to both MS and retention data, the presence of HH1 and HH2 was also suspected. It should be noted that the difficulty to find out the masses for specific sub-units of odd DARs may also come from the presence of additional heterogeneity, resulting from potential degradation mechanisms (deamidation, oxidation, glycation. . .). On the other hand, several possible sub-units of DAR 3 could not be detected such as H0, H2 and HHL2, suggesting that their corresponding positional isomers may be either absent or present in low abundance. Taking into account firstly the detected sub-units and secondly the relative increase in their peak intensities when the sample was stressed (Fig. 9b), it was possible to definitely pointing out the presence of the first three positional isomers listed in Fig. 9a (i.e. 3A, 3B and 3C) and hence, that of DAR 3. Whereas the peak intensity increase for L0, HL0, L1, HL1, HL2 and H3 was significant, H1 intensity remained constant. Thus, there may be still a certain uncertainty about the presence of positional isomer 3D. Similarly, based on the difficulty to clearly identify HH1 and HH2, the isomers 3E to 3H are undoubtedly present, but probably in lower abundance than the first three positional isomers.

The sub-units resulting from the three possible positional isomers of DAR 5 (5A, 5B and 5C) are listed in Fig. 10a. The ^{1}D-retention time of DAR 5 in HIC should be within 50 min (DAR 4) and 58 min (DAR 6). No significant change was observed within this time range when the sample was stressed, neither in the HIC profiles shown in Fig. 6, nor in the 2D-contour plots shown in Fig. 7. However, the observation of the ^{2}D-separations of ^{1}D-fractions at 52.5 min and 54 min (Fig. 10.b) points out slight differences which may demonstrate the presence of low amount of DAR 5. Both fractions were in the tail of DAR 4 peak. For the fraction at 52.5 min, L0, L1 HH2, HL2, H2 and H3 could be identified by deconvoluting mass spectra. In the case of H2 (at 57 s), a mass difference of +106 Da compared to the theoretical mass (Table 2) was observed but remain unexplained. It is indeed neither related to known variants [13], nor to a change in the amino acid sequence but may potentially originate from a change in the linker structure after stress degradation. Peptide mapping and/or thorough study of the chemical mechanisms involved under stressed conditions could be useful to understand this difference. However, considering both its retention time and deconvoluted mass spectrum, the peak at 57 s could be unambiguously identified as H2. H2 is a specific sub-unit of DAR 5 and, as

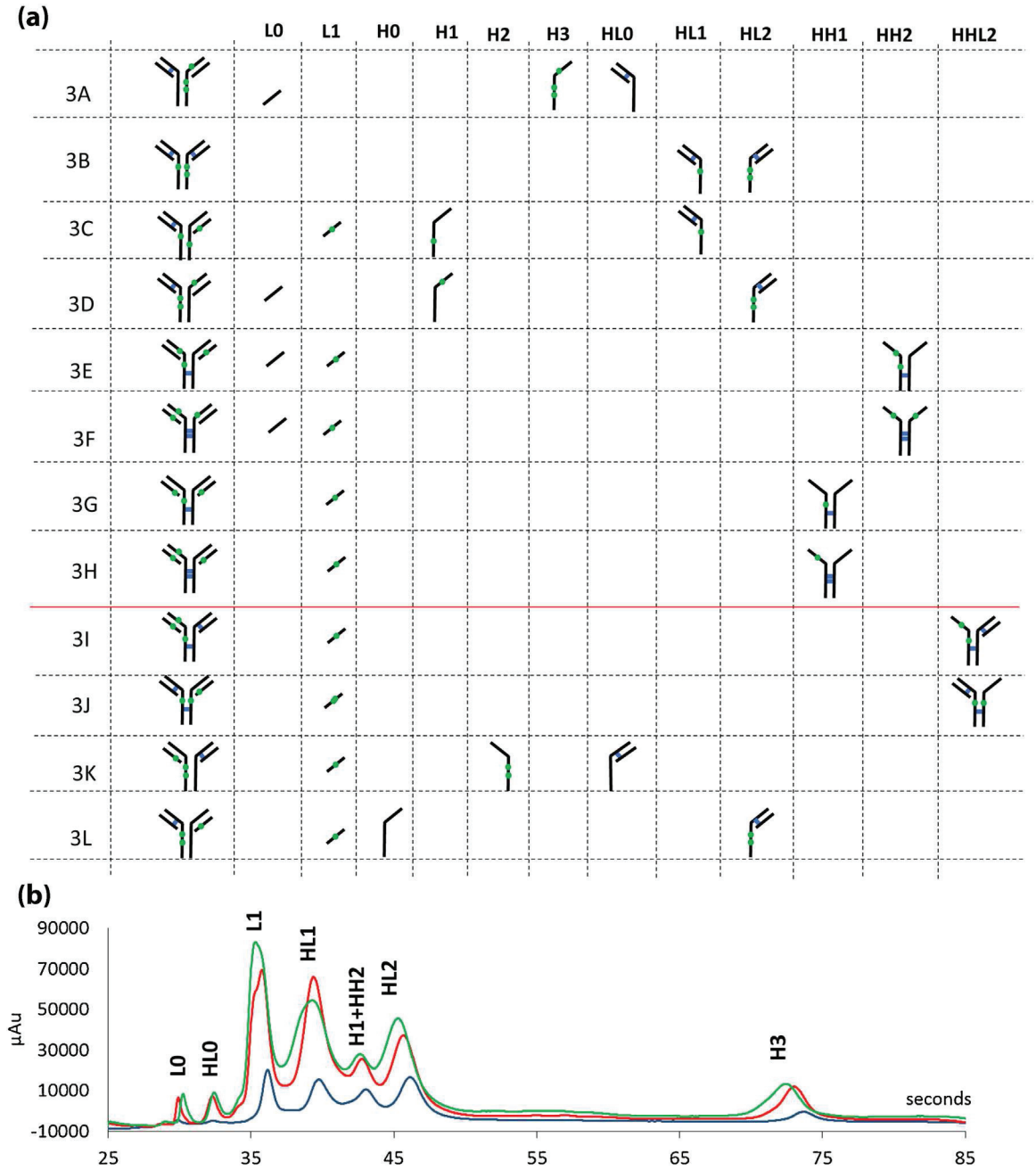

Fig. 9. (a) Possible positional isomers for DAR 3 and their expected sub-units resulting from denaturing conditions in RPLC (hinge region-isomers were not represented) and (b) overlay of the ^{2}D RPLC-separations of sub-units corresponding to the most concentrated fractions in ^{1}D for DAR 3 (indicated as horizontal grey lines at 45 min in Fig. 7), for non-stressed (blue), one-month stressed (red) and two-months stressed (green) ADC samples. The full red line delimits the positional isomers (above) that could be unambiguously identified. Abbreviations are defined as "L" for light chain; "H" for heavy chain with numbers 1, 2, 3 and 4 referring to the number of drugs (for interpretation of the references to colour in this figure legend, the reader is referred to the web version of this article).

shown in Fig. 10b, its corresponding peak cannot be observed with non-stressed sample. Its presence with stressed samples suggests the existence of the positional isomer 5A in RPLC, and hence of DAR 5 in HIC. L1, HH2, HL2 and H3 are also present in DAR 4 and their presence could be explained by the strong peak tailing of DAR 4 in HIC. However, while the peak intensity of HH2 (not related to DAR 5) decreases with the stressed sample, those of L1, HL2 and H3 (related to both DAR 4 and DAR 5) slightly increase, suggesting a balance between decrease in DAR 4 and increase in DAR 5. The peak intensity of L0 (specific sub-unit of odd DARs) increases, thereby also suggesting the presence of the positional isomer 5C. For the fraction at 54 min, a small peak appears at 51 s for stressed samples. This peak could not be clearly identified by deconvoluted mass spectra. It was suspected to correspond to HH3 by means of the variation of sub-unit retention times with the drug load number (Fig. 11). Finally, considering the likely presence of HH3 in stressed samples, the presence of the positional isomer 5 B was also highly suspected which could signify that the isomer 5 B was slightly separated from 5A and 5C in HIC. Thus, similarly to the presence of DAR 1 and DAR 3, there is converging evidence pointing out the presence of DAR 5, especially in stressed samples. Based on these observations, the average drug-to-antibody ratio (avDAR) should be more accurately determined by also taking into account odd DARs. Accordingly, Table 3 shows the average DAR values calcu-

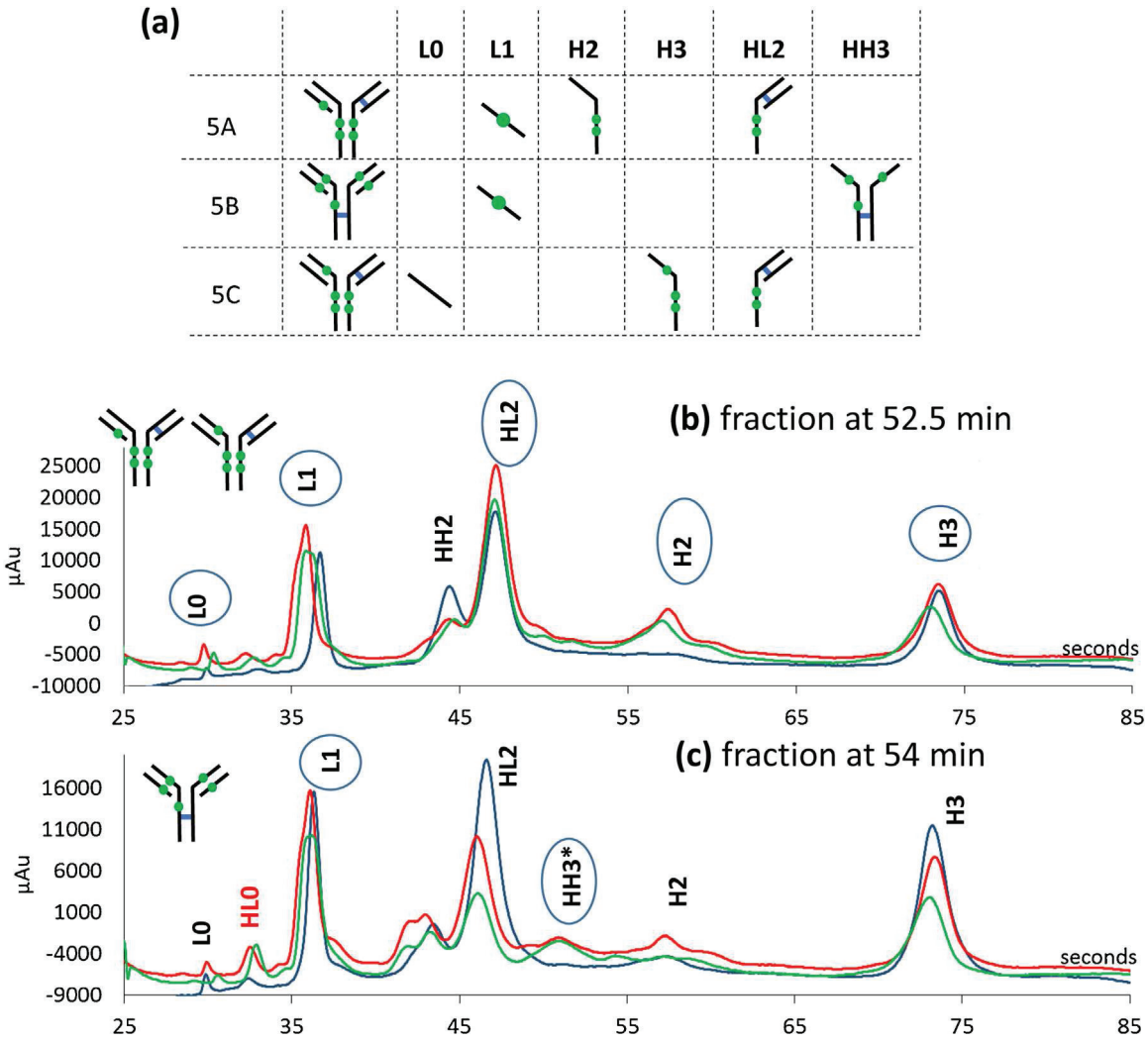

Fig. 10. (a) Possible positional isomers for DAR 5 and their expected sub-units resulting from denaturing conditions in RPLC (hinge region-isomers were not represented) and overlay of the ^{2}D RPLC-separations of sub-units corresponding to the fraction at (b) 52.5 min and (c) 54 min in ^{1}D, for non-stressed (blue), one-month stressed (red) and two-months stressed (green) ADC samples. Sub-units related to the corresponding positional isomers mentioned at the top of the figure were circled (for interpretation of the references to colour in this figure legend, the reader is referred to the web version of this article).

lated from the peak areas of all DARs. It appears that the value obtained for non-stressed ADCs (i.e. 3.9) was the same as the one obtained when only even DARs were considered [11]. This is due to the low abundance of odd DARs in a cysteine conjugated ADC (<2%). In contrast, since the relative abundance of odd DAR species was higher when the ADC sample was stressed, the average DAR value was significantly impacted and decreases down to 2.5 with one month stress and 2.0 with two-month stress duration.

The retention times for all sub-units identified for even and odd DARs were plotted as a function of the drug load number in Fig. 11. As shown for two sub-unit configurations namely H (with 1, 2 and 3 drugs) and HL (with 0, 1 and 2 drugs), the three experimental data, were very well fitted with a straight line (R^2 higher than 0.999). Such a retention behavior also exists in gradient elution with homologous series, when the carbon number is increased. Similarly, it seems that the drug number is the driving force for RPLC retention behavior of the sub-unit. This observation is confirmed when considering the behavior of the HH, HL and HHL sub-units. For a given drug number, the retention times of the series L and HH were exactly the same in RPLC and those of the series HL and HHL were close to each other. The series H was the most retained, with a regression line exhibiting a very high slope value compared to the other series. All these regression lines make it possible to predict the retention time of any sub-unit, provided that the retention times of at least two sub-units, having the same configuration but different drug number, are known. As example, the retention time of HH3 was predicted at 51 s, which is in good agreement with the retention time of the unknown peak in Fig. 10b.

3.3. On-line HICxRPLC-UV as a rapid method for quality assessment of ADCs

As demonstrated, on-line HICxRPLC-UV/MS method provides a huge amount of information. In one single injection, the determination of avDAR in HIC allows a qualitative evaluation of ADC structures, while the identification of sub-units in RPLC–MS provides essential data to deeply characterize the ADC. Our analytical strategy can be employed in the early stage of ADC development for extensive characterization. In addition, the high reliability of HICxRPLC-UV technique could allow its use in the later stages of ADC development and maybe, in the near future, for its quality control. For a given ADC, once all sub-units have been identified, UV detection might be sufficient considering that UV sensitivity was similar to or even better than MS for such species. As shown in Fig. 7 for degraded ADC, 2D-contour plots obtained in UV could be conveniently compared to each other in order to assess differ-

Table 2
Summary of experimental values for the different sub-units identified for suspected odd DARs: retention times in the second dimension and molecular weights obtained from deconvoluted mass spectra. Abbreviations are defined as "L" for light chain; "H" for heavy chain with numbers 1, 2, 3 and 4 referring to the number of drugs.

Sub-units		L0	HL0	HHL0	L1	HH1	HL1	HHL1	H1	HH2	HL2	HH3	H2	H3
^{2}D retention time (s)		29.8	32.4	33.8	36.3	36.3	39.8	40.5	42.9	43.3	46.7	51.8	57.0	73.1
		MW (Da)												
DAR 1	Non stressed	23723.4		ND	25041.1			ND						
	1-month stressed	23723.3		Highly Suspected	25040.3			Highly Suspected						
	2-month stressed	23723.0		Highly Suspected	25041.1			Highly Suspected						
DAR 3	Non stressed	23723.8	74043.0		25040.4	ND	ND		51636.3	ND	76675.1			54270.4
	1-month stressed	23723.3	74043.0		25040.5	Highly Suspected	Highly Suspected		51637.0	Highly Suspected	76680.4			54270.0
	2-month stressed	23828.0[b]	74047.2		25040.4	Highly Suspected	Highly Suspected		51636.0	Highly Suspected	76674.3			54265.6
DAR 5	Non stressed	23723.0	ND		25040.6					103282	76676.6	ND	ND	54269.0
	1-month stressed	23828.1[b]	74043.3		25040.7					Highly Suspected	76673.8	Highly Suspected	53059.0	54267.7
	2-month stressed	23723.8	74040.8		25040.4					Highly Suspected	76672.2	Highly Suspected	53056.8	54266.6
Average MW (Da)		23723.4	74043.5		25040.6				51636.4		76675.4		53057.9	54268.3
Theoretical MW[a] (Da)		23724.3	74042.8	124359	25040.1	101953	75358.6	75358.6	51636.3	103269	76674.4	104585	52952.1	54267.9
Δ mass (Da)		−0.9	0.7		0.5				0.1	13	1		105.8	0.4
Error (ppm)		38	9		20				2	125	13		1998	7

[a] calculated from [12].
[b] Structure related to L0.

Fig. 11. Retention times *vs.* drug load number for all sub-units identified in this study.

Table 3
Average DAR calculation for non-stressed, one-month stressed and two-month stressed ADC considering both even and odd DARs.

Number of drug load	HIC peak area (%)		
	Non-stressed	One-month stressed	Two-month stressed
DAR 0	5.7	7.2	9.1
DAR 1	1.1	7.5	9.8
DAR 2	25.3	20.4	17.4
DAR 3	1.8	6.4	7.6
DAR 4	41.3	25.6	20.8
DAR 6	17.1	8.5	4.6
DAR 8	7.5	3.7	2.5
Average DAR	3.9	2.5	2.0

ences between ADC batches as recently proposed by Vanhoenacker et al. [14] for the specific case of therapeutic monoclonal antibodies peptide mapping.

4. Conclusions

This work shows that on-line comprehensive 2D-LC–MS is a powerful technique for rapid characterization of inter-chain cysteine-linked ADCs. The combination of HIC and RPLC–MS leads to the determination of DARs in HIC and, at the same time, to the identification of the predominant positional isomers in RPLC–MS. Compared to the off-line mode, the on-line mode allows to obtain extensive information on all regions of the HIC-chromatogram and to avoid any risk of sample loss and/or sample contamination. Furthermore, the total analysis time is significantly lower and remains reasonable, the present 2D-separation being achieved within an analysis time of only 75 min.

In addition to even DARs (2, 4, 6, 8), the presence of odd DARs (1, 3 and 5) was clearly attested by a thorough study of HIC × RPLC–UV/MS data obtained on both non-stressed and stressed samples. Additionally, the relative abundance of their different positional isomers could be assessed.

It was finally demonstrated that the retention data obtained in HIC x RPLC with UV detection were of prime importance to assist ADC characterization. Indeed, the high complementarity between UV and MS detection in association with retention times in both dimensions was extremely helpful to identify sub-unit and hence characterize DARs. Furthermore, it was shown that the obtained contour plots were significantly different depending on ADC degradation conditions, suggesting that HIC x RPLC-UV contour plot

could be used as a convenient representation for assessing the conformity of ADCs in their later stage of development as well as in quality control.

Acknowledgments

Sabine Heinisch and Morgan Sarrut wish to thank Christelle Margoum and Philippe Bados (IRSTEA, France) for the loan of their Waters Q-Tof instrument. They also want to thank Waters for the generous gift of the 2D-ICLASS instrument and for making Maxent software available in their Lab. Davy Guillarme wishes to acknowledge the Swiss National Science Foundation for support through a fellowship to Szabolcs Fekete (31003A 159494).

References

[1] B. Wiggins, L. Liu-Shin, H. Yamaguchi, G. Ratnaswamy, Characterization of cysteine-linked conjugation profiles of immunoglobulin G1 and immunoglobulin G2 antibody–drug conjugates, J. Pharm. Sci. 104 (2015) 1362–1372, http://dx.doi.org/10.1002/jps.24338.

[2] M. Haverick, S. Mengisen, M. Shameem, A. Ambrogelly, Separation of mAbs molecular variants by analytical hydrophobic interaction chromatography HPLC: overview and applications, mAbs 6 (2014) 852–858, http://dx.doi.org/10.4161/mabs.28693.

[3] B.-Q. Shen, K. Xu, L. Liu, H. Raab, S. Bhakta, M. Kenrick, et al., Conjugation site modulates the in vivo stability and therapeutic activity of antibody-drug conjugates, Nat. Biotechnol. 30 (2012) 184–189, http://dx.doi.org/10.1038/nbt.2108.

[4] Y.T. Adem, K.A. Schwarz, E. Duenas, T.W. Patapoff, W.J. Galush, O. Esue, Auristatin antibody drug conjugate physical instability and the role of drug payload, Bioconjug. Chem. 25 (2014) 656–664, http://dx.doi.org/10.1021/bc400439x.

[5] B. Bender, D.D. Leipold, K. Xu, B.-Q. Shen, J. Tibbitts, L.E. Friberg, A mechanistic pharmacokinetic model elucidating the disposition of trastuzumab emtansine (T-DM1), an antibody–drug conjugate (ADC) for treatment of metastatic Breast cancer, AAPS J. 16 (2014) 994–1008, http://dx.doi.org/10.1208/s12248-014-9618-3.

[6] L.N. Le, J.M.R. Moore, J. Ouyang, X. Chen, M.D.H. Nguyen, W.J. Galush, Profiling antibody drug conjugate positional isomers: a system-of-equations approach, Anal. Chem. 84 (2012) 7479–7486, http://dx.doi.org/10.1021/ac301568f.

[7] A. Wakankar, Y. Chen, Y. Gokarn, F.S. Jacobson, Analytical methods for physicochemical characterization of antibody drug conjugates, mAbs 3 (2011) 161–172, http://dx.doi.org/10.4161/mabs.3.2.14960.

[8] A. Beck, G. Terral, F. Debaene, E. Wagner-Rousset, J. Marcoux, M.-C. Janin-Bussat, et al., Cutting-edge mass spectrometry methods for the multi-level structural characterization of antibody-drug conjugates, Expert Rev. Proteomics. 13 (2016) 157–183, http://dx.doi.org/10.1586/14789450.2016.1132167.

[9] F. Debaene, A. Bœuf, E. Wagner-Rousset, O. Colas, D. Ayoub, N. Corvaïa, et al., Innovative native MS methodologies for antibody drug conjugate characterization: high resolution native MS and IM-MS for average DAR and DAR distribution assessment, Anal. Chem. 86 (2014) 10674–10683, http://dx.doi.org/10.1021/ac502593n.

[10] R.E. Birdsall, H. Shion, F.W. Kotch, A. Xu, T.J. Porter, W. Chen, A rapid on-line method for mass spectrometric confirmation of a cysteine-conjugated antibody-drug-conjugate structure using multidimensional chromatography, mAbs 7 (2015) 1036–1044, http://dx.doi.org/10.1080/19420862.2015.1083665.

[11] M. Sarrut, A. Corgier, S. Fekete, D. Guillarme, D. Lascoux, M.-C. Janin-Bussat, et al., Analysis of antibody-drug-conjugates by comprehensive on-line two-dimensional hydrophobic interaction chromatography × reversed phase liquid chromatography hyphenated to high resolution mass spectrometry. I – Optimization of separation conditions, J. Chromatogr. B (2016), http://dx.doi.org/10.1016/j.jchromb.2016.06.048.

[12] M.-C. Janin-Bussat, M. Dillenbourg, N. Corvaia, A. Beck, C. Klinguer-Hamour, Characterization of antibody drug conjugate positional isomers at cysteine residues by peptide mapping LC–MS analysis, J. Chromatogr. B 981-982 (2015) 9–13, http://dx.doi.org/10.1016/j.jchromb.2014.12.017.

[13] A. Beck, E. Wagner-Rousset, D. Ayoub, A. Van Dorsselaer, S. Sanglier-Cianférani, Characterization of therapeutic antibodies and related products, Anal. Chem. 85 (2013) 715–736, http://dx.doi.org/10.1021/ac3032355.

[14] G. Vanhoenacker, I. Vandenheede, F. David, P. Sandra, K. Sandra, Comprehensive two-dimensional liquid chromatography of therapeutic monoclonal antibody digests, Anal. Bioanal. Chem. 407 (2015) 355–366, http://dx.doi.org/10.1007/s00216-014-8299-1.

CONCLUSIONS

Le développement d'une approche HICxRPLC-UV/MS a permis l'obtention, en une seule injection (temps d'analyse = 72 min), d'informations orthogonales telles que le DAR moyen des ADCs analysés et des informations structurales concernant les isomères de positions des différents DARs pairs.

La méthode a été optimisée afin (i) d'augmenter la capacité de pics grâce à l'utilisation d'outils prédictifs en HIC et un choix de phase mobile approprié en ^{2}D, (ii) d'augmenter la sensibilité grâce à l'ajout de sel dans l'échantillon, à l'utilisation de l'effet de concentration en ^{2}D malgré de larges volumes injectés et à l'ajout d'acide formique dans la phase mobile ^{2}D combiné à un split pour favoriser l'ionisation en MS, (iii) d'éviter toute précipitation entre les deux dimensions grâce à l'encadrement du volume transféré par un créneau d'eau et (iv) d'assurer le couplage avec la MS grâce à l'utilisation d'une vanne permettant d'éviter la contamination de la source par le créneau de sel lié à l'injection en ^{2}D.

Une étude fine des données de rétention de ^{1}D et ^{2}D et la complémentarité des modes de détection UV et MS ont permis d'identifier pour la première fois la présence de DARs impairs et de proposer des structures relatives à ces espèces.

Cette méthode HICxRPLC-UV-MS pourrait être utilisée lors d'étapes en amont du développement pour caractériser de façon exhaustive un ADC. De plus, du fait de sa bonne répétabilité, la cartographie 2D-UV générée peut-être un bon outil de contrôle de la qualité de la fabrication des ADCs ainsi que de leur stabilité.

RÉFÉRENCES

[1] A. Beck, J.M. Reichert, Antibody-drug conjugates, mAbs. 6 (2014) 15–17. doi:10.4161/mabs.27436.
[2] A. Beck, E. Wagner-Rousset, D. Ayoub, A. Van Dorsselaer, S. Sanglier-Cianférani, Characterization of Therapeutic Antibodies and Related Products, Anal. Chem. 85 (2013) 715–736. doi:10.1021/ac3032355.
[3] J.X. Shen, R.J. Motyka, J.P. Roach, R.N. Hayes, Minimization of ion suppression in LC–MS/MS analysis through the application of strong cation exchange solid-phase extraction (SCX-SPE), J. Pharm. Biomed. Anal. 37 (2005) 359–367. doi:10.1016/j.jpba.2004.10.035.
[4] Y.T. Adem, K.A. Schwarz, E. Duenas, T.W. Patapoff, W.J. Galush, O. Esue, Auristatin Antibody Drug Conjugate Physical Instability and the Role of Drug Payload, Bioconjug. Chem. 25 (2014) 656–664. doi:10.1021/bc400439x.
[5] B. Bender, D.D. Leipold, K. Xu, B.-Q. Shen, J. Tibbitts, L.E. Friberg, A Mechanistic Pharmacokinetic Model Elucidating the Disposition of Trastuzumab Emtansine (T-DM1), an Antibody–Drug Conjugate (ADC) for Treatment of Metastatic Breast Cancer, AAPS J. 16 (2014) 994–1008. doi:10.1208/s12248-014-9618-3.
[6] S. Fekete, D. Guillarme, P. Sandra, K. Sandra, Chromatographic, Electrophoretic, and Mass Spectrometric Methods for the Analytical Characterization of Protein Biopharmaceuticals, Anal. Chem. 88 (2016) 480–507. doi:10.1021/acs.analchem.5b04561.
[7] D.R. Stoll, J. Danforth, K. Zhang, A. Beck, Characterization of Therapeutic Antibodies and Related Products by Two-Dimensional Liquid Chromatography Coupled with UV Absorbance and Mass Spectrometric Detection, J. Chromatogr. B. (2016).

CHAPITRE 5 – DÉVELOPPEMENT DU COUPLAGE ENTRE LA CHROMATOGRAPHIE LIQUIDE ET LA CHROMATOGRAPHIE EN PHASE SUPERCRITIQUE POUR LA SÉPARATION DE COMPOSÉS NEUTRES

Ce chapitre a fait l'objet d'une publication :

Article 6 (chapitre 5)

"Potential and limitations of on-line comprehensive reversed phase liquid chromatography × supercritical fluid chromatography for the separation of neutral compounds: An approach to separate an aqueous extract of bio-oil";

M. Sarrut, A. Corgier, G. Crétier, A. Le Masle, S. Dubant, S. Heinisch J. Chromatogr. A. 1402 (2015) 124–133. doi:10.1016/j.chroma.2015.05.005.

INTRODUCTION

L'absence de corrélation entre les rétentions dans les deux dimensions, plus simplement appelée orthogonalité, peut-être déterminante pour maximiser la capacité de pics lors d'analyses bidimensionnelles.

Alors que des conditions offrant un degré d'orthogonalité élevé sont aisément identifiables pour des molécules ionisables grâce à l'utilisation de phases mobiles de pH différents et/ou grâce à la combinaison de différents modes chromatographiques (IEXxRPLC par exemple), celles-ci sont plus difficiles à trouver pour des composés neutres.

Le couplage entre la chromatographie en phase normale (NPLC) et la RPLC fournit une très bonne orthogonalité puisque les deux mécanismes de rétention sont différents [1]. Cependant, la compatibilité des phases mobiles entre les deux dimensions représente un problème majeur. Pour contourner cette difficulté, un faible volume doit être transféré vers la ^{2}D au prix d'une diminution importante de la sensibilité.

Ces difficultés ont donc souvent mené les chromatographistes à privilégier le couplage RPLCxRPLC malgré un faible degré d'orthogonalité [2]. La RPLC présente en effet l'avantage (i) d'être adaptée à de nombreux types d'échantillons, (ii) d'offrir différentes sélectivités du fait des nombreux greffages disponibles, (iii) de nécessiter des faibles temps d'équilibrage, (iv) de délivrer une grande efficacité et (v) d'être compatible avec la spectrométrie de masse [2].

Dans ce chapitre, la possibilité de coupler la chromatographie en fluide supercritique (SFC) et la RPLC (RPLCxSFC) en ligne pour l'analyse « comprehensive » d'un mélange complexe de composés neutres a été explorée. Le potentiel en terme d'orthogonalité entre ces deux techniques a déjà été souligné en mode hors ligne [3,4]. De plus, la faible viscosité de la phase mobile en SFC permet des analyses très rapides comme celles requises en ^{2}D. En revanche, la recherche de conditions permettant le transfert de l'échantillon entre les deux dimensions est un challenge clé pour le développement de telles méthodes.

A. DÉVELOPPEMENT DU COUPLAGE LCXSFC EN LIGNE POUR LA SÉPARATION DE COMPOSÉS NEUTRES

Article 6 (chapitre 5)

“Potential and limitations of on-line comprehensive reversed phase liquid chromatography × supercritical fluid chromatography for the separation of neutral compounds: An approach to separate an aqueous extract of bio-oil“;

M. Sarrut, A. Corgier, G. Crétier, A. Le Masle, S. Dubant, S. Heinisch J. Chromatogr. A. 1402 (2015) 124–133. doi:10.1016/j.chroma.2015.05.005.

Journal of Chromatography A, 1402 (2015) 124–133

Contents lists available at ScienceDirect

Journal of Chromatography A

journal homepage: www.elsevier.com/locate/chroma

Potential and limitations of on-line comprehensive reversed phase liquid chromatography × supercritical fluid chromatography for the separation of neutral compounds: An approach to separate an aqueous extract of bio-oil

Morgan Sarrut[a], Amélie Corgier[a], Gérard Crétier[a], Agnès Le Masle[b], Stéphane Dubant[c], Sabine Heinisch[a,*]

[a] Université de Lyon, Institut des Sciences Analytiques, UMR CNRS UCBL ENS 5280, 5 rue de la Doua, 69100 Villeurbanne, France
[b] IFP Energies nouvelles, Rond-Point de l'échangeur de Solaize, BP3, 69360 Solaize, France
[c] Waters SAS, BP608, 78056 St Quentin en Yvelines, France

ARTICLE INFO

Article history:
Received 28 January 2015
Received in revised form 29 April 2015
Accepted 4 May 2015
Available online 13 May 2015

Keywords:
Supercritical fluid chromatography (SFC)
On-line RPLCxSFC
Comprehensive two-dimensional chromatography
Complex samples
Bio-oils
Biomass

ABSTRACT

On-line comprehensive Reversed Phase Liquid Chromatography × Supercritical Fluid Chromatography (RPLCxSFC) was investigated for the separation of complex samples of neutral compounds. The presented approach aimed at overcoming the constraints involved by such a coupling. The search for suitable conditions (stationary phases, injection solvent, injection volume, design of interface) are discussed with a view of ensuring a good transfer of the compounds between both dimensions, thereby allowing high effective peak capacity in the second dimension. Instrumental aspects that are of prime importance in on-line 2D separations, were also tackled (dwell volume, extra column volume and detection). After extensive preliminary studies, an on-line RPLCxSFC separation of a bio-oil aqueous extract was carried out and compared to an on-line RPLCxRPLC separation of the same sample in terms of orthogonality, peak capacity and sensitivity. Both separations were achieved in 100 min. For this sample and in these optimized conditions, it is shown that RPLCxSFC (with Hypercarb and Acquity BEH-2EP as stationary phases in first and second dimension respectively) can generate a slightly higher peak capacity than RPLCxRPLC (with Hypercarb and Acquity CSH phenyl-hexyl as stationary phases in first and second dimension respectively) (620 vs 560). Such a result is essentially due to the high degree of orthogonality between RPLC and SFC which may balance for lesser peak efficiency obtained with SFC as second dimension. Finally, even though current limitations in SFC instrumentation (i.e. large extra-column volume, large dwell volume, no ultra-high pressure) can be critical at the moment for on-line 2D-separations, RPLCxSFC appears to be a promising alternative to RPLCxRPLC for the separation of complex samples of neutral compounds.

1. Introduction

Over the last decades, on-line comprehensive two-dimensional liquid chromatography (LCxLC) has grown significantly in many application fields [1–4]. Liquid chromatography provides a wide variety of separation modes including Reversed Phase Liquid Chromatography (RPLC), Normal Phase Liquid Chromatography (NPLC), Size Exclusion Chromatography (SEC), Ion Exchange Chromatography (IEC) and Hydrophilic Interaction Liquid Chromatography (HILIC). On-line coupling two of these different techniques *via* an appropriate interface may produce a separation system capable of generating a very high effective peak capacity in a reasonable analysis time while avoiding sample loss and/or sample contamination [5].

To maximize the potential of a two-dimensional system, one of the key problems is to find orthogonal conditions between the two dimensions in order to obtain a separation that uses the largest possible fraction (γ) of the separation space [6]. In this regard, NPLCxRPLC was shown to be very attractive for the separation of pharmaceutical compounds [7]. However, in spite of a lower degree of orthogonality, RPLCxRPLC has often been preferred to avoid peak deterioration associated with the incompatibility of the mobile phase of first dimension with that of second dimension (stronger eluting power or immiscibility) [2,8,9] and finally to obtain an

* Corresponding author. Tel.: +33 437 423 551.
E-mail address: sabine.heinisch@univ-lyon1.fr (S. Heinisch).

http://dx.doi.org/10.1016/j.chroma.2015.05.005
0021-9673/

Table 1
Physical and chemical properties of some bio-oil representative compounds.

	Compound	Chemical family	Molecular Formula	MW (g/mol)	log *P*
1	α-angelica lactone	Lactone	$C_5H_6O_2$	98.10	0.236
2	2-phenylethanol	Alcohol	$C_8H_{10}O$	122.16	1.504
3	5-methylfurfural	Furan	$C_6H_6O_2$	110.11	0.670
4	Phenol	Phenol	C_6H_6O	94.11	1.540
5	o-cresol	Phenol	C_7H_8O	108.14	1.962
6	m-cresol	Phenol	C_7H_8O	108.14	2.043
7	2,4,6-trimethylphenol	Phenol	$C_9H_{12}O$	136.19	2.935
8	α-hydroxycumene	Phenol	$C_9H_{12}O$	136.19	2.861
9	guaiacol	Guaiacol	$C_7H_8O_2$	124.14	1.341
10	syringol	Syringol	$C_8H_{10}O_3$	154.16	1.218
11	1-indanone	Enone	C_9H_8O	132.16	1.419
12	anisole	Aromatic ether	C_7H_8O	108.14	2.170

interesting sample peak capacity for the overall comprehensive system.

Bio-oil samples are mainly composed of small neutral compounds. Two very recent papers [10,11] presented successful separation of aqueous bio-oil extracts by on-line RPLCxRPLC with a percentage of retention space coverage close to 50% only, the retention space being delimited by the retention times of the least and the most retained compounds in both dimension. NPLCxRPLC could be a possible solution to increase the utilized portion of the available space. In this work, we experiment another option which consists in coupling RPLC to supercritical fluid chromatography (RPLCxSFC). West and Lesellier showed that polar stationary phases in SFC tend to behave as in NPLC [12]. Slightly polar stationary phases were also found to be attractive with SFC mobile phases as recently reported in a study which compared their use in SFC and RPLC [13]. On-line SFCxRPLC was investigated by François et al. [14] for the separation of fatty acids in fish oils and compared to on-line RPLCxRPLC for the separation of the same sample. 92% of the separation space was occupied in SFCxRPLC vs 55% in RPLCxRPLC. However, SFCxRPLC arrangement needed a particular interface composed of two two-position/ten-port switching valves equipped with two loops packed with octadecyl silica allowing both the depressurization of the supercritical fluid and the trapping and focusing of the analytes after an addition of water to the first dimension eluent and before the transfer to the second dimension. The potential of RPLCxSFC was highlighted by Stevenson et al. [15] in off-line mode. On-line RPLCxSFC has never been investigated yet. Here we describe our development of on-line RPLCxSFC for the separation of aromatic neutral compounds and an aqueous extract of bio-oil. With a liquid eluent in the first dimension, the interface between the two dimensions is simpler than that used in SFCxRPLC and similar to that used in RPLCxRPLC. Moreover, in the second dimension, the low viscosity of SFC mobile phase allows very fast analysis, which is of prime importance to increase peak capacity in on-line two-dimensional separations. This paper deals with the choice of SFC stationary phase, the study of phenomena resulting from the injection of a polar sample solvent into a supercritical mobile phase and the experimental and instrumental aspects related to the interface. Finally, a comparison between RPLCxSFC and RPLCxRPLC separations of the same aqueous bio-oil extract is proposed in terms of orthogonality, effective peak capacity and sensitivity.

2. Experimental

2.1. Material and reagents

Acetonitrile (ACN) (HPLC grade), methanol (MeOH) and acetone were purchased of HPLC grade from Sigma–Aldrich (Steinheim, Germany). Water was obtained from an Elga water purification system (Veolia water STI, Le Plessis Robinson, France). Pressurized liquid CO_2 3.0 grade (99.9%) was obtained from Air Liquide (Pierre Bénite, France).

The synthetic sample for RPLCxSFC experiments was composed of different compounds known to be representative of those found in bio-oil aqueous samples [10]. It contains α-hydroxycumene, phenol, 2,4,6-trimethylphenol, 1-indanone, syringol, angelica lactone, m-cresol, o-cresol, anisole, guaiacol, 5-methylfurfural and phenylethanol. They were dissolved in water/ACN 85/15 v/v at the concentration of 50 mg/L. Physical properties of these twelve compounds are reported in Table 1. The compounds were either obtained from Sigma–Aldrich or provided by IFP Energies nouvelles (Solaize, France). The bio-oil aqueous sample was provided by IFP Energies nouvelles.

2.2. Columns

Four columns from Waters (Milford, MA, USA) were used under SFC conditions: Acquity UPC^2 BEH-2EP, Acquity UPC^2 BEH, Acquity UPC^2 CSH Fluoro-Phenyl (all 50 mm × 2.1 mm, 1.7 μm, 100 Å) and Acquity UPC^2 HSS C18 (50 mm × 2.1 mm, 1.8 μm, 130 Å). Three columns were used under RPLC conditions: XBridge C18 (50 mm × 1.0 mm, 3.5 μm) from Waters, Hypercarb (100 mm × 1 mm, 5 μm) from Thermo Scientific (Cheshire, UK) and Acquity CSH Phenyl-Hexyl (50 mm × 2.1 mm, 1.7 μm) from Waters.

2.3. Apparatus

2.3.1. 1D-SFC system

Waters Acquity UPC^2 system was equipped with a binary solvent delivery pump, a 250 μL mixing chamber, an autosampler with a 10 μL loop, two column ovens compatible with temperature up to 90 °C and including two 6-channel column selection valves, a UV detector with a 8 μL flow-cell withstanding a pressure up to 414 bar and a backpressure regulator (BPR). The maximum allowable flow rate is 4 mL/min. The maximum allowable pressure is 414 bar for flow-rates below 3.25 mL/min. The maximum allowable pressure linearly decreases to 293 bar when the flow rate increases from 3.25 mL/min to 4 mL/min. Data acquisition was performed by Empower software (Waters). The extra-column volume and extra-column variance were measured under liquid chromatographic conditions. They were equal to 83 μL and 132 μL^2 respectively. The system dwell volume was estimated at 300 μL (see Section 2.4.1).

2.3.2. RPLCxRPLC system

The RPLCxRPLC system was a 2D-IClass liquid chromatograph from Waters. This instrument includes two high-pressure binary solvent delivery pumps, an autosampler with a flow-through needle of 15 μL, a column manager composed of two column ovens with an allowed maximum temperature of 90 °C and two 6-port high pressure two-position valves acting as interface between the two separation dimensions, a UV detector and a diode array

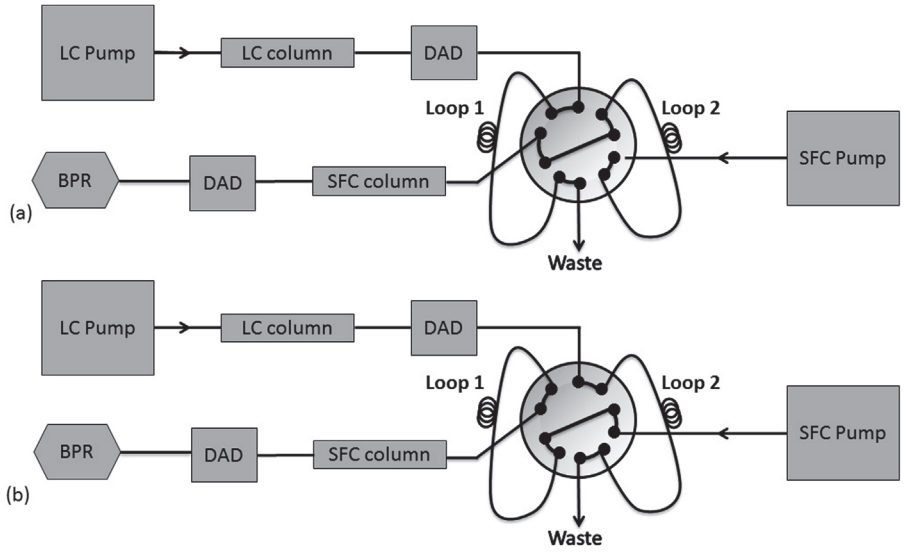

Fig. 1. RPLCxSFC setup. (a) The eluent of first dimension is stored in loop 1 while the content of loop 2 is injected in second dimension and (b) vice versa.

detector equipped with 500 nL flow-cells withstanding pressure up to 70 bar. The upper maximum allowable pressure is 1285 bar for the two pumps. Beyond a flow-rate of 1 mL/min, the upper limit decreases depending on both flow-rate and mobile phase composition. In case of low flow-rates (e.g. 10 μL/min in ^{1}D), a small i.d. tubing (30 cm × 25 μm) was placed just behind the column in order to generate a sufficient working pressure to ensure a good gradient run repeatability. The measured dwell volume was 110 μL and 120 μL for the first and second dimension respectively. A total extra-column volume of 12 μL and 17 μL and an extra-column variance of 4 μL^2 and 9 μL^2 were determined for the first and the second dimension respectively.

To ensure a fair comparison between RPLCxRPLC and RPLCxSFC experiments, the original interface made of two 6-port valves was replaced by a 10-port high pressure 2-position valve (Vici Valco Instruments, Houston, USA) equipped with two identical loops of 20 μL. Data acquisition, the instrumental control of the two dimensions and the programming of the 10-port high pressure 2-position valve interface were performed by Masslynx software (Waters).

2.3.3. RPLCxSFC setup

The first dimension was the same as in RPLCxRPLC, namely consisting of the high-pressure binary solvent delivery pump, the autosampler and the diode array detector of the 2D-IClass apparatus. The second dimension consisted of the high-pressure binary solvent delivery pump, the UV detector and the BPR of the Acquity UPC^2 apparatus, set at 140 bar. The column manager of the 2D-IClass instrument was used for both first and second dimension columns.

As in RPLCxRPLC, the 10-port high pressure 2-position valve was used as interface between the two dimensions. It was equipped with two identical loops of 3 or 5 μL. A 30 cm × 175 μm i.d. tubing was used between the mixer of SFC pump and the 10-port 2-position valve. A 56 cm × 175 μm i.d. tubing was connected between the valve and the 31.8 cm × 175 μm i.d. preheater of the second dimension column. Finally, the UV detector was connected to the column outlet by 30 cm × 175 μm i.d. tubing. Instrumental characteristics were determined for the SFC second dimension: 300 μL for the dwell volume, 57 μl for the extra-column volume and 50 μL^2 for the extra-column variance. The RPLCxSFC setup is presented in Fig. 1.

Both instrument control for the first dimension and interface programming were performed by Masslynx software. Data acquisition and instrument control for the second dimension were performed by Empower software dedicated to Acquity UPC^2 instrument. Synchronization between both dimensions was obtained by connecting electrically the two systems and by using external events in the first dimension method controlled by Masslynx software.

2.4. Chromatographic procedures

2.4.1. 1D-SFC

For V_D determination, SFC mobile phases are composed of CO_2 as solvent A and MeOH + 0.1% acetone as solvent B. It was found that when the initial composition of the programmed gradient was rich in CO_2 (e.g. 1%B), the obtained gradient profile was not perfectly linear, which led to a high uncertainty Δt on the gradient middle time t^* and consequently on the dwell volume V_D (Fig. 2a). From the experiment shown in Fig. 2a, V_D was in fact estimated at 600 ± 300 μL. This abnormal behavior is likely to be due to the supercritical nature of the mobile phase at high percentages of CO_2. In order to correctly assess the dwell volume of our SFC instrument, the gradient was therefore started with a higher percentage of MeOH + 0.1% acetone (i.e. 69% B) in order to get a quasi-liquid phase since the beginning of the gradient. Under these conditions the observed gradient profile was actually linear as shown in Fig. 2b and thus, the dwell volume measurement was much more reliable (i.e. 300 ± 40 μL).

The compatibility of the four SFC stationary phases (Acquity UPC^2 HSS C18, Acquity UPC^2 CSH FP, Acquity UPC^2 BEH and Acquity UPC^2 BEH-2EP) with LC injection solvents composed of different water/ACN proportions was tested in isocratic conditions, namely 95/2.5/2.5 CO_2/MeOH/ACN. The temperature, the flow rate, the BPR, the wavelength and the sampling rate were set at 45 °C, 2.7 mL/min, 140 bar, 215 nm (compensation from 350 nm to 450 nm) and 40 Hz respectively for all the experiments. The effect of injection solvent composition on the peak shape of o-cresol was only studied with the Acquity UPC^2 BEH-2EP column. The flow rate was set at 2.2 mL/min. Other conditions were those mentioned above.

2.4.2. RPLCxSFC

RPLCxSFC experiments related to the effect of RPLC solvent injection on pressure increase in second dimension were

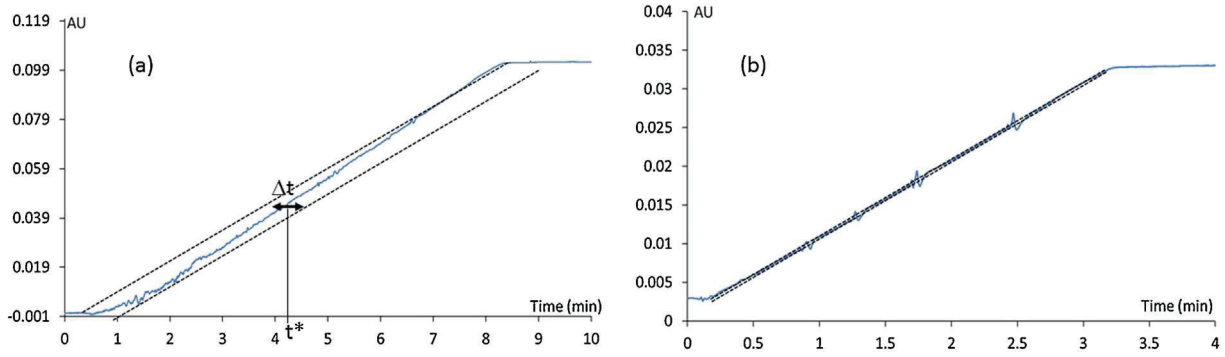

Fig. 2. Influence of gradient profile on the dwell volume measurement in SFC. Mobile phases: A = CO_2, B = MeOH + 0.1% acetone. Temperature = 30 °C. BPR = 140 bar. Detection wavelength = 254 nm. Programmed gradient: (a) 1–99%B in 8 min at 1 mL/min, (b) 69–99%B in 3 min at 1.5 mL/min. Dotted lines are the tangents to the obtained gradient profile. Δt represents the uncertainty at half part of the UV signal with t^* being the corresponding time.

performed with the following conditions. In first dimension, X-Bridge BEH C18 column was used with mobile phase consisted in Water (A) and ACN (B); the gradient profile was: 0 min, 1% B; 29.3 min, 55% B; 31.05 min, 1% B; 55 min, 1% B; the flow rate was 10 μL/min. In second dimension Acquity UPC^2 CSH FP and Acquity UPC^2 BEH were used at 2.0 mL/min and 2.6 mL/min respectively in isocratic conditions, namely CO_2/MeOH/ACN 95/2.5/2.5 (v/v/v) at 45 °C and 140 bar as BPR. The sampling time was 0.3 min. The loop volume of the interface was 3 μL.

The conditions of the RPLCxSFC separation of both synthetic sample and aqueous bio-oil extract are given in Tables 2 and 3 respectively.

2.4.3. RPLCxRPLC

The conditions of the RPLCxRPLC separation of aqueous bio-oil extract are given in Table 3. It should be noted that the maximum pressure allowed by the system with the second dimension was only 900 bar.

3. Calculations

The experimental sample peak capacities were calculated according to

$$^{j}\mathrm{n} = \frac{t_\mathrm{n} - t_1}{w} \quad (1)$$

t_n and t_1 are the retention times of the most and the least retained compound respectively and w is the average 4σ peak width (13.4% of peak height). Exponent j stands for the dimension number.

Effective sample peak capacities were calculated by the following relationship [10]:

$$n_{2\mathrm{D,effective}} = \alpha \times {}^{1}n \times (1-\gamma) + \gamma \times (\alpha \times {}^{1}n \times {}^{2}n) \quad (2)$$

γ is the correction factor corresponding to the ratio of the practical to the theoretical retention area. Its calculation is detailed in reference [6]. α is the undersampling rate introduced by Davis et al. [16]:

$$\alpha = \frac{1}{\sqrt{1 + 0.21\left(6/\tau\right)^2}} \quad (3)$$

where τ is the sampling rate of the 2D-separation (i.e. the number of fractions sent to ^{2}D per 6σ peak width in ^{1}D).

2D-data were processed using calculation tools developed under Excel 2007 and Matlab V7.12.0635.

4. Results and discussion

4.1. Theoretical considerations

The peak capacity in the second dimension ^2n increases with the ratio of the gradient time to the column dead time, $^2t_\mathrm{G}/^2t_0$. It is important to note that the increase in ^2n can be significant in the range of low $^2t_\mathrm{G}/^2t_0$ values which are usually considered in the second dimension. It is therefore of prime importance to do everything possible to enhance this ratio. As previously discussed [4], this ratio can be expressed by

$$\frac{^2t_\mathrm{G}}{^2t_0} = \frac{t_s}{^2t_0} - \left[\frac{^2V_\mathrm{D}}{^2V_0} + (1+x)\right] \quad (4)$$

where t_s is the sampling time, $^2V_\mathrm{D}$ the ^{2}D dwell volume, $^2V_0$ the ^{2}D column dead volume and x is the number of column volume required for ^{2}D column equilibration between two gradient runs.

Eq. (4) highlights the need for (i) low $^2t_0$ and therefore the use of a short ^{2}D column providing high efficiency, i.e. packed with sub 2 μm particles and/or the use of a high linear velocity as that usually required under SFC conditions, (ii) low $^2V_\mathrm{D}/^2V_0$ which is not favorable for SFC as second dimension because a rather large

Table 2
Experimental conditions for the RPLCxSFC separation of the 12 representative compounds (see list in Table 1).

	RPLC (^{1}D)	SFC (^{2}D)
Stationary phase	X Bridge BEH C18	Acquity UPC^2 BEH-2EP
Column geometry	50 mm × 1.0 mm, 3.5 μm	50 mm × 2.1 mm, 1.7 μm
Mobile phase	A: Water B: ACN	A: CO_2 B: MeOH/ACN 1:1 (v/v)
Flow rate	10 μL/min	2 mL/min
Gradient	8–51% (B) in 23 min	Isocratic 5% (B)
BPR	/	140 bar
Temperature	30 °C	45 °C
UV	220 nm	215 nm (compensation from 350 nm to 450 nm)
Vinj	2 μL	5 μL[a]

[a] 0.5 min as sampling time.

Table 3
Experimental conditions for both RPLCxSFC and RPLCxRPLC separations of the bio-oil aqueous sample.

	RPLC (^{1}D)[a]	SFC (^{2}D)	RPLC (^{2}D)
Stationary phase	Hypercarb	Acquity UPC^2 BEH-2EP	Acquity CSH Phenyl Hexyl
Column geometry	100 mm × 1.0 mm, 5 μm	50 mm × 2.1 mm, 1.7 μm	50 mm × 2.1 mm, 1.7 μm
Mobile phase	A: Water B: ACN	A: CO_2 B: MeOH/ACN 1:1 (v/v)	A: Water + 0.1% FA[b] B: ACN + 0.1% FA
Flow rate	10 μL/min	2 mL/min	1.2 mL/min
Gradient	5–99% (B) in 102.5 min	15–50% (B) in 0.12 min	5–55% (B) in 0.18 min
BPR	/	140 bar	/
Temperature	30 °C	45 °C	80 °C
UV	220 nm	220 nmCompensation from 350 nm to 450 nm	220 nm
Injected volume	5 μL	5 μL[c]	5 μL[c]

[a] RPLC (^{1}D) conditions are the same for RPLCxSFC separation and RPLCxRPLC separation.
[b] FA means formic acid.
[c] 0.5 min as sampling time.

dwell volume is present in the current SFC instrumentation, (iii) few column volumes to equilibrate the ^{2}D column (i.e. low × value) and (iv) a substantial sampling time t_s. However t_s affects the injection volume in ^{2}D, ^2V_i, according to

$$^2V_i = t_s \times {}^1F \quad (5)$$

where ^{1}F is the flow-rate in ^{1}D.

Critical injection effects have been reported under SFC conditions, especially when using polar injection solvents and/or large injection volumes [17,18]. With RPLC as first dimension, the injection solvent in ^{2}D is composed of water and an organic solvent, typically ACN. To the best of our knowledge, no study has been devoted to large injection volumes in hydro-organic solvents in SFC. Thus, the two following sections present a thorough study to determine the maximum injection volume depending on both mobile phase composition in ^{1}D and stationary phase in ^{2}D.

In order to minimize ^2V_i and since flow-splitting is impossible between the first RPLC dimension and the second SFC dimension to avoid CO_2 depressurization when the valve is switched, ^1F was set at the lowest value (10 μL/min) recommended in gradient elution for the UHPLC instrument. As a result a 1 mm i.d. column was found to be the most appropriate column geometry for the first dimension.

4.2. Effect of injection of a large water volume on inlet pressure increase

In SFC, when the injection solvent contains water, we observed a pressure increase (denoted ΔP) which occurs a few seconds after the injection process. Then, the pressure slowly decreases to its initial value. This phenomenon can be observed in 1D-SFC conditions as well as in RPLCxSFC conditions. The injection process is different between these two configurations. In 1D-SFC, the sample is pressurized before injection thanks to a particular design of the UPC^2 injection system. This pressurization step results in an immediate sharp pressure increase followed by a sharp decrease down to the working pressure, P_w, which is the working pressure generated by our experimental conditions. In RPLCxSFC the injection system of the UPC^2 instrument is not used. The sample is sent from the ^{1}D RPLC column to the sample loop and then injected in the SFC ^{2}D column when the 10-port valve is switched. As a result, the preceding sharp increase does not occur. However, in both cases, the same pressure increase ΔP can be observed. We have measured ΔP under different conditions in 1D-SFC. The experiments were focused on the behavior of 4 different SFC stationary phases subjected to 3 different injection volumes (1, 5 and 10 μL) with 3 different injection solvents differing in their water content (95%, 50% and 5%). A recent study in SFC [19] underlined the complementarity of the four studied stationary phases, with a polar character for Acquity BEH and Acquity BEH-2EP while much less polar for Acquity CSH FP and Acquity HSS C18. The obtained results, given in Fig. 3, clearly show that ΔP increases both with the injection volume and with the percentage of water in the injection solvent. It is also very interesting to note that the pressure increase is markedly higher with less polar stationary phases (Fig. 3a and b) resulting in an inlet pressure exceeding the pressure limit authorized by the instrument for 10 μL injected in 95% water. In this situation, ΔP was much higher than 80 bar while it remained lower than 40 bar for the two polar stationary phases (Fig. 3c and d). For 5 μL injected, ΔP is still high on less polar stationary phases compared to polar stationary phases (50 bar vs 5 bar at 95% water and 10 bar vs 2 bar at 50% water).

The problem of pressure increase was found to be much more critical during a RPLCxSFC separation as highlighted in Fig. 4. The inlet pressure of the ^{2}D SFC instrument was recorded when an Acquity CSH FP column (Fig. 4a) and an Acquity BEH column were used in ^{2}D (Fig. 4b). SFC conditions were strictly identical for both columns, except flow rate. Due to difference in pressure increase, the flow-rate was set at 2.0 mL/min while 2.6 mL/min with Acquity CSH FP and Acquity BEH respectively. The sampling time was 0.3 min. Consequently 3 μL of liquid solvent were injected in the ^{2}D SFC column every 0.3 min. The composition of this liquid injection solvent changes gradually as the gradient in the ^{1}D column progresses. This variation is easily assessed by means of the ^{1}D gradient profiles given in Fig. 4a and b. With a non-polar stationary phase (Fig. 4a), whereas the inlet pressure at the time of injection was 315 bar, it reached 400 bar after 10 runs. This pressure that is very close to the instrument pressure limit was kept nearly constant during 20 min before slowly decreasing down to the initial inlet pressure when the percentage of water becomes lower than 70%. This phenomenon was not observed with polar stationary phases (Fig. 4b). To explain this, we suggest that, unlike polar stationary phases, non-polar ones are poorly wetted by injection solvents rich in water, which finally results in local change of mobile phase nature. Due to the short analysis time in the second SFC dimension (0.3 min), these successive modifications have no time to be swept away. They eventually accumulate to form a multiphase plug (composed of CO_2, water, MeOH and ACN) which is more viscous than the original monophasic mobile phase (CO_2–MeOH–ACN mixture).

This significant pressure increase observed with non-polar stationary phases prevents from working at high flow-rates in ^{2}D. Furthermore, the sharp decrease in pressure observed in Fig. 4a might lead to change in retention between two consecutive fractions which could be very detrimental for the 2D-reconstruction.

In addition to this critical problem of pressure increase, significant baseline fluctuations are observed on Fig. 4c for the fractions that are separated during the pressure plate. Conversely no baseline fluctuation is noted for fractions that are analyzed when the

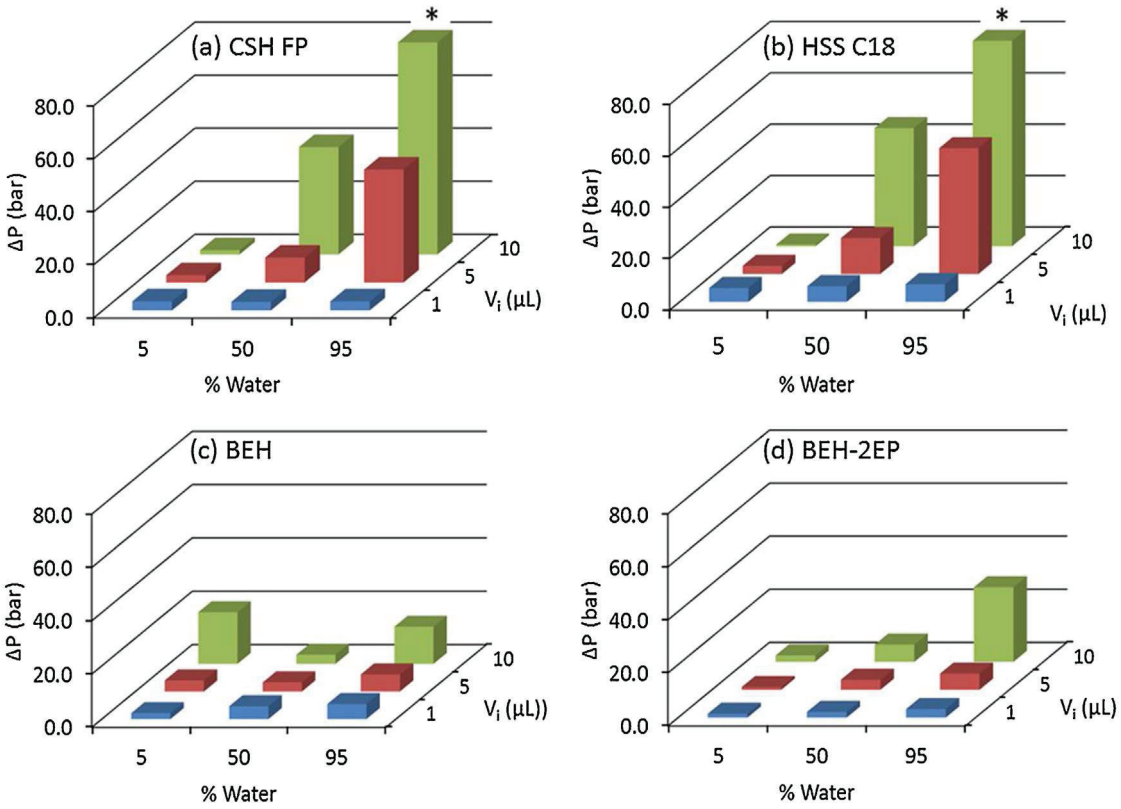

Fig. 3. Pressure increase ΔP in 1D-SFC as a function of water content of the injection solvent and injection volume V_i on (a) Acquity UPC^2 CSH FP column, (b), Acquity UPC^2 HSS C18 column, (c) Acquity UPC^2 BEH column and (d) Acquity UPC^2 BEH-2EP column. Column geometry: 50 mm × 2.1 mm, 1.7 μm; flow rate = 2.7 mL/min; temperature = 45 °C; BPR = 140 bar; injection solvent = mixture of water and acetonitrile. '*' means that ΔP could not be measured because the pressure limit (414 bar) was reached.

inlet pressure is back to normal (Fig. 4e). With ^{2}D polar stationary phases the ^{2}D inlet pressure remains constant during the whole RPLCxSFC separation (Fig. 4b) and no fluctuation of the baseline is visible whatever the considered fractions (Fig. 4d and f).

In the light of these results, it is clear that a polar stationary phase should be preferably used for the SFC second dimension. Re-injection of very low injection volumes (<1 μL) in ^{2}D could probably circumvent the problems encountered with non-polar stationary phase but it should lead to quite unrealistic sampling time (<0.1 min). Another alternative would be to start the RPLC gradient with water content lower than 70%. However this option is not possible for compounds that are poorly retained in RPLC such as small polar compounds. Considering the above results, Acquity BEH-2EP was chosen as ^{2}D SFC stationary phase for the rest of this study.

4.3. Effect of injection volumes and injection solvent composition on peak shapes in 1D-SFC

In SFC, it was recently shown [18] that the injection solvent composition strongly influences peak shapes. Very polar solvents such as DMSO and MeOH were found to lead to significant peak distortions even for small injected volumes, these distortions being more pronounced for less retained compounds. The effect of small injection volumes of ionizable compounds with pure water or water/ACN mixtures as injection solvent was recently studied [20]. For 90% of the tested compounds (acidics and basics), no significant injection effect were found. In an extensive work Abrahamsson et al. [17] also studied the effect of various injection solvents in accordance with the stationary phase. They pointed out that injection solvent may interact with stationary phase, mobile phase and solute, thereby affecting either positively or negatively peak shape. We have therefore studied the impact of injected volume on peak shape when the solute is dissolved in different water/ACN mixtures. Results obtained with CO_2/ACN/MeOH 95/2.5/2.5 (v/v/v) as SFC mobile phase and o-cresol as solute are shown in Fig. 5. Surprisingly, when the injected volume does not exceed 5 μL (i.e. 5% of the column dead volume), a very high content of ACN in injection solvent (i.e. 95%) seems to be more damaging for the peak shape than a high content of water (Fig. 5a and b). Conversely, it is possible to inject up to 5 μL of sample dissolved in a solvent containing 50–95% water without strong peak distortion. Obviously, for 10 μL injected (Fig. 5c) which represents 10% of the column dead volume, the peak shapes are very bad for all studied injection solvents. The results shown in Fig. 5 also point out the retention shift that increases with both the percentage of water in the injection solvent and the injection volume. It is likely to be due to two combined effects: (i) good affinity of water for the polar sites of the stationary phase and (ii) high affinity of o-cresol for water. Consequently, when the injection plug enters the column, o-cresol interacts preferentially with the stationary phase thereby increasing retention. Such retention shift could be damaging for 2D-chromatogram reconstruction due to difficulty in peak assignment between consecutive fractions analysis. However, this problem does not really arise in RPLCxSFC since the injection solvent composition slightly varies between the 2 and 4 consecutive ^{2}D runs that are required in comprehensive two-dimensional chromatography to minimize undersampling [16].

In view of this study, it was decided to inject a maximum of 5 μL in the second SFC dimension. Since flow splitting between ^{1}D and ^{2}D was not possible with a LCxSFC configuration, injection volume in ^{2}D was directly related to both ^{1}D flow-rate and sampling time. Accordingly, with 10 μL/min as ^{1}D flow-rate, the sampling time could not be higher than 30 s.

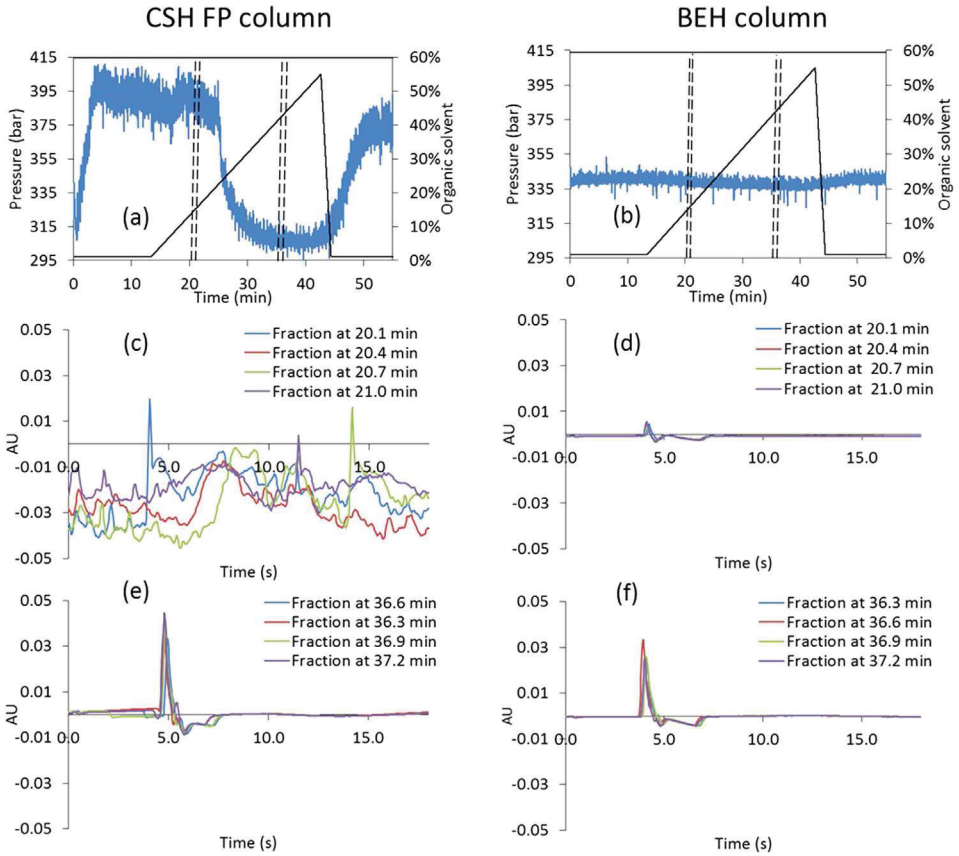

Fig. 4. Influence of ^{2}D stationary phase on the course of a RPLCxSFC experiment. (a) and (b): SFC inlet pressure vs run time. (c) and (d): ^{2}D analysis of fractions eluted from ^{1}D between 20.1 min and 21.0 min. (e) and (f): ^{2}D analysis of fractions eluted from ^{1}D between 36.3 min and 37.2 min. Sampling time = 0.3 min. RPLC conditions: column dimensions = 50 mm × 1.0 mm, stationary phase = 3.5 μm Xbridge C18, solvent A = water, solvent B = ACN, gradient from 1% B to 55% B in 29.3 min, flow rate = 10 μL/min, temperature = 30 °C. SFC conditions: column dimensions = 50 mm × 2.1 mm, stationary phase = (a,c,e) 1.7 μm Acquity UPC^{2} CSH FP; (b,d,f) 1.7 μm Acquity UPC^{2} BEH, isocratic mobile phase = CO_2/MeOH/ACN 95/2.5/2.5 (v/v/v), flow rate = (a,c,e) 2.0 mL/min; (b,d,e) 2.6 mL/min, temperature = 45 °C, BPR = 140 bar. Full lines show the gradient profile in ^{1}D outlet. Dotted lines show the time windows for the selected fractions.

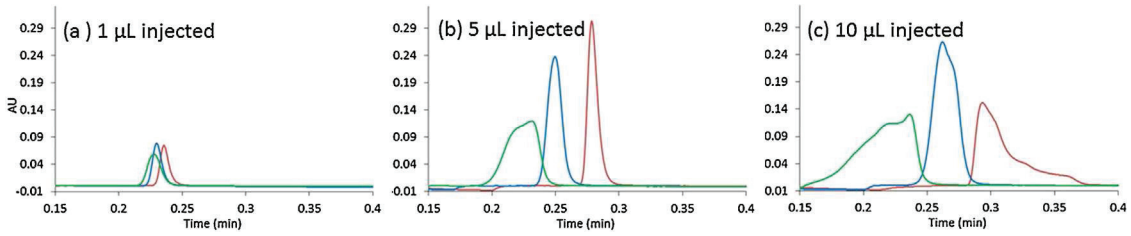

Fig. 5. Effect of injection solvent and injected volume peak shape. Solute: o-cresol with (a) 1 μL, (b) 5 μL, (c) 10 μL. Injection solvent composition: Water/ACN 95/5 (v/v) (——), 50/50 (v/v) (——) and 5/95 (v/v) (——). Column: Acquity UPC^{2} BEH-2EP, 50 mm × 2.1 mm, 1.7 μm. Flow rate = 2.2 mL/min; mobile phase: CO_2/MeOH/ACN 95/2.5/2.5 (v/v/v). Temperature = 45 °C. BPR = 140 bar. Detection wavelength = 215 nm (compensation from 350 nm to 450 nm).

4.4. Application to the RPLCxSFC separation of a sample of aromatic compounds

In order to validate the choices made previously to carry out the on-line RPLCxSFC experiments, 12 aromatic compounds were separated. The experimental conditions are given in Table 2. The sampling time and the ^{1}D flow rate being equal to 0.5 min and 10 μL/min respectively, two identical sample loops of 5 μL were installed on the 10-port switching valve in order to completely fill the sample loop. In LCxLC, partial loop injection is always preferred in order to avoid any sample loss due to the parabolic flow profile. Sample loops are therefore most commonly oversized. In LCxSFC, full loop injection is necessary to avoid dissolving issues as highlighted in Fig. 6. When the sample loop is in inject position, it is filled with the SFC mobile phase. When the sample loop comes back in load position, it is depressurized allowing some droplets of organic modifier covering the walls of the loop. Whereas this droplets can be well solubilized in the RPLC mobile phase coming from ^{1}D (Fig. 6a) they may cause troublesome issues with the SFC mobile phase if the sample loop is partially filled (Fig. 6b). In addition, the presence of air to push the sample plug can have a detrimental effect with SFC mobile phase which is better dissolved in the hydro-organic liquid solvent. However, unlike in LCxLC, full loop injection is a possible solution in LCxSFC since the loop is filled with air prior to the injection process thereby allowing the flow profile to be radial and hence preventing from any sample loss.

The obtained RPLCxSFC separation is presented in Fig. 7a. It is interesting to notice the large occupation of the retention space by the 12 compounds, underlining the great interest of this coupling in terms of orthogonality. Furthermore, as highlighted in Fig. 8b

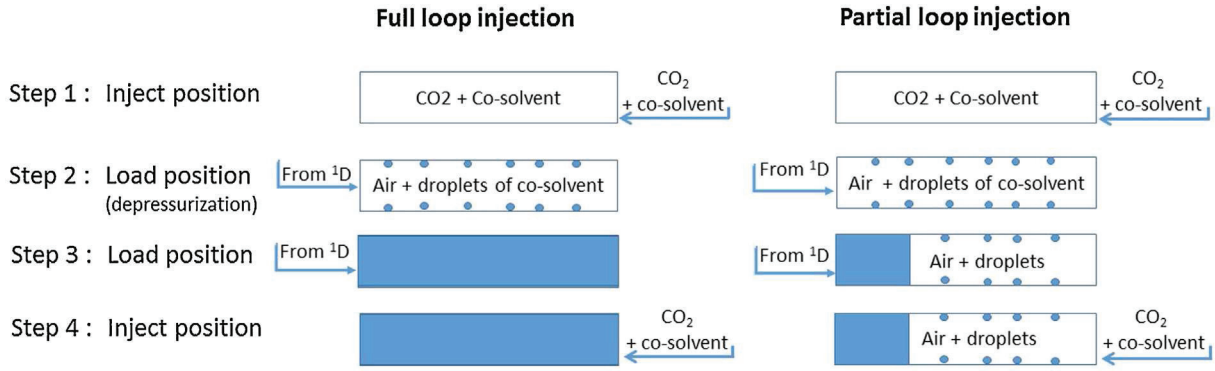

Fig. 6. Four step representation of the injection process in the second dimension of RPLCxSFC depending on the use of full or partial loop injection. After valve switching (Step 2) CO_2 is depressurized, producing some droplets of co-solvent on the wall of the loop.

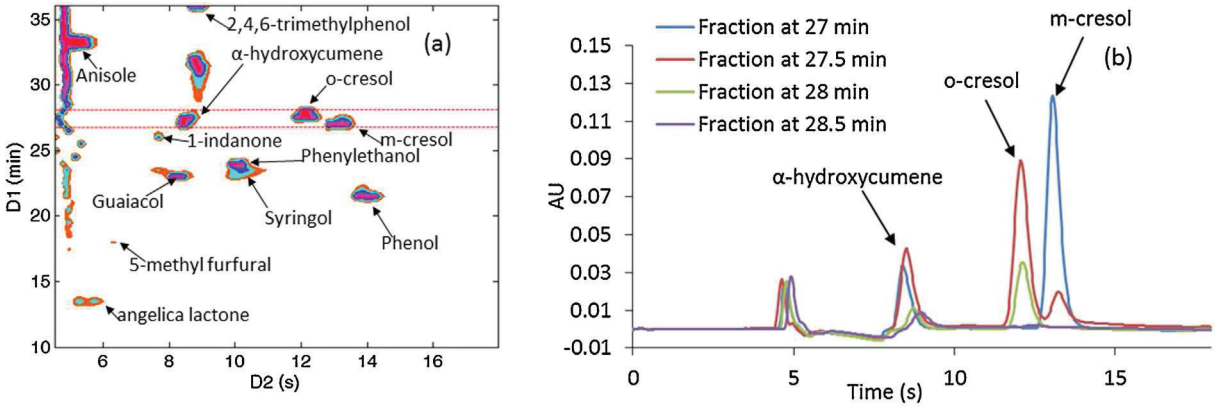

Fig. 7. On-line RPLCxSFC separation of 12 aromatic compounds. (a) Contour plot UV and (b) overlay of SFC separation of the fractions from 27 min to 28.5 min (red dotted lines in the contour plot). See Table 1 for solutes and Table 3 for experimental conditions. (For interpretation of the color information in this figure legend, the reader is referred to the web version of the article.)

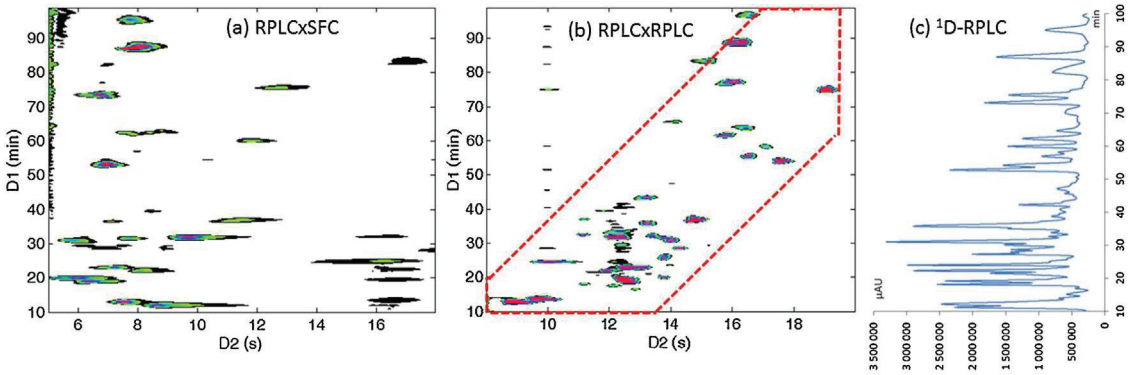

Fig. 8. Comparison of (a) on-line RPLCxSFC and (b) on-line RPLCxRPLC for the separation of a bio-oil aqueous extract. The red dotted lines in (b) delimit the separation space. (c) Chromatogram obtained in ^{1}D-RPLC. Experimental conditions and performance calculations are summarized in Tables 3 and 4 respectively. (For interpretation of the color information in this figure legend, the reader is referred to the web version of the article.)

showing the separation of four consecutive fractions, peak shapes are quite symmetrical as could be expected from our preliminary studies. With 0.83 s as average 4σ peak width the sample peak capacity is close to 15 in the second dimension.

4.5. Comparison of RPLCxRPLC and RPLCxSFC systems for the separation of a bio-oil sample

An extensive knowledge of the bio-oil composition is strongly required to optimize the pyrolysis process. As discussed in a preceding study, dealing with the RPLCxRPLC separation of bio-oil [10], LCxLC should be complementary to two dimensional gas chromatography (GCxGC) due to the presence of compounds with low volatility and/or poor thermal stability such as molecules coming from the thermal cracking of natural polymers or cracked sugars. Unlike GC, both LC and SFC are expected to be suitable separation techniques for this kind of compounds. In this study, RPLCxSFC was compared to RPLCxRPLC for the separation of a real sample consisting in an aqueous extract of a bio-oil. The conditions of the first dimension were similar to those used in our previous study on RPLCxRPLC [10] except the gradient time, much lower in the present work to reduce the analysis time. In order to elute all

Table 4
Experimental results of RPLCxSFC and RPLCxRPLC.

	γ	α	^1n	$^2w_{4\sigma}$ (s)	^2n	$^1n \times {}^2n$	$n_{2D,effective}$
RPLCxSFC	1	0.85	56	1.09	13	730	620
RPLCxRPLC	0.59	0.85	56	0.60	20	1120	560

^1n and ^2n were calcutated according to Eq. (1); γ was calculated according [6]; α was calculated according to Eq. (3); $n_{2D,effective}$ was calculated according to Eq. (2).

the compounds in ^{2}D SFC conditions, a gradient from 15% to 50% MeOH/ACN (1:1) was needed. The contour plot of the RPLCxSFC separation is presented in Fig. 8a. For comparison, Fig. 8b shows the RPLCxRPLC separation of the same sample performed using the same ^{1}D conditions as the RPLCxSFC separation. The ^{1}D-separation is shown in Fig. 8c. For a better comparison of the two separations, the sampling time was also kept identical (i.e. 30 s). As a consequence, ^1n (Eq. (1)) and α (Eq. (4)) were identical for both separations. Experimental conditions are given in Table 3.

Fig. 8 clearly underlines that the RPLCxSFC system offers much higher degree of orthogonality (γ close to 1) compared to the RPLCxRPLC configuration (γ close to 0.6). It is important to note that this latter configuration and the corresponding conditions displayed in Table 3 were found to provide the highest effective peak capacity among the different studied RPLCxRPLC systems [10].

In RPLCxSFC, thanks to tremendous enhancement of the available retention space the effective peak capacity was slightly higher as shown in Table 4 although ^2n was lower in SFC (12 vs 20 in RPLCxRPLC). This significant difference in ^{2}n can be essentially ascribed to

(i) More extra-column band broadening in SFC second dimension with 50 μL^2 as measured extra-column variance compared to 9 μL^2 in RPLC second dimension. This is essentially due to larger tubing internal diameter as well as larger cell volume (175 μm and 8 μL respectively in SFC compared to 65 μm and 0.5 μL respectively in RPLC). A recent study dealt with these problems of extra-column volumes in SFC [21], especially in case of short and narrow bore columns.
(ii) Injection issues that still exist in RPLCxSFC despite the precautions that need to be taken as discussed in Section 4.1. Conversely, no injection effect was observed in RPLCxRPLC.
(iii) Less broad composition range in SFC (35% vs 45% in RPLC).

It should also be noted that ^2n improvement was strongly expected in SFC as a result of flow-rate increase and hence $^2t_s/^2t_0$ increase but, in the end, $^2t_G/^2t_0$ which is of major importance in peak capacity assessment, was just slightly higher (2.3 in SFC vs 2.1 in RPLC). According to Eq. (4), these quite identical values can be explained by the fact that (i) the dwell volume was larger in SFC (300 μL vs 120 μL in LC) increasing $^2V_D/^2V_0$ and (ii) an additional time of 0.2 min was required by the software for data processing between two consecutive runs, thus increasing the time for column equilibration (3.4t_0 in SFC vs 2t_0 in RPLC) while 2t_0 only are sufficient for good run-to-run repeatability in UHPLC conditions [22–24] as well as in SFC conditions for neutral compounds (data not shown).

Larger extra-column volumes as well as more injection effects in SFC generated larger peak widths (1.09 s as average value vs 0.6 s in RPLC) and hence lower peak heights. Moreover, whereas the peak widths were nearly the same for all peaks in RPLC (10% as RSD), the peak shapes varied in SFC depending on the compounds resulting in a high variability in peak width values (23% as RSD). As a result the signal was 3–20 times lower in SFC compared to RPLC (7 times on average). At the same time, the UV-detector noise was more important in SFC (about two times higher). More significant UV-noise in SFC is probably due to pressure fluctuations and resulting refractive index changes [25].

In the present study, the combination of both lower signal and more significant noise resulted in a signal to noise ratio about 15 times lower in RPLCxSFC than in RPLCxRPLC.

Finally, despite the addressed instrumental issues which could be overcome in the future for some of them, our results show that RPLCxSFC can be a good alternative to RPLCxRPLC for the separation of biomass by-products and more generally for the separation of neutral compounds.

5. Conclusions

The goal of this work was to evaluate the potential of on-line RPLCxSFC for the separation of neutral compounds. Suitable stationary phase and injection volume for the ^{2}D SFC were chosen thanks to preliminary studies aiming at overpassing the lack of compatibility between the mobile phases used as first and second dimension. Polar stationary phases in SFC seem to be the most adapted stationary phases. On the other hand it was shown that a maximum of 5 μL of a mixture of water/acetonitrile was appropriate to inject in the second SFC dimension. An on-line RPLCxSFC separation of a real aqueous bio-oil sample was successfully carried out achieving full orthogonality ($\gamma = 1$) using a Hypercarb column in ^{1}D and an Acquity BEH 2-EP column in ^{2}D. With the optimized RPLCxRPLC configuration, using the same Hypercarb column in ^{1}D and an Acquity CSH phenyl-hexyl in ^{2}D, the γ-coefficient could not exceed 0.59. Accordingly, although wider peaks were observed in SFC as second dimension, the effective peak capacity was slightly higher with RPLCxSFC configuration (620 vs 560 with RPLCxRPLC). However, it should be noted that the peak capacity in ^{2}D-SFC was limited by the high dwell volume of the apparatus as well as software issues due to this unusual coupling. Consequently, we are sure that there is still room for further improvements. Furthermore, the signal to noise ratio was found to be markedly higher in RPLCxRPLC (10-fold higher) due to both larger peaks in SFC resulting from significant extra-column volumes and still more pronounced injection effects and more significant UV-detector noise in SFC.

Finally, in the light of these results, on-line RPLCxSFC can be considered as an interesting alternative for the separation of neutral compounds compared to RPLCxRPLC.

Acknowledgements

M.S., S.H. and G.C. wish to thank Waters for the loan of the UPC^2 system and especially Philippe Mériglier for his help in LCxSFC setting up. S.H. would like to thank Davy Guillarme for stimulating discussions and valuable advice on different aspects of SFC.

References

[1] P. Dugo, F. Cacciola, T. Kumm, G. Dugo, L. Mondello, Comprehensive multidimensional liquid chromatography: theory and applications, J. Chromatogr. A 1184 (2008) 353–368, http://dx.doi.org/10.1016/j.chroma.2007.06.074
[2] I. François, K. Sandra, P. Sandra, Comprehensive liquid chromatography: fundamental aspects and practical considerations—a review, Anal. Chim. Acta 641 (2009) 14–31, http://dx.doi.org/10.1016/j.aca.2009.03.041
[3] P.Q. Tranchida, P. Donato, F. Cacciola, M. Beccaria, P. Dugo, L. Mondello, Potential of comprehensive chromatography in food analysis, TrAC Trends Anal. Chem. 52 (2013) 186–205, http://dx.doi.org/10.1016/j.trac.2013.07.008

[4] M. Sarrut, G. Crétier, S. Heinisch, Theoretical and practical interest in UHPLC technology for 2D-LC, TrAC Trends Anal. Chem. 63 (2014) 104–112, http://dx.doi.org/10.1016/j.trac.2014.08.005
[5] G. Guiochon, N. Marchetti, K. Mriziq, R.A. Shalliker, Implementations of two-dimensional liquid chromatography, J. Chromatogr. A 1189 (2008) 109–168, http://dx.doi.org/10.1016/j.chroma.2008.01.086
[6] A. D'Attoma, C. Grivel, S. Heinisch, On-line comprehensive two-dimensional separations of charged compounds using reversed-phase high performance liquid chromatography and hydrophilic interaction chromatography. Part I: Orthogonality and practical peak capacity considerations, J. Chromatogr. A 1262 (2012) 148–159, http://dx.doi.org/10.1016/j.chroma.2012.09.028
[7] I. François, A. De Villiers, P. Sandra, Considerations on the possibilities and limitations of comprehensive normal phase–reversed phase liquid chromatography (NPLC × RPLC), J. Sep. Sci. 29 (2006) 492–498, http://dx.doi.org/10.1002/jssc.200500451
[8] K.J. Mayfield, R.A. Shalliker, H.J. Catchpoole, A.P. Sweeney, V. Wong, G. Guiochon, Viscous fingering induced flow instability in multidimensional liquid chromatography, J. Chromatogr. A 1080 (2005) 124–131, http://dx.doi.org/10.1016/j.chroma.2005.04.093
[9] P. Jandera, Column selectivity for two-dimensional liquid chromatography, J. Sep. Sci. 29 (2006) 1763–1783, http://dx.doi.org/10.1002/jssc.200600202
[10] A. Le Masle, D. Angot, C. Gouin, A. D'Attoma, J. Ponthus, A. Quignard, et al., Development of on-line comprehensive two-dimensional liquid chromatography method for the separation of biomass compounds, J. Chromatogr. A 1340 (2014) 90–98, http://dx.doi.org/10.1016/j.chroma.2014.03.020
[11] D. Tomasini, F. Cacciola, F. Rigano, D. Sciarrone, P. Donato, M. Beccaria, et al., Complementary analytical liquid chromatography methods for the characterization of aqueous phase from pyrolysis of lignocellulosic biomasses, Anal. Chem. 86 (2014) 11255–11262, http://dx.doi.org/10.1021/ac5038957
[12] C. West, E. Lesellier, Characterisation of stationary phases in subcritical fluid chromatography by the solvation parameter model: II. Comparison tools, J. Chromatogr. A 1110 (2006) 191–199, http://dx.doi.org/10.1016/j.chroma.2006.02.002
[13] A. Grand-Guillaume Perrenoud, J.-L. Veuthey, D. Guillarme, Comparison of ultra-high performance supercritical fluid chromatography and ultra-high performance liquid chromatography for the analysis of pharmaceutical compounds, J. Chromatogr. A 1266 (2012) 158–167, http://dx.doi.org/10.1016/j.chroma.2012.10.005
[14] I. François, P. Sandra, Comprehensive supercritical fluid chromatography × reversed phase liquid chromatography for the analysis of the fatty acids in fish oil, J. Chromatogr. A 1216 (2009) 4005–4012, http://dx.doi.org/10.1016/j.chroma.2009.02.078
[15] P.G. Stevenson, A. Tarafder, G. Guiochon, Comprehensive two-dimensional chromatography with coupling of reversed phase high performance liquid chromatography and supercritical fluid chromatography, J. Chromatogr. A 1220 (2012) 175–178, http://dx.doi.org/10.1016/j.chroma.2011.11.020
[16] J.M. Davis, D.R. Stoll, P.W. Carr, Effect of first-dimension undersampling on effective peak capacity in comprehensive two-dimensional separations, Anal. Chem. 80 (2008) 461–473, http://dx.doi.org/10.1021/ac071504j
[17] V. Abrahamsson, M. Sandahl, Impact of injection solvents on supercritical fluid chromatography, J. Chromatogr. A 1306 (2013) 80–88, http://dx.doi.org/10.1016/j.chroma.2013.07.056
[18] J.N. Fairchild, J.F. Hill, P. Iraneta, Influence of sample solvent composition for SFC separations, LC-GC N. Am. 31 (2013) 326–333.
[19] S. Khater, C. West, E. Lesellier, Characterization of five chemistries and three particle sizes of stationary phases used in supercritical fluid chromatography, J. Chromatogr. A 1319 (2013) 148–159, http://dx.doi.org/10.1016/j.chroma.2013.10.037
[20] L. Nováková, A. Grand-Guillaume Perrenoud, R. Nicoli, M. Saugy, J.-L. Veuthey, D. Guillarme, Ultra high performance supercritical fluid chromatography coupled with tandem mass spectrometry for screening of doping agents. I: Investigation of mobile phase and MS conditions, Anal. Chim. Acta 853 (2015) 637–646, http://dx.doi.org/10.1016/j.aca.2014.10.004
[21] A. Grand-Guillaume Perrenoud, C. Hamman, M. Goel, J.-L. Veuthey, D. Guillarme, S. Fekete, Maximizing kinetic performance in supercritical fluid chromatography using state-of-the-art instruments, J. Chromatogr. A 1314 (2013) 288–297, http://dx.doi.org/10.1016/j.chroma.2013.09.039
[22] A.P. Schellinger, D.R. Stoll, P.W. Carr, High-speed gradient elution reversed-phase liquid chromatography of bases in buffered eluents: Part I. Retention repeatability and column re-equilibration, J. Chromatogr. A 1192 (2008) 41–53, http://dx.doi.org/10.1016/j.chroma.2008.01.062
[23] A.P. Schellinger, D.R. Stoll, P.W. Carr, High speed gradient elution reversed phase liquid chromatography of bases in buffered eluents: Part II. Full equilibrium, J. Chromatogr. A 1192 (2008) 54–61, http://dx.doi.org/10.1016/j.chroma.2008.02.049
[24] C. Grivel, J.-L. Rocca, D. Guillarme, J.-L. Veuthey, S. Heinisch, Selection of suitable operating conditions to minimize the gradient equilibration time in the separation of drugs by Ultra-High-Pressure Liquid Chromatography with volatile (mass spectrometry-compatible) buffers, J. Chromatogr. A 1217 (2010) 459–472, http://dx.doi.org/10.1016/j.chroma.2009.11.059
[25] T.A. Berger, B.K. Berger, Minimizing UV noise in supercritical fluid chromatography. I. Improving back pressure regulator pressure noise, J. Chromatogr. A 1218 (2011) 2320–2326, http://dx.doi.org/10.1016/j.chroma.2011.02.030.

CONCLUSIONS

Le couplage RPLCxSFC en ligne a été appliqué à l'analyse d'une bio-huile principalement composée de molécules neutres.

L'avantage d'utiliser une combinaison RPLCxSFC par rapport à un montage RPLCxRPLC est clairement montré d'un point de vue de l'orthogonalité. Néanmoins, la compatibilité des phases mobiles entre les deux dimensions ainsi que la variance extra-colonne bien supérieure en ^{2}D-SFC comparée à la ^{2}D-RPLC limitent le gain final en terme de capacité de pics. Ces paramètres contribuent également à la plus faible sensibilité observée en RPLCxSFC. Une diminution du volume extra-colonne, du volume de délai et une augmentation de la pression maximale de l'appareillage en SFC sont des pistes à suivre pour augmenter les performances de ce couplage.

Finalement, le couplage RPLCxSFC en ligne est une solution viable et intéressante pour la séparation de composés neutres. Son potentiel pour des analyses achirales (^{1}D-RPLC) puis chirales (^{2}D-SFC) dans le domaine pharmaceutique est également très intéressant [5].

RÉFÉRENCES

[1] I. François, A. De Villiers, P. Sandra, Considerations on the possibilities and limitations of comprehensive normal phase–reversed phase liquid chromatography (NPLC×RPLC), J. Sep. Sci. 29 (2006) 492–498. doi:10.1002/jssc.200500451.

[2] D. Li, C. Jakob, O. Schmitz, Practical considerations in comprehensive two-dimensional liquid chromatography systems (LCxLC) with reversed-phases in both dimensions, Anal. Bioanal. Chem. 407 (2014) 153–167. doi:10.1007/s00216-014-8179-8.

[3] I. François, P. Sandra, Comprehensive supercritical fluid chromatography × reversed phase liquid chromatography for the analysis of the fatty acids in fish oil, J. Chromatogr. A. 1216 (2009) 4005–4012. doi:10.1016/j.chroma.2009.02.078.

[4] P.G. Stevenson, A. Tarafder, G. Guiochon, Comprehensive two-dimensional chromatography with coupling of reversed phase high performance liquid chromatography and supercritical fluid chromatography, J. Chromatogr. A. 1220 (2012) 175–178. doi:10.1016/j.chroma.2011.11.020.

[5] C.J. Venkatramani, M. Al-Sayah, G. Li, M. Goel, J. Girotti, L. Zang, L. Wigman, P. Yehl, N. Chetwyn, Simultaneous achiral-chiral analysis of pharmaceutical compounds using two-dimensional reversed phase liquid chromatography-supercritical fluid chromatography, Talanta. 148 (2016) 548–555. doi:10.1016/j.talanta.2015.10.054.

CONCLUSIONS GÉNÉRALES ET PERSPECTIVES

Nous avons pu confirmer dans ce travail que la chromatographie en phase liquide bidimensionnelle « comprehensive » en ligne est une technique séparative à très fort potentiel qui permet de répondre à des problématiques complexes très diverses.

Il a été montré qu'une mise au point rationnelle des conditions opératoires est indispensable. Une nouvelle méthodologie basée sur une approche « Pareto-optimal » a été développée afin d'optimiser simultanément la capacité de pics, le facteur de dilution et le temps d'analyse. Celle-ci tient compte à la fois des conditions opératoires mais aussi des contraintes instrumentales. Les conditions optimales peuvent ainsi être appliquées à des séparations réelles dans un environnement instrumental donné. Cette approche théorique a ainsi été appliquée en RPLCxRPLC pour l'analyse de mélanges complexes de peptides. Les résultats expérimentaux obtenus sont tout à fait cohérents avec les résultats prédits. Par ailleurs, il est montré que des conditions opératoires complètement différentes peuvent aboutir à des performances chromatographiques comparables et qu'il appartient au chromatographiste de faire un choix final en fonction de critères additionnels. En ce qui concerne la séparation de peptides, il est particulièrement intéressant de remarquer que la plus grande capacité de pics atteinte en 1D-RPLC (1600 en 40h, colonne monolithique de 4 mètres) ne nécessite qu'1h en RPLCxRPLC dans nos conditions optimisées. D'autre part, cette capacité de pics obtenue en RPLCxRPLC est 4 fois supérieure à celle obtenue dans des conditions optimisées en 1D-RPLC avec le meilleur standard de l'instrumentation actuelle (HT-UHPLC, sub-2µm). Enfin des capacités de pics similaires en 1D-RPLC et RPLCxRPLC ont été obtenues pour des temps de gradient de seulement 3-4 min.

Une méthode HICxRPLC-UV/MS en ligne a été optimisée dans le but de caractériser de façon exhaustive des biomolécules à visée thérapeutique à très hauts poids moléculaires que sont les anticorps conjugués (environ 150 kDa). Ce couplage a permis, en une seule injection de 70 min, de calculer le DAR moyen de l'échantillon d'anticorps conjugués (Brentuximab Vedotin) grâce à la ^{1}D mais également d'obtenir des renseignements structuraux grâce à la spectrométrie de masse associée à la détection UV de la ^{1}D et de la ^{2}D. Cette complémentarité a rendu possible l'identification de DAR impairs jusqu'alors non décrits dans la littérature pour cet ADC commercial. Pour obtenir ces résultats, un développement de méthode a été nécessaire et nous a conduit à (i) optimiser les conditions de gradient d'élution en HIC pour la séparation des différents DARs, (ii) ajouter du sel dans l'échantillon d'ADC afin d'améliorer la sensibilité, (iii) encadrer le créneau de sel provenant de la ^{1}D par de l'eau pour éviter toute précipitation lors de l'injection en ^{2}D, (iv) sélectionner le modificateur organique de ^{2}D pour maximiser la capacité de pics, (v) utiliser une vanne de sélection afin d'éliminer le créneau de sel avant son entrée dans la MS et (vi) augmenter la sensibilité MS grâce au split du débit de ^{2}D et à l'ajout d'acide formique. Il est à noter que la cartographie UV obtenue grâce à cette méthode pourrait être

utilisée pour le contrôle de la fabrication de ces molécules et/ou de leur stabilité. Le couplage avec la MS pourrait être utilisé lors d'étude en « early development » pour une caractérisation exhaustive de l'échantillon et/ou après la détection d'anomalies observées avec la méthode UV.

Enfin le développement d'un couplage RPLCxSFC en ligne a été pour la première fois décrit. Appliqué à des mélanges complexes de composés neutres, les sélectivités différentes fournit par ces deux modes chromatographiques sont un réel avantage par rapport à une approche RPLCxRPLC. Un travail particulier concernant les conditions de transfert de l'échantillon de la ^{1}D vers la ^{2}D a été réalisé. Il a abouti à une interface simple constituée d'une vanne 10-ports/2pos composée de deux boucles d'échantillonnages classiques (boucles vides). Celles-ci doivent être complètement remplies par la phase mobile liquide de ^{1}D afin d'éviter la présence d'air et ainsi assurer une meilleure solubilisation par la phase mobile de ^{2}D (CO_2+modificateur organique). L'utilisation de phases stationnaires polaires est recommandée en ^{2}D pour éviter des problèmes de surpressions et de fluctuations de la ligne de base lors de l'injection. Seuls des volumes inférieurs à 5 µL (5% $^{2}V_0$) permettent de limiter les effets à l'injection. Il est ici important de noter l'impossibilité d'utiliser un split pour réduire $^{2}V_i$ du fait de la remontée du CO_2 par dépressurisation lors de la rotation de la vanne à l'interface. Finalement une méthode RPLCxSFC en ligne a été comparée à une méthode RPLCxRPLC optimisée pour l'analyse d'un extrait aqueux d'une bio-huile. Des capacités de pics similaires ont été obtenues démontrant que le couplage RPLCxSFC représente une alternative viable pour la séparation de ce type d'échantillon. L'amélioration de paramètres instrumentaux (volume de délai, volume externe) en SFC pourrait accroitre l'intérêt pour un tel couplage en termes de capacité de pics et de sensibilité.

L'essor des techniques bidimensionnelles est croissant avec la complexité des échantillons mais aussi avec les demandes des différentes règlementations qui poussent les chimistes/biologistes à caractériser toujours davantage leurs échantillons. L'apport de méthodes orthogonales est donc primordiale et leur couplage en ligne avantageux. Pour bénéficier pleinement de l'apport de ces techniques en ligne, le travail d'optimisation doit être poursuivi afin d'affiner les prédictions théoriques et simplifier le travail d'optimisation. Le développement d'outils prédictifs plus ciblés appliqués à la séparation d'une ou plusieurs paires de pics critiques pourrait également être envisagé.

Le couplage avec la spectrométrie de masse peut faire l'objet d'améliorations comme la possibilité de travailler à très hauts débits sans limiter la sensibilité. Cela éviterait l'utilisation d'un split en amont du spectromètre de masse et donc une source de dispersion supplémentaire. Un meilleur compromis entre le temps de balayage et la sensibilité MS permettrait de profiter pleinement du pouvoir de résolution d'une séparation 2D. En effet, la MS ne peut pas toujours décrire de façon correcte les pics

générés en ^{2}D (entre 0.3s et 2s de largeur à la base selon les composés) tout en gardant une sensibilité suffisante.

Le domaine des biomolécules pourrait être un vecteur de développement de méthodes 2D. En effet, ces molécules sont très complexes et possèdent des propriétés qui conviennent parfaitement à des analyses 2D. Leur caractérisation requiert, l'utilisation de méthodes non dénaturantes et dénaturantes avec l'utilisation de différents modes chromatographiques tels que les modes HIC, SEC, RPLC, IEX, HILIC, qui sont intrinsèquement orthogonaux. L'intérêt de méthodes 2D en ligne serait alors d'obtenir les informations inhérentes aux deux techniques en une seule injection tout en permettant la compatibilité avec la spectrométrie de masse parfois impossible avec la méthode ^{1}D (cf. chapitre 4). De la même façon, le couplage LCxSFC peut être envisagé pour obtenir la séparation de diastéréoisomères en ^{1}D achirale puis d'énantiomères en ^{2}D chirale.

L'évaluation de la réduction des effets matrices grâce au pouvoir de séparation des méthodes LCxLC doit être poursuivie. En effet, cela pourrait permettre de limiter les étapes de traitement d'échantillon qui ne sont pas toujours aisément automatisables et ainsi gagner en productivité. Toutefois, ces études devront intégrer un aspect quantitatif qui reste un domaine encore peu exploré en LCxLC en ligne. L'apparition de logiciels permettant un traitement automatisé complet des données ainsi que leur quantification est un enjeu primordial pour l'essor définitif de ces techniques couplées « comprehensive » en ligne.